Paolo Bollella was born in 1989 in Rome (ITALY). He received his MSc in Analytical Chemistry in 2014 at the Faculty of Science of Sapienza University of Rome. During his MSc studies he joined to the biosensor laboratory at the department of Chemistry and Drug Technologies. In this period, his project was focused on the study of intaractions between Anabolic Androgenic Steroids and liposomes by means of surface plasmon resonance as a part of collaboration with the Italian Antidoping Institute in Rome led by Prof. Francesco Botrè.

He started his PhD studies in Pharmaceutical Science with speciality in Analytical Chemistry under the supervision of Prof. Riccarda Antiochia at the Department of Chemistry and Drug Technologies. During this period he moved for at least two years to the Division of Biochemistry and Structural Biology – Department of Chemistry at Lund University in Sweden. In this department, he joined to the bioelectrochemistry laboratory led by Prof. Lo Gorton, who carefully co-supervised my experimental work on the development of new nanostructuration approaches to study the electron transfer between redox enzymes and solid electrodes for applications into carbohydrate amperometric biosensors and enzymatic fuel cells

SAPIENZA
UNIVERSITÀ DI ROMA

PAOLO BOLLELLA

Biosensors & Enzymatic Fuel Cells based on Direct Electron Transfer of Dehydrogenases: Characterization and Applications

SAPIENZA
UNIVERSITÀ DI ROMA

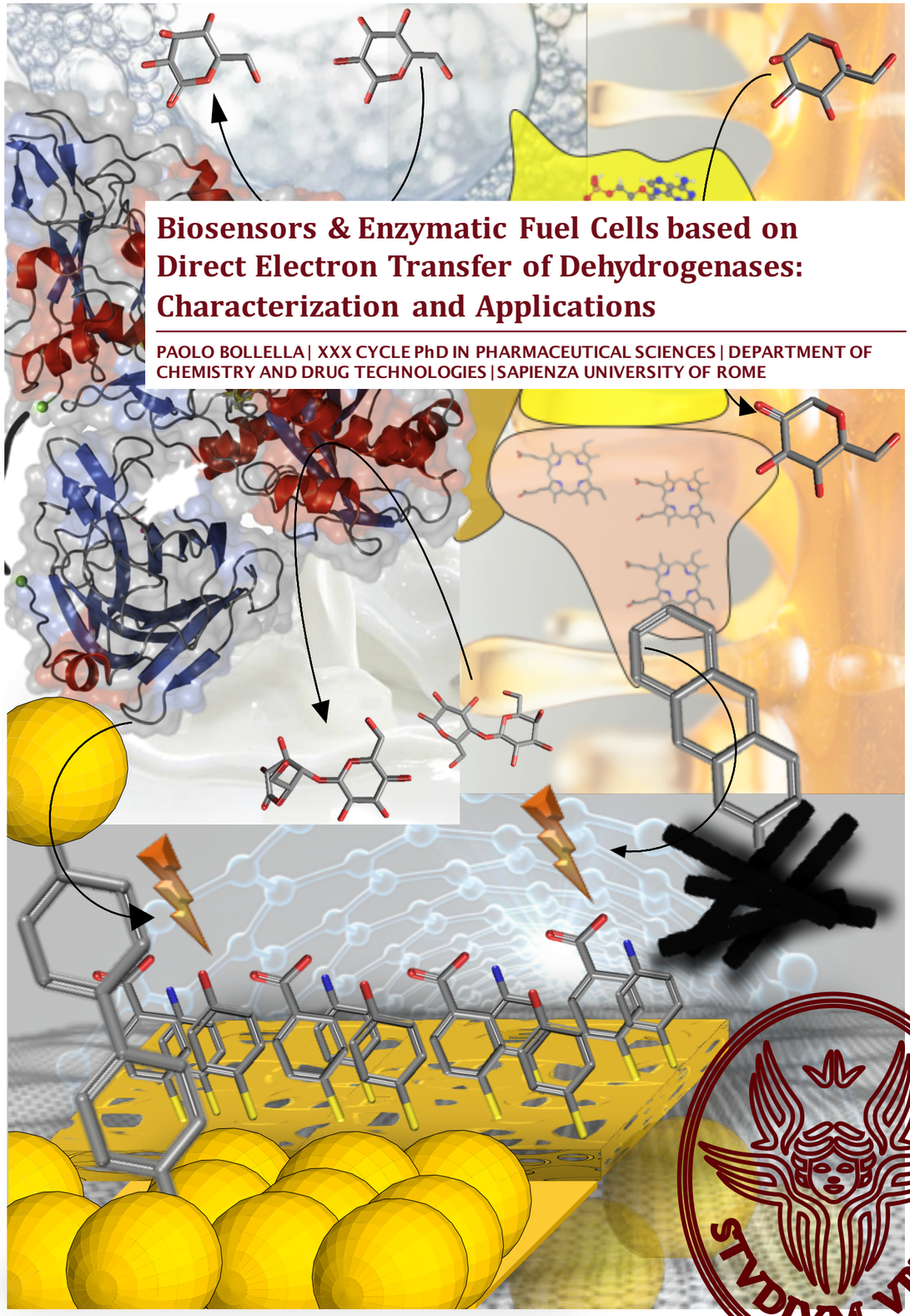

Biosensors & Enzymatic Fuel Cells based on Direct Electron Transfer of Dehydrogenases: Characterization and Applications

PAOLO BOLLELLA | XXX CYCLE PhD IN PHARMACEUTICAL SCIENCES | DEPARTMENT OF CHEMISTRY AND DRUG TECHNOLOGIES | SAPIENZA UNIVERSITY OF ROME

SAPIENZA
UNIVERSITÀ DI ROMA

Biosensors & Enzymatic Fuel Cells based on Direct Electron Transfer of Dehydrogenases: Characterization and Applications

Department of Chemistry and Drug Technologies - Sapienza University of Rome

PhD course in Pharmaceutical Sciences

Supervisor:

Prof. Riccarda Antiochia, PhD

Co-supervisor:

Prof. Lo Gorton, PhD

PhD Student:

Paolo Bollella
1272856

Dissertation date: 18th December 2017

Contents

“Most people say that it is the intellect
which makes a great scientist.
They are wrong: it is character.”
A. Einstein

To Whom warmly believed and supported Me…

LIST OF PUBLICATIONS

I. **Green synthesis and characterization of gold and silver nanoparticles and their application for development of a third generation lactose biosensor.**

Paolo Bollella*, Christopher Schulz, Gabriele Favero, Franco Mazzei, Roland Ludwig, Lo Gorton, Riccarda Antiochia* Electroanalysis, 29 (2017), 77-86. DOI: 10.1002/elan.201600476.

II. **Improved DET communication between cellobiose dehydrogenase and a gold electrode modified with a rigid self-assembled monolayer and green metal nanoparticles: the role of an ordered nanostructuration.**

Paolo Bollella*, Franco Mazzei, Gabriele Favero, Giovanni Fusco, Roland Ludwig, Lo Gorton, Riccarda Antiochia.* Biosensors & Bioelectronics, 88 (2017), 196-203. DOI: 10.1016/j.bios.2016.08.027.

III. **A glucose/oxygen enzymatic fuel cell based on gold nanoparticles modified graphene screen-printed electrode. Proof-of-concept in human saliva.**

Paolo Bollella*, Cristina Tortolini, Daniela Stevar, Lo Gorton, Roland Ludwig, Su Ma, Harry Boer, Anu Koivula, Giovanni Fusco, Gabriele Favero, Riccarda Antiochia, Franco Mazzei.* Sensors & Actuators B: Chemical, 256 (2018), 921-930. DOI: 10.1016/j.snb.2017.10.025

IV. **A Third Generation Glucose Biosensor Based on Cellobiose Dehydrogenase Immobilized on a Glassy Carbon Electrode Decorated with Electrodeposited Gold Nanoparticles: Characterization and Application in Human Saliva.**

Paolo Bollella*, Lo Gorton, Roland Ludwig, Riccarda Antiochia*. Sensors, 17 (2017), 1912. DOI: 10.3390/s17081912.

V. **Cellobiose Dehydrogenase: Insights on the Nanostructuration of Electrodes for Improved Development of Biosensors and Biofuel Cells.**
Paolo Bollella*, Roland Ludwig, Lo Gorton.* Applied Material Today, 9 (2017), 319-332. DOI: 10.1016/j.apmt.2017.08.009.

VI. **The Influence of pH and Divalent/Monovalent Cations on the Internal Electron Transfer (IET), Enzymatic Activity and Structure of Fructose Dehydrogenase.**
Paolo Bollella*, Yuya Hibino, Kenji Kano, Lo Gorton, Riccarda Antiochia.* Analytical and Bioanalytical Chemistry, *Submitted.*

VII. **Enhanced Direct Electron Transfer of Fructose Dehydrogenase Rationally Immobilized on 2-Amino Anthracene Diazonium Cation Grafted Single-Walled Carbon Nanotube Based Electrode.**
Paolo Bollella*, Yuya Hibino, Kenji Kano, Lo Gorton, Riccarda Antiochia. In manuscript.*

VIII. **Highly Sensitive Membrane-less Fructose Biosensor Based on Fructose Dehydrogenase Immobilized onto Aryl Thiols Modified Highly Porous Gold Electrode: Characterization and Application in Food Samples.**
Paolo Bollella*, Yuya Hibino, Kenji Kano, Lo Gorton, Riccarda Antiochia. In manuscript.*

Appendix Publications

1. **DNA-based biosensors for Hg^{2+} determination by polythymine-methylene blue modified electrodes.** *Cristina Tortolini, Paolo Bollella, Marta Letizia Antonelli, Riccarda Antiochia, Franco Mazzei, Gabriele Favero.* Biosensors & Bioelectronics, 67 (2015), 524-531. DOI: 101016/j.bios.2014.09.031.

2. **Recent trends in electrochemical nanobiosensors for environmental analysis.** *Franco Mazzei, Gabriele Favero, Paolo Bollella, Cristina*

Tortolini, Luisa Mannina, Marcelo E. Conti, Riccarda Antiochia. International Journal of Environment and Health, 7 (2015), 267-291. DOI: 10.1504/IJENVH.2015.073210.

3. **Inhibition-based biosensor for atrazine detection.** *Cristina Tortolini, Paolo Bollella, Riccarda Antiochia, Gabriele Favero, Franco Mazzei.* Sensors & Actuators B: Chemical, 224 (2016), 552-558. DOI: 10.1016/j.snb.2015.10.095.

4. **Inhibition-based first-generation electrochemical biosensors: theoretical aspects and application to 2,4-dichlorophenoxy acetic acid detection.** *Paolo Bollella, Giovanni Fusco, Cristina Tortolini, Gabriella Sanzò, Riccarda Antiochia, Gabriele Favero, Franco Mazzei*. Analytical and Bioanalytical Chemistry, 408 (2016), 3203-3211. DOI: 10.1007/s00216-016-9389-z.

5. **Beyond graphene: electrochemical sensors and biosensors for biomarkers detection.** *Paolo Bollella, Giovanni Fusco, Cristina Tortolini, Gabriella Sanzò, Gabriele Favero, Lo Gorton, Riccarda Antiochia.* Biosensors & Bioelectronics, 89 (2017), 152-166. DOI: 10.1016/j.bios.2016.03.068.

6. **Nanotechnology-based Surface Plasmon Resonance Affinity Biosensors for in-vitro Diagnostics.** *Riccarda Antiochia, Paolo Bollella, Gabriele Favero, Franco Mazzei*. International Journal of Analytical Chemistry, 2016, ID: 2981931, 15 pages. DOI: 10.1155/2016/2981931.

7. **AuNPs-functionalized PANABA-MWCNTs Nanocomposite-based Impedimetric Immunosensor for 2,4-Dichlorophenoxy Acetic Acid Detection.** *Giovanni Fusco, Francesca Gallo, Cristina Tortolini, Paolo Bollella, Federica Ietto, Antonella De Mico, Andrea D'Annibale, Riccarda Antiochia, Gabriele Favero, Franco Mazzei*. Biosensors & Bioelectronics, 93 (2017), 52-56. DOI: 10.1016/j.bios.2016.10.016.

8. **Catalase-based modified graphite electrode for hydrogen peroxide detection in different beverages.** *Giovanni Fusco, Paolo Bollella, Franco Mazzei, Gabriele Favero, Riccarda Antiochia, Cristina Tortolini*. Journal of Analytical Methods in Chemistry, 2016, ID: 8174913, 12 pages. DOI: 10.1155/2016/8174913.

9. **Highly Sensitive, Stable and Selective Hydrogen Peroxide Amperometric Biosensors Based on Peroxidases from Different Sources Wired by Os-polymer: A Comparative Study.** *Paolo Bollella, Luca Medici, Merid Tessema, Andrey A. Poloznikov, Dmitry M. Hushpulian, Vladimir I. Tishkov, Rafael Andreu, Dónal Leech, Massimo Marcaccio, Lo Gorton, Riccarda Antiochia.* Solid State Ionics, IN PRESS.

10. **A novel starch binding laccase from the wheat pathogen Zymoseptoria tritici highlights the functional diversity of ascomycete laccases.** *Majid H. Momeni, Paolo Bollella, Roberto Ortiz, Esben Thormann, Riccarda Antiochia, Lo Gorton, Maher A. Hachem.* BBA Proteins and Proteomics, submitted.

11. **Sunlight Photocurrent Generation from Thylakoid Membranes on Gold Nanoparticle Modified Screen-Printed Electrodes.** *Hussein Kanso, Galina Pankratova, Paolo Bollella, Dónal Leech, David Hernandez, Lo Gorton.* Journal of Electroanalytical Chemistry, in revision.

Books

A. **Sensori e Biosensori.** *Marta Letizia Antonelli, Paolo Bollella, Cristina Tortolini*. ISBN: 9788868125912.

B. Book Chapter: *Riccarda Antiochia, Cristina Tortolini, Federico Tasca, Lo Gorton, Paolo Bollella**, **Graphene and 2D-like nanomaterials: different biofunctionalization pathways for electrochemical biosensors development**, Graphene Bioelectronics Ed. Ashutosh Tiwari, Elsevier. ISBN: 9780128133491. *Corresponding Author.

MY CONTRIBUTIONS TO THE PUBLICATIONS

I performed the experiments, analyzed the data and wrote the first draft of the manuscript (**PAPERS I, II, IV** and from **VI** to **VIII**). I planned the experiments, helped in the data evaluation and wrote the first draft of the manuscript (**PAPER III**). I wrote the first draft of the manuscript (**PAPER V**).

LIST OF ABBREVIATIONS

2-ANT	2-amino anthracene
4-APh	4-aminothiophenol
4-MBA	4-mercaptobenzoic acid
4-MPh	4-mercaptophenol
$Ag\|AgCl_{sat}$	Silver/silver chloride reference ele ctrode (KCl saturated)
AgNPs	Silver nanoparticles
AuNPs	Gold nanoparticles
ATP	adenosine triphosphate
BFC	Biofuel cell
BPDT	biphenyl-4,4'-dithiol
CA	Chronoamperometry
CDH	Cellobiose dehydrogenase
CE	Counter electrode
Ct	*Corynascus thermophilus*
CV	Cyclic voltammetry
CYT_{CDH}	cytochrome domain of CDH
CYT_{FDH}	Cytochrome domain of FDH
DCIP	2,6-dichloroindophenol
DET	direct electron transfer
DH_{CDH}	Dehydrogenase domain of CDH
DH_{FDH}	Dehydrogenase domain of FDH
DLS	Dynamic light scattering
EFC	Enzymatic fuel cell
$E^{0,}$	Formal potential
ET	Electron transfer
FAD	Flavin adenine dinucleotide (oxidized)
$FADH_2$	Flavin adenine dinucleotide (reduced)
FDH	Fructose dehydrogenase
FIA	Flow injection analysis
GA	Glutaraldehyde
GalOx	Galactose oxidase

GPH	Graphene
GMC	Glucose-methanol-choline
h-PG	highly porous gold
IET	Internal electron transfer
IPE	Ideal polarized electrode
Lcs	Laccase
LSV	Linear sweep voltammetry
MFC	Microbial fuel cell
MNP	metal nanoparticles
MWCNT	Multi walled carbon nanotubes
NADH	Nicotinamide adenine dinucleotide (reduced)
NHE	Normal hydrogen electrode
Pc	*Phanerochaete chrysospotium*
PVA-SbQ	N-methyl-4(4'-formylstyryl)pyridinium methosulfate acetal
SAM	Self-assembled monolayer
SEM	Scanning electron microscopy
SWCNTs	Single walled carbon nanotubes
TEM	Transmission electron microscopy
Th	*Trametes hirsuta*
Tv	*Trametes villosa*
WE	Working electrode
XRD	X-Ray diffraction spectroscopy

POPULAR ABSTRACT

Il lavoro svolto durante i tre anni di dottorato è stato indirizzato verso lo sviluppo di nuovi metodi di sintesi ed elettrosintesi di nanomateriali metallici o carboniosi per il miglioramento del trasferimento elettronico diretto tra l'enzima e l'elettrodo. Questo miglioramento si traduce in un notevole incremento della sensibilità, stabilità e selettività dei biosensori sviluppati nonché della potenza generata da una pila enzimatica a biocombustibile, (Biofuel Cell).

La prima parte della tesi riguarda lo studio e l'ottimizzazione del trasferimento elettronico diretto della cellobiosio deidrogenasi (CDH), un enzima appartenente alle flavoemeossidoreduttasi, costituito da due subunità dotate rispettivamente di cofattore FAD (subunità I) e heme *b* (subunità II). In questa parte abbiamo sintetizzato nanoparticelle di oro e di argento con un nuovo metodo "green", che impiega come agente riducente la quercetina, un noto flavonoide presente in numerosi alimenti e bevande (es. tè, capperi, mirtilli, etc.). La reazione è stata condotta a temperatura ambiente e a pressione atmosferica senza ulteriore purificazione in quanto la quercetina è nota avere un comportamento stabilizzante delle sospensioni colloidali. Le suddette nanoparticelle sono state impiegate nella costruzione di biosensori per la determinazione del lattosio e di una pila a biocombustibile glucosio/ossigeno. Successivamente, abbiamo sviluppato un nuovo metodo per l'elettrodeposizione di nanoparticelle di oro in modo da ottenere una superficie nanostrutturata ordinata che ha portato allo sviluppo di un biosensore per la determinazione del glucosio nella saliva.

La seconda parte della tesi riguarda lo studio del meccanismo del trasferimento elettronico diretto della fruttosio deidrogenasi (FDH), con particolare attenzione rivolta all'influenza dei cationi monovalenti e bivalenti, all'influenza della forma delle nanoparticelle sulla catalisi enzimatica, all'individuazione dei siti "heme" coinvolti nel trasferimento elettronico diretto attraverso l'accesso ad una porzione idrofobica dell'enzima, ed infine allo sviluppo di un biosensore per la determinazione del fruttosio realizzato immobilizzando la FDH su elettrodi di oro altamente poroso.

SCIENTIFIC ABSTRACT

The aim of this thesis is the study and the enhancement of the direct electron transfer of two different dehydrogenases, by means of a proper nanostructuration of the electrodes, for biosensors and enzymatic fuel cells (EFCs) development.

Cellobiose dehydrogenase (CDH) is an extracellular enzyme belonging to the oxidoreductase group. CDH contains two subunits: (a) subunit I is the dehydrogenase domain (DH_{CDH}), similar to the domain of other oxidoreductases, which belongs to the glucose-methanol-choline (GMC) oxidoreductase superfamily with a flavin adenine dinucleotide (FAD) co-factor covalently bound to the enzyme structure; (b) subunit II is the cytochrome domain (CYT_{CDH}), which contains a heme *b* and acts as a built-in mediator by shuttling the electrons to a modified electrode. Both subunits are connected through a flexible linker responsible of the modulation of the internal electron transfer (IET) rate by varying the experimental conditions, such as changes of pH and divalent cations the concentration.

Fructose dehydrogenase (FDH) is a membrane-bound flavocytochrome oxidoreductase which also belongs to the hemoflavoproteins family. FDH is a heterotrimeric membrane-bound enzyme complex with a molecular mass of 146.4 kDa, consisting of three subunits: (a) subunit I (DH_{FDH}) is the catalytic domain with a covalently bound flavin adenine dinucleotide (FAD) cofactor, where D-(-)-fructose is involved in a $2H^+/2e^-$ oxidation to 5-dehydro-D-(-)-fructose; (b) subunit II (CYT_{FDH}) acts as a built-in electron acceptor with three heme *c* moieties covalently bound to the enzyme scaffold and two of them involved in the electron transfer pathway; (c) subunit III is not involved in the electron transfer but plays a key role for the enzyme complex stability.

The central target of the present thesis is the possibility to improve the electron transfer through the electrode nanostructuration, which can be realized by exploiting new nanomaterials as well as new nanostructuration methods (e.g. “green” synthesized metal nanoparticles, electrodeposition etc.).

In the thesis much attention has been paid also to the understanding of the electron transfer pathway of FDH, which would be of fundamental interest in the near future for the development of highly sensitive biosensors and efficient EFCs. The

biosensors realized and optimized in this thesis are prototypes of devices that, hopefully, will be commercially available on the market in the next future.

1. INTRODUCTION

1.1 Biosensors & Biofuel cells: general aspects

A biosensor has been defined for the first time as an analytical device integrating a biological element/bioreceptor (e.g. tissues, organelles, cells, plants, enzymes, antibody, aptamer, DNA) with a physicochemical transducer (e.g. electrical, acoustic, mechanical, photometric etc.), which produces either discrete or continuous electronic digital signal directly related to the analyte(s) investigated. The general scheme of a biosensor is reported in Figure 1.1 [1, 2].

The bioreceptor produces a physicochemical signal due to the selective interaction with the analyte, while the transducer converts the biochemical recognition reaction into a quantifiable output signal [3]. Both the bioreceptor and the transducer are crucial issues for the development of a sensitive biosensor [4]. However, the physicochemical changes may be considered (i) the variation of the heat due to a chemical reaction which can be estimated as enthalpy (ΔH), entropy (ΔS) or Gibb's energy (ΔG); (ii) the movement of electrons generated through a redox reaction; (iii) the variation of the light absorbed as consequence of a chemical reaction; (iv) the change of the mass due to a biorecognition reaction. Based on the different transduction methods, the biosensors can be divided into several groups: calorimetric, electrochemical, optical, piezoelectric devices, ion channel switch, field-effect transistor (FET) etc. [5-9]. Due to their high sensitivity, selectivity and short time of detection, the electrochemical transducers have been the most widely used during the past history of biosensors [10-12].

In 1962, Leland Clark Jr. and Champ Lyons referred for the first time about an enzyme based biosensor for glucose detection, as schematically reported in Figure 1.1. In this work, the authors immobilized glucose oxidase (GOx) by using a permeable

membrane, where GOx was oxidizing β-D-glucose to β-D-glucono-δ-lactone through the simultaneous reduction of its redox cofactor, the flavin adenine dinucleotide (FAD), giving $FADH_2$ (hydroquinone form). Thus, the $FADH_2$ was oxidized from the final electron acceptor, the molecular oxygen (O_2), giving hydrogen peroxide (H_2O_2) with the final hydrolyzation of β-D-glucono-δ-lactone to D-gluconic acid. According to this reaction mechanism, the proposed biosensor was monitoring the O_2 consumption through the combination of the GOx immobilized onto the permeable membrane and a Clark's oxygen electrode [13, 14].

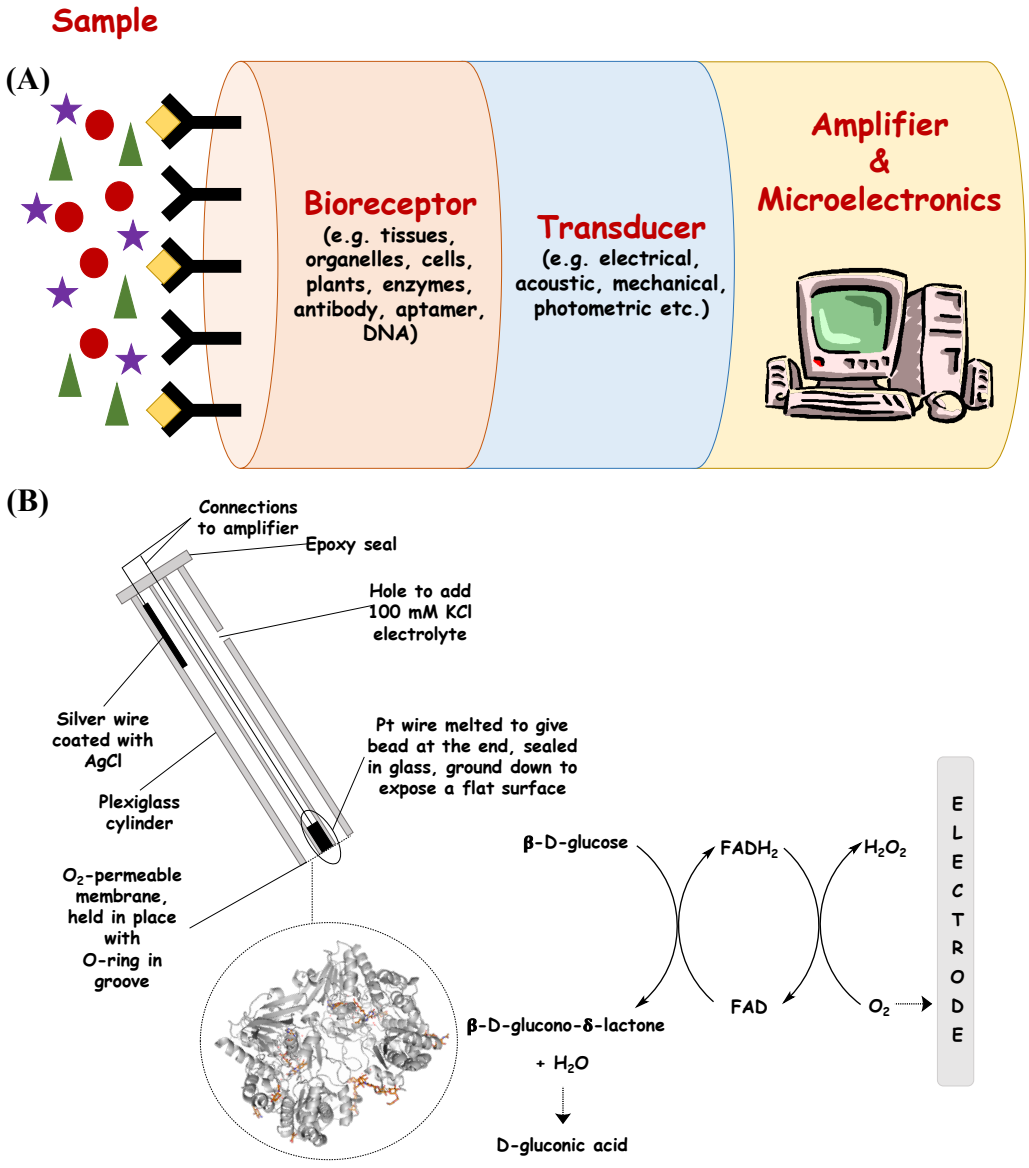

Figure 1.1 **(A)** General scheme of the biosensor; **(B)** schematic representation of the first glucose biosensor based on Clark's oxygen electrode combined with an O_2-permeable membrane modified with GOx.

During 1960s, the biosensor field has attracted an increasing interest by the scientific community mainly due to the possibility of an instantaneous and continuous monitoring of metabolites, drugs and proteins by using miniaturized and portable devices, rising up to 1972-75, when it was successfully commercialized the first biosensor for glucose detection in whole blood from Yellow Springs Instruments. Afterwards, the economic interest toward other biomarkers (e.g. lactate, hydrogen peroxide, lactose, alpha-fetoprotein etc.) boosted the interest of many start-up companies (today multinational corporations) to find out the best solution for a fast, sensitive, selective and non-invasive clinical trial [15-17].

Another intriguing field during the last century is represented from the biological fuel cells (BFCs) [18]. Since the world energy consumption has dramatically increased mainly due to the world population enhancement, there was a boost in the transition between the non-renewable resources and the renewable "green" resources [19]. In addition, there was a trend toward the miniaturization and portability of computing and communications devices. Both "green" energy and small dimensions require mini-, lightweight power sources which are able to sustain operation over long periods of time. An ideal BFCs should provide a solution due to their small dimensions, lightweight and sustainable power sources by using renewable fuels (e.g., alcohols, sugars). These devices have three main features: high conversion efficiency, operability at room temperature and possibility to scale down. In particular, the most effective advantage is the scalability due to the recent progress in medical sciences, with an increasing development of implantable electrically operated devices (e.g., pacemakers), which need small power sources that can supply energy over a long period of time, avoiding any maintenance and replacement issues that would require a surgery [20, 21].

BFCs can be classified on the basis of the different biological entities used in the anodic part, enzymatic fuel cells (EFCs) based on the redox enzymes and microbial fuel cells (MFCs) based on the whole microbial cells that catalyze the electrochemical fuel oxidation [22, 23]. MFCs require continuous maintenance of whole living cells to sustain physiological process, severely limiting the working conditions in order to produce an adequate power output. Promising results can be achieved by using the EFCs, based on the redox enzymes, obtained through the extraction and purification from the living organisms, and directly applied as a biocatalyst in a BFCs [24].

In principle, the EFCs work as a fuel cell, so it consists of an oxidative electrode called anode, and a reductive electrode called cathode. The anode and cathode are

connected externally through a circuit. Since anode and cathode work in a different electrochemical environment, they are separate through ion-selective membrane to distinguish the anodic and the cathodic compartments. Nevertheless, the ion-selective barrier plays a key role because it prevents immediate crossover of fuel and oxidant from one compartment to the other (i.e., low permeability) and also because it serves to manage the flow of positive ions from the anode compartment to the cathodic compartment (i.e., high ionic conductivity) so as to maintain a balance of charge during the flow of electrons from the anode to the cathode through an external circuit [25]. A schematic representation of EFCs is reported in Figure 1.2.

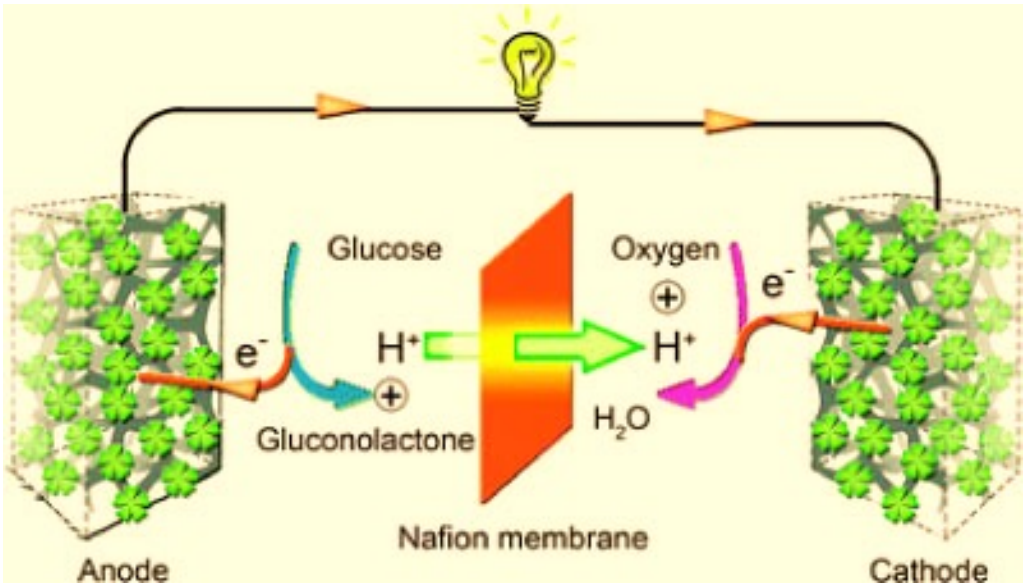

Figure 1.2 Schematic representation of EFCs work flow: the sugar (e.g. glucose) is oxidized at the anode donating two electrons that are forced into the external circuit flowing to the cathode in which the oxygen is reduced to water. In the end it results in the conversion of chemical energy into electrical energy.

1.2. Aim of the thesis

This thesis is devoted to the study and the improvement of the direct electron transfer (DET) of two sugar oxidizing enzymes, namely cellobiose dehydrogenase (CDH) and fructose dehydrogenase (FDH). In this regard, the thesis is mainly focused on the development of new synthesis methods of nanomaterials (e.g. metal nanoparticles) and new chemical electrode modification approaches in order to drastically improve the electron transfer (ET) rate between the enzymes and the electrodes, which would largely affect the sensitivity of the developed biosensors.

The thesis has been organized either following the division according to the analyte detected, so far lactose, glucose and fructose, or considering the enzymes used in this project, CDH and FDH. In the first part of the thesis metal nanoparticles (MNPs) have been synthesized by using quercetin as reducing agent developing a new "green" synthesis approach. The MNPs have been used in the first three papers with three different immobilization methods (e.g. adsorption, chemical modification and physical entrapment) in order to develop two biosensors for lactose detection and an EFC in which CDH was combined with a multi-copper oxidase namely laccase as biocathode. Afterwards, methods for both metal nanostructures electrodeposition and electrochemical modification of nanostructured electrodes have been developed and optimized. The continuous research of new approaches to enhance the ET rate by exploiting only the surface modification had a clear influence on the output of this thesis. Nevertheless, both theoretical and practical aspects concerning the topics will be deeply discussed in the following chapters.

2. BASICS OF BIOELECTROCHEMISTRY

2.1 Enzymes

Enzyme is a word of Greek derivation, which means “en” in, and “zýmē” yeast, literally “in the yeast”. Enzymes are big biological molecules catalysing a lot of life-sustaining chemical reaction. Enzymes are able to convert a substrate to a product with high selectivity and low energy barrier. The selectivity was explained by Emil Fisher as an interaction between two complementary parts [26, 27].

Generally, enzymes are globular proteins consisting of polypeptide chains. The amino acids sequence gives the final structure and function once folded [28]. The enzyme active site corresponds to the site in which the conversion from substrate to product takes place. Some enzymes need a cofactor in order to be fully active in catalysis; the cofactor could be both an organic (e.g. flavin) and inorganic molecule (e.g. metal ion or iron-sulfur cluster). The inorganic cofactors are bound to the enzyme while the organic cofactors can be either bound, so called prosthetic groups, or released during the reaction, so called coenzymes, like nicotinamide adenine dinucleotide (NADH) or adenosine triphosphate (ATP). Without the cofactor the enzyme is called apoenzyme while when the cofactor is bound it is called holoenzyme.

The enzyme activity is defined in terms of international units as the amount of enzyme able to produce a micromole of product per minute under specific experimental conditions [29]. The enzymes are classified based on the reaction catalyzed (divided into 6 groups) and get a number called “enzyme commission number, E.C. number):

E.C. 1 Oxidoreductases catalyze oxidation/reduction reactions like CDH, FDH, multicopper oxidases, which are the most used in the thesis;

E.C. 2 Transferases transfer a functional group from one compound to another;

E.C. 3 Hydrolases give two products from one molecule of substrate through hydrolysis;

E.C. 4 Lyases perform a non-hydrolytic addition/removal of a functional group from a compound;
E.C. 5 Isomerases catalyze intramolecular rearrangements;
E.C. 6 Ligases merge two molecules through C-O, C-N, C-S or C-C bonds formation with the ATP cleavage.

By considering the above mentioned classification, it is possible to guess a systematic name for the identification of new enzymes. Nevertheless, it is possible to use other identifiers on other protein data banks (PDB), where thousands of amino acids sequences are available to identify new proteins.

The present thesis is mainly devoted to exploit two cellobiose dehydrogenases (CDH) from *Trametes villosa* and *Corynascus thermophilus* (recombinant and C291Y mutant), fructose dehydrogenase (FDH) from *Gluconobacter japonicus* and laccase from *Trametes hirsuta*, which belongs to the multi copper oxidoreductases group. These enzymes have been used to realize biosensors and EFCs based on lactose, glucose and fructose as substrates. The two dehydrogenases have a lot of similarities with other glucose-methanol-choline (GMC) oxidoreductases due to the presence of the cofactor FAD.

2.1.1 Cellobiose dehydrogenase (CDH)

Cellobiose dehydrogenase (CDH; E.C 1.1.99.18) is an extracellular enzyme, belonging to the oxidoreductase group, secreted by wood-degrading, phytopatogenic and saprotrophic fungi within the phyla of Basidiomycota and Ascomycota [30]. In 1974, Westermark and Eriksson reported for the first time about the enzymatic activity in *Trametes versicolor* and *Phanaerochaete chrysosporium* observing the oxidation of guiacol while adding cellobiose [31]. During the last 40 years, a lot of efforts have been addressed to elucidate the full electron transfer mechanism, enzyme catalytic activity towards several substrates (e.g. cellobiose, lactose, glucose etc.), enzyme structure and bioengineering pathways to adapt the enzyme to some commercial/industrial purposes [32, 33].

CDH is the only extracellular flavocytochrome oxidoreductase belonging to the hemoflavoproteins family which includes also mandelate dehydrogenase, fumarate dehydrogenase, bacterial cytochrome P-450, nitric oxidase synthase and flavocytochrome b_2. CDH contains two subunits: subunit I is the dehydrogenase domain

(DH_{CDH}) similar to DH domain of other oxidoreductases belonging to the glucose-methanol-choline (GMC) oxidoreductase superfamily with a flavin adenine dinucleotide (FAD) co-factor covalently bound to enzyme structure; subunit II is the cytochrome domain (CYT_{CDH}), which contains a heme *b* and acts as a built-in mediator by shuttling the electrodes to a modified electrode [34, 35]. Both subunits are connected through a flexible linker responsible for the modulation of the internal electron transfer (IET) rate by varying the experimental conditions such as changing the pH or the concentration of divalent cations [36-38]. The oxidation of the natural substrate cellobiose fully reduces FAD in a $2e^-/2H^+$ process and the electrons are sequentially transferred one by one through IET to the CYT_{CDH} domain resulting in reduced heme *b*, finally donating the electrons to the electrode [39].

Based on the phyla of fungi secreting CDH, it is possible to divide them into two classes: class I and class II, from Basidiomycota and Ascomycota, respectively. The CDHs belonging to class I exhibit a shorter enzyme sequence (c.a) and a lower molecular weight (c.a. 80 kDa) compared to class II as well as a highly conserved linker region, an acidic working pH (3.5-4.5) and a poor oxidizing capacity towards glucose and monosaccharides.. Conversely, class II CDHs are able to oxidize both disaccharides and monosaccharides, exhibit a more complex and longer enzyme sequence (including also a cellulose binding module), a higher molecular weight (c.a. 115 kDa) and some have a neutral working pH (7.4) [40-42].

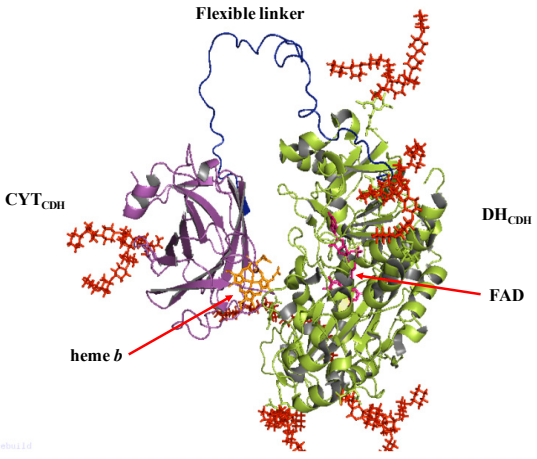

Figure 2.1 Schematic representation of cellobiose dehydrogenase (CDH): in green the DH_{CDH} domain with the FAD cofactor in pink, in violet the CYT_{CDH} domain with the heme *b* cofactor in orange, in blue the flexible linker responsible for the modulation of internal electron transfer (IET) and in red all the potential glycosylation sites.

The crystal structure of the separated domains of CDH has been reported for the first time by the group of C. Divne for *Phanerochaete chrysosporium* (*Pc*CDH) considering separately CYT_{CDH} domain (PDB 1D7C) and then DH_{CDH} domain (1KDG) [43, 44], as shown in Figure 2.1. Unfortunately, only one crystal structure is now available for the whole enzyme, which is *Neurospora crassa* CDH published by the same group in 2015 [45]. Nevertheless, the crystal structure of CYT_{CDH} showed a sandwich fold of two antiparallel β sheets with an exposed heme *b* cofactor, like in cytochromes. The heme *b* is hexacoordinated so that the propionate residues are sufficiently exposed and affecting the internal electron transfer (IET). FAD cofactor and heme *b* cofactor present a chemical structure reported in Figure 2.2.

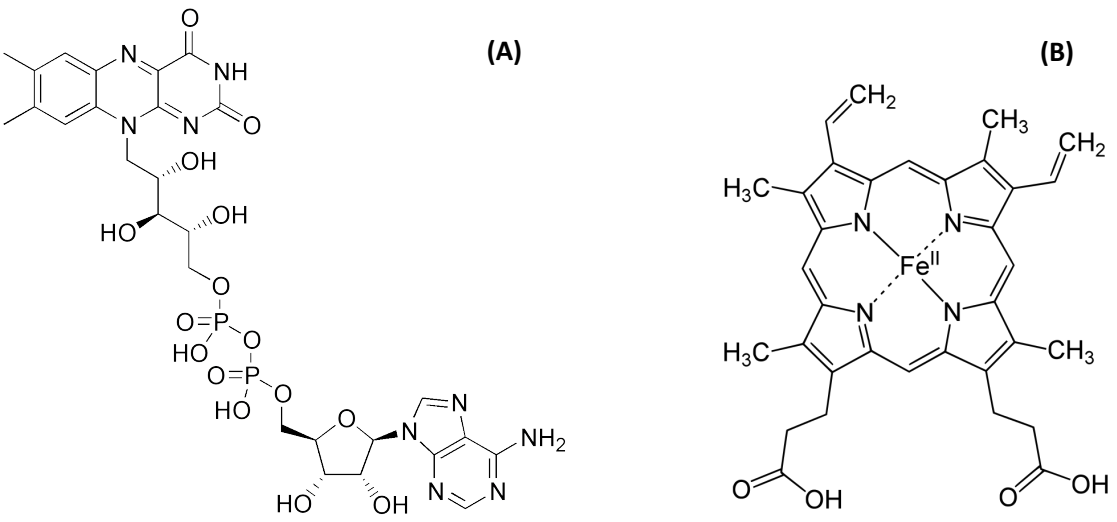

Figure 2.2 (A) chemical structure of FAD cofactor; (B) chemical structure of heme *b* cofactor

From the bioelectrochemical aspect according to the theory by Guo and Hill, the enzymes can be classified in intrinsic enzymes, where the ET occurs close to the prosthetic group, and extrinsic enzymes with redox acceptors allowing the electron-tunnelling towards the electrode [46, 47]. Therefore, CDH is defined as an extrinsic redox enzyme due to its built-in electron transport chain in which the electrons are transferred between the DH_{CDH} domain and the CYT_{CDH} domain. The electrons are transferred from the substrate oxidation occurring at DH_{CDH} either to the built-in mediator (CYT_{CDH} domain) or to redox soluble mediators (e.g. quinones, $Fe(CN)_6^{3-/4-}$) and redox polymers immobilized onto the electrode surface.

The electron transfer reaction between the DH_{CDH} domain and the electrode occurs mainly according to three different routes [48]. In a first reaction the sugar substrate, an aldose, is oxidised at the C1 position (only the β-anomer is a substrate for CDH) into its corresponding lactone and concurrently the FAD in the active site of the DH_{CDH} is fully reduced to $FADH_2$-DH_{CDH}, as shown in Reaction (2.1):

$$\text{aldose} + \text{FAD–DH}_{\text{CDH}} \rightarrow \text{lactone} + \text{FADH}_2\text{–DH}_{\text{CDH}} \quad (2.1)$$

The reoxidation of $FADH_2$-DH_{CDH} can be accomplished by a $2e^-$, $2H^+$ acceptor such as quinone (Q) or an equivalent aromatic redox compound according to Reaction (2.2):

$$\text{FADH}_2\text{–DH}_{\text{CDH}} + \text{Q} \rightarrow \text{FAD–DH}_{\text{CDH}} + \text{QH}_2 \quad (2.2)$$

the reduced quinone, QH_2, will be reoxidised at the electrode if the applied potential (E_{app}) is set higher than the formal potential of the Q/QH_2 redox couple, $E^{\circ\prime}_{Q/QH_2}$, as in Reaction (2.3);

$$\text{QH}_2 \xrightarrow{E_{app} > E^{\circ\prime}_{Q/QH_2}} \text{Q} + 2\text{H}^+ + 2\text{e}^- \quad (2.3)$$

alternatively a $1e^-$, non-H^+ acceptor, e.g., an Os^{3+}-complex (Os^{3+}), accepts the electrons sequentially from the $FADH_2$-DH_{CDH}, whereby Os^{2+}-complex (Os^{2+}) and the enzyme stabilised semiquinone of the bound FAD, FADH•-DH_{CDH}, are formed in Reaction (2.4);

$$\text{FADH}_2\text{-DH}_{\text{CDH}} + \text{Os}^{3+} \rightarrow \text{FADH}\bullet\text{-DH}_{\text{CDH}} + \text{Os}^{2+} + \text{H}^+ \quad (2.4)$$

this reaction is then followed by the second electron transfer to a second Os^{3+}, whereby the fully oxidised DH_{CDH} is regained, as shown in Reaction (2.5);

$$\text{FADH}\bullet\text{-DH}_{\text{CDH}} + \text{Os}^{3+} \rightarrow \text{FAD-DH}_{\text{CDH}} + \text{Os}^{2+} + \text{H}^+ \quad (2.5)$$

The two Os^{2+} formed will be reoxidised at the electrode if E_{app} is set higher than the formal potential of the $Os^{3+/2+}$ redox couple, $E^{\circ\prime}_{Os^{3+/2+}}$, according to Reaction (2.6);

$$2\text{Os}^{2+} \xrightarrow{E_{app} > E^{\circ\prime}_{Os^{3+/2+}}} 2\text{Os}^{3+} + 2\text{e}^- \quad (2.6)$$

the electrons can also be transferred from $FADH_2$-DH_{CDH} to the CYT_{CDH} sequentially in an internal electron transfer(IET) process, according to Reaction (2.7);

$$\text{FADH}_2\text{-DH}_{\text{CDH}} - \text{CYT}_{\text{CDH}} \xrightarrow{\text{IET}} \text{FADH}\bullet\text{-DH}_{\text{CDH}} - \text{CYT}_{\text{CDH}}{}^{\bullet-} + \text{H}^+ \quad (2.7)$$

this first electron transfer step is followed by the reoxidation of the reduced CYT_{CDH}, $CYT_{CDH}^{\bullet -}$, by an e^- acceptor such as Os^{3+} or cytochrome *c* (or by the electrode, see below), however, the second electron from the DH_{CDH} will then be transferred to the CYT_{CDH} simultaneously, as shown in Reaction (2.8);

$$FADH^{\bullet}\text{-}DH_{CDH}\text{-}CYT_{CDH}^{\bullet -} + Os^{3+} \rightarrow FAD\text{-}DH_{CDH}\text{-}CYT_{CDH}^{\bullet -} + Os^{2+} \quad (2.8)$$

Finally the last electron will be transferred from the CYT_{CDH} to a second 1 e^- acceptor molecule, as in Reaction (2.9),

$$FAD\text{-}DH_{CDH}\text{-}CYT_{CDH}^{\bullet -} + Os^{3+} \rightarrow FAD\text{-}DH_{CDH}\text{-}CYT_{CDH} + Os^{2+} \quad (2.9)$$

When CDH is immobilised on the electrode surface and in the absence of any competing e^- acceptors, the reoxidation of the reduced enzyme can be summarised as follows, as shown in Reaction (2.10);

$$FADH_2\text{-}DH_{CDH}\text{-}CYT_{CDH} \xrightarrow{\text{1st IET step}} FADH^{\bullet}\text{-}CYT_{CDH}^{\bullet -} \quad (2.10)$$

this step is followed by a first electron transfer (ET) step to the electrode, which is immediately followed by a second IET step delivering the second electron from the DH_{CDH} to the CYT_{CDH}, according to Reaction (2.11);

$$FADH^{\bullet}\text{-}DH_{CDH} - CYT_{CDH}^{\bullet -} \xrightarrow{\text{1st ET to electrode and 2nd IET step}} FAD\text{-}DH_{CDH} - CYT_{CDH}^{\bullet -} + e^-(\text{electrode}) \quad (2.11)$$

Finally, the second electron is then delivered to the electrode, as reported in Reaction (2.12).

$$FAD\text{-}DH_{CDH} - CYT_{CDH}^{\bullet -} \xrightarrow{\text{2nd ET to electrode}} FAD\text{-}DH_{CDH} - CYT_{CDH} + e^-(\text{electrode}) \quad (2.12)$$

In the present thesis, CDH has been widely employed to develop biosensors for lactose and glucose detection (**PAPERS I, II, III** and **IV**). In **PAPERS I** and **II**, a CDH from *Trametes villosa* (basidiomycete, class I) and a CDH from *Corynascus thermophilus* (ascomycete, class II) have been used in order to develop lactose biosensors with enhanced electron transfer thanks to the different approaches of electrode nanostructuration. Afterwards, a mutant of *Ct*CDH with an enhanced turnover number for glucose and reduced cross-reactivity with maltose, namely *Ct*CDH C291Y, has been used to develop a glucose biosensor for the detection of glucose in human saliva

(**PAPER IV**) and an EFC tested as proof of concept in saliva, as a possible future application of self-powered biosensors (**PAPER III**).

2.1.2 Fructose dehydrogenase (FDH)

Fructose dehydrogenase (FDH; EC 1.1.99.11) is a membrane-bound oxidoreductase extracted by bacteria belonging to the acetic acid bacteria (AAB) family, which is a group of Gram-negative bacteria able to oxidize sugars and ethanol to produce acetic acid during fermentation [49]. Among the AAB family, only two genera of AAB exhibited oxidizing activity towards D-fructose producing 5-keto-D-fructose, which are *Acetobacter* and *Gluconobacter* [50]. In particular, *Acetobacter* can oxidize ethanol to carbon dioxide and water through Krebs cycle enzymes, while *Gluconobacter* does not oxidize ethanol due to lack of some Krebs cycle enzymes. In 1960, Weidenhagen and Bernsee isolated from *Acetobacter suboxydans* a D-fructose oxidation product identified as 6-aldo-D-fructose. Subsequently, Terada and his co-workers isolated from *Gluconobacter cerinus* a similar dicarbonylhexose, described as 5-keto-D-fructose. Afterwards, Whiting's and Avigada's groups gave a great contribution in the field confirming that the oxidation product is 5-keto-D-fructose, as previously hypotized by Terada et al.[51].

FDH is a membrane-bound flavocytochrome oxidoreductase also belonging to the hemoflavoproteins family. FDH from *Gluconobacter japonicus* NCBR 3260 is a heterotrimeric membrane-bound enzyme complex with a molecular mass of 146.4 kDa, consisting of three subunits, namely: subunit I (DH_{FDH}) is the catalytic domain with a covalently bound flavin adenine dinucleotide (FAD) cofactor, where D-(-)-fructose is involved in a $2H^+/2e^-$ oxidation to 5-dehydro-D-(-)-fructose; subunit II (CYT_{FDH}) acts as built-in electron acceptor with three heme *c* moieties covalently bound to the enzyme scaffold and two of them involved in the electron transfer pathway; subunit III is not involved in the electron transfer but plays a key role for the enzyme complex stability [49].

Unfortunately, the crystal structure of FDH is not yet available because it is not so easy to obtain crystals of a membrane bound protein with a high molecular weight (ca. 146 kDa). Although the obvious difficulties, in the last few years a lot of efforts have been addressed in this regard considering new crystallization methods. The crystal

structure would be a fundamental finding to clarify the electron transfer mechanism of this enzyme with particular attention to the co-factor involved.

The last part of the PhD thesis (**PAPERS VI, VII** and **VIII**) has been addressed on the investigation of the electron transfer mechanism in order to improve it through a correct orientation of the enzyme onto the electrode surface. In **PAPER VI**, the possible influence of monovalent and divalent cations on the catalytic current by means of structural changes has been investigated. Since other research groups supposed that only two of the three heme *c* are involved in the whole ET mechanism, we studied the hydrophobic region, which is actually located in the subunit II close to two heme *c* groups herein contained (**PAPER VII**), as shown in Figure 2.3, and isolated the contribution of two heme *c* groups in the ET mechanism. Finally, in **PAPER VIII** different enzyme orientations by means of electrostatic interaction between the enzyme and the different re-charged highly porous gold electrode were carefully studied and evaluated

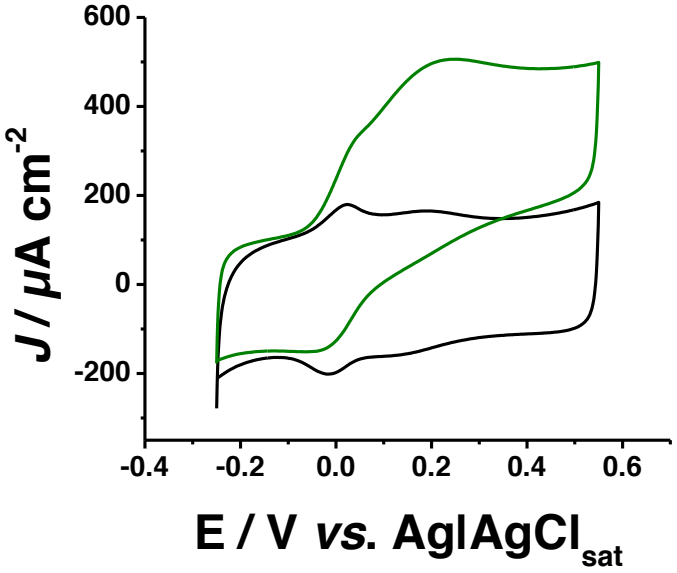

Figure 2.3 Cyclic voltammograms performed in 50 mM NaAc pH 4.5 in absence (black) and in presence (green) of 10 mM D-fructose at scan rate 10 mV s^{-1}. In the turnover measurement (green), it is clearly visible the contribution of each heme *c* to the catalysis (**PAPER VII**).

2.1.3 “Blue” multi-copper oxidases

Copper plays a key role as cofactor in many living systems, which are involved in the metabolism of O_2 and NO_x compounds [52]. Among all the copper forms in terms of oxidation state, Cu^{3+} is not biologically relevant due to its high formal potential, while Cu^{2+} owns a six-coordinate tetragonal (distorted octahedral) geometry or five-coordinate (square-pyramidal or bipyrimidal) geometry, and Cu^{+} contributes to the reduction of O_2, with a formal potential ($E^{0'}$) up to 500 mV but highly affected by the coordination geometry and the amino acids involved as linker. This $E^{0'}$ value is certainly much higher compared to $E^{0'}$ for Cu^{2+}/Cu^{+} couple in water (+150 mV vs. NHE) [53]. Moreover, the “biological” copper sites are divided into three classes based on their spectroscopic features strictly related to the geometric and electronic structure of the active site: type 1 (T1) or blue copper (e.g. azurin), type 2 (T2) or normal copper (e.g. galactose oxidase), and type 3 (T3) or coupled binuclear copper centres. The most representative proteins for each different type of copper are reported below [54, 55].

Type 1 – Azurin is a small copper protein with a low MW (9-14 kDa) containing a mononuclear copper of T1 type. The crystal structure of azurin is well-known in which the copper is coordinated by cysteine, two histidines and an axial methionine. The redox potential of azurin depends on the origin and ranges from 270 to 320 mV vs. NHE. The most characterized azurin is from *Pseudomonas aeruginosa* [56].

Type 2 – Galactose oxidase (GalOx) was first isolated in 1959. This protein is a single polypeptide with a MW of 68 kDa arranged in three domains, in which the active site contains a T2 Cu located in the solvent accessible surface of domain II. GalOx exists in three different redox states, namely oxidized/active (Cu^{2+} and C-Y•), semi-oxidized/inactive (Cu^{2+} and C-Y) and reduced (Cu^{+} and C-Y). The $E^{0'}$ for the redox couple $Cu^{2+/}Cu^{+}$ was found to be 159 mV vs NHE at pH 7 [57].

Type 3 – Tyrosinase exhibits a coupled binuclear copper active site (T3 site). This enzyme is able to catalyze the hydroxylation of monophenols (Figure 2.4, small pathway) and two-electron oxidation of *o*-diphenols to *o*-quinones (Figure 2.4, big pathway). Tyrosinases are produced in a large number of eukaryote systems (e.g. plant, animal and fungi). The two copper atoms in the active site react with oxygen giving a highly reactive intermediate, which interacts with the *o*-diphenol (e.g. catechol)

presenting a similar activity to catechol oxidase, being grouped as polyphenol oxidases [58].

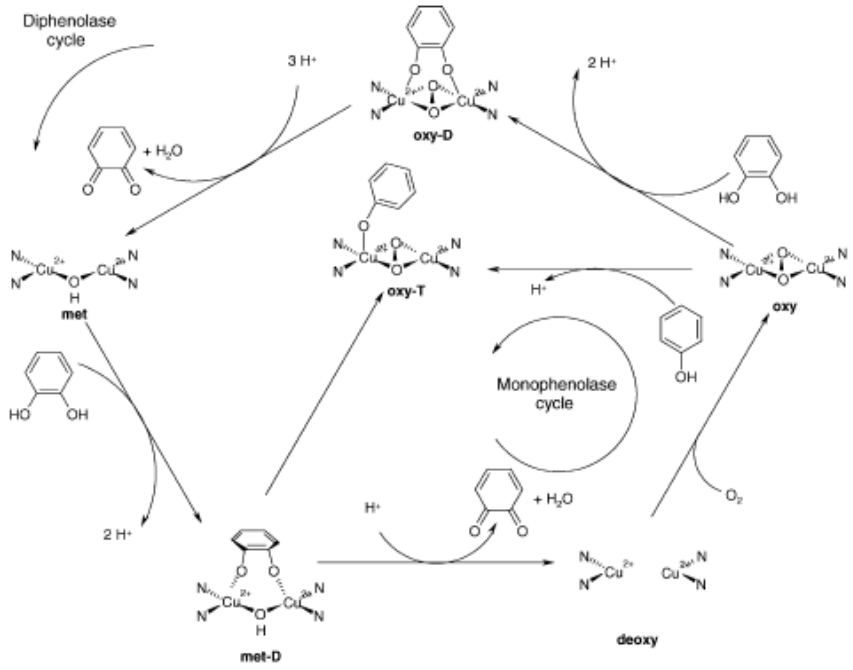

Figure 2.4 Schematic representation of reaction patterns of T3 type copper based proteins for the hydroxylation reaction (small pathway) and for the two electrons oxidation of *o*-diphenols to *o*-quinone.

Contrary to single type of copper oxidases, "blue" multicopper oxidases are able to oxidize their substrates by accepting the electrons at the mononuclear centre T1 and transferring them to a trinuclear centre T2/T3 type, in which O_2 binds giving a 4 electron reduction to two molecules of water. The family of "blue" multicopper oxidases includes: ceruloplasmin, laccase, bilirubine oxidase, ascorbate oxidase and nitrite reductase. Particular attention has been paid in this thesis to laccases [59, 60].

Laccase (benzendiol: oxygen oxidoreductases, E.C. 1.10.3.2) is able to catalyze the oxidation of ortho- and paradiphenols, amino-phenols, polyphenols, polyamines, lignins and aryl diamines as well as some inorganic ions coupled to the reduction of molecular dioxygen to water. Laccase was first described by Yoshida in 1883 [61]. The enzyme owns a broad substrate specificity considering also the redox mediators, and for this reason it is considered a promising enzyme for many applications. Laccases are classified into two groups according to their source: plant and fungi [60]. Nevertheless, laccases have been identified also in bacterial microorganisms [62]. The laccase from fungi is a monomer, which could be divided into 3 domains structurally similar to

azurin and plastocyanin, although there are some differences like the loop in the substrate-binding pocket. The key characteristic of laccases is the standard redox potentials of their redox centres, T1, T2, and T3 sites. The value of the redox potential of the T1 Cu-site has been determined using potentiometric titrations with redox mediators for a great number of different Lcs and varies between 430 and 780 mV versus NHE [63]. Recently, laccases have been divided into three classes according to the formal potential of T1 site: low, middle and high potential laccases [53]. The low potential group includes laccases from trees, e.g., *Rhus vernicifera* with a potential of the T1 site of about 430 mV vs. NHE. The middle group includes laccases from basidiomycetes like *Myceliophthora thermophile*, *Rhizoctonia solany*, and *Coprinus cinereus*. The enzymes have a potential of the T1 site ranging from 470 to 710 mV versus NHE. The high potential laccases (e.g., those from *Trametes (Polyporus, Coriolus) hirsuta (hirsutus)*, *T. versicolor*, *T. villosa*) all have a potential of the T1 site of about 780 mV vs. NHE [64].

The direct electron transfer of high potential laccases has been widely investigated due to their importance from the application point of view as a potential cathode in an EFC [65]. Laccase ET was deeply investigated also in presence of inhibitors like fluoride ions and azide showing different behaviors for low and high potential laccases: for low potential laccases no changes in the cyclic voltammograms were observed while for the high potential ones an increase in the cathodic and anodic peaks was observed. Moreover, we should take into account that the direct electron transfer (DET) mechanism is rather different based on the electrode material like carbon based and gold electrode. From recent findings, it seems that the DET at carbon electrodes occurs through the T1 site, while at gold surface it occurs through the T2/T3 site [66]. Finally, laccases ET have been widely investigated due to their role both for biosensors development (e.g. polyphenol detection, dopamine detection, etc.) and for EFC development especially considering the high redox potential laccases used as potential biocathode [67].

In this regard, *Trametes hirsuta* laccase has been used in **PAPER III**, immobilized through a drop-casting procedure on a AuNPs/graphene modified screen printed electrode (SPE) to develop a potential biocathode for an EFC. The EFC was further scaled-down and reduced on one SPE, in which the laccase was deposited onto the counter electrode used in combination with *Ct*CDH, deposited onto the modified working electrode, as shown in Figure 2.5.

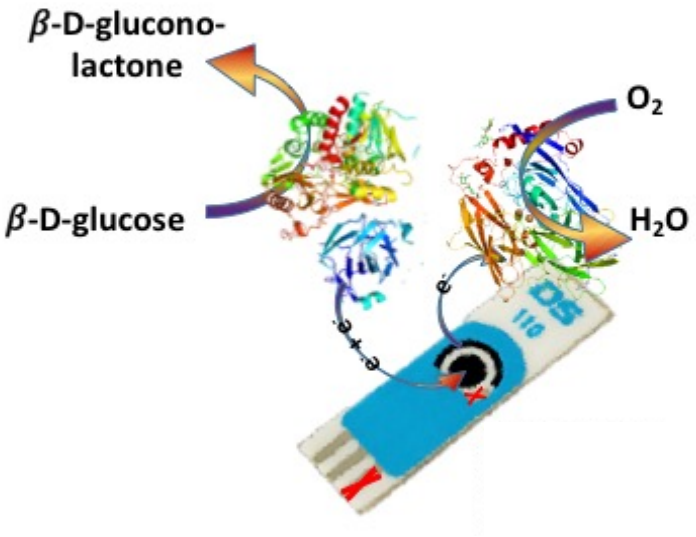

Figure 2.5 Schematic representation of one-SPE enzymatic fuel cell.

2.2 Electron transfer in redox protein

The electron transfer (ET) is the most important processes in chemistry and biology [68-71]. ET has been widely investigated during the XX century and classified into inner-sphere ET and outer-sphere ET. ET is defined according to IUPAC as: "The transfer of an electron from one molecular entity to another, namely the acceptor A and the donor D, or between two localized sites in the same molecular entity".

The inner sphere or bonded electron transfer is a redox chemical reaction proceeding through a covalent bond between the acceptor and the donor. In the inner sphere (IS) electron transfer (ET), a ligand bridges the two redox centers during the electron transfer event, so far rare in biological systems, where A and D are usually shielded by the protein scaffold. The bridging ligand could be virtually any entity that can convey electrons. Typically, such a ligand has more than one lone electron pair, such that it can serve as an electron donor to both A and D. Common bridging ligands include halides, pseudohalides, such as hydroxide and thiocyanate, oxalate, malonate and pyrazine. The ET occurs once the bridged complex is formed. The inner sphere ET mechanism was discovered by H. Taube, awarded the Nobel Prize in Chemistry in 1983 [72]. His findings were resumed as follow "When $Co(NH_3)_5Cl^{2+}$ is reduced by Cr^{2+} in 1M $HClO_4$, 1 Cl^- appears attached to Cr for each Cr(III) which is formed or Co(III) reduced. When the reaction is carried on in a medium containing radioactive Cl, the mixing of the Cl^- attached to Cr(III) with that in solution is less than 0.5%. This

experiment shows that transfer of Cl to the reducing agent from the oxidizing agent is direct…"

Contrary to the inner sphere ET, in the outer sphere ET the chemical species D and A are not connected to each other. This process is commonly observed in biological systems like redox enzymes.

The first accepted model to describe the outer sphere ET was proposed by Rudolph A. Marcus in 1956 [73, 74]. This theory is based on the Franck–Condon principle concerning the separation of fast electronic motion and slow nuclear motion. According to this model, the electrons are transferred by tunnelling between two chemical species producing nuclear vibrational surfaces. The activation energy for the process arises from the reorganization of the nuclear and solvent coordinates required to bring the reactant system to a configuration in which the electron can transfer adiabatically to the product surface. The rate constant for the outer sphere ET is:

$$k_{ET} = \frac{2\pi}{\hbar} \frac{H_{DA}^2}{\sqrt{4\pi\lambda RT}} e^{-\frac{(\Delta G^0+\lambda)^2}{4\lambda RT}} \quad (2.13)$$

where k_{ET} is the electron transfer rate, $\hbar$ is the reduced Planck constant, R is the universal gas constant and T is the absolute temperature in K [75]. The reorganization energy (λ) includes the vibrational components (inner-sphere or intramolecular reorganizational energy, λ_i) and components from the polarization changes in the dielectric solvent environment (outer-sphere or solvent reorganization energy, λ_0). ET is mainly affected by the driving force, which depends on the Gibbs free energy $\Delta G^0 = -nF\Delta E^0$ of a redox reaction, so directly obtained from the difference between the reduction potentials of D and A, and by the reorganization energy (λ) occurring during the ET. The theory states two regions where k_{ET} decreases when $-\Delta G^0$ changes while the maximum corresponds to $-\Delta G^0 = \lambda$. H_{DA} is the function describing the probability for electron tunneling between D and A. The model has been developed for inorganic species but it can be considered valid also for redox proteins [76].

ET in redox enzymes has been widely investigated during the last 30 years. This is a key issue for the development of biosensors and EFCs and represent one of the important aspects of the thesis. From a bioelectrochemical point of view, the enzymes can be divided in intrinsic and extrinsic enzymes. In the former, the ET takes place within the vicinity of the prosthetic group, while for the extrinsic ones an electro-donating/accepting centre (e.g. cofactor) is required to create an ET pathway between the enzyme active site and the electroactive part, which would interact with the

electrode surface [77]. Therefore, the ET can occur with intrinsic enzymes only if the catalytic site is close to the protein surface and if there is a deformation without any activity loss, good orientation of the active site towards the electrode surface, and through enzyme bioengineering [77, 78].

2.3 Kinetic models for enzyme

The first kinetic models for enzyme have been introduced by Michaelis and Menten at the beginning of the last century, successively adapted by Briggs and Aldane to more general conditions (1923) [79, 80]. The Michaelis-Menten reaction for the enzymatic conversion of a single substrate (S) into its product (P) can be resumed as follows in Equation 2.14:

$$\mathbf{E + S} \underset{k_{-1}}{\overset{k_1}{\rightleftharpoons}} \mathbf{ES} \xrightarrow{k_2} \mathbf{E + P} \tag{2.14}$$

In the first step the substrate (S) reacts with the enzyme (E) forming the enzyme-substrate complex (ES) with a reaction rate of k_1; then the ES complex may be converted in product (P) and leave the enzyme (E) in its native state, with a reaction rate of k_2, if $k_2 >> k_{-1}$, otherwise the reverse equilibrium can give back the dissociation of the ES complex with a reaction rate of k_{-1}. This mechanism can be proposed by assuming a few boundary conditions: constant enzyme concentration, enzyme concentration lower than substrate concentration and product concentration equal to zero at the beginning.

According to the aforementioned boundary conditions, at low substrate concentration, the reaction rate is linearly dependent on [S] (first-order kinetics), while proceeding at higher concentrations the half maximum rate ($V_{max}/2$) corresponds to the Michaelis-Menten constant K_M. At high substrate concentrations, it asymptotically approaches its maximum rate, being independent of [S] (zero-order kinetics), as shown in Figure 2.6.

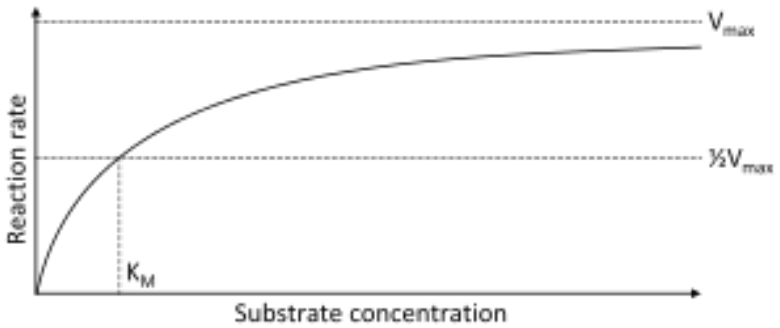

Figure 2.6 Variation of th initial velocity with the substrate concentration for a single substrate-enzyme interaction.

By considering the formation of the ES complex as the rate limiting step, it is possible to use the following equation:

$$\frac{d[ES]}{dt} = k_1[E][S] - k_{-1}[ES] - k_2[ES] \tag{2.15}$$

At steady state [ES] would be constant, therefore $\frac{d[ES]}{dt} = 0$, which means that the rate of formation and decomposition of ES is the same, thus we can write:

$$k_1[E][S] - k_{-1}[ES] - k_2[ES] = 0 \tag{2.16}$$

$$k_1[E][S] = k_{-1}[ES] + k_2 = (k_{-1} + k_2)[ES] \tag{2.17}$$

The enzyme concentration is defined as follow:

$$[E]=[E_t]-[ES] \tag{2.18}$$

where $[E_t]$ is the total enzyme concentration and $[ES]$ the enzyme-substrate complex. Therefore, it is possible to re-write equation 2.17 by substituting $[E]$ with equation 2.18, as follows:

$$k_1([E_t] - [ES])[S] = (k_{-1} + k_2)[ES] \tag{2.19 a}$$

$$k_1[E_t][S] - k_1[ES][S] = (k_{-1} + k_2)[ES] \tag{2.19 b}$$

$$k_1[E_t][S] = (k_{-1} + k_2)[ES] + k_1[ES][S] \tag{2.19 c}$$

$$[ES] = \frac{k_1[E_t][S]}{k_{-1}+k_2+k_1[S]} \tag{2.19 d}$$

$$[ES] = \frac{\frac{\cancel{k_1}[E_t][S]}{\cancel{k_1}}}{\frac{k_{-1}+k_2}{k_1}+\frac{\cancel{k_1}[S]}{\cancel{k_1}}} \tag{2.19 e}$$

$$[ES] = \frac{[E_t][S]}{\frac{k_{-1}+k_2}{k_1}+[S]} \tag{2.19 f}$$

which is re-written by considering the Michaelis-Menten constant, K_M:

$$K_M = \frac{(k_{-1}+k_2)}{k_1} \tag{2.20}$$

$$[ES] = \frac{[E_t][S]}{K_M+[S]} \quad (2.20\text{ a})$$

K_M is defined as the substrate concentration at which half of the enzyme molecules are complexed to give ES complex. Moreover, the K_M gives also an estimation of the affinity enzyme-substrate. Therefore, small K_M implies a strong ES complex so far giving a small linear range in the V_0 vs. [S] plot, while large K_M implies a weak ES complex, giving a larger linear range.

By substituting equation 2.20a into V_0 namely the rate of P formation, it is possible to write:

$$V_0 = k_2[ES] \quad (2.21\text{ a})$$

$$V_0 = \frac{k_2[E_t][S]}{K_M+[S]} \quad (2.21\text{ b})$$

By considering [ES]=[E_t] at the saturation we can define V_{max}=k_2[E_t], thus writing the Michaelis-Menten equation:

$$V_0 = \frac{V_{max}[S]}{K_M+[S]} \quad (2.22)$$

Finally, with the experimental data fitted by using the Michaelis-Menten equation it is possible to determine V_{max} and K_M. The fitting is carried out by using the linear form considering the Lineweaver-Burk, Eadie-Hofstee or the Hanes equations:

- Lineweaver-Burk $\frac{1}{V} = \frac{1}{V_{max}} + \frac{K_M}{V_{\max}[S]}$ (2.23)
- Eadie-Hofstee $V = V_{max} - K_M \frac{V}{[S]}$ (2.24)
- Hanes $\frac{[S]}{V} = \frac{[S]}{V_{max}} + \frac{K_M}{V_{max}}$ (2.25)

All three equations will result in linear graphs by plotting 1/V vs. 1/[S] for Lineweaver-Burk, V vs. V/[S] for Eadie-Hofstee and [S]/V vs. [S] for Hanes. Nevertheless, these graphs will exhibit a linear trend if the enzymatic reaction is controlled by the enzyme

kinetics. However, the Lineweaver-Burk equation [81] may deviate from linearity if the enzymatic reaction is mass transfer controlled and the Eadie-Hofstee [82, 83] or the Hanes equations are usually preferred if the reaction is not strictly kinetically controlled [84]. In this PhD thesis (from **PAPER I** to **PAPER VIII**), the Lineweaver-Burk equation was used to calculate the kinetic parameters related to cellobiose dehydrogenases (CDH) from *Trametes villosa* and *Corynascus thermophilus* (recombinant and C291Y mutant), fructose dehydrogenase (FDH) from *Gluconobacter japonicus* and laccase from *Trametes hirsuta*, such as K_M and V_{max}.

Generally, the redox enzymes obey the ping-pong mechanism, which is a non-sequential mechanism because the enzyme bounces back and forth from an intermediate state to its standard state. Therefore, the oxidoreductases change their oxidation state while reacting with the first substrate, going back to the initial oxidation state after the reaction with the second substrate [85-87].

3. ELECTROCHEMICAL TECHNIQUES

The aim of this chapter is to give a short introduction in the field of electrochemistry, referring for further details to two excellent books: 'Electrochemical Methods: Fundamentals and Applications' by Allen J. Bard and Larry R. Faulkner, and for practical aspects 'The Handbook of Electrochemistry' edited by Cynthia G. Zoski [88, 89].

Electrochemistry is a branch of physical chemistry dealing with the study of the interaction between electrical energy and chemical change occurring at the solution/electrode interface. A lot of basic principles and relationships have been completely elucidated prior to the electron discovery by Joseph J. Thompson in 1893. At the beginning of XIX century, Alessandro Volta invented the first battery, then known as a voltaic pile, which consists of two electrodes, namely copper and zinc, separated by paper soaked in a diluted solution of H_2SO_4. Since this discovery, the electrochemistry rapidly became a top subject in physical and analytical chemistry. In 1835, Michael Faraday defined a few basic concepts such as anode, cathode, electrode, electrolyte and ion in order to make possible a comprehensive description of electrochemistry, while the positive and negative mathematical convention for electrical charge was attributed to Benjamin Franklin.

3.1 Fundaments of electrochemistry

Electrochemical techniques can be divided into two major classes, static ($i = 0$, e.g. potentiometry) and dynamic ($i \neq 0$, amperometry, cyclic voltammetry etc.) techniques, as reported in Table 3.1. In the present thesis dynamic techniques have mainly been utilized.

The electrodes used to perform the electrochemical measurements can also be classified into two groups: ideal polarized electrodes (IPE) and ideal non-polarized electrodes (I*n*PE). In the IPE no actual charge crosses the electrode-electrolyte interface, regardless

of the applied potential, behaving like a capacitor, while I*n*PEs allow free and unimpeded exchange of charges across the electrode-electrolyte interface (e.g. Ag|AgCl reference electrode). None of existing electrodes behaves as an IPE, but under particular experimental conditions a few electrodes approach this behaviour, like a mercury electrode immersed in a deaerated potassium chloride solution, or gold surface modified with a self-assembled monolayer.

<table>
<tr><td rowspan="10">Controlled Potential</td><td rowspan="3">Potential step</td><td>Amperometry</td><td colspan="2">Chronoamperometry; Double Potential Step Chronoamaperometry</td></tr>
<tr><td colspan="3">Chronocoulometry; Double Potential Step Coulometry</td></tr>
<tr><td colspan="3">Sampled Current Voltammetry; Differential Pulse Voltammetry; Square Wave Voltammetry</td></tr>
<tr><td rowspan="4">Potential Sweep</td><td rowspan="4">Voltammetry</td><td rowspan="2">Stationary</td><td>Linear Sweep Voltammetry</td></tr>
<tr><td>Cyclic Voltammetry</td></tr>
<tr><td rowspan="2">Hydrodynamic</td><td rowspan="2">Rotating Disk Electrode; Rotating Ring Disk Electrode</td></tr>
<tr><td colspan="2">Anodic Stripping Voltammetry (Stationary/Hydrodynamic)</td></tr>
<tr><td rowspan="2">Constant Potential</td><td rowspan="2">Bulk Electrolysis</td><td colspan="2">Stirred Solution</td></tr>
<tr><td colspan="2">Flow Electrolysis</td></tr>
<tr><td rowspan="5">Controlled Current</td><td colspan="2" rowspan="4">Chronopotentiometry</td><td colspan="2">Constant Current</td></tr>
<tr><td colspan="2">Linearly Increasing Current</td></tr>
<tr><td colspan="2">Current Reversal</td></tr>
<tr><td colspan="2">Cyclic</td></tr>
<tr><td colspan="2">Coulometry</td><td colspan="2">Coulometric Titration</td></tr>
<tr><td colspan="4">Electrolysis</td></tr>
<tr><td>Controlled Charge</td><td colspan="2">Charge Step</td><td colspan="2">Coulostatic Methods</td></tr>
<tr><td rowspan="2">Impedence Techniques</td><td colspan="4">AC Voltammetry (AC Polarography)</td></tr>
<tr><td colspan="4">Electrochemical Impedence Spectroscopy</td></tr>
</table>

Table 3.1 Scheme of the dynamic techinques used in electrochemistry.

A capacitor, also know as a condenser, is able to store the electrical charge between two metal plates separated by a dielectric material, so called capacitance, which can be defined as q/E=C, where q is the charge, E is the potential between the electrode and the solution and C is the capacitance. In a similar way, the electrode-solution interface behaves as a capacitor and a model for this interface was created. According to this model, when an electrode is immersed into a solution, a special phenomenon called double layer effect occurs at the electrode/electrolyte interface. Therefore, two layers of polarized ions are generated by applying a voltage: one in the surface lattice structure of the electrode, and the other one, with opposite charge, comes from the solvated ions distributed in the electrolyte, as represented in Figure 3.1. These two layers are separated by a monolayer of solvent molecule, called inner Helmoltz plane (IHP), adsorbed onto the electrode surface, which behaves as a molecular dielectric.

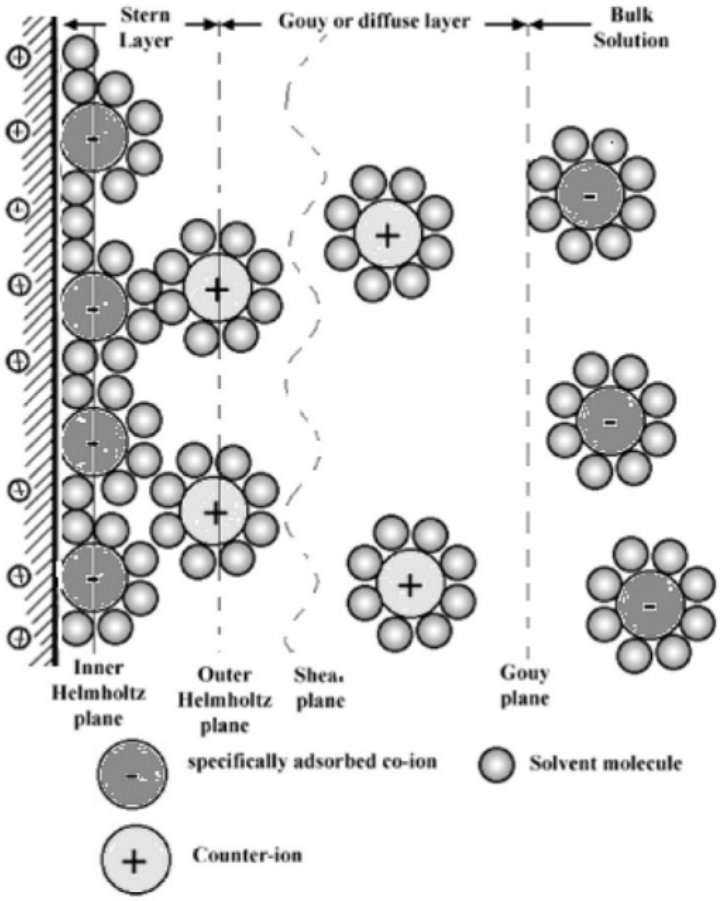

Figure 3.1 A schematic representation of the electrical double layer.

The inner electrode charge is exactly balanced by an equal amount of opposite charges in the outer Helmholtz plane (OHP), finally forming the electrical double layer. The double layer capacitance can be defined as a non-faradic process. Conversely, in a faradic process there is an electron transfer from the solution to the electrode due to a redox reaction governed by Faraday's Law, which says that the amount of chemical reaction caused by the flow of current is proportional to the amount of electricity passed.

There are two different electrochemical cells where faradic processes can occur, the Galvanic and the electrolytic cell. The Galvanic (Voltaic) cell produces electrical energy by means of chemical redox reactions spontaneously occurring at the electrodes. For example, in **PAPER III** two enzyme based electrodes, reacting with carbohydrates (anodic side) and molecular oxygen (cathodic side), are used combined in an EFC to produce electricity. This topic will be further treated in the next chapter. On the other hand, the electrolytic cell is an energy consuming device, where the applied potential affects the redox reactions at the electrode/electrolyte interface.

A simple redox reaction can be written as follows:

$$Ox + ne^- \rightleftharpoons Red \tag{3.1}$$

where *Ox* is the oxidized species, *Red* the reduced one, and *n* the number of electrons transferred between *Ox* and *Red*. The Gibbs free energy relationship for the aforementioned equilibrium is:

$$\Delta G = \Delta G^0 + RT \ln \frac{a_{Red}}{a_{Ox}} \tag{3.2}$$

where R is the gas constant (8.3145 J mol^{-1} K^{-1}) and T (K) is the temperature. By considering the ratio between a_{Red} and a_{Ox}, the Gibbs free energy can be expressed as:

$$\Delta G = -nFE \tag{3.3}$$

where E is the maximum potential difference between the two electrodes, the open circuit potential (OCV) or the equilibrium potential, present when no current flows through the cell. F is the Faraday's constant (1F = 96 485.3 C mol^{-1}). Under standard conditions it can be written:

$$\Delta G^0 = -nFE^0 \tag{3.4}$$

Afterwards, by substituting ΔG and ΔG^0 with equation 3.3 and 3.4 it is possible to obtain equation 3.5:

$$-nFE = -nFE^0 + RT \ln \frac{a_{Red}}{a_{Ox}} \tag{3.5}$$

which would be further rearranged through several mathematical steps to give the Nernst equation as reported in 3.6:

$$E = E^0 + \frac{RT}{nF} \ln \frac{a_{Ox}}{a_{Red}} \tag{3.6}$$

By assuming $a_i = \gamma_i[\mathrm{I}]$ and $\gamma_i = 1$ so $a_i = [\mathrm{I}]$ therefore it is possible to exchange the standard potential with formal potential and rewrite the Nernst equation in the final form:

$$E = E^{0\prime} + \frac{RT}{nF} \ln \frac{[Ox]}{[Red]} \tag{3.7}$$

Finally, the cell potential can be estimated by combining the half-cells reactions:

$$E = E_{cathode} - E_{anode} \tag{3.8}$$

In order to estimate the rate of a redox reaction taking place in an electrochemical cell, the relationship between the faradic current and the electrolysis rate:

$$i = \frac{dQ}{dt} \tag{3.9}$$

where i (A) is the faradic current for the redox reaction considered in a certain time t (s), while Q (C) is the charge given by Faraday's law:

$$Q = nFN \tag{3.10}$$

with F (Faraday's constant, 1F = 96 485.3 C mol^{-1}), n the number of electrons transferred per mole of product, N. By deriving the above reported equation by the time, it is possible to write:

$$i = \frac{dQ}{dt} = nF \frac{dN}{dt} = Rate\ (mol\ sec^{-1}) \tag{3.11 a}$$

This equation is valid for heterogeneous reactions occurring at the interface electrode-solution. In this case, equation 3.9 should be normalized by the electrode area A (cm^{-2}):

$$Rate\ (mol\ sec^{-1} cm^{-2}) = \frac{i}{nFA} = \frac{j}{nF} \tag{3.11 b}$$

where j is the current density (A cm^{-2}).

Moreover, the redox reaction rate at the electrode surface is governed by four main factors, as shown in Figure 3.2:

1. Mass transfer from/to the bulk solution to/from the electrode surface;
2. Kinetics of the electron transfer (ET) at the electrode surface;
3. Homogeneous and heterogeneous chemical reactions preceding or following the ET;
4. Surface phenomena such as adsorption, desorption and crystallization.

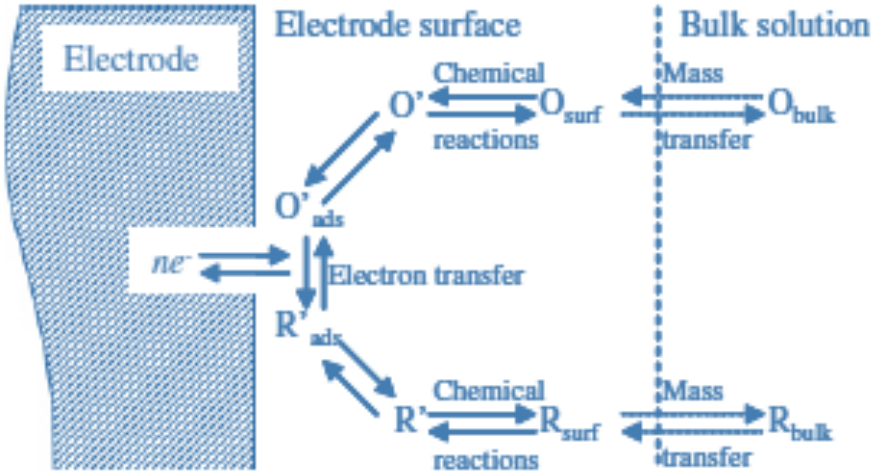

Figure 3.2 Schematic representation of the ET at the electrode/solution interface.

In general terms, the electrochemical systems can be controlled by kinetic and mass-transfer effects. In the first case there is a slow ET, while for the mass-transfer controlled system the ET rate constant is usually high at the electrode/solution interface where the rate limiting step can be the movement of molecules through the double layer and the bulk solution. The mass transfer can be achieved in three ways:

1. Migration of charged particles under the influence of an electrical field;
2. Diffusion along a concentration gradient;
3. Convection of molecules, e.g. by stirring.

The Butler-Volmer equation can be used to estimate the current of a system as a function of the overpotential without any mass-transfer limitation. Assuming the general redox reaction (for a 1 electron process according to Butler-Volmer):

$$Ox + e^- \underset{k_b}{\overset{k_f}{\rightleftharpoons}} Red \tag{3.12}$$

where k_f (cm sec^{-1}) and k_b (cm sec^{-1}) are the heterogeneous rate constants for the forward and backward reaction, respectively. The total current can be defined as the difference between the cathodic and the anodic current:

$$i = i_c - i_a \tag{3.13}$$

Both currents are related to the corresponding heterogeneous rate constant:

$$i_c = FAk_f C_O(0,t) \tag{3.14}$$

$$i_a = FAk_b C_R(0,t) \tag{3.15}$$

where F is Faraday's constant, A (cm^2) is the area of the electrode, and $C_j(x,t)$ (mol

cm^{-3}) is the concentration of species *j* at the distance x (cm) from the electrode the time t (s). The equation can be written as the ratio between the forward and backward rate constant:

$$k^0 = \frac{k_b}{k_f} = e^{f(E-E^0)} \tag{3.16}$$

where *f* is a factor containing (*RT/nF*). The complete *current-potential characteristic* can be written through the combination of the last equations:

$$i = FAk^0[C_O(0,t)e^{-\alpha f(E-E^0)} - C_R(0,t)e^{(1-\alpha)f(E-E^0)}] \tag{3.17}$$

where α is the electron transfer coefficient. This equation is used for every assumption on the heterogeneous electrode kinetics, including the Butler-Volmer equation. By considering a system in equilibrium, there is no net current:

$$i_0 = |i_a| = |i_c| \tag{3.18}$$

where i_0 is the exchange current:

$$i_0 = FAk^0 \tag{3.19}$$

where C_j* (mol cm^{-3}) is the bulk concentration for the *j* species. From the equations the *current-overpotential equation* is defined:

$$i = i_0[\frac{C_O(0,t)}{C_O^*}e^{-\alpha f\eta} - \frac{C_R(0,t)}{C_R^*}e^{(1-\alpha)f\eta}] \tag{3.20}$$

where n is the overpotential. By considering an efficient mass-transfer the concentration of the bulk solution would be equal to the solution at the electrode surface and it is possible to obtain the Butler-Volmer equation:

$$i = i_0[e^{-\alpha f\eta} - e^{(1-\alpha)f\eta}] \tag{3.21}$$

Finally, we should consider two approximations:

-a low overpotential: $i = -i_0 f\eta$

-high overpotentials well-known as the Tafel behaviour: $i = i_0 e^{-\alpha f\eta}$

which could be rearranged in a simple form: $\eta = a + b \log i$, where $a = \frac{2.3RT}{\alpha F}\log i_0$ and $b = -\frac{2.3RT}{\alpha F}$ allowing the extraction of kinetic parameters from *Tafel plot*.

3.2 Potential step techniques

Chronoamperometry (CA)

Potential step methods include techniques in which the potential of the working electrode is stepped and the resulting current from faradic process is recorded vs. time such as chronoamperometry (CA). In particular, the shape of the curve is mainly

affected by the mass-transfer from/to bulk solution/electrode surface. Whenever the potential is applied, the current achieves its highest value (high concentration of electroactive species at the electrode surface), decreasing after the steady state (electroactive species are consumed at the electrode surface) under diffusion control. In these experimental conditions, the Cottrell equation [90], derived from Fick's second law, can be used to predict the current trend with time. The current is then diffusion controlled. This equation is valid for a planar macroscale electrode:

$$i = \frac{nFAD_O^{1/2}C_O^*}{\pi^{1/2}t^{1/2}} \tag{3.22}$$

where D_O (cm^{-2} sec^{-1}) is the diffusion coefficient for O, F is Faraday's constant (1F = 96 485.3 C mol^{-1}), n the number of electrons involved in the faradic process, C_O^* (mol cm^{-3}) is the bulk concentration for O and A (cm^2) is the electrode area. This is the general Cottrell equation but for large amplitude potentials steps also the geometry of the electrode should be taken into account. Plotting the steady-state current i vs. $t^{-1/2}$ diffusion coefficients and electroactive area of electrodes can be calculated.

Chronoamperometry (CA) under convection: Flow Injection Analysis (FIA)

Flow injection analysis (FIA) is accomplished by injecting a plug of sample into a continuously flowing carrier stream. The sample is transported by the carrier stream through a detector to a waste container. FIA was first developed by Ružička and Hansen in Denmark in the mid '70 [91-93]. FIA instrumentation consists of a pump, used to move the carrier stream through a narrow tube and an injection port, through which a well-defined volume of a sample solution is injected into the carrier stream in a reproducible manner. Finally, the sample is sensed by a flow-through detector (in this thesis an enzyme based electrode) and recorded with a potentiostat. A bypass loop allows passage of carrier when the injection valve is in the load position, as reported in Figure 3.3. A typical recorder output has the shape of a sharp asymmetric peak. Once the sample is injected, it will be affected by the laminar flow, which is a combination of diffusive forces contributing to the sample dilution before reaching the detector. The dilution is highly reproducible by using FIA.

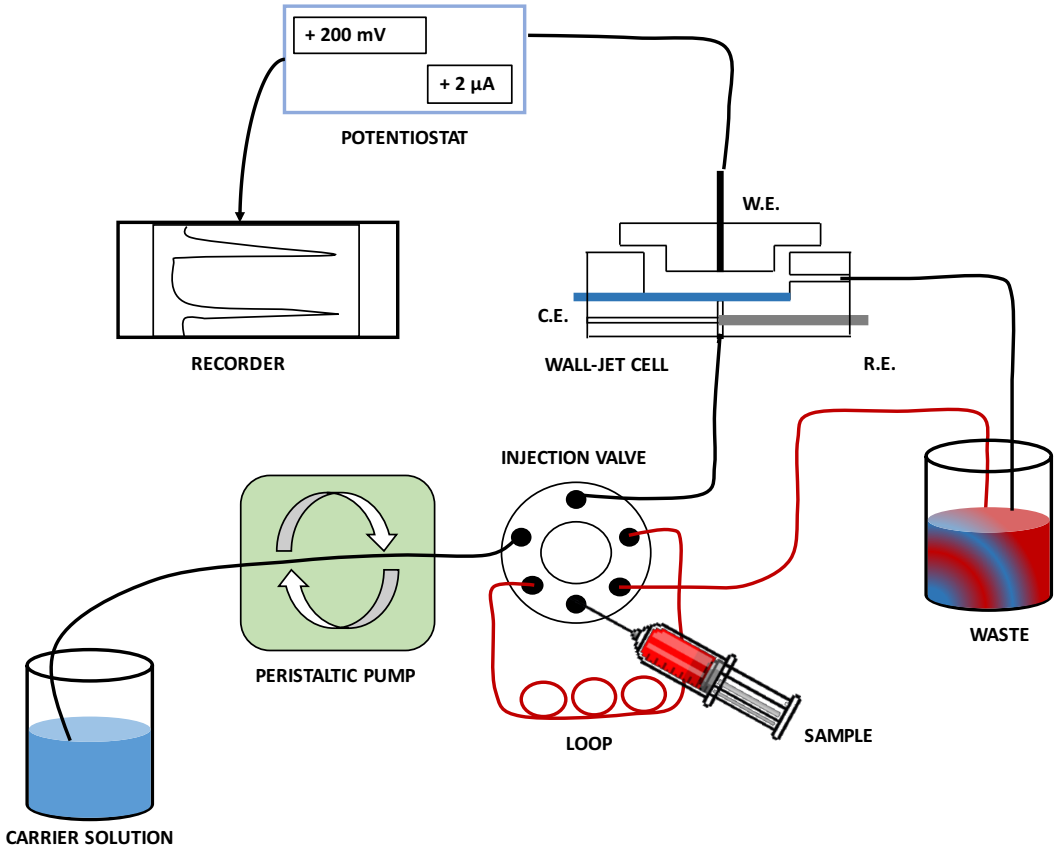

Figure 3.3 Schematic representation of FIA system.

The dispersion can be controlled through the dispersion factor (D), defined as the ratio of the analytical read out before (C^O) and after (C^{max}) the dispersion process in the carrier stream:

$$D = \frac{c^o}{c^{max}} \tag{3.23}$$

The value D is then used to correct the concentration values obtained during the experimental work. Dispersion is classified into limited (D = 1 to 3), medium (D = 3-10) and large (D > 10). In this thesis all the amperometry experiments were performed under limited dispersion.

The thesis reported the use of a FIA system combined with a wall-jet cell where an enzyme based electrode was used as the amperometric detector. A wall-jet cell consists of two halves constructed to be screwed together [94]. The distance between the working electrode and the inlet can be varied continuously by screwing the two halves more or less apart [95]. The inlet section of the cell contains the Ag|AgCl reference electrode (R.E.) in a circular chamber filled with 0.1 M KC1 from an external syringe. The chamber is connected with sample stream through four holes. The working electrode (W.E.) is fitted into a Teflon holder in order to expose the top of the electrode

to the carrier stream while the counter electrode (C.E.) is a platinum wire encircling the outlet chamber. In FIA measurements a selected constant potential (E_{app}) is applied to the WE in order to achieve the highest current possible.

The equation which describes the steady-state current recorded in a wall-jet cell when the inlet diameter is much smaller than the electrode has been reported by Yamada and Matsuda:

$$i = 0.898nFCD^{2/3}v^{-5/12}a^{-1/2}A^{3/8}U^{3/4} \quad (3.24)$$

where *a* is the diameter of the inlet nozzle, *A* is the electrode surface area, *C* is the concentration of the electrochemically active compound, *F* is the Faraday constant, *D* is the diffusion coefficient, ν is the kinematic viscosity, *U* is the average volume flow rate, n is the number of electrons involved in the faradic process [96].

Finally, FIA is a powerful analytical tool since it exhibits several advantages such as a fast, precise and accurate read out, it requires low sample volumes, it shows a low signal to noise ratio, and it is highly reproducible, easy and cheap.

3.3 Potential sweep techniques

During the experimental work of the thesis, several potential sweep techniques have been used such as linear sweep voltammetry (LSV) in which the potential is swept from the starting potential (E_1) to the end potential (E_2) recording the current. In a similar way, also cyclic voltammetry (CV) is a sweep technique but in this case the potential is reversed once reached the E_2.

Cyclic voltammetry for diffusing species

In CV the potential is swept *vs*. the time between two limiting potentials recording the resulting current. A redox reaction can be defined as a Nernstian system when the electron transfer kinetics is faster compared to the sweep rate. In a general CV experiment, where the electron transfer at a planar electrode is diffusion-controlled, the curve starts at E_1, increases while approaching to the formal potential ($E^{0'}$) of the redox couple due to the oxidation reaction therefore the surface concentration of reduced species drops, hence the flux to the surface and the faradaic current increases. After that, the potential is switched back and the reduction half-reaction occurs, as shown in the graphs reported in Figure 3.4.

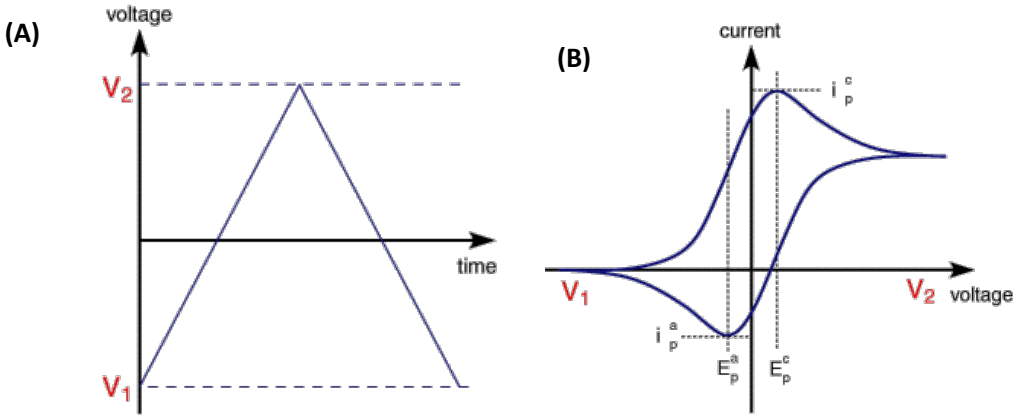

Figure 3.4 Graphical representation of CV. **(A)** the potential waveform and **(B)** a typcal CV for an electrochemical reaction where E_p^a and E_p^c stand for anodic and cathodic peak potentials, respectively, while i_p^a and i_p^c are the anodic and the cathodic peak current.

The electrochemistry of this method is governed by Randles-Sevčik equation [97-99], where the faradic peak current is proportional to the square root of the sweep rate. By considering a few boundary conditions like a reversible system in semi-infinite linear diffusion (planar diffusion-controlled process), it is possible to solve the equation as follows:

$$i_p = (2.69\ 10^5) n^{3/2} A D_O^{1/2} C_O^* v^{1/2} \tag{3.25}$$

The plot i_p vs. $v^{1/2}$ should be linear and considering its slope and intercept it is possible to obtain the diffusion coefficient.

The peak potential can be defined as:

$$E_p = E_{1/2} - 1.109 \frac{RT}{nF} = {}^{28.5}/_{n}\, mV\ at\ 25\ °C \tag{3.26}$$

where, F is the Faraday constant, R the constant of the ideal gases, T temperature [C], D_0 diffusion coefficient of the oxidized species [mol cm^{-3}], C_0* the concentration of the oxidized species [M], ν the sweep rate [V/s] and i_p the peak current [A].

A reversible system should match all the following criteria:

$$i_p \propto v^{1/2} \tag{3.27}$$

$$E_p\ non - dependent\ of\ v \tag{3.28}$$

$$\Delta E_p = E_{pa} - E_{pc} = \frac{59}{n} mV\ at\ 298\ K \tag{3.29}$$

$$\left| E_p - E_{p/2} \right| = \frac{59}{n} mV\ at\ 298\ K \tag{3.30}$$

$$\left| \frac{i_a}{i_c} \right| = 1 \tag{3.31}$$

$$E_{pa} \text{ or } E_{pc} \text{ should be independent on } v \text{ with the increase in } v$$

$$E_{\lambda} > \frac{59}{n} mV \text{ beyond } E_p, \text{then } E_p \text{ is independent on } v \quad (3.32)$$

In case the system does not fulfill all the aforementioned conditions, some kinetic restriction should be considered (quasireversible or irreversible systems). In case of irreversible system, the following equations should be applied:

$$i_{pa} \text{ or } i_{pc} \propto v^{1/2} \quad (3.33)$$

$$\left|\frac{i_a}{i_c}\right| \neq 1 \quad (3.34)$$

$$E_{pa} \text{ or } E_{pc} \text{ should shift to higher overpotentials with an increase in } v \quad (3.35)$$

$$\left|E_p - E_{p/2}\right| = \frac{48}{\alpha n} mV \text{ at } 298\ K \quad (3.36)$$

Since the fully reversible ET is always mass-transfer controlled it is hard to calculate k^0 using CV. Nevertheless, it should be possible for quasireversible and irreversible systems, with a slower rate of ET compared to the reversible ones.

For a one-step quasireversible electrochemical reaction in which the kinetic parameter $\Psi = k^0[\pi DnvF/(RT)]^{-1/2}$ is varied up to 0.1 and (ΔEp x n) not exceeding 200 mV, the Nicholson and Shain method [100] can be used considering the working curve Ψ-$\Delta Ep\ x\ n$ followed by a Ψ-$v^{-1/2}$ plot. On the other hand, Klingler and Kochi method [101] allows calculation of the ET rate constant k^0 for an irreversible system by following the equation below reported:

$$k^0 = 2.18 \left[\frac{D\beta nvF}{RT}\right]^{\frac{1}{2}} e^{-(\frac{\beta^2 nF}{RT})(E_p^a - E_p^c)} \quad (3.37)$$

where β is the ET coefficient for the redox process considered and E_p^a-E_p^c the peak-to-peak separation between the anodic and the cathodic peak, which should be higher than 200 mV out of Nicholson and Shain method. In the present thesis, the evaluation of the ET rate constant k^0 was performed by using an extended method reported from Lavagnini et al., which can be applied to all redox systems (quasireversible and irreversible) over the whole peak separation interval [102]. The equation 3.37 was rearranged as follows:

$$\Psi = 2.18 \left[\frac{\beta}{\pi}\right]^{\frac{1}{2}} e^{-\frac{\beta^2 F}{RT} n\Delta E_p} \quad (3.38)$$

where the symbols have their usual meaning. Finally k^0 could be easily calculated from the slope of the graph Ψ-$[\pi DnF/(RT)]^{-1/2}\ v^{-1/2}$. This method has been employed in

PAPER I, II, III and **IV** to evaluate the ET kinetic parameters of the modified electrodes considering the redox couple ferri/ferrocyanide $Fe(CN)_6^{3-/4-}$.

Cyclic voltammetry for immobilized species

The CV of an electroactive layer adsorbed onto the electrode surface is different compare to the CV of the same dissolved species freely diffusing. In this cases, we must consider the assumptions about (a) the degree to which adsorption equilibrium is attained before the start of the electrochemical experiment (i.e., how long after the formation of a fresh electrode surface the experiment is initiated) and (b) the relative rate of electron transfer to the adsorbed species compared to that for the dissolved species.

By assuming that the net reaction involves the electrolysis of diffusing O as well as O adsorbed on the electrode, to produce R that diffuses away and R that remains adsorbed, the mass-transfer equation resulted to be:

$$D_O \left[\frac{\partial C_O(x,t)}{\partial x}\right]_{x=0} - \frac{\partial \Gamma_O(t)}{\partial t} = -\left[D_R \left(\frac{\partial C_R(x,t)}{\partial x}\right)_{x=0} - \frac{\partial \Gamma_R(t)}{\partial t}\right] = \frac{i}{nFA} \tag{3.39}$$

where $\Gamma_O(t)$ and $\Gamma_R(t)$ are the amounts of O and R adsorbed at time *t* (mol/cm^2), while $C_O(x,t)$ and $C_R(x,t)$ are the concentration of O and R dissolved (freely diffusing) and the other constants have their usual meaning. The introduction of these terms requires additional equations relating Γ to C. Most frequently, the Langmuir isotherms can be used, as reported below:

$$\Gamma_O(t) = \frac{\beta_O \Gamma_{O,s} C_O(0,t)}{1+ \beta_O C_O(0,t) + \beta_R C_R(0,t)} \tag{3.40}$$

$$\Gamma_R(t) = \frac{\beta_R \Gamma_{R,s} C_R(0,t)}{1+ \beta_O C_O(0,t) + \beta_R C_R(0,t)} \tag{3.41}$$

with initial conditions $\Gamma_O = \Gamma_O^*$ *and* $\Gamma_R = 0$. By considering a sweep rate larger compare to the diffusion rate, so that O does not have time to diffuse appreciably to the electrode surface, it is possible to write the equation 3.42 as follows:

$$-\frac{\partial \Gamma_O(t)}{\partial t} = \frac{\partial \Gamma_R(t)}{\partial t} = \frac{i}{nFA} \tag{3.42}$$

Equation 3.42 implies that reduction of adsorbed O produces adsorbed R with no adsorbtion/desorption occurring during the scan. The previous equation along with the initial conditions yields

$$\Gamma_O(t) + \Gamma_R(t) = \Gamma_O^* \tag{3.43}$$

By considering the Langmuir isotherms, it is possible to write:

$$\frac{\Gamma_O(t)}{\Gamma_R(t)} = \frac{\beta_O \Gamma_{O,s} C_O(0,t)}{\beta_R \Gamma_{R,s} C_R(0,t)} = \frac{b_O C_O(0,t)}{b_R C_R(0,t)} \tag{3.44}$$

where $b_O = \beta_O \Gamma_{O,s}$ and $b_R = \beta_R \Gamma_{R,s}$. By considering a nernstian process, it is possible to write:

$$\frac{C_O(0,t)}{C_R(0,t)} = \exp\left[\left(\frac{nF}{RT}\right)\left(E - E^{0\prime}\right)\right] \tag{3.45}$$

further rearranged substituting equation 3.44 into 3.45, as follows:

$$\frac{\Gamma_O(t)}{\Gamma_R(t)} = \left(\frac{b_O}{b_R}\right)\exp\left[\left(\frac{nF}{RT}\right)\left(E - E^{0\prime}\right)\right] \tag{3.46}$$

By using the previous equation with equation 3.42, it is possible to obtain the equation for the i-E curve:

$$i = \frac{n^2F^2}{RT}\frac{vA\Gamma_O^*\left(\frac{b_O}{b_R}\right)\exp\left[\left(\frac{nF}{RT}\right)\left(E-E^{0\prime}\right)\right]}{\left[1+\left(\frac{b_O}{b_R}\right)\exp\left[\left(\frac{nF}{RT}\right)\left(E-E^{0\prime}\right)\right]\right]^2} \tag{3.47}$$

when $E = E^{0\prime}$, the peak current is given by:

$$i_p = \frac{n^2F^2}{4RT}\, vA\Gamma_O^* \tag{3.48}$$

The peak potential is obtained by:

$$E_p = E^{0\prime} - \left(\frac{RT}{nF}\right)\ln\left(\frac{b_O}{b_R}\right) \tag{3.49}$$

The peak current, and indeed the current at each point on the wave, is proportional to v, in contrast to the $v^{1/2}$ dependence observed for nernstian waves of diffusing species. For an ideal nernstian reaction under Langmuir isotherm conditions, $E_{pa} = E_{pc}$, and the total width at half-height of either the cathodic or anodic wave is given by:

$$\Delta E_{p,1/2} = 3.53\frac{RT}{nF} = \frac{90.6}{n} mV \; at \; 25\,°C \tag{3.50}$$

However, for the case where adsorbed O undergoes a totally irreversible one-step reduction, the langmuirian-nernstian boundary condition reported in equation can be replaced by kinetic one, obtaining a different expression for the i-E curve:

$$i = FAk_f\Gamma_O^* \exp\left[\left(\frac{RT}{\alpha F}\right)\left(\frac{k_f}{v}\right)\right] \quad (3.51)$$

The shape of the i-E curve is independent of v and k^0 so that the peak values are given by

$$i_p = \frac{\alpha F^2}{2.718RT}\, vA\Gamma_O^* \quad (3.52)$$

$$E_p = E^{0\prime} - \left(\frac{RT}{nF}\right)\ln\left(\frac{RT}{\alpha F}\frac{k^0}{v}\right) \quad (3.53)$$

$$\Delta E_{p,1/2} = 2.44\frac{RT}{\alpha F} = \frac{62.5}{\alpha} mV \; at \; 25\,°C \quad (3.54)$$

where α is the electron transfer coefficient while the other constants have their usual meaning. The heterogeneous electron transfer rate constant (k_s) for adsorbed species can be calculated as follows:

$$\log k_s = \alpha\log(1-\alpha) + (1-\alpha)\log(RT/nFv) - \alpha(1-\alpha)\, nF\Delta E_p/2.3RT \quad (3.55)$$

where α is the electron transfer coefficient while the other constants have their usual meaning. In this equation we should consider two different cases:

- $n\Delta E_p$ > 200 mV α can be calculated considering the graph E_p=f(log v), where there are two straight lines with a slope equal to m_c=-2.3RT/αnF for the cathodic peak, and m_a=2.3RT/(1-α)nF for the anodic peak;
- $n\Delta E_p$ < 200 mV α = 0.5 can be used because ΔE_p does not depend very much on α.

The equation 3.55 was used in **PAPERS II**, **III**, **IV** and **VII** to evaluate the ET rate of CDH and FDH adsorbed onto modified electrodes.

4. BIOELECTRONICS

There are three different ways to pursue the increasing of the performance of bioelectronics in terms of ET and current output. The first is the protein engineering, the second is the electrode nanostructuration and the third is the immobilization method. The present thesis is mainly devoted on the design and development of different nanostructuration and immobilization methods.

4.1 Electrode material, nanostructuration and modification

The ET rate and the amount of protein immobilized onto the electrode surface could be highly increased through an efficient nanostructuration of the surface by using several nanomaterials, such as metal nanoparticles (e.g. gold nanoparticles AuNPs, silver nanoparticles AgNPs), highly porous gold (h-PG), graphene, single and multi-walled carbon nanotubes (SWCNTs) or their combination as nanocomposite materials, like for example graphene decorated with AuNPs. These improvements would affect directly the analytical and electrochemical performance of bioelectronics such as biosensors and EFCs in terms of catalytical properties, sensitivity, chemical and electrochemical stability, selectivity, anti-fouling properties and introduction of other functional groups for further electrode modification. The aforementioned nanostructuration methods used in the thesis will be further discussed. For deeper insight into the nanomaterials several papers reported in literature are highly recommended [103-106].

Electrode materials

Graphite (**PAPERS I** and **VI**), glassy carbon (GC, **PAPERS IV** and **VII**), screen-printed (**PAPER III**) and gold polycrystalline (AuE, **PAPERS II** and **VIII**) based electrodes have been employed.

Graphite electrodes consist of several graphene sheets in a polycrystalline arrangement in which both planes, basal and edge plane sites, are present on the electrode surface with a random composition. However, graphite electrodes own high porosity and high charging current. On the electrode surface there are several oxygen functionalities or electrochemically active quinone groups, which may act as mediators with enzymes, so they should be consider during control experiments in order to exclude their contribution in the electrochemical process [107].

Glassy carbon (GC) electrodes merge glassy and ceramic properties with graphite properties. GC electrodes exhibit low density, low porosity and low electrical resistance. Their structure has been widely discussed in the last 50 years proposing several models, assuming the presence of both sp^2 and sp^3 carbon atoms or the presence of only sp^2 hybridized carbon or a fullerene like structure, but further investigations are needed to clarify this debate. GC electrodes are inert for the hydronium ion reduction [108].

In the last twenty years, screen-printed electrodes (SPEs) have received great attention for the on-site monitoring as a good compromise between high-volume and low-cost electrodes production, although not yet highly reproducible and reliable single-use sensors. Therefore, the use of screen-printing technology in the serial production of disposable low-cost electrodes for the electrochemical determination of a wide range of substances is currently undergoing widespread growth. Furthermore, SPEs are highly customizable in terms of working electrode modification (e.g. graphite, gold, palladium, copper, graphene, MWCNTs and AuNPs etc.), combined with the possibility to miniaturize the electrochemical cell [16, 109, 110].

Polycrystalline gold electrodes (AuE) own a really well-defined surface, lower charging current and a better reproducibility when comparing with graphite electrodes. Since gold is an inert material, it would prevent the formation of heterogeneous oxygen species which would affect the catalysis. AuEs need a pre-modification step with polymers or SAM because the protein directly adsorbed onto the metal surface gets easily denatured giving poor results in terms of electrochemistry [111, 112].

Metal nanoparticles (MNPs)

Nanosized metals exhibit a larger range of optical and electronic properties compared to relative bulk metals, such as larger surface area-to-volume ratio, larger surface energies, plasmon excitation, quantum confinement, etc [113, 114]. Due to its unique properties

gold is the most widely investigated metal. The properties of gold nanoparticles are strongly dependent upon size and shape. From the historical point of view, the most famous archaeological finds made of gold nanoparticles mixed with molten glass is certainly the *Lycurgus Cup* (4th century, roman empire age), which was changing colour depending on the location of the light source [115].

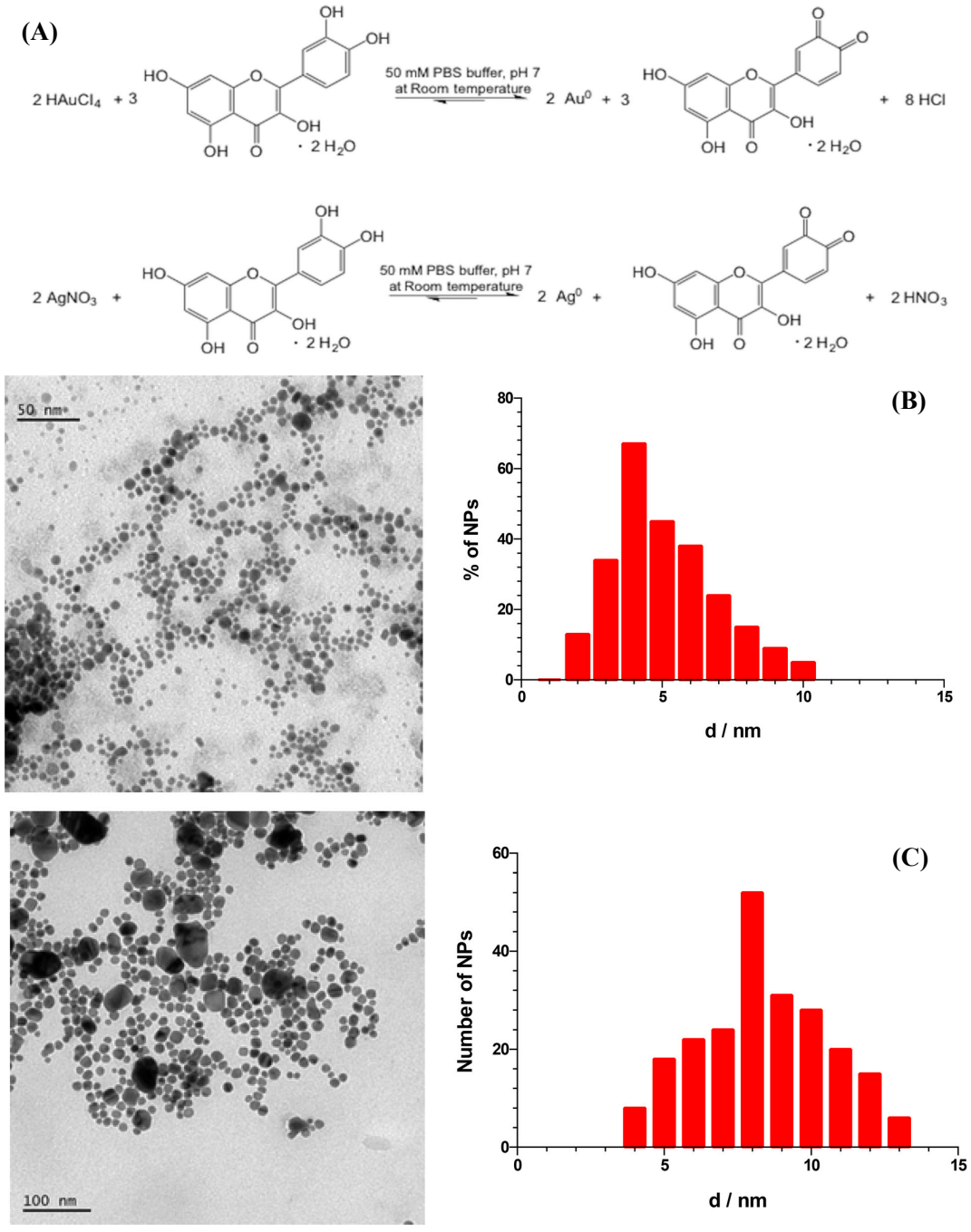

Figure 4.1 (A) Synthesis reaction of AuNPs and AgNPs; **(B)** TEM image of AuNPs with size distribution graph; **(C)** TEM image of AgNPs with size distribution graph (**PAPER I**). Reproduced with permission of Whiley & Co. from reference [121].

Nevertheless, the scientific community attributed the first colloidal gold to Michael Faraday (1857), who prepared colloidal gold by reducing a solution of gold chloride with phosphorus, then called "activated gold" [116]. This discovery was then followed by Richard Adolf Zsigmondy [117] (1898), who prepared the first colloidal gold diluted solution, Theodor Svedberg for the ultracentrifugation and Gustav Mie (1908) for his fundamental contribution on the theory for scattering and adsorption by spherical particles [118, 119]. During the last century, metal nanoparticles have attracted a great interest of the whole scientific community concerning both theoretical and practical aspects. The synthesis methods are generally divided into three main groups: chemical, physical and electrochemical methods [120].

In **PAPERS I, II, III** and **IV**, chemical and electrochemical methods have been used to synthesize metal nanoparticles. Chemical methods usually involve the chemical reduction of a metal precursor solution (e.g. gold chloride, silver nitrate etc.) in aqueous or organic solvent by using a reducing agent, like sodium borohydride ($NaBH_4$), sodium citrate or others. The synthesized MNPs present a "coating" layer which ensures a high dispersion in the colloidal suspension. A chemical method can be considered as a bottom-up approach proceeding through several steps from the reduction occurring to the metal ions, followed by nucleation taking place because the supersaturated solution is thermodynamically unstable, and finally the growth. The primary growth occurs after the nuclei formation from the solution through the deposition of soluble species onto the solid surface (molecular addition). Generally, the synthesis should be quit before any secondary growth process take place to avoid aggregation phenomena (combination of stable particles with smaller unstable nuclei). The size and the shape of metal nanoparticles are affected mainly by pH and type of reducing agent. Nowadays, also the synthesis of MNPs has been addressed toward green chemistry in order to minimize the use and the generation of hazardous chemicals. In this regard, the method used in this work involves the reduction of chloroauric acid ($HAuCl_4$) for AuNPs (**PAPERS I, II** and **III**) and silver nitrate ($AgNO_3$) for AgNPs (**PAPER I** and **II**), respectively [121, 122]. The reaction was carried out in aqueous solvent by using quercetin as reducing agent, as reported in Figure 4.1. Quercetin is a plant polyphenol from the flavonoid group, found in many fruits, vegetables, leaves, and grains. Quercetin reduces $AuCl_4^-$ ions to neutral gold atoms and Ag^+ ions to neutral silver atoms, which start to aggregate in sub-nanometer particles followed by a final growth to appropriate dimensions. Thus,

the reaction was quit after 20 minutes obtaining AuNPs with a core diameter of ~ 5 nm and after 30 minutes obtaining AgNPs of ~8 nm under mild experimental conditions, like room temperature and neutral pH.

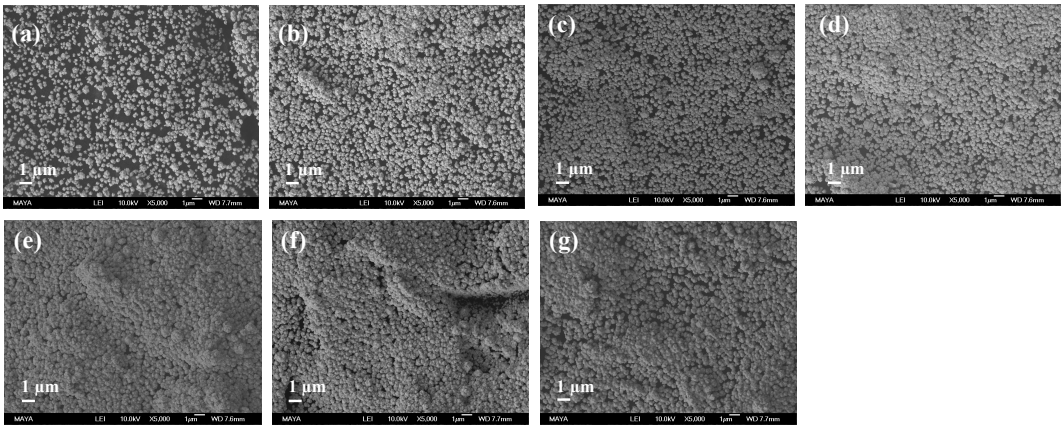

Figure 4.2 SEM images of AuNPs-modified GCEs obtained by sweeping the potential between 1.1 and −0.1 V vs. $Ag|AgCl_{sat}$ for a given number of scans in 10 mM $HAuCl_4$ (0.5 M H_2SO_4): (a) 5, (b) 10, (c) 15, (d) 20, (e) 25, (f) 30 and (g) 35 (**PAPER IV**). Reproduced with permission of MDPI from reference [125].

Besides the classical synthesis methods for MNPs, also the electrochemical deposition methods have been widely used to synthesize MNPs. The electrodeposition is realised directly on the electrode surface immersing the electrode in the precursor solution [123, 124]. Herein, the metal precursor concentration, the supporting electrolyte, the applied potential and the electrodeposition time are affecting the size, shape and thickness of the NPs layer. The electrochemical methods can be divided into potential sweep methods and potential step methods. In the first methods the electrode is scanned over a certain number of cycle (cyclic voltammetry), while in the latter case the potential is stepped for a certain time (chronoamperometry). In this PhD thesis, AuNPs have been electrodeposited onto glassy carbon electrodes studying the effect of the cycle number on the NPs layer thickness, performing the electrodeposition in 10 mM $HAuCl_4$ solution in 0.5 M H_2SO_4 (**PAPER IV**) [125]. Figure 4.2 shows the morphology of the electrode surface while increasing the scan number by 5, each time leading to aggregates and multi-layers which negatively affected the ET rate of the modified electrode.

MNPs are generally characterized by using several surface techniques like scanning electron microscopy (SEM), transmission electron microscopy (TEM), atomic

force microscopy (AFM) or other techniques like X-Ray diffraction spectroscopy (XRD), dynamic light scattering (DLS) and UV-Vis spectroscopy [126-129].

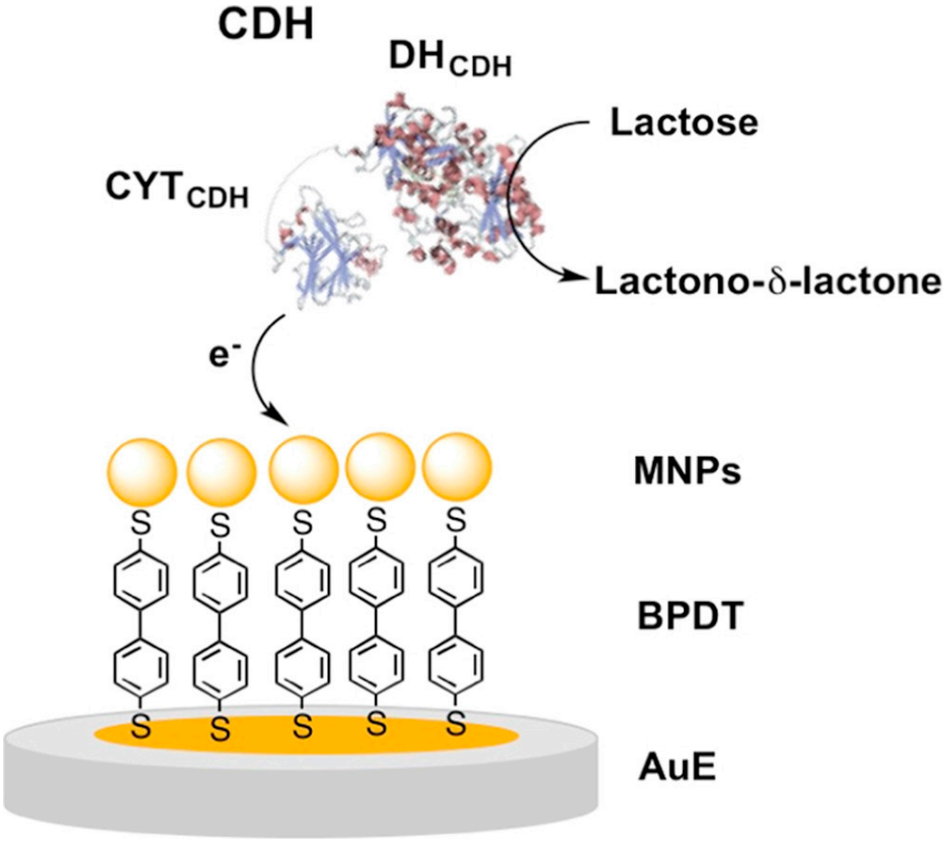

Figure 4.3 *Ct*CDH/MNPs/BPDT/AuE platform and DET between *Ct*CDH and the modified electrode (**PAPER II**). Reproduced with permission of Elsevier Ltd. from reference [122]

After a preliminary characterization, MNPs are widely used in biosensors construction especially in combination with redox enzymes according to different modification pathways. In particular, the first approach was the drop-casting of AuNPs and AgNPs onto graphite rod electrodes (**PAPER I**). In **PAPER II** both AuNPs and AgNPs have been covalently linked to the gold electrode surface by using a rigid SAM, diphenyl-4,4'-dithiol (BPDT), as shown in Figure 4.3, which exhibits high conjugation through the two aromatic rings (high conductivity) and a certain rigidity considering only the rotation along the σ bond connecting the phenyl rings as possible molecular rearrangements. Moreover, AuNPs have been used also in combination with graphene to develop an efficient CDH based bioanode using a cross-linking photopolymer to immobilize the AuNPs onto the modified electrode (**PAPER III**). Then, the AuNPs obtained through the electrochemical method were further modified using a mixed

SAM based on 4-mercaptobenzoic acid (4-MBA) and 4-mercaptophenol (4-MPh) as reported in **PAPER IV**.

Highly porous gold (h-PG)

Highly porous gold (*h-PG*) has been widely studied during the last twenty years mainly due to its particular properties, such as low bulk density, great specific surface area, low thermal conductivity, good penetrability, etc. [130-132]. Among all synthesis methods, de-alloying, free-template electrochemical deposition, template electrochemical deposition, self-assembly, sputter, and spray are the most commonly used. In **PAPER VIII** particular attention has been addressed to the free-template electrodeposition, which gives a multimodal distribution of *h-PG,* performing a two steps electrodeposition in 10 mM $HAuCl_4$ in 2.5 M NH_4Cl, as shown in Figure 4.4.

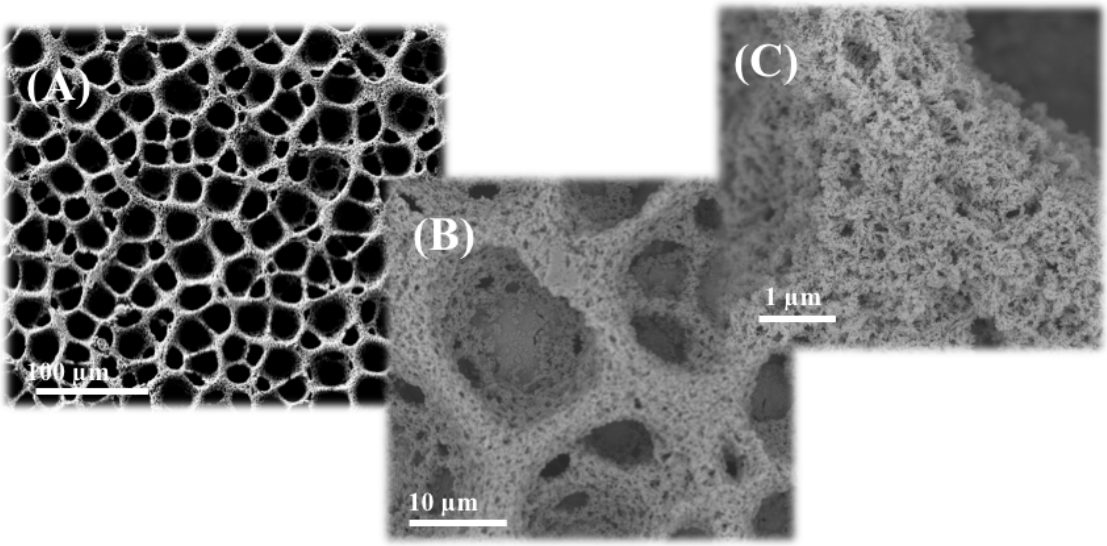

Figure 4.4 SEM images at different magnification (A) 100 µm (B) 10 µm (C) 1 µm of h-PGE obtained through a two steps electrodeposition: i) sweeping the potential for 25 scans between +0.8 V and 0 V vs. Ag|AgClsat, ii) applying a fixed potential -3 V vs. $Ag|AgCl_{sat}$ for 120 s; both steps have been carried out in 10 mM $AuCl_3 \cdot H_2O$ containing 2.5 M NH_4Cl (**PAPER VIII**).

The first step is responsible for the homogeneous deposition of a gold layer by cycling the electrode in the precursor solution while in the second step a negative potential is applied for 120 s in order to ensure the hydrogen bubbling at the electrode surface. In this procedure the hydrogen bubbles work as a template since the gold is electrodeposited in the interstitial space. Free-template electrodeposition is a time-saving method compared to the template electrodeposition since the template-removal

step is not needed. The so prepared *h-PG* electrodes were further modified with different SAM of 4-MBA, 4-MPh and 4-mercaptoaminothiophenol (4-APh) in order to obtain a different charged porous surface allowing a reorientation of the enzyme through electrostatic interactions.

Carbon nanomaterials

Carbon is a versatile atom which can be involved in *sp*, sp^2 and sp^3 hybridized structures. Carbon (C) itself exhibits a lot of allotropes such as diamond (where C atoms are bonded in tetrahedral lattice), graphite (C atoms arranged in several sheets with honeycomb lattice structure), graphene (which is one layer of graphite structure) and fullerenes (C atoms arranged in spherical or tubular structures). The most widely used carbon based nanomaterials in biosensors development are single walled carbon nanotubes (SWCNTs), multi walled carbon nanotubes (MWCNTs) and graphene (GPH) [133, 134]. CNTs are perfectly straight tubules with a diameter in the nanometer range. CNTs were accidentally discovered by Sumio Iijiama in 1991, giving to rise new input in carbon research through new structures [135]. CNTs own particular electronic properties due to the honeycomb lattice network developed along the diameter to give tubules with a certain helicity, which introduces several changes in the electronic density of states [136, 137]. Moreover, CNTs exhibit a lot of mechanical properties like high stability, strength and stiffness, low density and finally offer a great chemical features due to the introduction of terminal groups used for further reactions [138].

Among CNTs, there are two types which differ for the arrangement of graphene cylinders. MWCNTs are based on several concentric cylinders while SWCNTs are based on one cylinder. In order to modify these structures, several reaction approaches can be adopted:

- Covalent bond (sidewall halogenation, cycloaddition, electrophilic additions, nucleophilic addition, grafting of polymers etc.);
- Non-covalent adsorption (polymers);
- Encapsulation of biomolecules;
- Other side reaction.

In **PAPER VII**, a GC electrode was modified through drop-casting of a SWCNTs suspension, then grafted with 2-aminoanthracene (2-ANT) through the diazonium coupling technique in order to get access to the hydrophobic portion of the redox protein close to the heme *c* groups thus enhancing the ET rate.

Another intriguing carbon based nanomaterial is GPH. GPH exhibits as single- or double- layer of carbon atoms linked by sp^2 bond in a honeycomb lattice. The different graphene layers are held together by weak Van der Waals interactions along the distance of 3.35 Å. However, graphene displays peculiar properties mainly due to the chemical structure where each carbon atoms is sp^2 covalently linked with other 3 carbon atoms in the 2D-plane, so that one electron is freely moving in the third dimension generating high electronic conduction, as shown in Figure 4.5 [139].

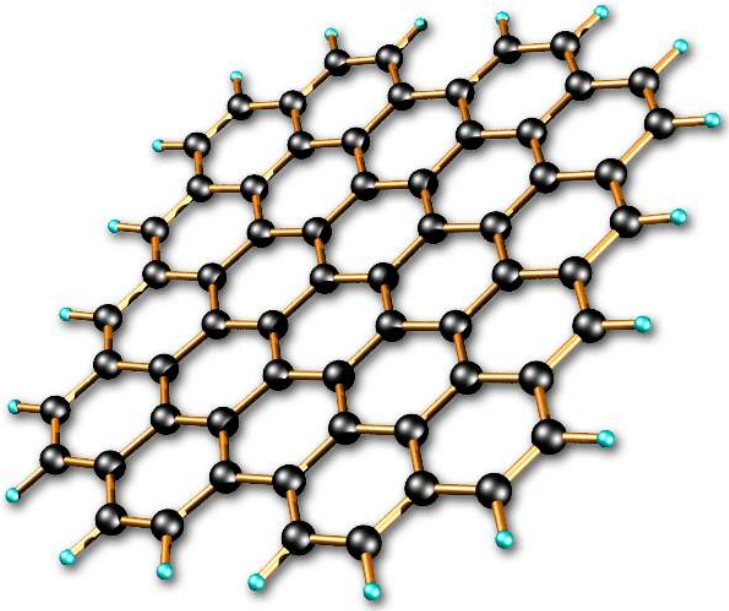

Figure 4.5 Structure of graphene.

During the last decade, several methods to synthesize graphene have been developed. There are basically two different classes of methods which can be resumed in top-down methods (e.g. graphite exfoliation through physical, chemical or electrochemical procedures) and bottom-up methods (e.g. chemical vapor deposition CVD). The top-down methods are based on mechanical procedures which reduce interatomic Van der Waals interactions between the graphene sheets while the bottom-up methods consider mainly a chemical production with a low yield which does not allow to scale up the procedure to an industrial production. The raw material mainly employed to synthesize graphene is graphite which is naturally available with purity levels ranging between 80% and 98% due to the presence of nickel or iron as impurities, while considering the synthetic graphite is possible to achieve purity levels above 99% depending on the quality of carbon source and its thermal treatment [105, 140].

Historically, graphene was synthesized the first time by using the mechanical exfoliation which allowed the fabrication of graphene sheets with minimal structural defects as detailed reported from Andre Geim and Konstantin Novosolev (both awarded with Nobel prize in Physics in 2010) using adhesive tape to separate graphene sheets from crystalline graphite [141, 142]. Unfortunately, this method cannot be used for large scale production while it is useful to investigate physical properties and for some selected applications (e.g. field-effect transistor). The exfoliation can be also realized through the electrochemical oxidation of a carbon-based working electrode (e.g. highly oriented pyrolytic graphite HOPG) in a three-electrodes electrochemical setup (working, reference and auxiliary electrode usually platinum). The oxidation experiment is carried out in electrolyte diluted such as sulfuric acid or surfactant solution like poly(styrenesulfunate) in water diluted sodium dodecyl sulfate (SDS), which acts during the intercalation process of negative charge from the electrolyte.

In **PAPER III**, a GPH based SPE was further modified through drop-casting with a colloidal suspension of gold nanoparticles to support the enzymatic layer of *Ct*CDH immobilized by using a cross-linked photopolymer, called poly(vinyl alcohol), N-methyl-4(4'-formylstyryl)pyridinium methosulfate acetal (PVA-SbQ).

Self-Assembled monolayers (SAMs)

Self-Assembled monolayers (SAMs) reaction occurs through the spontaneous and ordered adsorption of organic molecules onto the electrode surface. SAMs are generated through the chemisorption of head groups of the molecules followed by a slow organization of tail groups. The organization step takes place because of some forces acting between the spacer chain and the tail groups mainly Van der Waals, electrostatic and steric interactions [103, 143]. Thiols and dithiols are widely used as SAMs due to their spontaneous chemisorption on metal electrodes like gold. SAMs are really popular for biosensors development mainly because of the ease of preparation, long term stability, relatively low toxicity, wide potential window and dense monolayer formation. Moreover, SAMs present a lot of functional groups as tail groups like carboxyl, hydroxyl, amino etc. SAMs offer multiple choices concerning the spacers, which could be aromatic or aliphatic and in terms of length representing a really versatile and easy procedure to chemically modify the electrode surface [144, 145].

In the thesis work SAMs have been actively employed in **PAPERS II, IV** and **VIII**. In particular, in **PAPER II** biphenyl-4,4'-dithiol (BPDT) was used to covalently

link AuNPs and AgNPs followed by the enzyme drop-casting. In **PAPER IV** a mixed SAM namely 4-MBA and 4-APh was deposited onto the AuNPs/GC modified electrode where the CtCDH was cross-linked by using glutaraldehyde (GA). Finally, in **PAPER VIII** the h-PG electrodes were further modified with 4-MBA, 4-MPh and 4-APh used separately to exploit the electrostatic interaction between the charged electrode surface and the enzyme namely FDH.

Covalent reactions at carbon electrodes

Carbon based electrodes can be modified through chemical and electrochemical methods. On the surface of carbon electrodes there are a lot of oxygen containing functionalities like carboxylic, hydroxyl or ketones groups. Covalent bonds with –COOH usually occur with amines or alcohols. Also ketones and aldehydes can react with amines on the surface of the enzymes. Moreover, the spontaneous reaction of diazonium cations and carbon based electrodes is described [146, 147].

Since the first report of carbon based electrode modification using diazonium salts on 1992, a very large number of publications can be found using this method for surfaces modification [148-150]. Diazonium coupling offers a lot of modification possibilities with different functional groups that can influence the enzyme orientation. This aspect is important for biosensors and EFCs development. The electrochemical reduction of aryl diazonium salts is normally made in an aprotic medium with a supporting electrolyte or in acidic water conditions at room temperature. Besides the classical methods like ultrasound, microwave or UV light, it is possible to electrodeposit the *in situ* generated aryl diazonium cations, as shown in Figure 4.6. The thickness of this layer is mainly affected by the number of cycles applied to the carbon based electrode.

Figure 4.6 Diazotation of the aniline derivate, followed by the electroreduction of diazonium cation with a final covalent linkage.

In **PAPER VII**, SWCNTs suspension was drop-cast onto the GC electrode surface and let it dry; afterwards, the *in situ* generated diazonium cation of 2-amino anthracene was electrochemical reduced onto the electrode surface making the surface highly hydrophobic in order to get access to the hydrophobic region of the subunit II through π-π interaction. This approach allowed to exploit the contribution of each heme on the catalytic behaviour of FDH arising a current density two times higher compared to the electrode modified with SWCNTs on which FDH is randomly oriented.

4.2 Immobilization of the enzymes

Besides the electrode materials employed, nanostructuration and modification, enzyme immobilization represents a key issue in biosensors and EFCs development. The enzyme immobilization consists of a confinement onto the support surface (e.g. electrode), being a different phase from the one for substrates and products. An ideal immobilization matrix should be affordable, inert, robust, stable [151-153], increase the enzyme specificity/activity and reduce the product inhibition, non-specific adsorption and microbial contamination. The immobilization methods can be divided into three main categories: adsorption, chemical methods (e.g. covalent bond and cross-linking) and physical entrapment (e.g. polymers like chitosan, collagen, nafion or PVA-SbQ). In the present thesis, adsorption (**PAPERS I** and **VI**), cross-linking (**PAPERS IV**) and physical entrapment (**PAPER III**) methods have been used features, advantages and drawbacks of each method will be clarified below

Adsorption

Enzyme adsorption is mainly due to hydrophobic interactions and salt linkages by easily drop-casting the enzyme onto the support and let it dry [154]. Thereafter the molecules that are not adsorbed are washed away. This is a really weak immobilization method but easy to perform. Considering its reversibility, it should be taken into account that changes in pH, ionic strength, substrate concentration and temperature would contribute to detach enzyme molecules from the electrode surface. Carbon based electrodes (e.g. graphite, SWCNTs etc.) but also gold porous electrodes due to their porosity are suited for this kind of immobilization method. Therefore, it was used in **PAPERS I** and **VI** on graphite electrodes.

Cross-linking

Cross-linking is a strong chemical coupling method which requires the use of a cross-linking reagent, like glutaraldehyde or polyethylene glycol to link the biomolecules to the modified electrode surface [155, 156]. In this case, the main disadvantage is related to the activity loss of the enzyme. Cross-linking was used in **PAPER IV** to link *Ct*CDH to the electrode surface modified with a mixed SAM 4-MBA/4-APh by using glutaraldehyde. The so prepared biosensor was further characterized and used to detect glucose in human saliva.

Physical entrapment

Enzymes can be immobilized in three-dimensional matrices such as an electropolymerized film, an amphiphilic network composed of polydimethylsiloxane (PDMS), a photopolymer, a silica gel, a polysaccharide or a carbon paste. This immobilization is easy to perform. Enzyme, mediators and additives can be simultaneously deposited in the same sensing layer [157, 158]. There is no modification of the biological element so that the activity of the enzyme is preserved during the immobilization process. Biosensors based on physically entrapped enzymes are often characterized by increased operational and storage stability. However, limitations such as leaching of biocomponent and possible diffusion barriers can restrict the performances of the systems. In this regard, the N-methyl-4(4'-formylstyryl)pyridinium methosulfate acetal (PVA-SbQ) has been used to entrap *Ct*CDH (**PAPER III**) onto the modified electrode surface through photopolymerization, as shown in Figure 4.7.

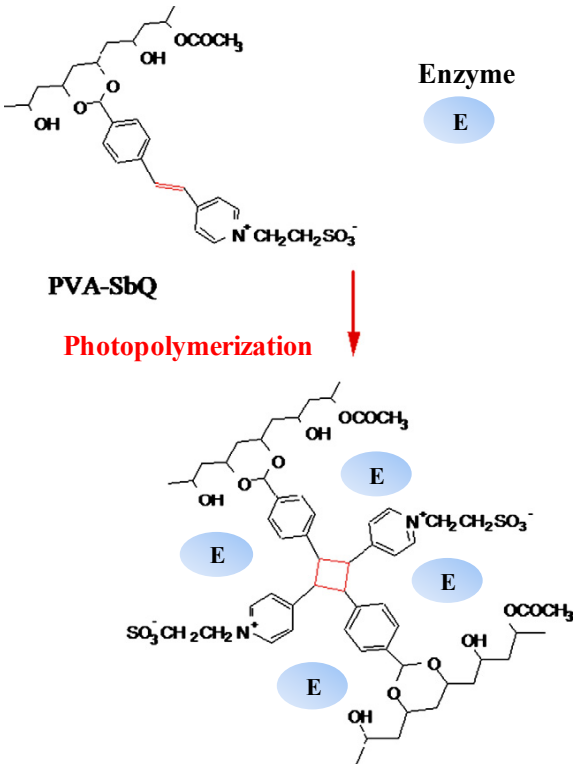

Figure 4.7 PVA-SbQ entrapment of the enzyme.

4.3 Enzyme biosensors

Besides the general concept of "biosensors" previously discussed in the introduction section, the catalytic or enzymatic biosensors that catalyse the conversion of the substrate (analyte) in product will be deeply explored [159, 160]. According to the communication way between enzyme and electrode, enzymatic biosensors can be divided into 1st generation, 2nd generation and 3rd generation biosensors [161-163], as shown in Figure 4.6.

In the 1st generation biosensors, the substrate is converted into a product, which is an electroactive molecule oxidised/reduced onto the electrode surface. The main problem is represented by the interferences for the analytical detection [164]. These interferences can be reduced by using an artificial mediator immobilized onto the electrode surface, which is able to shuttle the electrons between the active site and the electrode surface, giving rise to the 2nd generation biosensors [165]. Finally, some enzymes have their active sites or a redox ET pathway very close to the surface of the enzyme. In this case the electrode is able to electrically contact the enzyme without the use of any other molecule. This mechanism is called direct electron transfer (DET) and

the biosensors are called 3rd generation biosensors [166, 167]. All three generations are reported in Figure 4.8.

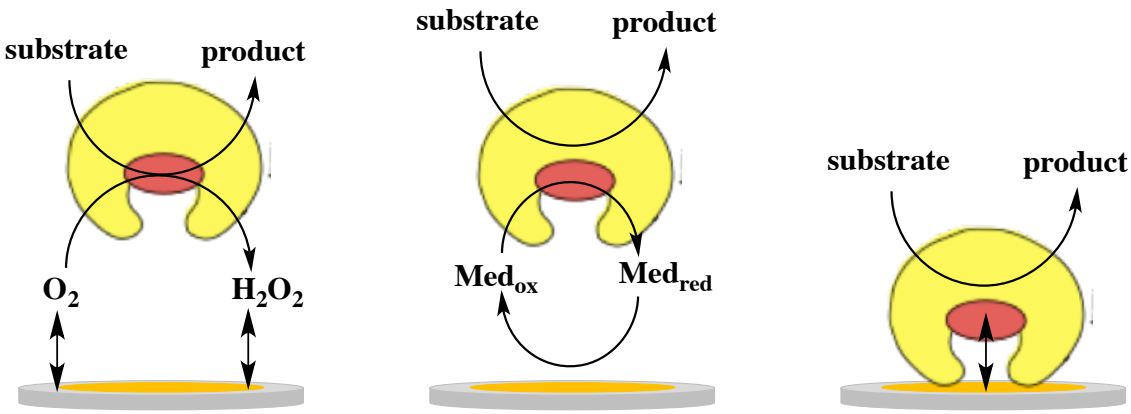

Figure 4.8 Biosensors types. Left, first generation, center second generation and right, third generation.

For biosensors based on DET, third generation biosensors, the absence of mediators is the main advantage, providing them with superior selectivity, both because they should operate in a potential window closer to the redox potential of the enzyme itself, and therefore, less prone to interfering reactions and also because of the lack of other reagents in the reaction sequence [168]. Another attractive feature of the systems based on DET is the possibility of modulating the desired properties of an analytical device using protein modification with genetic or chemical engineering techniques on one hand, and novel interfacial technologies on the other hand. The very first reports on DET with a redox active protein were published already in 1977 when Eddowes-Hill [169] and Yeh-Kuwana [170] independently showed that cytochrome c with gold and tin doped indium oxide electrodes, respectively, showed virtually reversible electrochemistry as revealed by cyclic voltammetry [169].

The development of amperometric biosensors was boosted from the big request of glucose sensors on the market mainly due to the increase of diabetes in the world population. Nowadays a lot of glucose sensors are available on the market mainly based on 1st or 2nd generation biosensors with PQQ-dependent GDH or FAD-dependent GDH with a mediator (e.g. glucocontour XT from Bayer) [171, 172]. Recently, the first 3rd generation lactose biosensor kit has been commercialized by DirectSens GmbH.

In the present thesis third generation biosensors for lactose detection (**PAPERS I** and **II**), glucose detection (**PAPER IV**) and fructose detection (**PAPERS VII** and **VIII**) have been developed

4.4 Enzymatic fuel cells (EFCs)

As already discussed in advance, a fuel cell is a galvanic cell. It consists of a fuel compartment and an oxidant compartment where two electrodes are submerged. The fuel is oxidised at the anode while the oxidant is reduced at the cathode, with electrons flowing from the anode towards the cathode generating electrical power to power-up electronic devices [173]. Over the last 30 years' biofuel cells (BFCs) have received great attention because they work in mild experimental conditions, without separator between the two halves and offer some possibilities towards the miniaturization process compares to classical fuel cells [20, 174, 175]. In the BFCs there is substitution of metal catalysts in both compartments with enzymes or microorganisms able to oxidize the fuel and reduce the oxidant. The limiting aspect is the power output, which is in the milli- or micro-Watts [176], rather lower than the one obtainable from classical fuel cells. The main advantage is represented from the mild operational conditions like normal temperature and pressure.

To date, the first enzymatic fuel cell was reported by Yahiro and co-workers in 1964. The cell consisted of platinum based electrodes immerged in phosphate buffer solutions for both compartments separated by a membrane. Glucose and glucose oxidase were placed into the anodic compartment while the cathodic side was purged with oxygen. With this setup, the cell gave an open circuit potential (OCV) of about 625-750 mV with a small current density [21]. The poor performance was probably the result of the absence of any mediator to transfer electrons between glucose oxidase and the electrode. It is well known that glucose oxidation at Pt occurs at high potential, therefore it is unclear whether the enzymes were functioning at all. This work was followed by Hill and co-workers in 1981 reporting a methanol-oxidizing fuel cell based on bacterial methanol dehydrogenase in which the performances were not so satisfying due to the low OCV but higher current density close to 0.5 mA cm^{-2}. Other research groups have been contributing to the improvement of EFCs like Yue and Lowther, Willner and co-workers, and Armstrong, who demonstrated the first EFCs for the H_2 oxidation as well as Karyakin and his co-worker [177-181].

Few parameters should be considered for a completed EFCs characterization [182], as below listed:

- Power output: power generated from the EFC calculated from P=E x I as a derivation of the Ohm's law (I=V/R);
- Open circuit voltage (OCV): maximum voltage associated with the EFC, also called resting potential or zero-current potential, because it is the potential at which no net current is flowing in the circuit;
- Short circuit potential: the potential at which the anode and the cathode are electrically connected without an applied load, no useful electrical work is done.

An example of EFCs characterization is shown in Figure 4.9.

As already discussed the ET between enzymes and electrodes takes place either in a DET- or a MET-pathway. MET based EFCs give in general much higher current densities due to the efficient ET between the active site of the enzyme and the electrode. Nevertheless, the use of DET compared to MET has many advantages, like less components (e.g. no mediators) and higher open-circuit potential (OCV) due to direct connection of the enzyme resulting in the OCV as the difference between the formal potential of cathode and anode. This makes DET EFC the most advantageous ones for future miniaturization and implantation in the human body [183-185].

In the present thesis work, the anode construction based on a nanocomposite material (graphene and AuNPs) has been optimized with different immobilization methods, drop-casting, nafion membrane and PVA-SbQ, which showed the best results. This electrode was used in combination with a *Trametes hirsuta* laccase based electrode, as biocathode The EFC was further scaled down according to three steps: (i) two SPEs separated by a proton-exchange membrane, (ii) two SPEs without any separator, (iii) only one SPE, which has been tested as proof-of-concept in saliva (**PAPER III**), as better described in the next paragraphs

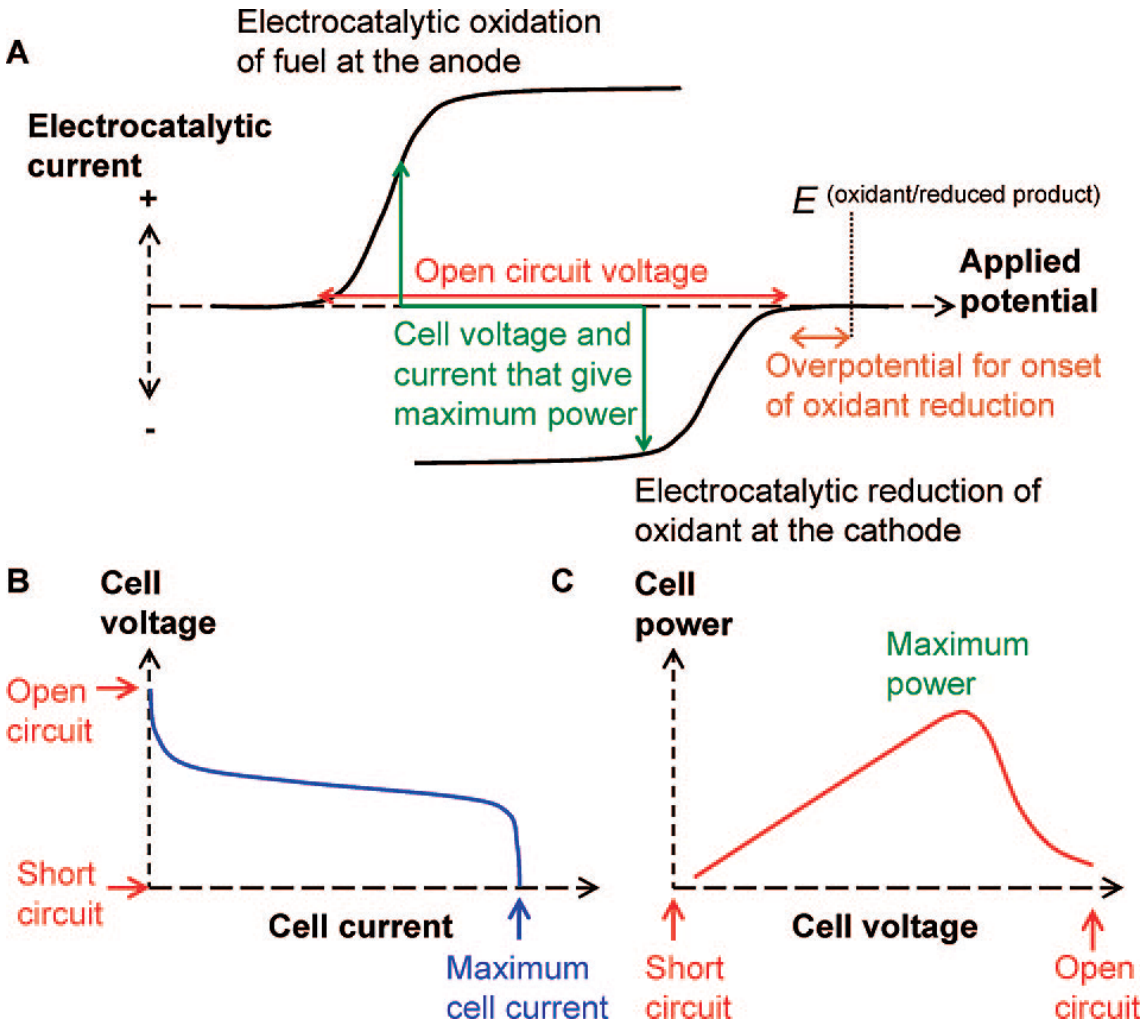

Figure 4.9 Voltage and current response for a pair of fuel cell electrodes tested separately (A) or operating together in a fuel cell (B and C). Features that determine fuel cell performance are highlighted.

5. SUMMARY OF RESEARCH

In the first part of the thesis has been focused on the "green" synthesis of metal nanoparticles to modify the electrode surface through different immobilization approaches, like drop-casting (**PAPER I**), covalent modification of gold surface through SAM (**PAPER II**) and physical entrapment by using a photopolymer,PVA-SbQ (**PAPER III**).

In **PAPER I** a facile, cost effective and environmental friendly green synthesis method of gold and silver nanoparticles (NPs) by using quercetin as reducing agent has been reported The obtained NPs were characterized by transmission electron microscopy (TEM), energy dispersive spectroscopy (EDS), dynamic light scattering (DLS) and UV-Vis spectroscopy and parameters such as pH, ionic strength and temperature, effectively affecting shape and size of NPs, have been carefully studied and optimized. The obtained results showed that the synthesized NPs were circular in shape with an average diameter of 5 and 8 nm for AuNPs and AgNPs, respectively. The "green" NPs, showing increased electroactive areas (A_{EA}) and electronic transfer rate constants (k^0), were successively used to fabricate a novel third generation lactose biosensor based on cellobiose dehydrogenase from *Trametes villosa* (TvCDH). The TvCDH/AuNPs based lactose biosensor revealed the best results showing very efficient DET and a detection limit for lactose of 3.5 μM, a large linear range from 10 to 300 μM, a high sensitivity (5.4 μA μM^{-1} cm^{-2}) and long-term stability.

In **PAPER II**, an efficient direct electron transfer (DET) between cellobiose dehydrogenase from *Corynascus thermophilus* (*Ct*CDH) and a novel gold electrode platform was achieved through the covalent linking of the "green" AuNPs and AgNPs modified with a dithiol self-assembled monolayer, consisting of biphenyl-4,4-dithiol (BPDT). The green AuNPs and AgNPs were synthesized using quercetin as reducing agent at room temperature. TEM experiments showed that AuNPs and AgNPs were circular in shape with an average diameter of 5 and 8 nm, respectively. Cyclic voltammetry of *Ct*CDH immobilized onto AuNPs/BPDT/AuE and AgNPs/BPDT/AuE

electrode platforms was carried out and compared with naked AuE, BPDT/AuE, AuNPs/AuE, and AgNPs/AuE. A pair of well-defined redox waves in neutral pH solution due to the efficient DET of *Ct*CDH was present with both MNPs/BPDT/AuE platforms. No DET communication was found with platforms without MNPs linked to BPDT. The apparent heterogeneous electron transfer rate constants (k_S) of *Ct*CDH were calculated to be 21.5 ± 0.8 s^{-1} and 10.3 ± 0.7 s^{-1}, for the AuNPs/BPDT/AuE and the AgNPs/BPDT/AuE platforms, respectively. The modified electrodes were successively used to develop an eco-friendly biosensor for lactose detection. The *Ct*CDH/AuNPs/BPDT/AuE based biosensor showed the best analytical performances with an excellent stability, a detection limit of 3 μM, a linear range between 5 and 400 μM and a sensitivity of 27.5 ± 2.5 μA cm^{-2} mM^{-1}. Such performances were favourably compared with other lactose biosensors reported in literature. The biosensor was successively tested to quantify lactose content in real milk and cream samples. No significant interference present in the sample matrices was observed.

In **PAPER III**, the development of a new direct electron transfer based-miniaturized glucose/oxygen enzymatic fuel cell (EFC) has been described. The operating ability of the proposed EFC has been tested in real human saliva samples. The bioanode and biocathode are a graphene working electrode and a graphite counter electrode localized on the same screen printed electrode (SPE) modified with poly(vinyl alcohol) N-methyl-4(4'-formylstyryl)pyridinium methosulfate acetal (PVA-SbQ)/cellobiose dehydrogenase from *Corynascus Thermophilus* (*Ct*CDH) C291Y/AuNPs and with *Trametes Hirsuta* laccase (*Th*Lac)/AuNPs, respectively.

In order to optimize the bioanode, several CDH immobilization procedures were adopted, such as drop-casting, use of Nafion membrane and PVA-SbQ photopolymer. The photopolymer showed the best performance in terms of stability and reliability. The biocathode was a partially optimized laccase electrode modified with nanomaterials drop-casted onto the gold nanoparticles (AuNPs) modified SPE, in order to reduce the overpotential of O_2/H_2O redox reaction catalyzed by *Trametes Hirsuta* Laccase (*Th*Lac). The performances of bioanode and biocathode were tested separately. Initially the two enzymes were immobilized onto separated graphene SPEs. An efficient direct electron transfer was achieved for both elements, obtaining an apparent heterogeneous electron transfer rate constant (k_s) of 0.99 ± 0.05 s^{-1} for *Ct*CDH C291Y and 5.60 ± 0.05 s^{-1} for *Th*Lac. Both electrodes were then assembled in a two compartments EFC obtaining a maximal power output of 5.16 ± 0.15 μW cm^{-2} at a cell voltage of 0.58 V and an open

circuit voltage (OCV) of 0.74 V. Successively, the bioanode and biocathode were assembled in a non-compartmentalized EFC and a remarkable 50% decrease of the maximum power output at the value of 2.15 ± 0.12 μW cm^{-2} at cell voltage of 0.48 V and an OCV of 0.62 V at pH 6.5 was registered. In order to reduce the cell dimensions for possible integration in biomedical devices, the bioanode and biocaythode were realized by immobilization of both enzymes onto the same SPE. Theminiaturized EFC delivered a maximal power output of 1.57 ± 0.07 μW cm^2 and 1.10 ± 0.12 μW cm^{-2} with an OCV of 0.58 V and 0.41 V in a 100 μM glucose solution and in human saliva, respectively.

In **PAPER IV**, an efficient direct electron transfer (DET) between a cellobiose dehydrogenase mutant from *Corynascus thermophilus* (*Ct*CDH C291Y) and a novel glassy carbon (GC)-modified electrode, obtained by direct electrodeposition of gold nanoparticles (AuNPs) was realized. The electrode was further modified with a mixed self-assembled monolayer of 4-aminothiophenol (4-APh) and 4-mercaptobenzoic acid (4-MBA), by using glutaraldehyde (GA) as cross-linking agent. The *Ct*CDH C291Y/GA/4-APh,4-MBA/AuNPs/GC platform showed an apparent heterogeneous electron transfer rate constant (*k*s) of 19.4 ± 0.6 s^{-1}, with an enhanced theoretical and real enzyme surface coverage (Γ_{theor} and Γ_{real}) of 5287 ± 152 pmol cm^{-2} and 27 ± 2 pmol cm^{-2}, respectively. The modified electrode was successively used as glucose biosensor exhibiting a detection limit of 6.2 M, an extended linear range from 0.02 to 30 mM, a sensitivity of 3.1 ± 0.1 μA mM^{-1} cm^{-2} (R^2 = 0.995), excellent stability and good selectivity. These performances compared favourably with other glucose biosensors reported in literature. Finally, the biosensor was tested to quantify the glucose content in human saliva samples with successful results in terms of both recovery and correlation with glucose blood levels, allowing further considerations on the development of non-invasive glucose monitoring devices.

PAPER V presents the results obtained during the last 20 years by combining new nanomaterials and hybrid nanocomposites with various CDHs in order to increase the overall performances of electrical devices (biosensors, EFCs etc.). It has also been shown that nanomaterials can be further chemically modified to facilitate electron transfer pathways between the biocomponent and the electrodes. Both carbon and metal based nanomaterials and their combinations have been used together with CDH to improve the performance.

The second part of the thesis regards the study of the ET mechanism of fructose dehydrogenase (FDH), highlighting the following points: a) the influence of divalent and monovalent cations on the catalytic current through structural changes (**PAPER VI**) b) the chemical modification of carbon based electrodes to get access to the hydrophobic region contained in the subunit II of FDH (**PAPER VII**); c) the modification of highly porous gold with different SAM to get various orientations of FDH through different electrostatic interactions between the enzyme and the re-charged surface to develop the most sensitive fructose biosensor (**PAPER VIII**).

In **PAPER VI** the influence of monovalent and divalent cations on the catalytic current and enzyme structure by using both spectrophotometric assays and amperometric measurements has been investigated. In particular, the spectrophotometric assays were carried out by using a monoelectronic acceptor namely cytochrome c and successively a bielectronic acceptor, which is 2,6-dichloroindophenol (DCIP). In the first case, it was possible to observe a remarkable increase of the absorbance up to 200% adding 10 mM of $CaCl_2$. By increasing the concentration of $CaCl_2$ up to 50 mM and 100 mM, it was possible to observe a decrease of the absorbance with a slight inhibition in correspondence of the highest $CaCl_2$ concentration. $MgCl_2$ showed surprisingly no effect on the ET as well as for the monovalent cations. Contrary to the previous assay, none of the cations tested seem to affect the catalysis with DCIP. These results were further confirmed through amperometric measurements in which the electrode was replacing the cytochrome c in terms of electron acceptor, so far interacting with the subunit II through the direct electron transfer mechanism. In order to confirm the results obtained by spectrophotometric assays and amperometric measurements, circular dichroism (CD) measurements have been performed showing a great structural change while increasing $CaCl_2$ concentration up to 50 mM, when the enzyme molecules start to agglomerate hindering the substrate access to the active site probably due to chelation reaction occurring at the enzyme surface with glutammate residues.

In **PAPER VII**, an efficient direct electron transfer (DET) between fructose dehydrogenase and a carbon based electrode SWCNTs/GC further modified through diazonium coupling was achieved. The diazonium salt was synthesized following the reaction of 2-amino anthracene with $NaNO_2$ in acidic media (0.5 M HCl) for 5 minutes at 0 °C. After the *in situ* reaction, the 2-amino anthracene diazonium salt was electrodeposited by running cyclic voltammograms from +1000 mV to -1000 mV vs.

$Ag|AgCl_{sat}$. Themodified electrode was further incubated with FDH. CVs of FDH/2-ANT/SWCNTs/GC were performed showing two couples of redox peaks possibly ascribed to heme c_1 and heme c_3. Nevertheless, in presence of 10 mM fructose it was possible to observe two catalytic waves clearly related to heme *c*. On the other hand, for the SWCNTs/GC electrode only one catalytic wave and one couple of peaks were observed, while in the absence of SWCNTs no electrochemistry of FDH was observed with also a slight catalytic effect. These findings could be explained by considering the hydrophobic pocket close to heme c_1 and heme c_3. The access to the heme groups is possible through the anthracene aromatic structure via π-π interactions between the aromatic sides chains of the amino acids present in the hydrophobic pocket of FDH.

PAPER VIII showed a new method to electrodeposit highly porous gold without any templates. The electrodeposition is carried out first cycling the electrode in 10 mM $HAuCl_4$ with 2.5 M NH_4Cl and then applying a negative potential for the production of hydrogen bubbles at the electrode surface. After that the modified electrode was characterized in sulphuric acid to estimate the real surface area (A_{real}) close to 30 cm^2. The electrode was further incubated overnight with different SAMs,4-mercaptobenzoic acid (4-MBA), 4-mercaptophenol (4-MPh) and 4-aminothiophenol (4-APh) in order to obtain different re-charged electrode surface. All modified electrodes were investigated by using cyclic voltammetry both in non-turnover and turnover conditions showing the best performance for the FDH/4-MPh/h-PG/AuE observing a clear electrochemistry of heme c_2 and heme c_3 and a great catalytic effect (about 1000 μA cm^{-2} in presence of 10 mM fructose), probably due to the correct orientation of FDH through the electrostatic interaction enzyme-modified electrode. The FDH/4-MPh/h-PG/AuE based biosensor showed the best analytical performances with an excellent stability (90% of retained activity over 90 days), a detection limit of 0.3 μM, a linear range between 0.05 and 5 mM and a sensitivity of 175 ± 15 μA cm^{-2} mM^{-1}. Such performances were favourably compared with other fructose biosensors reported in literature. The biosensor was successively tested to quantify fructose content in food and beverage samples. No significant interference present in the sample matrices was observed.

6. CONCLUSIONS AND FUTURE PERSPECTIVES

My PhD thesis deals with the ET processes between enzymes and electrodes. I have really enjoyed the time looking for new nanostructuration methods for biosensors and EFCs development and new synthesis method for metal nanoparticles, like the "green" synthesis by using quercetin. This work is a continuation of 25 years of research about the direct electron transfer of dehydrogenases, in particular CDH and FDH, because of their key role from the analytical and energetic points of view.

In this thesis I have presented new approaches on the nanostructuration as tools to improve the DET of dehydrogenases, first using chemical and then electrochemical methods. In the chemical approach, I have developed a "green" protocol to obtain AgNPs and AuNPs in a short time at normal temperature and pressure. Afterwards, I used the electrochemical methods for both metal and carbon based electrodes to obtain high reproducibility in the electrode modification.

The modified electrodes have been employed to obtain "bioelectronics", highly sensitive and selective biosensors for lactose, glucose and fructose detection employed as valid analytical screening methods for clinical and food samples like saliva, blood and dairy products.

The ET process of another dehydrogenase namely FDH was also explored, considering a great similarity for subunit I compare to all the GMC-oxidoriductases DH domains. On the other hand, the subunit II resulted to be rather different. One of the last findings is related to the fact that only two heme *c* are involved in the ET process, so for future investigations a series of FDH mutant should be investigated in order to fully understand the ET pathway that in this case is much more complex compared to CDH.

As future perspectives on the development of the best glucose/fructose biosensor and glucose/fructose EFC, I think that several approaches can be exploited in order to improve the ET of redox enzymes: (a) discovery of new nanomaterials and new

nanostructuration methods; (b) modify the nanostructured electrode matching the chemical-physic properties of the enzymes (e.g. isoelectric point pI, particular region surface exposed like hydrophobic region) in order to create a favourable environment for the enzyme immobilization preventing enzyme denaturation; and (c) the enzyme engineering through deglygosylation (reducing the enzyme dimensions the ET should be improved) or introducing redox groups or nanomaterials like gold nanoparticles in the vicinity of the prosthetic group.

7. ACKNOWLEDGMENTS

This thesis is the final resume of my research work performed during the PhD course. During this three years, I have been working for 18 months at the Division of Biochemistry and Structural Biology of Lund University in Sweden, where I have done the most part of the measurements included in this thesis. Of course, my greatest acknowledgments go to Prof. Lo Gorton also known as Luigi “Il Bello”. I really enjoyed the time in Sweden both in and out of the lab. I still remember that day, 9th april 2015, when I just arrived in Lund, Lo looked at me and said: Are You Paolo? He was a bit scared because of my huge luggage and I replied: Yes, I am. From that day, I have to say THANK YOU or as you prefer TACK SÅ MYCKET, you taught me the deep secrets of bioelectrochemistry. I enjoyed our conversation about science, music and politics. It was a great honour being a colleague and friend of all permanent people Galina, Christopher, Kamrul as well as the numerous visiting students, PostDocs, Doctors and Professors coming from all over the world with all kind of knowledge, personalities and peculiarities.

The second great acknowledgments go to Prof. Riccarda Antiochia, my supervisor to give me the great opportunity to begin the PhD course and to present me Prof. Lo Gorton. She strongly supported my crazy ideas about bioelectrochemistry and biosensors.

The third great acknowledgments go to people that have been directly involved in the project: Dr. Roland Ludwig and Dr. Su Ma to kindly donate CDH from *Trametes Villosa* and from *Corynascus thermophilus* (recombinant and C291Y); Prof. Kenji Kano and Dr. Yuya Hibino to kindly donate FDH from *Gluconobacter japonicus*; and Dr. Daniel Jacobsson, Dr. Crispin Hetherington and Gunnel Karlsson for their help with TEM and SEM characterization of modified electrodes.

I have to thank all my Italian lab mates and friends Cristina, Giovanni, Prof. Franco Mazzei, Prof. Gabriele Favero and all the students for the nice time and discussions about science and gossip.

Many thanks go to all the people from the Swedish department and the “Beer club” crew who made that place of work very enjoyable with lovable cakes at “Fika tid” and beers at 5 PM. Special thanks go to Magnus for being very helpful in fixing everything broken and to Adine for handling orders and taking care of all those little things you usually don’t notice.

I have to thank all my international friends from all over the world João, Marta, Thiago, Luigi, Alfredo, Roberto, Dmitry, Alireza etc. etc. the list is really long but I have wonderful memories of great moments with all of you…I will never forget!!!

I have to THANK my girlfriend for her strong support during this period especially during the last part “the thesis writing”. I would have never managed without her to arrive at end of this wonderful experience.

Last but not least I want to THANK my family: Mum, Dad and my brother Alessandro. I would like to thank you for your great support in taking crucial decision for my future. I have been happy and proud to show you another corner of the world: “Sweden” that now I feel like a second home. GRAZIE per il Vostro supporto materiale e mentale nel prendere decisioni piuttosto ardue per il mio futuro. Sono stato contento e mi sono sentito anche un po’ orgoglioso di avervi fatto conoscere un nuovo angolo di mondo…che ora più che mai sento essere la mia seconda casa…

8. REFERENCES

1. Mello, L. D.; Kubota, L. T., Review of the use of biosensors as analytical tools in the food and drink industries. *Food chemistry* **2002,** 77, (2), 237-256.
2. Turner, A. P., Current trends in biosensor research and development. *Sensors and Actuators* **1989,** 17, (3-4), 433-450.
3. Turner, A.; Karube, I.; Wilson, G. S., *Biosensors: fundamentals and applications*. Oxford university press: 1987.
4. Banica, F.-G., *Chemical sensors and biosensors: fundamentals and applications*. John Wiley & Sons: 2012.
5. Wang, J., Electrochemical glucose biosensors. *Chemical reviews* **2008,** 108, (2), 814-825.
6. Borisov, S. M.; Wolfbeis, O. S., Optical biosensors. *Chemical reviews* **2008,** 108, (2), 423-461.
7. Abel, A. P.; Weller, M. G.; Duveneck, G. L.; Ehrat, M.; Widmer, H. M., Fiber-optic evanescent wave biosensor for the detection of oligonucleotides. *Analytical Chemistry* **1996,** 68, (17), 2905-2912.
8. Walton, P.; O'Flaherty, M.; Butler, M.; Compton, P., Gravimetric biosensors based on acoustic waves in thin polymer films. *Biosensors and Bioelectronics* **1993,** 8, (9-10), 401-407.
9. Danielsson, B., Calorimetric biosensors. *Journal of biotechnology* **1990,** 15, (3), 187-200.
10. Thévenot, D. R.; Toth, K.; Durst, R. A.; Wilson, G. S., Electrochemical biosensors: recommended definitions and classification. *Biosensors and Bioelectronics* **2001,** 16, (1), 121-131.
11. Newman, J. D.; Turner, A. P., Home blood glucose biosensors: a commercial perspective. *Biosensors and Bioelectronics* **2005,** 20, (12), 2435-2453.
12. Wang, J., Carbon-nanotube based electrochemical biosensors: A review. *Electroanalysis* **2005,** 17, (1), 7-14.
13. Clark, L. C.; Lyons, C., Electrode systems for continuous monitoring in cardiovascular surgery. *Annals of the New York Academy of sciences* **1962,** 102, (1), 29-45.
14. Wang, J., Glucose biosensors: 40 years of advances and challenges. *Electroanalysis* **2001,** 13, (12), 983.
15. Oliver, N.; Toumazou, C.; Cass, A.; Johnston, D., Glucose sensors: a review of current and emerging technology. *Diabetic Medicine* **2009,** 26, (3), 197-210.
16. Albareda-Sirvent, M.; Merkoci, A.; Alegret, S., Configurations used in the design of screen-printed enzymatic biosensors. A review. *Sensors and Actuators B: Chemical* **2000,** 69, (1), 153-163.
17. Yoo, E.-H.; Lee, S.-Y., Glucose biosensors: an overview of use in clinical practice. *Sensors* **2010,** 10, (5), 4558-4576.
18. Atanassov, P.; Apblett, C.; Banta, S.; Brozik, S.; Barton, S. C.; Cooney, M.; Liaw, B. Y.; Mukerjee, S.; Minteer, S. D., Enzymatic biofuel cells. *Interface-Electrochemical Society* **2007,** 16, (2), 28-31.
19. Boyle, G., *Renewable energy: power for a sustainable future*. Taylor & Francis: 1997; Vol. 2.

20. Minteer, S. D.; Liaw, B. Y.; Cooney, M. J., Enzyme-based biofuel cells. *Current opinion in biotechnology* **2007,** 18, (3), 228-234.
21. Calabrese Barton, S.; Gallaway, J.; Atanassov, P., Enzymatic biofuel cells for implantable and microscale devices. *Chemical reviews* **2004,** 104, (10), 4867-4886.
22. Franks, A. E.; Nevin, K. P., Microbial fuel cells, a current review. *Energies* **2010,** 3, (5), 899-919.
23. Leech, D.; Kavanagh, P.; Schuhmann, W., Enzymatic fuel cells: Recent progress. *Electrochimica Acta* **2012,** 84, 223-234.
24. Shleev, S., Quo Vadis, Implanted Fuel Cell? *ChemPlusChem* **2017,** 82, (4), 522-539.
25. Falk, M.; Blum, Z.; Shleev, S., Direct electron transfer based enzymatic fuel cells. *Electrochimica Acta* **2012,** 82, 191-202.
26. Cornish-Bowden, A.; Cornish-Bowden, A., Fundamentals of enzyme kinetics. **2012**.
27. Fischer, E., Einfluss der Configuration auf die Wirkung der Enzyme. *European Journal of Inorganic Chemistry* **1894,** 27, (3), 2985-2993.
28. Fersht, A., A guide to enzyme catalysis and protein folding. *Structure and mechanism in protein science* **1999**, 508-539.
29. Committee, I. N., Units of enzyme activity. Recommendations 1978. Prepared by Karlson P, Bielka H, Horecker BL, Jakoby WB, Keil B, Liébecq C, et al. *Eur J Biochem* **1979,** 97, 319-20.
30. Zamocky, M.; Ludwig, R.; Peterbauer, C.; Hallberg, B.; Divne, C.; Nicholls, P.; Haltrich, D., Cellobiose dehydrogenase-a flavocytochrome from wood-degrading, phytopathogenic and saprotropic fungi. *Current protein and peptide science* **2006,** 7, (3), 255-280.
31. Henriksson, G.; Johansson, G.; Pettersson, G., A critical review of cellobiose dehydrogenases. *Journal of Biotechnology* **2000,** 78, (2), 93-113.
32. Ludwig, R.; Harreither, W.; Tasca, F.; Gorton, L., Cellobiose dehydrogenase: a versatile catalyst for electrochemical applications. *ChemPhysChem* **2010,** 11, (13), 2674-2697.
33. Ludwig, R.; Ortiz, R.; Schulz, C.; Harreither, W.; Sygmund, C.; Gorton, L., Cellobiose dehydrogenase modified electrodes: advances by materials science and biochemical engineering. *Analytical and bioanalytical chemistry* **2013,** 405, (11), 3637-3658.
34. Stoica, L.; Ludwig, R.; Haltrich, D.; Gorton, L., Third-generation biosensor for lactose based on newly discovered cellobiose dehydrogenase. *Analytical chemistry* **2006,** 78, (2), 393-398.
35. Cameron, M. D.; Aust, S. D., Cellobiose dehydrogenase–an extracellular fungal flavocytochrome. *Enzyme and microbial technology* **2001,** 28, (2), 129-138.
36. Schulz, C.; Ludwig, R.; Micheelsen, P. O.; Silow, M.; Toscano, M. D.; Gorton, L., Enhancement of enzymatic activity and catalytic current of cellobiose dehydrogenase by calcium ions. *Electrochemistry Communications* **2012,** 17, (Supplement C), 71-74.
37. Kielb, P.; Sezer, M.; Katz, S.; Lopez, F.; Schulz, C.; Gorton, L.; Ludwig, R.; Wollenberger, U.; Zebger, I.; Weidinger, I. M., Spectroscopic Observation of Calcium-Induced Reorientation of Cellobiose Dehydrogenase Immobilized on Electrodes and its Effect on Electrocatalytic Activity. *ChemPhysChem* **2015,** 16, (9), 1960-1968.

38. Kracher, D.; Zahma, K.; Schulz, C.; Sygmund, C.; Gorton, L.; Ludwig, R., Inter-domain electron transfer in cellobiose dehydrogenase: modulation by pH and divalent cations. *The FEBS Journal* **2015,** 282, (16), 3136-3148.
39. Tavahodi, M.; Ortiz, R.; Schulz, C.; Ekhtiari, A.; Ludwig, R.; Haghighi, B.; Gorton, L., Direct Electron Transfer of Cellobiose Dehydrogenase on Positively Charged Polyethyleneimine Gold Nanoparticles. *ChemPlusChem* **2017,** 82, (4), 546-552.
40. Igarashi, K.; Yoshida, M.; Matsumura, H.; Nakamura, N.; Ohno, H.; Samejima, M.; Nishino, T., Electron transfer chain reaction of the extracellular flavocytochrome cellobiose dehydrogenase from the basidiomycete Phanerochaete chrysosporium. *The FEBS journal* **2005,** 272, (11), 2869-2877.
41. Harreither, W.; Sygmund, C.; Augustin, M.; Narciso, M.; Rabinovich, M. L.; Gorton, L.; Haltrich, D.; Ludwig, R., Catalytic properties and classification of cellobiose dehydrogenases from ascomycetes. *Applied and environmental microbiology* **2011,** 77, (5), 1804-1815.
42. Tasca, F.; Gorton, L.; Harreither, W.; Haltrich, D.; Ludwig, R.; Nöll, G., Comparison of direct and mediated electron transfer for cellobiose dehydrogenase from Phanerochaete sordida. *Analytical chemistry* **2009,** 81, (7), 2791-2798.
43. Hallberg, B. M.; Henriksson, G.; Pettersson, G.; Divne, C., Crystal structure of the flavoprotein domain of the extracellular flavocytochrome cellobiose dehydrogenase. *Journal of molecular biology* **2002,** 315, (3), 421-434.
44. Hallberg, B. M.; Bergfors, T.; Bäckbro, K.; Pettersson, G.; Henriksson, G.; Divne, C., A new scaffold for binding haem in the cytochrome domain of the extracellular flavocytochrome cellobiose dehydrogenase. *Structure* **2000,** 8, (1), 79-88.
45. Tan, T.-C.; Kracher, D.; Gandini, R.; Sygmund, C.; Kittl, R.; Haltrich, D.; Hällberg, B. M.; Ludwig, R.; Divne, C., Structural basis for cellobiose dehydrogenase action during oxidative cellulose degradation. *Nature communications* **2015,** 6, 7542.
46. Guo, L.-H.; Allen, H.; Hill, O., Direct electrochemistry of proteins and enzymes. *Advances in inorganic chemistry* **1991,** 36, 341-375.
47. Hill, H., The electrochemistry of metalloproteins. *Pure and Applied Chemistry* **1990,** 62, (6), 1047-1050.
48. Bollella, P.; Ludwig, R.; Gorton, L., Cellobiose dehydrogenase: Insights on the nanostructuration of electrodes for improved development of biosensors and biofuel cells. *Applied Materials Today* **2017,** 9, (Supplement C), 319-332.
49. Kawai, S.; Goda-Tsutsumi, M.; Yakushi, T.; Kano, K.; Matsushita, K., Heterologous overexpression and characterization of a flavoprotein-cytochrome c complex fructose dehydrogenase of Gluconobacter japonicus NBRC3260. *Applied and environmental microbiology* **2013,** 79, (5), 1654-1660.
50. Yamada, Y.; Aida, K.; Uemura, T., A new enzyme, D-fructose dehydrogenase. *Agricultural and Biological Chemistry* **1966,** 30, (1), 95-96.
51. Ikeda, T.; Matsushita, F.; Senda, M., Amperometric fructose sensor based on direct bioelectrocatalysis. *Biosensors and Bioelectronics* **1991,** 6, (4), 299-304.
52. Solomon, E. I.; Sundaram, U. M.; Machonkin, T. E., Multicopper oxidases and oxygenases. *Chemical reviews* **1996,** 96, (7), 2563-2606.
53. Solomon, E. I.; Baldwin, M. J.; Lowery, M. D., Electronic structures of active sites in copper proteins: contributions to reactivity. *Chemical Reviews* **1992,** 92, (4), 521-542.

54. Shleev, S.; Tkac, J.; Christenson, A.; Ruzgas, T.; Yaropolov, A. I.; Whittaker, J. W.; Gorton, L., Direct electron transfer between copper-containing proteins and electrodes. *Biosensors and Bioelectronics* **2005,** 20, (12), 2517-2554.
55. Morozova, O.; Shumakovich, G.; Gorbacheva, M.; Shleev, S.; Yaropolov, A., "Blue" laccases. *Biochemistry (Moscow)* **2007,** 72, (10), 1136-1150.
56. Nar, H.; Messerschmidt, A.; Huber, R.; van de Kamp, M.; Canters, G. W., Crystal structure analysis of oxidized Pseudomonas aeruginosa azurin at pH 5· 5 and pH 9· 0: A pH-induced conformational transition involves a peptide bond flip. *Journal of molecular biology* **1991,** 221, (3), 765-772.
57. Avigad, G.; Amaral, D.; Asensio, C.; Horecker, B., The D-galactose oxidase of Polyporus circinatus. *Journal of Biological Chemistry* **1962,** 237, (9), 2736-2743.
58. Nelson, J.; Dawson, C., Tyrosinase. *Advances in Enzymology and Related Areas of Molecular Biology, Volume 4* **2006**, 99-152.
59. Yaropolov, A.; Skorobogat'Ko, O.; Vartanov, S.; Varfolomeyev, S., Laccase. *Applied Biochemistry and Biotechnology* **1994,** 49, (3), 257-280.
60. Mayer, A. M.; Staples, R. C., Laccase: new functions for an old enzyme. *Phytochemistry* **2002,** 60, (6), 551-565.
61. Thurston, C. F., The structure and function of fungal laccases. *Microbiology* **1994,** 140, (1), 19-26.
62. Sharma, P.; Goel, R.; Capalash, N., Bacterial laccases. *World Journal of Microbiology and Biotechnology* **2007,** 23, (6), 823-832.
63. Shleev, S.; Jarosz-Wilkolazka, A.; Khalunina, A.; Morozova, O.; Yaropolov, A.; Ruzgas, T.; Gorton, L., Direct electron transfer reactions of laccases from different origins on carbon electrodes. *Bioelectrochemistry* **2005,** 67, (1), 115-124.
64. Frasconi, M.; Favero, G.; Boer, H.; Koivula, A.; Mazzei, F., Kinetic and biochemical properties of high and low redox potential laccases from fungal and plant origin. *Biochimica et Biophysica Acta (BBA)-Proteins and Proteomics* **2010,** 1804, (4), 899-908.
65. Mano, N.; de Poulpiquet, A., O2 Reduction in Enzymatic Biofuel Cells. *Chemical Reviews* **2017**.
66. Dagys, M.; Laurynėnas, A.; Ratautas, D.; Kulys, J.; Vidžiūnaitė, R.; Talaikis, M.; Niaura, G.; Marcinkevičienė, L.; Meškys, R.; Shleev, S., Oxygen electroreduction catalysed by laccase wired to gold nanoparticles via the trinuclear copper cluster. *Energy & Environmental Science* **2017,** 10, (2), 498-502.
67. Johannes, C.; Majcherczyk, A., Laccase activity tests and laccase inhibitors. *Journal of Biotechnology* **2000,** 78, (2), 193-199.
68. Newton, M. D.; Sumi, H.; Skourtis, S. S.; Beratan, D. N.; Vanmaekelbergh, D.; Hammes-Schiffer, S.; Piotrowiak, P.; Endicott, J. F.; Fox, M. A.; Andersson, A.-M., Electron transfer in chemistry. **2001**.
69. Bartlett, P. N., *Bioelectrochemistry: fundamentals, experimental techniques and applications*. John Wiley & Sons: 2008.
70. Kuznetsov, A. M.; Ulstrup, J., *Electron transfer in chemistry and biology: an introduction to the theory*. John Wiley & Sons Ltd: 1999.
71. McNaught, A. D.; McNaught, A. D., *Compendium of chemical terminology*. Blackwell Science Oxford: 1997; Vol. 1669.

72. Taube, H.; Myers, H.; Rich, R. L., Observations on the Mechanism of Electron Transfer in Solution1. *Journal of the American Chemical Society* **1953,** 75, (16), 4118-4119.
73. Marcus, R., On the Theory of Oxidation-Reduction Reactions Involving Electron Transfer. II. Applications to Data on the Rates of Isotopic Exchange Reactions. *The Journal of Chemical Physics* **1957,** 26, (4), 867-871.
74. Marcus, R. A., Electron transfer reactions in chemistry. Theory and experiment. *Reviews of Modern Physics* **1993,** 65, (3), 599.
75. Marcus, R. A., Chemical and electrochemical electron-transfer theory. *Annual Review of Physical Chemistry* **1964,** 15, (1), 155-196.
76. Marcus, R., Electron transfer at electrodes and in solution: comparison of theory and experiment. *Electrochimica Acta* **1968,** 13, (5), 995-1004.
77. Frew, J. E.; Hill, H. A. O., Direct and indirect electron transfer between electrodes and redox proteins. *The FEBS Journal* **1988,** 172, (2), 261-269.
78. Armstrong, F. A.; Hill, H. A. O.; Walton, N. J., Direct electrochemistry of redox proteins. *Accounts of Chemical Research* **1988,** 21, (11), 407-413.
79. Michaelis, L.; Menten, M., Die Kinetik der InwertinWirkung. *Biochem.* **1913**, (49), 333-369.
80. Briggs, G. E.; Haldane, J. B. S., A note on the kinetics of enzyme action. *Biochemical journal* **1925,** 19, (2), 338.
81. Lineweaver, H.; Burk, D., The determination of enzyme dissociation constants. *Journal of the American Chemical Society* **1934,** 56, (3), 658-666.
82. Eadie, G., The inhibition of cholinesterase by physostigmine and prostigmine. *Journal of Biological Chemistry* **1942,** 146, (1), 85-93.
83. Hofstee, B., On the evaluation of the constants Vm and Km in enzyme reactions. *Science* **1952,** 116, (3013), 329-331.
84. Hanes, C. S., Studies on plant amylases: the effect of starch concentration upon the velocity of hydrolysis by the amylase of germinated barley. *Biochemical Journal* **1932,** 26, (5), 1406.
85. Cleland, W., The kinetics of enzyme-catalyzed reactions with two or more substrates or products: I. Nomenclature and rate equations. *Biochimica et Biophysica Acta (BBA)-Specialized Section on Enzymological Subjects* **1963,** 67, 104-137.
86. Cleland, W., The kinetics of enzyme-catalyzed reactions with two or more substrates or products: II. Inhibition: nomenclature and theory. *Biochimica et Biophysica Acta (BBA)-Specialized Section on Enzymological Subjects* **1963,** 67, 173-187.
87. Cleland, W., The kinetics of enzyme-catalyzed reactions with two or more substrates or products: III. Prediction of initial velocity and inhibition patterns by inspection. *Biochimica et Biophysica Acta (BBA)-Specialized Section on Enzymological Subjects* **1963,** 67, 188-196.
88. Bard, A. J.; Faulkner, L. R.; Leddy, J.; Zoski, C. G., *Electrochemical methods: fundamentals and applications*. wiley New York: 1980; Vol. 2.
89. Zoski, C. G., *Handbook of electrochemistry*. Elsevier: 2006.
90. Cottrell, F. G., Der Reststrom bei galvanischer Polarisation, betrachtet als ein Diffusionsproblem. *Zeitschrift für Physikalische Chemie* **1903,** 42, (1), 385-431.
91. Ŗužička, J.; Hansen, E., Flow injection analyses: Part I. A new concept of fast continuous flow analysis. *Analytica Chimica Acta* **1975,** 78, (1), 145-157.

92. Růžička, J.; Stewart, J., Flow injection analysis: Part II. Ultrafast determination of phosphorus in plant material by continuous flow spectrophotometry. *Analytica Chimica Acta* **1975,** 79, 79-91.
93. Ruzicka, J.; Hansen, E. H., *Flow injection analysis*. John Wiley & Sons: 1988; Vol. 62.
94. Appelqvist, R.; Marko-Varga, G.; Gorton, L.; Torstensson, A.; Johansson, G., Enzymatic determination of glucose in a flow system by catalytic oxidation of the nicotinamide coenzyme at a modified electrode. *Analytica Chimica Acta* **1985,** 169, 237-247.
95. Glauert, M., The wall jet. *Journal of Fluid Mechanics* **1956,** 1, (6), 625-643.
96. Yamada, J.; Matsuda, H., Limiting diffusion currents in hydrodynamic voltammetry: III. Wall jet electrodes. *Journal of Electroanalytical Chemistry and Interfacial Electrochemistry* **1973,** 44, (2), 189-198.
97. Matheson, L.; Nichols, N., The cathode ray oscillograph applied to the dropping mercury electrode. *Transactions of The Electrochemical Society* **1938,** 73, (1), 193-210.
98. Randles, J. E. B., A cathode ray polarograph. Part II.—The current-voltage curves. *Transactions of the Faraday Society* **1948,** 44, 327-338.
99. Ševčik, A., Oscillographic polarography with periodical triangular voltage. *Collection of Czechoslovak Chemical Communications* **1948,** 13, 349-377.
100. Nicholson, R. S.; Shain, I., Theory of stationary electrode polarography. Single scan and cyclic methods applied to reversible, irreversible, and kinetic systems. *Analytical Chemistry* **1964,** 36, (4), 706-723.
101. Klingler, R.; Kochi, J., Electron-transfer kinetics from cyclic voltammetry. Quantitative description of electrochemical reversibility. *The Journal of Physical Chemistry* **1981,** 85, (12), 1731-1741.
102. Lavagnini, I.; Antiochia, R.; Magno, F., An extended method for the practical evaluation of the standard rate constant from cyclic voltammetric data. *Electroanalysis* **2004,** 16, (6), 505-506.
103. Love, J. C.; Estroff, L. A.; Kriebel, J. K.; Nuzzo, R. G.; Whitesides, G. M., Self-assembled monolayers of thiolates on metals as a form of nanotechnology. *Chemical reviews* **2005,** 105, (4), 1103-1170.
104. McCreery, R. L., Advanced carbon electrode materials for molecular electrochemistry. *Chem. Rev* **2008,** 108, (7), 2646-2687.
105. Bollella, P.; Fusco, G.; Tortolini, C.; Sanzò, G.; Favero, G.; Gorton, L.; Antiochia, R., Beyond graphene: Electrochemical sensors and biosensors for biomarkers detection. *Biosensors and Bioelectronics* **2017,** 89, 152-166.
106. Mazzei, F.; Favero, G.; Bollella, P.; Tortolini, C.; Mannina, L.; Conti, M. E.; Antiochia, R., Recent trends in electrochemical nanobiosensors for environmental analysis. *International Journal of Environment and Health* **2015,** 7, (3), 267-291.
107. Banks, C. E.; Moore, R. R.; Davies, T. J.; Compton, R. G., Investigation of modified basal plane pyrolytic graphite electrodes: definitive evidence for the electrocatalytic properties of the ends of carbon nanotubes. *Chemical Communications* **2004**, (16), 1804-1805.
108. Engstrom, R. C., Electrochemical pretreatment of glassy carbon electrodes. *Analytical Chemistry* **1982,** 54, (13), 2310-2314.
109. Renedo, O. D.; Alonso-Lomillo, M.; Martinez, M. A., Recent developments in the field of screen-printed electrodes and their related applications. *Talanta* **2007,** 73, (2), 202-219.

110. Taleat, Z.; Khoshroo, A.; Mazloum-Ardakani, M., Screen-printed electrodes for biosensing: a review (2008–2013). *Microchimica Acta* **2014,** 181, (9-10), 865-891.
111. Carvalhal, R. F.; Sanches Freire, R.; Kubota, L. T., Polycrystalline Gold Electrodes: A Comparative Study of Pretreatment Procedures Used for Cleaning and Thiol Self-Assembly Monolayer Formation. *Electroanalysis* **2005,** 17, (14), 1251-1259.
112. Hoogvliet, J.; Dijksma, M.; Kamp, B.; Van Bennekom, W., Electrochemical pretreatment of polycrystalline gold electrodes to produce a reproducible surface roughness for self-assembly: a study in phosphate buffer pH 7.4. *Analytical chemistry* **2000,** 72, (9), 2016-2021.
113. Zeng, S.; Yong, K.-T.; Roy, I.; Dinh, X.-Q.; Yu, X.; Luan, F., A review on functionalized gold nanoparticles for biosensing applications. *Plasmonics* **2011,** 6, (3), 491.
114. Saha, K.; Agasti, S. S.; Kim, C.; Li, X.; Rotello, V. M., Gold nanoparticles in chemical and biological sensing. *Chemical reviews* **2012,** 112, (5), 2739-2779.
115. Freestone, I.; Meeks, N.; Sax, M.; Higgitt, C., The Lycurgus cup—a roman nanotechnology. *Gold Bulletin* **2007,** 40, (4), 270-277.
116. Faraday, M., The Bakerian lecture: experimental relations of gold (and other metals) to light. *Philosophical Transactions of the Royal Society of London* **1857,** 147, 145-181.
117. Zsigmondy, R., Uber losliches Gold. *Zeitschr. Elektrochemie4* **1898,** 546.
118. Svedberg, T.; Pedersen, K. O., The ultracentrifuge. *The Ultracentrifuge.* **1940**.
119. Mie, G., Beiträge zur Optik trüber Medien, speziell kolloidaler Metallösungen. *Annalen der physik* **1908,** 330, (3), 377-445.
120. Daniel, M.-C.; Astruc, D., Gold nanoparticles: assembly, supramolecular chemistry, quantum-size-related properties, and applications toward biology, catalysis, and nanotechnology. *Chemical reviews* **2004,** 104, (1), 293-346.
121. Bollella, P.; Schulz, C.; Favero, G.; Mazzei, F.; Ludwig, R.; Gorton, L.; Antiochia, R., Green Synthesis and Characterization of Gold and Silver Nanoparticles and their Application for Development of a Third Generation Lactose Biosensor. *Electroanalysis* **2017,** 29, (1), 77-86.
122. Bollella, P.; Mazzei, F.; Favero, G.; Fusco, G.; Ludwig, R.; Gorton, L.; Antiochia, R., Improved DET communication between cellobiose dehydrogenase and a gold electrode modified with a rigid self-assembled monolayer and green metal nanoparticles: The role of an ordered nanostructuration. *Biosensors and Bioelectronics* **2017,** 88, (Supplement C), 196-203.
123. El-Deab, M. S.; Ohsaka, T., An extraordinary electrocatalytic reduction of oxygen on gold nanoparticles-electrodeposited gold electrodes. *Electrochemistry Communications* **2002,** 4, (4), 288-292.
124. Dai, X.; Compton, R. G., Direct electrodeposition of gold nanoparticles onto indium tin oxide film coated glass: application to the detection of arsenic (III). *Analytical sciences* **2006,** 22, (4), 567-570.
125. Bollella, P.; Gorton, L.; Ludwig, R.; Antiochia, R., A Third Generation Glucose Biosensor Based on Cellobiose Dehydrogenase Immobilized on a Glassy Carbon Electrode Decorated with Electrodeposited Gold Nanoparticles: Characterization and Application in Human Saliva. *Sensors* **2017,** 17, (8), 1912.

126. Haiss, W.; Thanh, N. T.; Aveyard, J.; Fernig, D. G., Determination of size and concentration of gold nanoparticles from UV− Vis spectra. *Analytical chemistry* **2007,** 79, (11), 4215-4221.
127. Mohanraj, V.; Chen, Y., Nanoparticles-a review. *Tropical Journal of Pharmaceutical Research* **2006,** 5, (1), 561-573.
128. Zhou, W.; Wang, Z. L., *Scanning microscopy for nanotechnology: techniques and applications*. Springer science & business media: 2007.
129. Wang, Z., Transmission electron microscopy of shape-controlled nanocrystals and their assemblies. In ACS Publications: 2000.
130. Du Toit, H.; Di Lorenzo, M., Electrodeposited highly porous gold microelectrodes for the direct electrocatalytic oxidation of aqueous glucose. *Sensors and Actuators B: Chemical* **2014,** 192, 725-729.
131. Du Toit, H.; Di Lorenzo, M., Glucose oxidase directly immobilized onto highly porous gold electrodes for sensing and fuel cell applications. *Electrochimica Acta* **2014,** 138, 86-92.
132. Sanzó, G.; Taurino, I.; Antiochia, R.; Gorton, L.; Favero, G.; Mazzei, F.; De Micheli, G.; Carrara, S., Bubble electrodeposition of gold porous nanocorals for the enzymatic and non-enzymatic detection of glucose. *Bioelectrochemistry* **2016,** 112, 125-131.
133. Yang, W.; Ratinac, K. R.; Ringer, S. P.; Thordarson, P.; Gooding, J. J.; Braet, F., Carbon nanomaterials in biosensors: should you use nanotubes or graphene? *Angewandte Chemie International Edition* **2010,** 49, (12), 2114-2138.
134. Gogotsi, Y.; Presser, V., *Carbon nanomaterials*. CRC press: 2013.
135. Iijima, S.; Ajayan, P.; Ichihashi, T., Growth model for carbon nanotubes. *Physical review letters* **1992,** 69, (21), 3100.
136. Ajayan, P.; Lijima, S., Smallest carbon nanotube. *Nature* **1992,** 358, (6381), 23-23.
137. Iijima, S., Growth of carbon nanotubes. *Materials Science and Engineering: B* **1993,** 19, (1-2), 172-180.
138. Hirsch, A., Functionalization of single-walled carbon nanotubes. *Angewandte Chemie International Edition* **2002,** 41, (11), 1853-1859.
139. Neto, A. C.; Guinea, F.; Peres, N. M.; Novoselov, K. S.; Geim, A. K., The electronic properties of graphene. *Reviews of modern physics* **2009,** 81, (1), 109.
140. Carbone, M.; Gorton, L.; Antiochia, R., An Overview of the Latest Graphene-Based Sensors for Glucose Detection: the Effects of Graphene Defects. *Electroanalysis* **2015,** 27, (1), 16-31.
141. Geim, A. K.; Novoselov, K. S., The rise of graphene. *Nature materials* **2007,** 6, (3), 183-191.
142. Geim, A. K., Graphene: status and prospects. *science* **2009,** 324, (5934), 1530-1534.
143. Ulman, A., Formation and structure of self-assembled monolayers. *Chemical reviews* **1996,** 96, (4), 1533-1554.
144. Schwartz, D. K., Mechanisms and kinetics of self-assembled monolayer formation. *Annual Review of Physical Chemistry* **2001,** 52, (1), 107-137.
145. Prime, K. L.; Whitesides, G. M., Self-assembled organic monolayers: model systems for studying adsorption of proteins at surfaces. *Science* **1991,** 252, (5009), 1164.
146. Downard, A. J., Electrochemically assisted covalent modification of carbon electrodes. *Electroanalysis* **2000,** 12, (14), 1085-1096.

147. Bahr, J. L.; Yang, J.; Kosynkin, D. V.; Bronikowski, M. J.; Smalley, R. E.; Tour, J. M., Functionalization of carbon nanotubes by electrochemical reduction of aryl diazonium salts: a bucky paper electrode. *Journal of the American Chemical Society* **2001,** 123, (27), 6536-6542.
148. Ortiz, R.; Ludwig, R.; Gorton, L., Highly Efficient Membraneless Glucose Bioanode Based on Corynascus thermophilus Cellobiose Dehydrogenase on Aryl Diazonium-Activated Single-Walled Carbon Nanotubes. *ChemElectroChem* **2014,** 1, (11), 1948-1956.
149. Liu, G.; Böcking, T.; Gooding, J. J., Diazonium salts: Stable monolayers on gold electrodes for sensing applications. *Journal of Electroanalytical Chemistry* **2007,** 600, (2), 335-344.
150. Gooding, J. J., Advances in interfacial design for electrochemical biosensors and sensors: aryl diazonium salts for modifying carbon and metal electrodes. *Electroanalysis* **2008,** 20, (6), 573-582.
151. Barlett, P.; Cooper, J., A review of the immobilization of enzymes in electropolymerized films. *Journal of Electroanalytical Chemistry* **1993,** 362, (1-2), 1-12.
152. Cosnier, S., Biomolecule immobilization on electrode surfaces by entrapment or attachment to electrochemically polymerized films. A review. *Biosensors and Bioelectronics* **1999,** 14, (5), 443-456.
153. Putzbach, W.; Ronkainen, N. J., Immobilization techniques in the fabrication of nanomaterial-based electrochemical biosensors: A review. *Sensors* **2013,** 13, (4), 4811-4840.
154. Nanduri, V.; Sorokulova, I. B.; Samoylov, A. M.; Simonian, A. L.; Petrenko, V. A.; Vodyanoy, V., Phage as a molecular recognition element in biosensors immobilized by physical adsorption. *Biosensors and Bioelectronics* **2007,** 22, (6), 986-992.
155. Gregg, B. A.; Heller, A., Cross-linked redox gels containing glucose oxidase for amperometric biosensor applications. *Analytical Chemistry* **1990,** 62, (3), 258-263.
156. Sassolas, A.; Blum, L. J.; Leca-Bouvier, B. D., Immobilization strategies to develop enzymatic biosensors. *Biotechnology advances* **2012,** 30, (3), 489-511.
157. Gupta, R.; Chaudhury, N., Entrapment of biomolecules in sol–gel matrix for applications in biosensors: Problems and future prospects. *Biosensors and Bioelectronics* **2007,** 22, (11), 2387-2399.
158. Ichimura, K., A convenient photochemical method to immobilize enzymes. *Journal of Polymer Science Part A: Polymer Chemistry* **1984,** 22, (11), 2817-2828.
159. Rubianes, M. D.; Rivas, G. A., Enzymatic biosensors based on carbon nanotubes paste electrodes. *Electroanalysis* **2005,** 17, (1), 73-78.
160. Newman, J. D.; Setford, S. J., Enzymatic biosensors. *Molecular biotechnology* **2006,** 32, (3), 249-268.
161. Gorton, L.; Lindgren, A.; Larsson, T.; Munteanu, F.; Ruzgas, T.; Gazaryan, I., Direct electron transfer between heme-containing enzymes and electrodes as basis for third generation biosensors. *Analytica Chimica Acta* **1999,** 400, (1), 91-108.
162. Karyakin, A. A.; Kotel'nikova, E. A.; Lukachova, L. V.; Karyakina, E. E.; Wang, J., Optimal environment for glucose oxidase in perfluorosulfonated ionomer membranes: improvement of first-generation biosensors. *Analytical chemistry* **2002,** 74, (7), 1597-1603.

163. Scheller, F. W.; Schubert, F.; Neumann, B.; Pfeiffer, D.; Hintsche, R.; Dransfeld, I.; Wollenberger, U.; Renneberg, R.; Warsinke, A.; Johansson, G., Second generation biosensors. *Biosensors and Bioelectronics* **1991,** 6, (3), 245-253.
164. Karyakin, A. A.; Gitelmacher, O. V.; Karyakina, E. E., Prussian blue-based first-generation biosensor. A sensitive amperometric electrode for glucose. *Analytical chemistry* **1995,** 67, (14), 2419-2423.
165. Heller, A.; Maidan, R.; Wang, D., Amperometric biosensors based on three-dimensional hydrogel-forming epoxy networks. *Sensors and Actuators B: Chemical* **1993,** 13, (1-3), 180-183.
166. Freire, R. S.; Pessoa, C. A.; Mello, L. D.; Kubota, L. T., Direct electron transfer: an approach for electrochemical biosensors with higher selectivity and sensitivity. *Journal of the Brazilian Chemical Society* **2003,** 14, (2), 230-243.
167. Gorton, L.; Jönsson-Pettersson, G.; Csöregi, E.; Johansson, K.; Domínguez, E.; Marko-Varga, G., Amperometric biosensors based on an apparent direct electron transfer between electrodes and immobilized peroxidases. Plenary lecture. *Analyst* **1992,** 117, (8), 1235-1241.
168. Ghindilis, A. L.; Atanasov, P.; Wilkins, E., Enzyme-catalyzed direct electron transfer: Fundamentals and analytical applications. *Electroanalysis* **1997,** 9, (9), 661-674.
169. Eddowes, M. J.; Hill, H. A. O., Novel method for the investigation of the electrochemistry of metalloproteins: cytochrome c. *Journal of the Chemical Society, Chemical Communications* **1977**, (21), 771b-772.
170. Yeh, P.; Kuwana, T., Reversible electrode reaction of cytochrome c. *Chemistry Letters* **1977,** 6, (10), 1145-1148.
171. Laurinavicius, V.; Razumiene, J.; Kurtinaitiene, B.; Lapenaite, I.; Bachmatova, I.; Marcinkeviciene, L.; Meskys, R.; Ramanavicius, A., Bioelectrochemical application of some PQQ-dependent enzymes. *Bioelectrochemistry* **2002,** 55, (1), 29-32.
172. Zafar, M. N.; Beden, N.; Leech, D.; Sygmund, C.; Ludwig, R.; Gorton, L., Characterization of different FAD-dependent glucose dehydrogenases for possible use in glucose-based biosensors and biofuel cells. *Analytical and bioanalytical chemistry* **2012,** 402, (6), 2069-2077.
173. Carrette, L.; Friedrich, K.; Stimming, U., Fuel cells–fundamentals and applications. *Fuel cells* **2001,** 1, (1), 5-39.
174. Bullen, R. A.; Arnot, T.; Lakeman, J.; Walsh, F., Biofuel cells and their development. *Biosensors and Bioelectronics* **2006,** 21, (11), 2015-2045.
175. Davis, F.; Higson, S. P., Biofuel cells—recent advances and applications. *Biosensors and Bioelectronics* **2007,** 22, (7), 1224-1235.
176. Moehlenbrock, M. J.; Minteer, S. D., Extended lifetime biofuel cells. *Chemical Society Reviews* **2008,** 37, (6), 1188-1196.
177. Rasmussen, M.; Abdellaoui, S.; Minteer, S. D., Enzymatic biofuel cells: 30 years of critical advancements. *Biosensors and Bioelectronics* **2016,** 76, 91-102.
178. Heller, A., Miniature biofuel cells. *Physical Chemistry Chemical Physics* **2004,** 6, (2), 209-216.
179. Willner, I.; Yan, Y. M.; Willner, B.; Tel-Vered, R., Integrated Enzyme-Based Biofuel Cells–A Review. *Fuel Cells* **2009,** 9, (1), 7-24.
180. Wait, A. F.; Parkin, A.; Morley, G. M.; dos Santos, L.; Armstrong, F. A., Characteristics of enzyme-based hydrogen fuel cells using an oxygen-tolerant

hydrogenase as the anodic catalyst. *The Journal of Physical Chemistry C* **2010,** 114, (27), 12003-12009.
181. Karyakin, A.; Morozov, S.; Karyakina, E.; Zorin, N.; Perelygin, V.; Cosnier, S., Hydrogenase electrodes for fuel cells. In Portland Press Limited: 2005.
182. Luckarift, H. R.; Atanassov, P. B.; Johnson, G. R., *Enzymatic fuel cells: From fundamentals to applications*. John Wiley & Sons: 2014.
183. Halámková, L.; Halámek, J.; Bocharova, V.; Szczupak, A.; Alfonta, L.; Katz, E., Implanted biofuel cell operating in a living snail. *Journal of the American Chemical Society* **2012,** 134, (11), 5040-5043.
184. Guiseppi-Elie, A.; Lei, C.; Baughman, R. H., Direct electron transfer of glucose oxidase on carbon nanotubes. *Nanotechnology* **2002,** 13, (5), 559.
185. Coman, V.; Ludwig, R.; Harreither, W.; Haltrich, D.; Gorton, L.; Ruzgas, T.; Shleev, S., A Direct Electron Transfer-Based Glucose/Oxygen Biofuel Cell Operating in Human Serum. *Fuel cells* **2010,** 10, (1), 9-16.

Paper I

Full Paper

Wiley Online Library

ELECTROANALYSIS

DOI: 10.1002/elan.201600476

SPECIAL ISSUE

Green Synthesis and Characterization of Gold and Silver Nanoparticles and their Application for Development of a Third Generation Lactose Biosensor

Paolo Bollella,[a] Christopher Schulz,[b] Gabriele Favero,[a] Franco Mazzei,[a] Roland Ludwig,[c] Lo Gorton,[b] and Riccarda Antiochia*[a]

Abstract: In this paper we report on a facile, cost effective and environmental friendly green synthesis method of gold and silver nanoparticles (NPs) by using quercetin as reducing agent. The obtained NPs were characterized by transmission electron microscopy (TEM), energy dispersive spectroscopy (EDS), dynamic light scattering (DLS) and UV-Vis spectroscopy and parameters such as pH, ionic strength and temperature, effectively affecting shape and size of NPs, have been carefully studied and optimized. The obtained results showed that the synthesized NPs were circular in shape with an average diameter of 5 and 8 nm for the AuNPs and the AgNPs, respectively. The "green" NPs, showing increased electroactive areas (A_{EA}) and electronic transfer rate constants (k^0), were successively used to fabricate a novel third generation lactose biosensor based on cellobiose dehydrogenase from *Trametes villosa* (*Tv*CDH). The *Tv*CDH/AuNPs based lactose biosensor revealed the best results showing very efficient DET and a detection limit for lactose of 3.5 mM, a large linear range from 10 to 300 mM, a high sensitivity (5.4 $\mu A\,mM^{-1}\,cm^{-2}$) and long-term stability.

Keywords: Green synthesis · Gold nanoparticles · Silver nanoparticles · Lactose biosensor · Cellobiose dehydrogenase

1 Introduction

Nanotechnology is one of the most active areas of modern research. New applications of nanoparticles (NPs) and nanomaterials are emerging rapidly. In the last decade metal nanoparticles (MNPs) have played an important role in the development of biofuel cells, ion batteries and (bio)sensing devices [1–4] especially in the medical diagnostics field. MNPs are commonly described as nanosized metals with dimensions within 1–100 nm with many opto-electronic properties such as larger surface area-volume ratio compared to their corresponding bulk material, large surface energies, plasmonic excitation and quantum confinement [5]. Historically, gold, silver and copper MNPs were the most largely synthesized, because of the particular properties of the noble metals, followed by iron oxide MNPs for their magnetic properties [6–8].

The integration of green chemistry principles to nanotechnology is one of the key issues of nanoscience research. Green synthesis has become the way for a sustainable and safe production of NPs and it has been proven to be an advantegeous method due to its slower kinetics, easy manipulation and control over crystal growth for stabilization of NPs [9,10].

The use of environmentally friendly materials, in particular plant extracts, fungi, bacteria and enzymes, for the synthesis of MNPs showed numerous benefits in pharmaceutical and other biomedical applications [11–13]. Green synthesis resulted also in being very cost effective and therefore can be used as a cheep suitable alternative for large-scale production of MNPs.

Several approaches have been reported in the literature using extracts from a variety of different plant species in combination with a variety of acids and metal salts. For example aqueous extracts of *Ferocactus echidne* have been used to reduce silver nitrate ($AgNO_3$) to form silver nanoparticles (AgNPs) within 6 h. It has been reported that both polyphenols and ascorbic acid present in aqueous *Ferocactus echidne* extracts can easily reduce silver ions and can also act as capping agents to prevent the agglomeration of AgNPs [12]. Recently, gold nanoparticles (AuNPs) have been synthesized within 30 min by reducing sodium tetrachloroaurate ($NaAuCl_4$) with extracts of

[a] P. Bollella, G. Favero, F. Mazzei, R. Antiochia
Department of Chemistry and Drug Technologies, Sapienza University of Rome, P.le Aldo Moro 5, 00185 – Rome, Italy
Tel.: +39 06 49913735
Fax: +39 06 49913133
*e-mail: riccarda.antiochia@uniroma1.it

[b] C. Schulz, L. Gorton
Department of Analytical Chemistry/Biochemistry and Structural Biology, Lund University, P. O.Box 124, SE-221 00 Lund, Sweden

[c] R. Ludwig
Food Biotechnology Laboratory, Department of Food Science and Technology, BOKU – University of Natural Resources and Life Sciences, Muthgasse 18, A-1190 Vienna, Austria

Supporting information for this article is available on the WWW under http://dx.doi.org/10.1002/elan.201600476

Darjeeling tea leaves. In that study it was demonstrated that catechins present in the extract acted as reducing agents, with epicatechins and epigallocatechins as stabilizing agents [14]. Alternatively, AuNPs were obtained by reduction of tetrachloroauric acid ($HAuCl_4$) with gallic acid at room temperature within 30 min. These NPs were successively modified with 3'- and 5'-alkanethiol-capped 12-base oligonucleotides to form two different nucleic acid probes [15]. The flower extract of *Rosa damascena* was used to produce AuNPs and AgNPs by reducing $HAuCl_4$ and $AgNO_3$ within 5 min and successively employed for electrode modification in order to increase the electroactive surface area and the electron transfer rate [16].

It has been demonstrated that the principal biomolecules present in plant extracts responsible for the reduction of metal ions to form NPs are proteins, polyphenols, vitamins and sugars, in particular L-ascorbic acid, caffeic acid, gallic acid and quercetin [17]. However, most synthesis methods utilizing these biomolecules require high temperatures such as the synthesis using starch and glucose as reducing agents at high temperature for 20 h [18] or the synthesis using L-ascorbic acid at 80 °C [19,20] or they require microwave assistance [21,22]. Moreover these methods are influenced by several variables which are difficult to control and can affect the method reproducibility [23–25].

Quercetin (QUC, 3,3',4',5,7-pentahydroxyflavone) belongs to the class of flavonoids, well-known polyphenolic compounds widely distributed in fruits, vegetables and plant-derived beverages such as green tea and red wine [26,27]. QUC is one of the most important flavonols present in nature and has attracted the attention of many researchers because of its biological and pharmaceutical properties. Many of the beneficial effects of QUC are related to its antioxidant properties, which may result from its ability to scavenge free radicals (e.g., peroxyl radicals) and in chelating metal ions (e.g., $Fe^{3+/2+}$, Cu^{2+}, Ag^{+}) [28]. Generally, the radical scavenging occurs through electron donation or hydrogen atom donation from free hydroxyls and the chelation has been attributed to the presence of 5-hydroxypyran-4-one, rather than the 3',4'-dihydroxy groups in the B ring. The ability of QUC in chelation depends on pH and the metal-ligand ratio [29]. The two catechol hydroxyl groups on the B ring can be oxidized at a very low positive potential and also this reaction is pH-dependent [30].

In this paper, we first report the synthesis of AuNPs and AgNPs by reduction of gold and silver ions using quercetin as reducing agent via a quasi-reversible reaction by donating electrons and protons from the 3'-4'-dihydroxyl groups in the B ring. The NPs were successively characterized by UV-Visible (UV-Vis), transmission electron microscopy (TEM), dynamic light scattering (DLS) and energy dispersive spectroscopy (EDS). Afterwards, the "green" NPs were used to modify graphite electrodes by a drop-casting procedure and the resulting NPs modified electrodes were characterized with cyclic voltammetry and electrochemical parameters such as electroactive surface area and electron transfer rate constants were carefully evaluated. Finally, cellobiose dehydrogenase (CDH) was physically adsorbed onto the AuNPs and AgNPs modified electrodes to fabricate a third generation lactose biosensor. The characterization and optimization of the proposed biosensors are also presented in this work.

2 Experimental

2.1 Reagents and Equipment

Cellobiose dehydrogenase (CDH; cellobiose: (acceptor) 1-oxidoreductase; EC 1.1.99.18) from *T. villosa* was purified at University of Natural Resources and Applied Life Sciences Vienna, Austria (volumetric activity (DCIP assay, pH 4.5, 30°) = 72.4 U mL^{-1}, specific activity = 6.5 U mg^{-1}).

Chloroauric acid ($HAuCl_4 \cdot 3H_2O$), silver nitrate ($AgNO_3$), potassium hexacyanoferrate(III) ($K_3Fe(CN)_6$), hexaammineruthenium chloride(III) ($Ru(NH_2)_6Cl_3$), quercetin (QUC, 2-(3,4-dihydroxyphenyl)-3,5,7-trihydroxy-4*H*-chromen-4-one), β-lactose, acetic acid (100%), sodium acetate (CH_3COONa), sodium phosphate monobasic (NaH_2PO_4), sodium phosphate dibasic (Na_2HPO_4) and potassium chloride were obtained from Sigma Aldrich Chemicals (Stockholm, Sweden). All chemicals were of analytical reagent grade and were used without further purification. Milli-Q water (Millipore 18.2 MΩ cm^{-1}, Millipore, Bedford, MA, USA) was used for all experiments.

UV-Visible spectra were recorded on a Shimadzu UV-2401 PC spectrophotometer (Kyoto, Japan) with samples contained in a quartz cuvette, operating at a resolution of 1 nm from 400 to 700 nm for AuNPs, and from 300 to 500 nm for AgNPs and quercetin. Milli-Q water was used as blank. The spectra recorded were re-plotted using GraphPad Prism 6.

The elemental composition was determined by using an energy dispersive detector on scanning electron microscopy (SEM)/Zeiss EVO MA10 Oxford instruments (Bucks, England). For performing EDS measurements two drops of the synthesized colloidal samples were deposited on a polymer thin copper grid followed by solvent evaporation under vacuum.

The shape and size of the NPs were investigated by using Philips/FEI BioTwin CM120 TEM transmission electron microscopy (Hillsboro, OR, USA). For doing TEM measurements two drops of the synthesized colloidal samples were deposited on a polymer thin copper grid followed by solvent evaporation under vacuum.

The particle size range of the NPs along with their polydispersity and the zeta potential were determined using a particle size analyser (Zetasizer Nano ZS90, Malvern Instruments Ltd, Malvern, United Kingdom). Particle size is based on measuring the time dependent fluctuation of scattering the laser light by the NPs undergoing

Brownian motion, whereas the zeta potential measurement is based on the direction and velocity of the NPs under the influence of a known electric field.

All electrochemical measurements were performed using a PalmSens potentiostat (model Emstat, Palm Instruments BV, Utrecht, The Netherlands) equipped with PSTrace, version 4.5. A conventional three-electrode electrochemical cell was used for all experiments performed with an Ag|AgCl (sat. KCl) as reference electrode, a Pt wire as counter electrode and bare-graphite or modified graphite electrodes as working electrodes. Graphite rods (Alfa Aesar GmbH & Co KG, AGKSP grade, ultra "F" purity, and 3.05 mm diameter, Karlsruhe, Germany) were polished on wet emery paper (Turfbak Durite, P1200) and then carefully rinsed with Milli-Q water. The experiments to evaluate the electroactive area and the electronic transfer rate constant were carried out at scan rates from 5 $mV\,s^{-1}$ to 1000 $mV\,s^{-1}$, whereas the experiments to investigate the electrocatalytic oxidation of NADH in plain buffer or with added $CaCl_2$ were performed at a scan rate of 1 $mV\,s^{-1}$. All measurements were performed in solutions saturated with N_2 at room temperature. The pH measurements were carried out with a Metrohm 827 pH LAB pH-meter (Metrohm Nordic AB, Kristianstad, Sweden) at room temperature. For FIA experiments a 50 mM acetate buffer (pH 4.5) was used as carrier buffer with a constant flow rate of 0.5 $mL\,min^{-1}$ by a peristaltic pump (Minipuls 2, Gilson, Villier-le-Bel, France). An electrically controlled six-port valve (LabPRO, Rheodyne EV750-100, USA) with a 50 µL injection loop was used for the injection of analytes into the carrier flow.

2.2 Synthesis of AuNPs and AgNPs

The synthesis of AuNPs and AgNPs was carried out using quercetin (QUC) to reduce $HAuCl_4$ and $AgNO_3$ for AuNPs and AgNPs, respectively. $HAuCl_4$ and $AgNO_3$ were solubilized in 50 mM PBS buffer at pH 7; quercetin was solubilized in a 1 M NaOH solution with a final concentration of 1 mM, then diluted in 50 PBS buffer at pH 7, adjusting the pH of the final solution to pH 7.0. The synthesis of both kinds of NPs was performed at a fixed QUC concentration of 50 µM and varying the concentration of $HAuCl_4$ and $AgNO_3$ from 10 µM to 500 µM, in a total reaction batch volume of 10 mL. The synthesis was realized at room temperature in 50 PBS buffer at pH 7, obtaining colloidal solutions of AuNPs and AgNPs.

2.3 Electrode Modification

NPs colloidal solution was drop-casted onto the top of graphite rods electrodes and then left to dry overnight at room temperature. Enzyme-modified electrodes were prepared by allowing 5 µL of a *Trametes villosa* cellobiose dehydrogenase solution (volumetric activity (DCIP assay, pH 4.5, 30°) = 72.4 $U\,mL^{-1}$, specific activity = 6.5 $U\,mg^{-1}$) to physically adsorb on the top of the NPs/graphite rod electrodes and to evaporate overnight at 4°, as described elsewhere [31].

3 Results and Discussion

3.1 Green Synthesis and Characterization of AuNPs and AgNPs

Both AuNPs and AgNPs were synthesized using QUC as reducing agent at room temperature, according to the reactions shown in Scheme 1. The reduction of Au and Ag ions to form NPs was monitored by UV-Vis spectrophotometry. The UV-Vis spectra of QUC, AuNPs and AgNPs clearly show the two typical absorption bands for QUC at λ = 322 nm and λ = 360 nm, and the characteristic surface

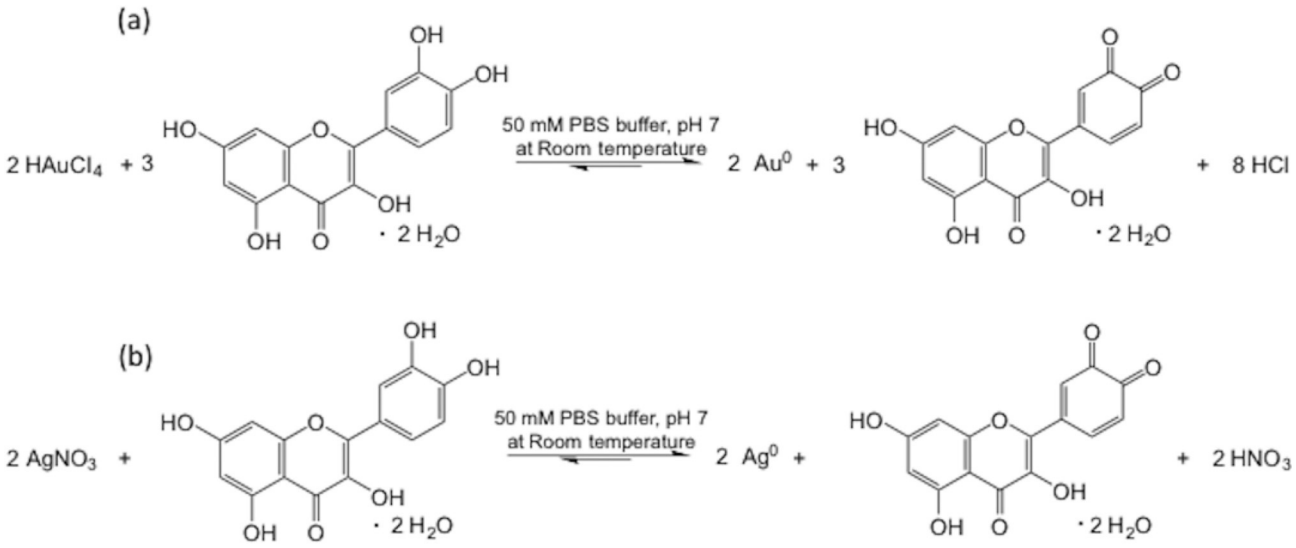

Scheme 1. Synthesis of metal nanoparticles through reduction of metal cations by quercetin: (a) $HAuCl_4$ and (b) $AgNO_3$.

plasmon resonance (SPR) bands for AuNPs and AgNPs recorded at $\lambda = 515$ nm and $\lambda = 403$ nm, respectively, as reported previously [32,33] (Figure S1, supplementary material).

Two important reaction parameters, reaction time and concentration of metal precursor, have been optimized with UV-Vis spectrophotometry. The reaction time was studied by following the change in absorbance at fixed wavelengths, $\lambda = 515$ nm for AuNPs and $\lambda = 403$ nm for AgNPs, versus time. The absorbance reached the maximum value after 20 min and 30 min for AgNPs and AuNPs, respectively, in the concentration range of 300–350 μM for both metal precursors (data not shown). In order to optimize the metal precursor concentration, UV-Vis spectra were recorded by following the absorbance of the colloidal solutions of AuNPs and AgNPs obtained through varying the concentrations of $HAuCl_4$ and $AgNO_3$, respectively, in the range of 50–500 μM (Fig. 1, a and b). It is possible to observe an increase in absorbance of the SPR band with a maximum in the concentration range of 300–350 μM. Therefore, 300 and 350 μM were chosen as optimal metal precursor concentrations for the synthesis of both AuNPs and AgNPs.

The concentrations of AuNPs were calculated using both 300 and 350 μM solutions of $HAuCl_4$ and found to be 2.37 nM and 2.72 μM by using a molar extinction coefficient of $1.10 \times 10^7\ M^{-1}\,cm^{-1}$ (λ_{max} 515 nm). Similarly, the concentrations of AgNPs were found to be 0.70 and 0.71 μM obtained with 300 and 350 μM solutions of $AgNO_3$, calculated using a molar extinction coefficient of $4.18 \times 10^9\ M^{-1}\,cm^{-1}$ ($\lambda_{max} = 405$ nm) [34,35].

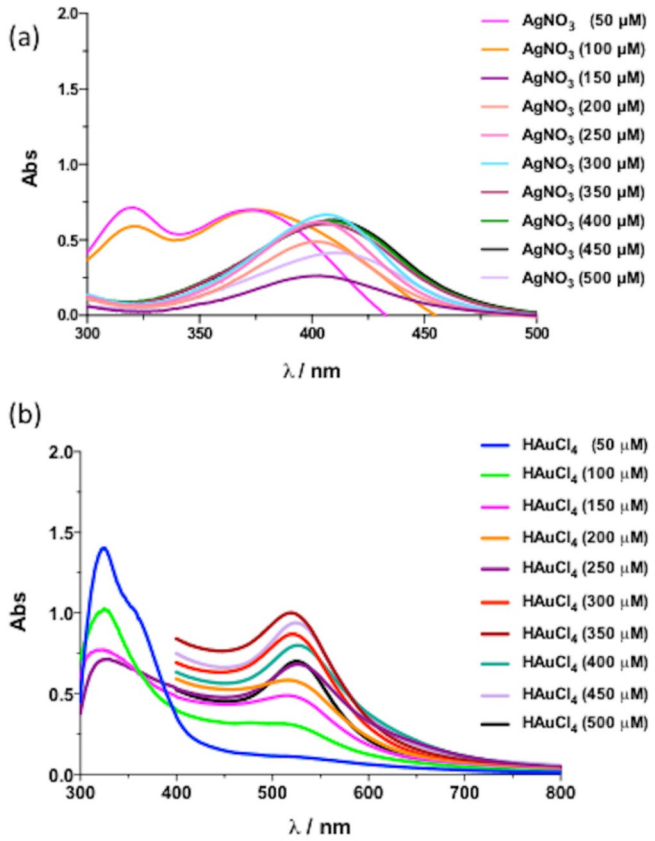

Fig. 1. (a) UV-Vis spectra of colloidal solutions of AgNPs after 20 min (diluted 1:4) in 50 mM PBS at pH 7; (b) UV-Vis spectra of colloidal solutions of AuNPs after 30 min (diluted 1:4) in 50 mM PBS at pH 7.

It is interesting to note in Fig. 1 that the λ_{max} values, 515 and 403 nm for AuNPs and AgNPs, respectively, are in good agreement with values reported in the literature for NPs with a diameter of about 5 nm [36,37], as it is known that the SPR band shows a clear λ shift to higher wavelengths from 515 to 530 nm and from 400 to 450 nm for AuNPs and AgNPs, respectively, when increasing the NPs diameter from 5 and 40 nm.

EDS spectroscopy of the MNPs was used in order to check the elemental composition of the colloidal suspensions. The patterns obtained perfectly match with the typical pattern of AuNPs and AgNPs reported in the literature (Fig. S2, a and b, Supplementary Material) [38,39].

In order to characterize the shape, the dimensions and size distributions of the MNPs, transmission electron microscopy (TEM) measurements were performed. The best results were obtained for AuNPs and AgNPs synthesized using a 300 μM metal precursor concentration, as shown in Fig. 2, a and b, where both samples show an almost homogeneous size distribution, spherical form and crystalline structure without aggregates and clusters, otherwise present in AuNPs and AgNPs samples obtained with a 350 mM metal precursor (data not shown) [40,41]. The real diameter of AuNPs and AgNPs resulted to be 5.5 ± 0.6 and 8.4 ± 0.3 nm, respectively.

In order to confirm the results obtained with TEM measurements, dynamic light scattering (DLS) experiments were carried out allowing the determination of the hydrodynamic diameter, called Z-average [42,43] (Fig. S3, a and b, supplementary material). Then, the zeta potential was measured to get some informations on the surface charge and the stability of the colloidal suspension [44,45]. It is possible to observe that the hydrodynamic diameter of both NPs is larger than the core diameter but the Z-average of AgNPs was similar to that of AuNPs, in particular 10.0 ± 0.6 nm for AgNPs and 9.5 ± 0.4 nm for AuNPs, with a low polydispersion index in both cases. The colloidal suspension of the AgNPs showed a zeta potential value of -39.0 ± 1.3 mV, slightly lower than that registered for the AuNP suspension, -28.5 ± 1.4 mV (measured at pH 7), which entails a major stability of the colloidal suspension of the AgNPs compared to AuNPs. It is possible to hypothesize that the colloidal suspension of AgNPs is more negatively charged, because of the presence of remaining QUC molecules adsorbed onto the surface of the AgNPs (see below), which are able to form chelates with AgNPs through a polymerization reaction [28,46]. The initial step of this reaction is the conversion of the catechol moiety in the B-ring to *o*-quinone with different condensation products depending on the pH. On the contrary, at the same quercetin concentration, in the synthesis of AuNPs, all ligand molecules

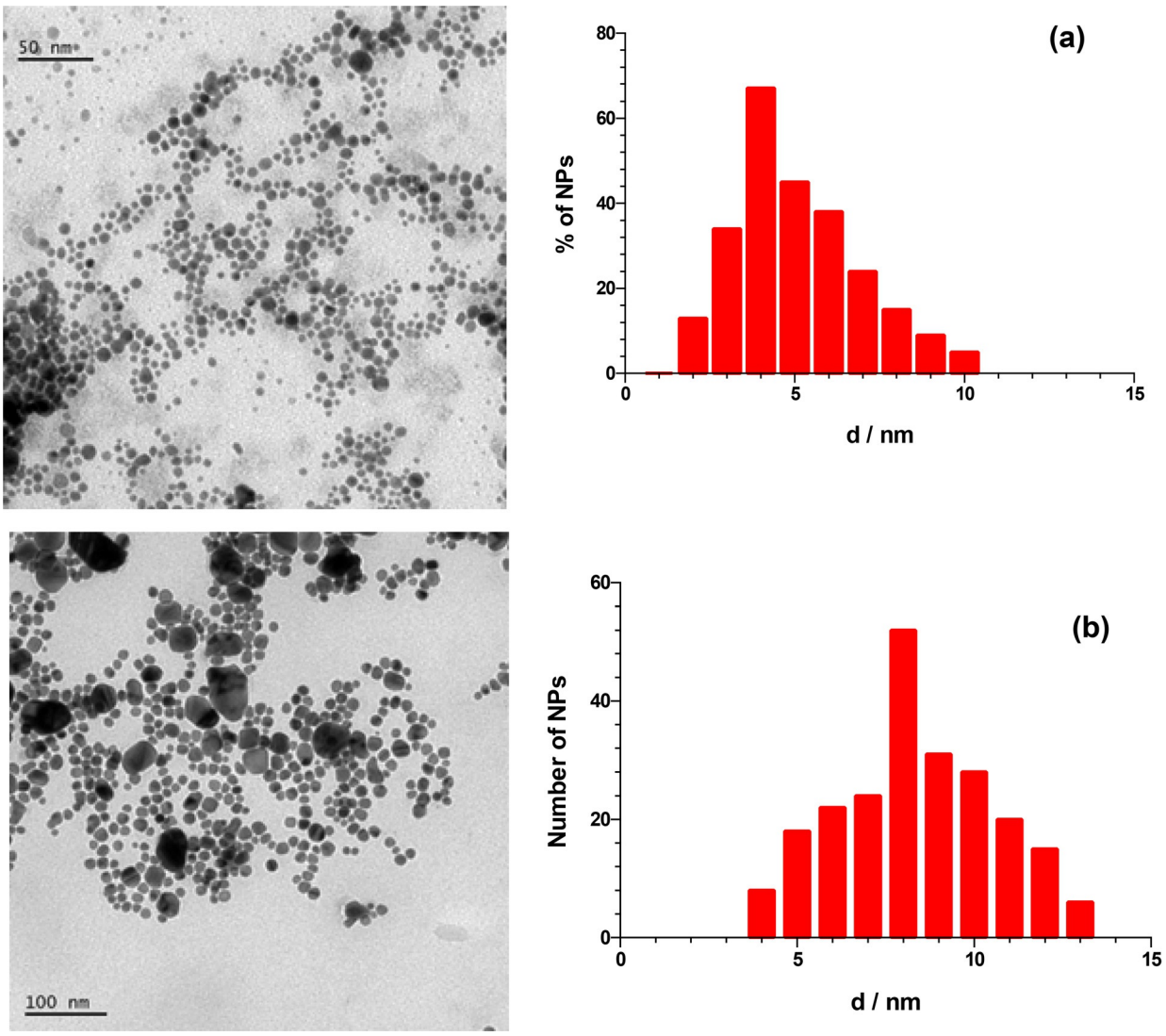

Fig. 2. (a) TEM image of a colloidal solution of AuNPs deposited on a copper grid (left) and size distribution (right); (b) TEM image of a colloidal solution of AgNPs deposited on a copper grid (left) and size distribution (right).

are involved in the reduction of Au^{3+} cations, because of the stoichiometry of the synthesis reaction (Scheme 1) and are not available for complexation reactions with the NPs [29]. The quinone produced according to the reaction sequence might contribute to the stabilization of the colloidal suspension of AuNPs, as also suggested by Huang et al. for the synthesis AuNPs using plant tannins as reducing agent [47]. Moreover, the synthesis of both NPs was carried out at pH 7, above the isoelectric point of quercetin, which can explain the negative charge of both NPs.

3.2 Electrochemical Characterization of Green AuNPs and AgNPs

After the preliminary characterization of NPs, cyclic voltammetry experiments were carried out in order to verify the possible employment of both kinds of NPs for development of electrochemical biosensing platforms. The NP suspensions were deposited onto the top of graphite rods electrodes by a drop casting technique. The amount of suspension was carefully optimized. This is a key issue in a surface nanostructuration process, because too large a volume of NPs may cause aggregation that can lead to the formation of metal multilayers, which in turn may hinder the electron transfer between the redox probe and the electrode surface [48,49]. The optimal volume of the suspension of NPs to be deposited onto the surface in order to prevent any cluster formation resulted in 4 μL for AuNPs and 6 μL for AgNPs. These results were obtained with cyclic voltammetry experiments using two different probes, $Ru(NH_3)_6^{3+/2+}$ and $Fe(CN)_6^{3-/4-}$ and both of them showed the same optimal volume of suspension of the respective NPs (Fig. S4, a and b, Supplementary Material). The most electrochemically reversible performance was obtained with ($Ru(NH_3)_6^{3+/2+}$) for both NPs.

This result can be ascribed to the fact that both NPs are negatively charged and $Ru(NH_3)_6^{3+/2+}$ is positively charged whereas $Fe(CN)_6^{3-/4-}$ is negatively charged and therefore to a possible adsorption effect due to electrostatic accumulation of $Ru(NH_3)_6^{3+/2+}$ onto the electrode surface [50].

Successively, the electrochemically active area (A_{EA}) and the electron transfer rate constant (k^0) have been evaluated with cyclic voltammetry experiments varying the scan rate form $5\,mV\,s^{-1}$ to $1000\,mV\,s^{-1}$ in 1 mM $Ru(NH_3)_6^{3+/2+}$ (results not shown). The A_{EA} was calculated by plotting the peak current vs. square root of the scan rate ($\upsilon^{1/2}$) and inserting the slope obtained into the Randles-Sevcik equation [51]. The k^0 was evaluated by plotting the peak potential (E_p) vs. log $\upsilon^{1/2}$, for both anodic and cathodic peaks by using a method that merges the Klingler & Kochi and Nicholson & Shain methods, as reported previously [52]. These experiments were repeated at different pHs in the range of pH 2–8 in 50 mM citrate-phosphate buffer and the results are shown in Fig. 3, a and b. The best A_{EA} and k^0 values for AuNPs were obtained at pH 7 and resulted in $A_{EA}=0.159\pm0.008\,cm^2$ and $k^0=7.2\pm0.2\times10^{-3}\,cm\,s^{-1}$, respectively, while for AgNPs the best results were recorded at pH 6.5 resulting in $A_{EA}=0.121\pm0.004\,cm^2$ and $k^0=5.6\pm0.5\times10^{-3}\,cm\,s^{-1}$, respectively. Therefore, both metal NPs showed better electrochemical performances then graphite naked electrode ($A_{EA}=0.097\pm0.007\,cm^2$ and $k^0=0.62\pm0.01\times10^{-3}\,cm\,s^{-1}$) at about neutral pHs.

In order to investigate any possible presence of remaining QUC molecules onto the NPs surface NADH oxidation experiments were carried out by using cyclic voltammetry [53,54], as QUC is known to be a mediator for the electrocatalytic oxidation of NADH. It is known from the literature that Ca^{2+} ions can increase the oxidation current of NADH if hydroxyl groups are present in the structure of the mediator, because of the formation of particular complexes between Ca^{2+} and –OH groups [55] making the mediator positively charged, which has a very beneficial effect on the rate between NADH and the mediator [56]. Figure 4 shows the voltammetric curves obtained with an AuNPs/graphite electrode (Fig. 4a) and an AgNPs/graphite electrode (Fig. 4b) in 50 mM Tris-HCl buffer at pH 7 (black curves), in the presence of 10 mM NADH before (blue curves) and after adding 20 mM $CaCl_2$ (red curves). As for the graphs performed with the AuNPs/graphite electrode, the cyclic voltammogram re-

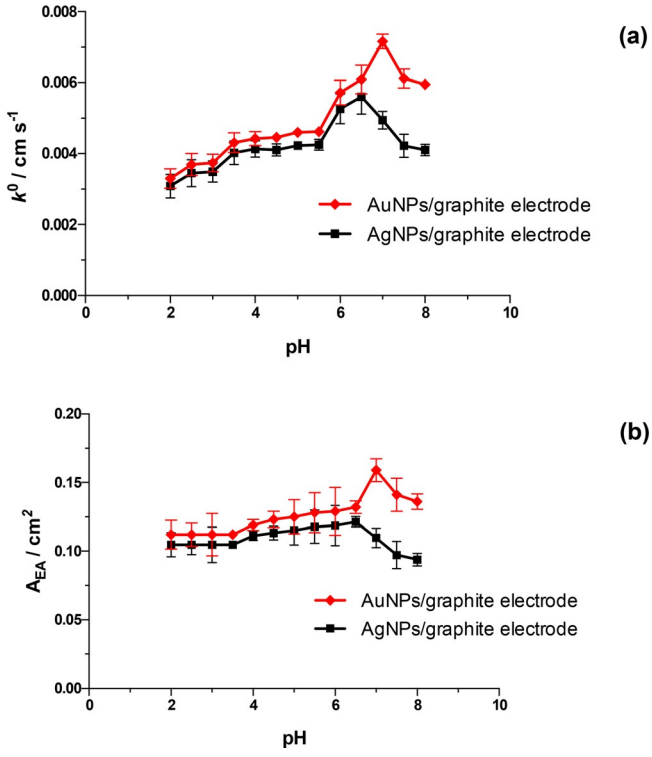

Fig. 3. (a) Electron transfer rate constant (k^0) vs. pH of a AuNPs/graphite electrode (red line) and a AgNPs/graphite electrode (black line) in 1 mM $Ru(NH_3)_6Cl_3$ in 50 mM citrate-phosphate buffer, pH 2–8. Measurements were performed with cyclic voltammetry (CV) at scan rates from $5\,mV\,s^{-1}$ to $1000\,mV\,s^{-1}$; (b) electroactive area (A_{EA}) vs. pH of a AuNPs/graphite electrode (red line) and a AgNPs/graphite electrode (black line) in 1 mM $Ru(NH_3)_6Cl_3$ in 50 mM citrate-phosphate buffer, pH 2–8. Measurements performed with cyclic voltammetry (CV) at scan rates from $5\,mV\,s^{-1}$ to $1000\,mV\,s^{-1}$.

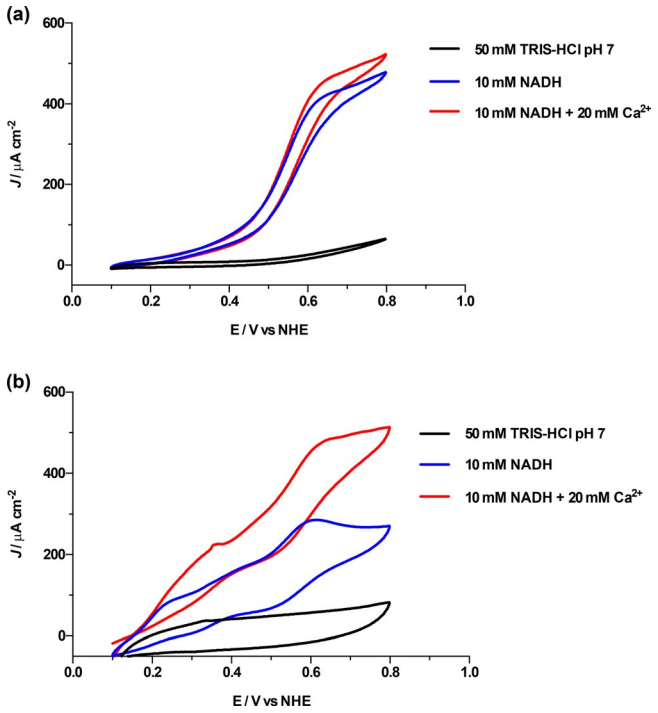

Fig. 4. (a) Cyclic voltammograms of a AuNPs/graphite electrode performed in 50 mM TRIS-HCl buffer, pH 7 (black line), in presence of 10 mM NADH (blue line) and 10 mM NADH + 20 mM Ca^{2+} (red line) at a scan rate of $1\,mV\,s^{-1}$; (b) cyclic voltammograms of a AgNPs/graphite electrode performed in 50 mM TRIS-HCl buffer, pH 7 (black line), in presence of 10 mM NADH (blue line) and 10 mM NADH + 20 mM Ca^{2+} (red line) at a scan rate of $1\,mV\,s^{-1}$.

corded in buffer solution shows no oxidation or reduction waves (black curve, Fig. 4a) and it is possible to observe a small difference in shape between the blue and the red curves recorded in absence and in presence of $CaCl_2$, respectively, thus allowing to state that there are no remaining quercetin molecules on the surface of the AuNPs. In contrast, in the case of the AgNPs/graphite electrode a quasi-reversible redox process with a formal potential (E°') of 0.323 V vs. NHE (pH 7) is observed in buffer solution (Fig. 4b, black curve) pointing to the fact that some QUC molecules remain adsorbed onto the surface of the AgNPs. Moreover, the large difference in shape and the large increase in the oxidation current of NADH shown by the blue and the red curves obtained before and after the addition of $CaCl_2$ (Fig. 4a and b) represent a clear confirmation of the presence of QUC molecules adsorbed onto the surface of the AgNPs.

It is interesting to note that the E°' value obtained with the graphite electrode modified with AgNPs (E°' = 0.323 vs. NHE) is substantially lower than that obtained with 50 μM QUC in 50 mM Tris-HCl buffer at pH 7 with a graphite electrode (Fig. S5, Supplementary material) which shows a quasi-reversible voltammogram with an E°' value of 0.459 vs. NHE. The substantial shift in E°'-value indicates that the oxidized rather than the reduced form of QUC is more strongly bound to the surface of the AgNPs than on graphite. This result can be expected as it is known in literature that the surface nanostructuration can shift the E°' value of redox substances immobilized onto the electrode surface [16,57,58].

3.3 Electrochemical Characterization of *Tv*CDH/AuNPs/Graphite Electrodes and *Tv*CDH/AgNPs/Graphite Electrodes

Figure 5 shows the CVs of *Tv*CDH drop-cast onto a naked graphite electrode, an AuNPs/graphite and an AgNPs/graphite electrode carried out in 50 mM acetate buffer pH 4.5. In the absence of substrate, no wave (anodic or cathodic) from the cytochrome domain is visible. When substrate is added it is possible to observe an oxidative, catalytic current due to the catalysis of the DH domain and the DET between the cytochrome domain of CDH and the electrode. In particular a small electrocatalytic current was registered with both *Tv*CDH/graphite (black curve) and *Tv*CDH/AgNPs/graphite electrodes (blue curve) while a very large catalytic current density was obtained with the *Tv*CDH/AuNPs/graphite electrode (red curve). This result could be ascribed to the fact that the AuNPs are slightly more positive charged than the AgNPs at pH 4.5 (the zeta potential values measured at pH 4.5 are 29.3 ± 1.7 mV and 21.1 ± 1.5 mV for AuNPs and AgNPs, respectively), due to some QUC molecules (pI 6.4) adsorbed onto the AgNPs surface, creating a less electrostatic repulsive environment for the cytochrome domain of CDH (pI 4.2), thus enhancing DET and allowing the enhancement of enzyme loading onto the electrode surface without influencing the electrochemical behavior of the enzyme.

3.4 Lactose Biosensor

Calibration curves for *Tv*CDH/AuNPs/graphite electrode, *Tv*CDH/AgNPs/graphite electrode and *Tv*CDH/graphite

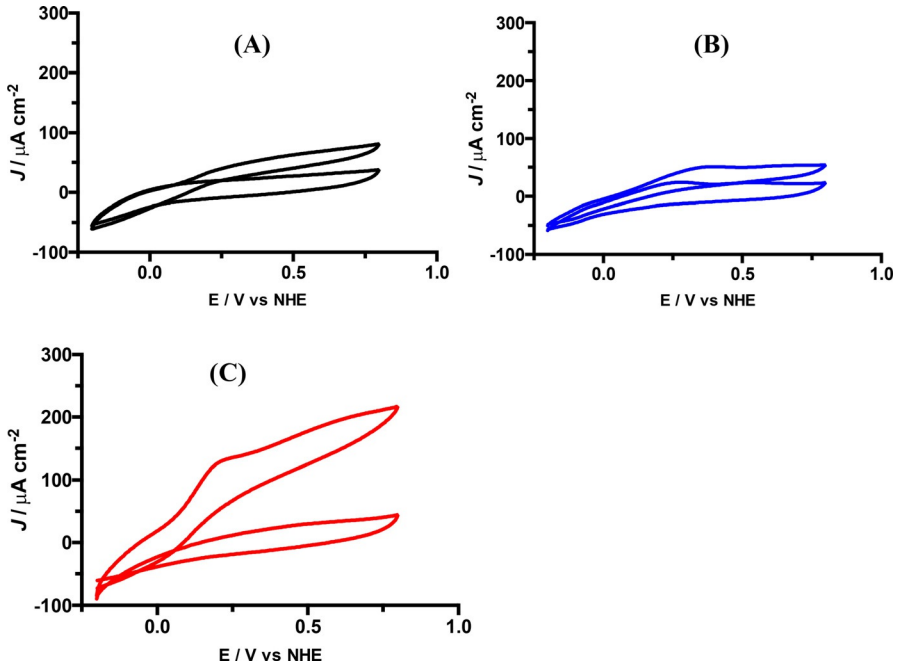

Fig. 5. Cyclic voltammograms of a *Tv*CDH/graphite electrode (black curves) (A), *Tv*CDH/AgNPs/graphite electrode (blue curves) (B) and *Tv*CDH/AuNPs/graphite electrode (red curves) (C) in the absence and in presence of 0.01 M β-lactose in acetate buffer at pH 4.5. Scan rate 10 mV s^{-1}.

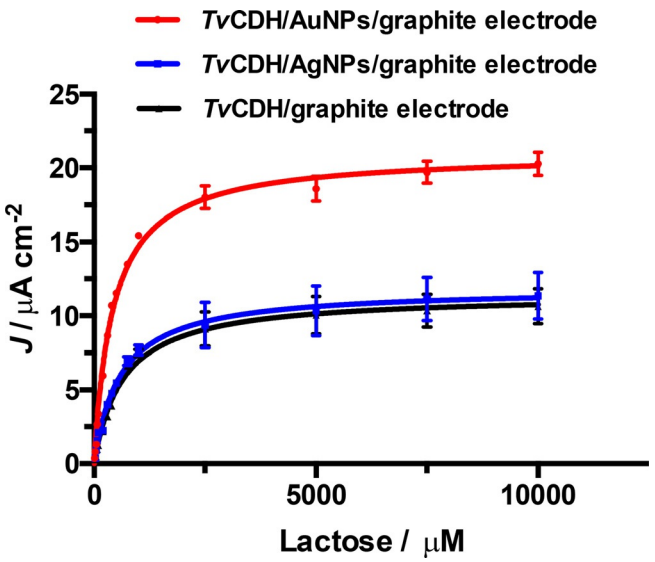

Fig. 6. Calibration curves for β-lactose with a *Tv*CDH/graphite electrode (black line), a *Tv*CDH/AuNPs/graphite electrode (red line) and a *Tv*CDH/AgNPs/graphite electrode (blue line), recorded amperometrically in a flow injection analysis (FIA) system. Buffer: 0.05 M acetate buffer at pH 4.5. Applied potential: 250 mV vs Ag|AgCl.

electrode were carried out with different lactose concentrations with FIA measurements and the results are shown in Fig. 6. The calibration curves show a linear range of 10–300 μM for the *Tv*CDH/AuNPs/graphite electrode, 25–200 μM for the *Tv*CDH/AgNPs/graphite electrode and 25–100 μM for the *Tv*CDH/graphite electrode, with a correlation coefficient (R^2) of 0.99. The detection limit was found to be 3.5 μM for *Tv*CDH/AuNPs/graphite electrode and 10 μM for both *Tv*CDH/AgNPs/graphite electrode and *Tv*CDH/graphite electrode, calculated using the relation 3 x S. D.a/b, where S. D.a is the absolute standard deviation of the intercept, and b is the slope of the calibration curve. The sensitivity was calculated to be 5.4 ± 0.3 μA $mM^{-1} cm^{-2}$ for *Tv*CDH/AuNPs/graphite electrode, 2.9 ± 0.4 μA $mM^{-1} cm^{-2}$ for *Tv*CDH/AgNPs/graphite electrode and 2.6 ± 0.2 μA $mM^{-1} cm^{-2}$ for *Tv*CDH/graphite electrode. The results clearly show a better performance with an extended linear range, lower LOD and higher sensitivity with the AuNPs/graphite platform confirming the better communication between CDH and the electrode.

Table 1 shows the apparent kinetic parameters (J_{max}, K_M^{app}) obtained by fitting the calibration curves. It is possible to observe a sensible reduction of the apparent Michaelis-Menten (K_M^{app}) with the AuNPs/graphite platform compared to the other two platforms with a value of 432.9 μM +/−SD, which is smaller than that obtained with CDH immobilized onto aryl diazonium modified single wall carbon nanotubes deposited on a glassy carbon electrode (0.7 mM) [59,60].

Table 1. Apparent kinetic parameters of *Tv*CDH immobilized on modified AuNPs/graphite, AgNPs/graphite and naked graphite electrode platforms with with β-lactose as substrate.

	TvCDH/AuNPs/graphite	TvCDH/AgNPs/graphite	TvCDH/graphite
J_{max}/μA cm^{-2}	21.01 ± 0.33	11.88 ± 0.21	11.45 ± 0.28
K_M^{app}/μM	432.9 ± 24.5	592.1 ± 35.4	655.1 ± 52.5

The stability of the *Tv*CDH/AuNPs/graphite electrodes was also tested. The decrease in the electrocatalytic current densities after 24 h of continuous injections was about 15.4%. The lifetime of the biosensor was also studied by consecutive measurements of the current densities with a 5 mM lactose concentration. The biosensor retained about 90% of its initial activity after 1 day of a 8h/day operation and about 50% after 1 week, under dry storage conditions, therefore showing a very good stability if compared to other lactose biosensors [60,61].

For comparison, in Table 2 are shown the analytical characteristics of different lactose biosensors reported in the literature. Among the results obtained with the biosensor based on different types of CDH enzymes, it is interesting to observe that the modification of the graphite electrode with the green Au/NPs results in a marked improvement of the sensitivity of the sensor. It is interesting to note also the comparison with a bi-enzymatic lactose biosensor based on β-galactosidase and glucose oxidase immobilized on a gold electrode [62]: it shows a very good sensitivity and the widest linear range but the detection limit is much higher than those reported for CDHs based biosensors. Moreover, it must be remembered that

Table 2. Comparisons between the main analytical parameters of lactose biosensors.

Biosensor platform	Linear range (μM)	LOD (μM)	Sensitivity (μA mM^{-1} cm^{-2})	Response time (s)	E (V) vs Ag-|AgCl	Reference
β-Gal-GOx-HRP/TTF/AuE	13–1000	3.8	11	300	0	[62]
CDH/MWCNTs/SPCEs	0.5–100	0.2	-	65	0.10	[63]
CDH/NH_2-PD/SWCNTs/GC	1–100	0.5	4.8	-	0.10	[60]
CDH/PEI@AuNPs/AuE	1–100	0.3	3.9	3	0.25	[64]
CDH/AuNPs/graphite	10–300	3.5	5.4	25	0.10	this work

Abbreviations: AuE, solid gold electrode; β-Gal, β-galactosidase; CDH, cellobiose dehydrogenase; GC, glassy carbon electrode; GOx, glucose oxidase; HRP, horseradish peroxidase; MPA, 3-mercaptopropionic acid; MWCNTs, multi wall carbon nanotubes; NH_2-PD, *p*-phenylenediamine; SPCE, screen printed carbon electrode; SWCNTs, single wall carbon nanotubes; TTF, tetrathiafulvalene.

the bi-enzymatic biosensor is based on the use of an artificial mediator to facilitate the electron transfer between the oxidising enzyme and the electrode (2nd generation biosensor) and not on DET as in the case of all CDHs based lactose biosensors [65].

4 Conclusions

Green synthesis was successfully employed to synthesize AuNPs and AgNPs using QUC as reducing agent in aqueous solution at room temperature. The key aspect is that the green pathway allowed the synthesis of the MNPs with a very small diameter, 5 nm for AuNPs and 8 nm for AgNPs, values absolutely comparable to those typical of the NPs obtained with traditional synthetic methods, but avoiding toxic waste products and the use of harmful chemicals. The other important issue is that the green process is cost effective and time saving as QUC is a natural flavonol present in many cheap food stuffs and beverages and the time required for the synthesis is only about 20 min for making the AgNPs and 30 min for the AuNPs. The main advantages related to the use of quercetin as reducing agent are therefore i) no need of extreme experimental conditions, ii) short reaction time, iii) high reaction yield and iv) great reproducibility.

The synthesized AuNPs and AgNPs were extensively characterized in terms of morphology, crystalline nature, structural and electrochemical properties. They showed great electrochemical properties such as enhanced electroactive surface and high electron transfer rate constants. Both types of green NPs were used to prepare a lactose biosensor based on cellobiose dehydrogenase from *Trametes villosa*. The *Tv*CDH/AuNPs/graphite biosensor gave the best result, showing a good linear range, low detection limit, high sensitivity, good stability and a fast response time. For these reasons, the green synthesis of AuNPs could be a promising low cost and eco-friendly synthesis method to obtain performing nanomaterials for the development of lactose biosensors for possible use in food industries.

Acknowledgements

The authors like to thank the Swedish Research Council and Sapienza University of Rome for financial support.

References

[1] H. Liao, C. L. Nehl, J. H. Hafner, *Future Medicine* **2006**, *1*, 201.
[2] J. Wang, *Microchim. Acta* **2012**, *177*, 245.
[3] Y. Qiao, C. M. Li, *J. Mater. Chem* **2011**, *21*, 4027.
[4] Z. Wang, L. Zhou, X. W. Lou, *Adv. Mater.* **2012**, *24*, 1903.
[5] T. K. Sau, A. L. Rogach, F. Jäckel, T. A. Klar, J. Feldmann, *Adv. Mater.* **2010**, *22*, 1805.
[6] A. Majdalawieh, M. C. Kanan, O. El-Kadri, S. M. Kanan, *J. Nanosci. Nanotechnol.* **2014**, *14*, 4757.
[7] A. P. Ingle, N. Duran, M. Rai, *Appl. Microbiol. Biotechnol.* **2014**, *98*, 1001.
[8] B. Karagoz, J. Yeow, L. Esser, S. M. Prakash, R. P. Kuchel, T. P. Davis, C. Boyer, *Langmuir* **2014**, *30*, 10493.
[9] S. Iravani, *Green Chem.* **2011**, *13*, 2638.
[10] V. V. Makarov, A. J. Love, O. V. Sinitsyna, S. S. Makarova, I. V. Yaminsky, M. E. Taliansky, N. O. Kalinina, *Acta Naturae* **2014**, *6*, 35.
[11] A. Singh, D. Jain, M. K. Upadhyay, N. Khandelwal, H. N. Verma, *J. Nanomater. Bios.* **2010**, *5*, 483.
[12] M. Cinelli, S. R. Coles, M. N. Nadagouda, J. Btaszczyński, R. Słowiński, R. S. Varma, K. Kirman, *Green Chem.* **2015**, *17*, 2825.
[13] A. T. Shah, M. I. Din, S. Bashir, M. A. Qadir, F. Rashid, *Anal. Lett.* **2015**, *48*, 1180.
[14] M. Daglia, R. Antiochia, A. P. Sobolev, L. Mannina, *Food Res. Int.* **2014**, 63, 275.
[15] W. Wang, Q. Chen, C. Jiang, D. Yang, X. Liu, S. Xu, *Colloid Surface A: Physicochem. Eng. Asp.* **2007**, *301*, 73.
[16] S. Ghoreishi, M. Behpour, M. Khayatkashani, *Physica E* **2011**, *44*, 97.
[17] B. Moyo, S. Oyedemi, P. J. Masika, V. Muchenje, *Meat Science* **2012**, *91*, 441.
[18] P. Raveendran, J. Fu, S. L. Wallen, *J. Am. Chem. Soc.* **2003**, *125*, 13940–941.
[19] N. Mat Zain, A. G. F. Stapley, G. Shama, *Carbohydrate Polymers* **2014**, *112*, 195–202.
[20] J. Xiong, Y. Wang, Q. Xue, X. Wu, *Green Chem.* **2011**, *13*, 900–904.
[21] M. Valodkar, S. Modi, A. Pal, S. Thakore, *Mat. Res. Bulletin* **2011**, *46*, 384–389.
[22] D. Singh, D. Rawat, Isha, *Bioresources and Bioprocessing* **2016**, *3*, 14–21.
[23] M. N. Nadagouda, R. S. Varma, *Green Chem.,* **2008**, *10*, 859–862.
[24] D. Philip, *Physica E: Low-dim. Syst. Nanostr.* **2010**, *42*, 1417–1424.
[25] M. Zargar, A. A. Amid, F. A. Bakar, M. N. Shamsudin, K. Shameli, F. Jahanshiri, F. Farahani, *Molecules* **2011**, *16*, 6667–6676.
[26] F. Das, *J. Ethnopharmacol.* **2012**, *143*, 383.
[27] M. Zhang, S. G. Swarts, L. Yin, et al., in *Oxygen Transport to Tissue XXIII*, (Eds: J. C. La Manna, M. A. Puchowicz, K. Xu, D. K. Harrison, D. F. Bruley), Springer, New York **2011**; pp. 283–289.
[28] Z. Jurasekova, A. Torreggiani, M. Tamba, S. Sanchez-Cortes, J. V. Garcia-Ramos, *J. Mol. Struct.* **2009**, *918*, 129.
[29] J. P. Cornard, J. C. Merlin, *J. Inorg. Biochem.* **2002**, *92*, 19.
[30] A. M. Oliveira Brett, M.-E. Ghica, *Electroanalysis* **2003**, *15*, 1745.
[31] L. Stoica, R. Ludwig, D. Haltrich, L. Gorton, *Anal. Chem.* **2006**, *78*, 393.
[32] I. Hussain, S. Graham, Z. Wang, B. Tan, D. C. Sherrington, S. P. Rennard, A. I. Cooper, M. Brust, *J. Am. Chem. Soc.* **2005**, *127*, 16398.
[33] N. Vigneshwaran, N. M. Ashtaputre, P. V. Varadarajan, R. P. Nachane, K. M. Paralikar, R. H. Balasubramanya, *Mat. Lett.* **2007**, *61*, 1413.
[34] Y. Sun, Y. Xia, *Analyst* **2003**, *128*, 686.
[35] X. Liu, M. Atwater, J. Wang, Q. Huo, *Colloid. Surface B: Biointerfaces* **2007**, *58*, 3.
[36] N. Ji, Y. Chen, P. Gong, K. Cao, D.-L. Peng, *Colloid Surface A: Physicochem. Eng. Aspects* **2015**, *480*, 11.
[37] N. A. Negm, S. M.; A. A. Tawfik Abd-Elaal, *J. Ind. Engineering. Chem.* **2015**, *21*, 1051.
[38] J. Y. Song, H.-K. Jang, B. S. Kim, *Proc. Biochem.* **2009**, *44*, 1133.

[39] J. Y. Song, B. S. Kim, *Bioprocess Biosyst. Eng.* **2009**, *32*, 79.
[40] A. V. Kozytskiy, A. E. Raevskaya, O. L. Stroyuk, I. E. Kotenko, N. A. Skorik, S. Y. Kuchmiy, *J. Mol. Catal. A: Chem.* **2015**, *398*, 35.
[41] L. Sun, S. Zhang, F. Liu, M. Han, *Superlattice. Microst.* **2015**, *86*, 418.
[42] S. Rajakannu, S. Shankar, S. Perumal, S. Subramanian, G. P. Dhakshinamoorthy, *Int. J. Curr. Microbiol. App. Sci.* **2015**, *4*, 944.
[43] E. Sulman, M. Sulman, I. Tyamina, V. Doluda, L. Nikoshvili, A. Sidorov, V. Matweeva, *Chem. Eng. Technol.* **2015**, *38*, 683.
[44] M. G. Carmeiro-da-Cunha, M. A. Cerqueira, B. W. S. Souza, J. A. Teixeira, A. A. Vicente, *Carbohyd. Polym.* **2011**, *85*, 522.
[45] R. J. Hunter, *Zeta Potential in colloid science*, Academic Press Inc., San Diego **1981**.
[46] A. Torreggiani, A. Trinchero, M. Tamba, P. Taddei, *J. Raman Spectrosc.* **2005**, *36*, 380.
[47] X. Huang, H. Wu, X. Liao, B. Shia, *Green Chem.* **2010**, *12*, 395.
[48] J. Jiang, L. Zhang, V. Shanbhang, *J. Electrochem. Soc.* **2014**, *161*, 3028.
[49] E. Costa Rama, M. B. González-García, A. Costa-García, *Sens. Actuat. B* **2014**, *201*, 567.
[50] Y.-S. Dyne Lin, L. M. H. Lai, J. Z. Ginges, E. Luais, J. R. Peterson, I. Y. Goon, R. Amal, J. J. Gooding, *Chem. Phys. Chem.* **2010**, 11, 2087–2813.
[51] K. Ngamchuea, S. Eloul, K. Tshulik, R. G. Compton, *J. Solid State Electrochem.* **2014**, *18*, 3251.
[52] I. Lavagnini, R. Antiochia, F. Magno, *Electroanalysis* **2004**, *16*, 505.
[53] R. Antiochia, I. Lavagnini, F. Magno, *Anal. Bioanal. Chem.* **2005**, *381*, 1355.
[54] Y. Dilgin, B. Kızılkayab, D. G. Dilgin, I. Gökc, L. Gorton, *Colloid Surface B* **2013**, *102*, 816.
[55] E. Katz, T. Lötzbeyer, D. D. Schlereth, W. Schuhmann, H.-L. Schmidt, *J. Electroanal. Chem.* **1994**, *373*, 189.
[56] L. Gorton, E. Domínguez, in *Encyclopedia of Electrochemistry*, (Series Eds. A. J. Bard, M. Stratmann, Vol. 9. Eds: G. S. Wilson Wiley-VCH), Weinheim **2002**, pp. 67–143
[57] W. Zhao, H. Wang, X. Qin, X. Wang, Z. Zhao, Z. Miao, L. Chen, M. Shan, Y. Fang, Q. Chen, *Talanta* **2009**, *80*, 1029.
[58] S. Chen, R. Yuan, Y. Chai, F. Hu, *Microchim. Acta* **2013**, *180*, 15.
[59] F. Tasca, W. Harreither, R. Ludwig, J. J. Gooding, L. Gorton, *Anal. Chem.* **2011**, *83*, 3042.
[60] F. Tasca, R. Ludwig, L. Gorton, R. Antiochia, *Sens. Actuators B* **2013**, *177*, 64.
[61] M. Ammam, J. Fransaer, *Sens. Actuators B* **2012**, *148*, 583.
[62] F. Conzuelo, M. Gamella, S. Campuzano, M. A. Ruiz, A. J. Reviejo, J. M. Pingarrón, *J. Agric. Food Chem.* **2010**, *58*, 7141.
[63] G. Safina, R. Ludwig, L. Gorton, *Electrochim. Acta* **2010**, *55*, 7690.
[64] M. Tavahodi, R. Ortiz, C. Schulz, A. Ekhtiari, R. Ludwig, B. Haghighi, L. Gorton, *Anal. Chem.*, submitted.
[65] P. Bollella, F. Mazzei, G. Favero, G. Fusco, R. Ludwig, L. Gorton, R. Antiochia, *Biosens. Bioelectron.* **2016**, DOI:10.1016/j.bios.2016.08.027.

Received: July 26, 2016
Accepted: September 16, 2016
Published online: October 10, 2016

Supplementary material:

Green synthesis and characterization of gold and silver nanoparticles and their application for development of a third generation lactose biosensor

Paolo Bollella, Christopher Schulz, Gabriele Favero, Franco Mazzei, Roland Ludwig, Lo Gorton, Riccarda Antiochia*

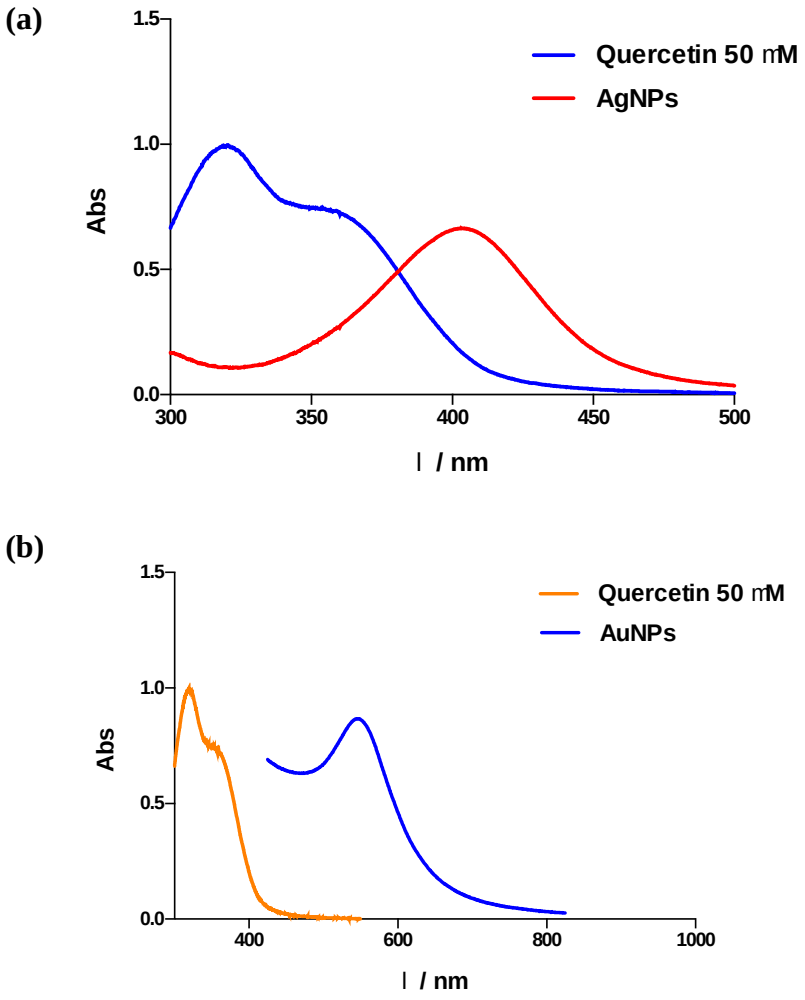

Figure S1. (a) UV-Vis spectra of a colloidal solution of AgNPs (diluted 1:4) in 50 mM PBS buffer at pH 7 and quercetin 50 µM; (b) UV-Vis spectra of a colloidal solution of AuNPs (diluted 1:4) in 50 mM PBS buffer at pH 7 and quercetin 50 µM.

(a)

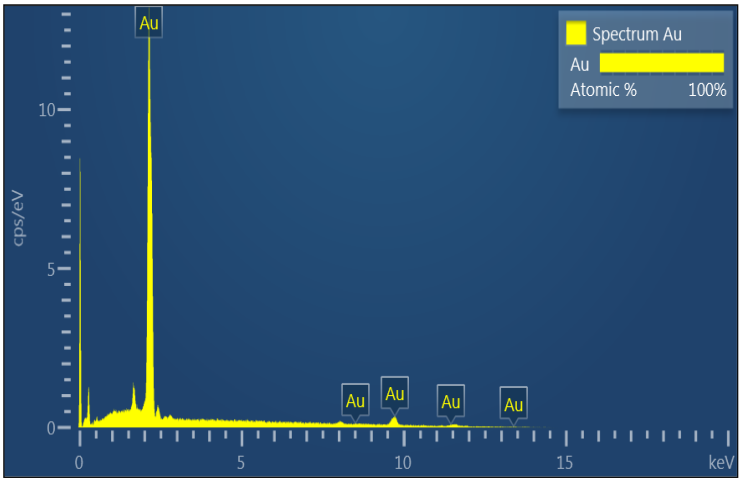

(b)

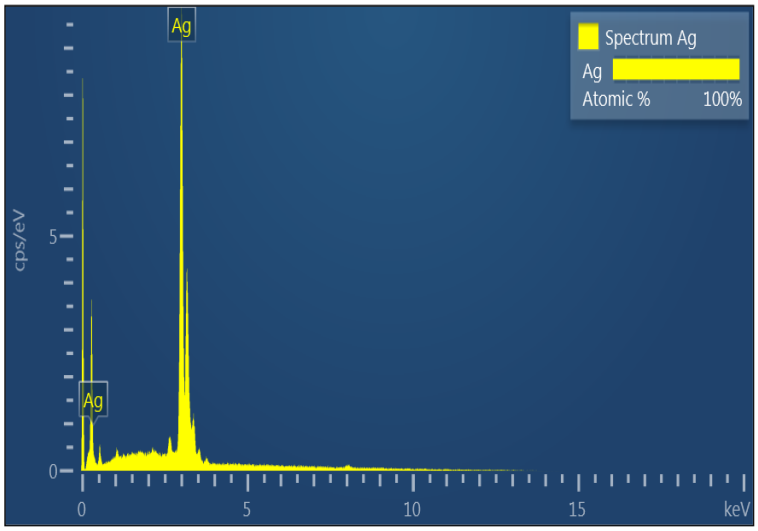

Figure S2. (a) Energy dispersive spectra of a colloidal solution of AuNPs deposited on a copper grid; (b) Energy dispersive spectra of a colloidal solution of AgNPs deposited on a copper grid.

(a)

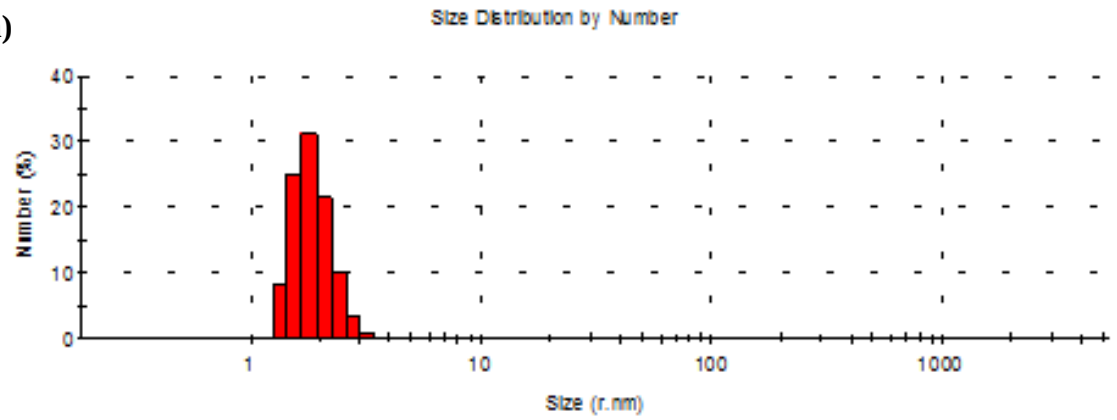

(b)

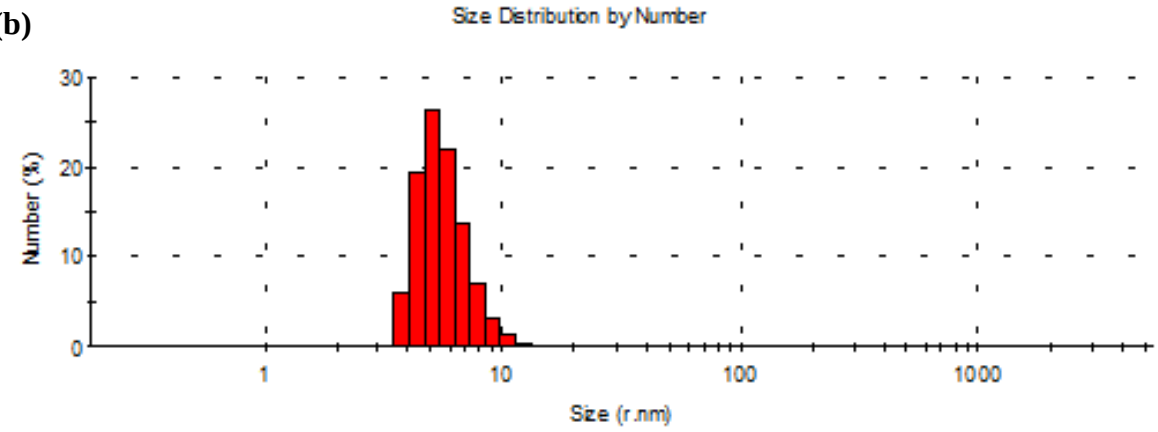

Figure S3. (a) Size distribution of a colloidal solution of AuNPs (diluted 1:4) in 50 mM PBS buffer at pH 7; (b) Size distribution of a colloidal solution of AgNPs (diluted 1:4) in 50 mM PBS buffer at pH 7.

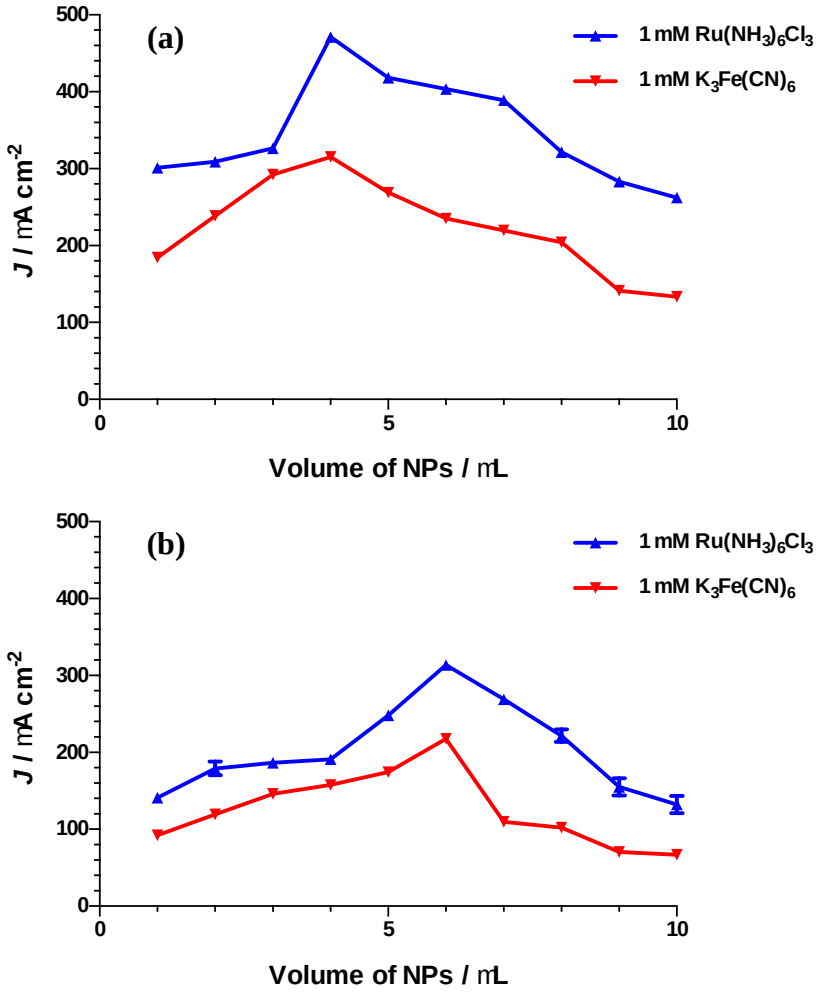

Figure S4. (a) Amperometric current response of AuNPs/SPGE in 1 mM $K_3Fe(CN)_6$ (red line) and in 1 mM $Ru(NH_3)_6Cl_3$ (blue line) in 50 mM PBS buffer, pH 7. Measurements performed with cyclic voltammetry at a scan rate of 50 mV s^{-1}; (b) Amperometric current response of AgNPs/SPGE in 1 mM $K_3Fe(CN)_6$ (red line) and in 1 mM $Ru(NH_3)_6Cl_3$ (blue line) in 50 mM PBS buffer, pH 7. Measurements performed with cyclic voltammetry at a scan rate of 50 mV s^{-1}.

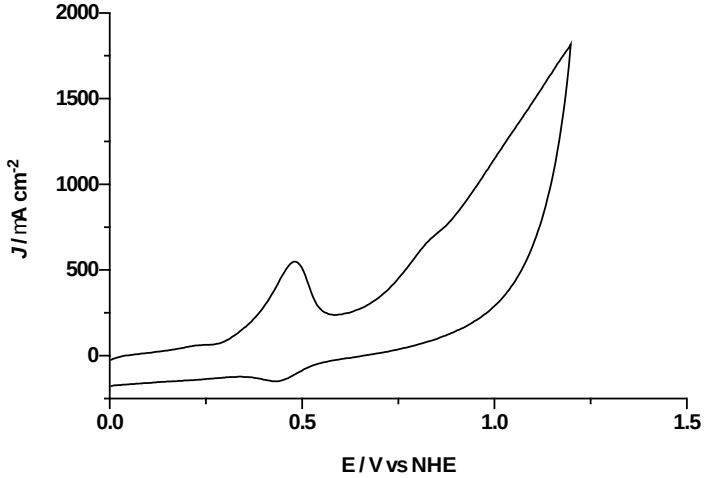

Figure S5. Cyclic voltammograms carried out in a 50 µM quercetin solution in 50 mM TRIS-HCl buffer, pH 7 with graphite electrode at a scan rate of 10 mV s^{-1}.

Paper II

Biosensors and Bioelectronics 88 (2017) 196–203

Contents lists available at ScienceDirect

Biosensors and Bioelectronics

journal homepage: www.elsevier.com/locate/bios

Improved DET communication between cellobiose dehydrogenase and a gold electrode modified with a rigid self-assembled monolayer and green metal nanoparticles: The role of an ordered nanostructuration

P. Bollella[a], F. Mazzei[a], G. Favero[a], G. Fusco[a], R. Ludwig[c], L. Gorton[b], R. Antiochia[a,*]

[a] Department of Chemistry and Drug Technologies, Sapienza University of Rome, P.le Aldo Moro 5, 00185 Rome, Italy
[b] Department of Analytical Chemistry/Biochemistry and Structural Biology, Lund University, P.O.Box 124, SE-221 00 Lund, Sweden
[c] Food Biotechnology Laboratory, Department of Food Science and Technology, BOKU – University of Natural Resources and Life Sciences, Muthgasse 18, A-1190 Vienna, Austria

ARTICLE INFO

Keywords:
Cellobiose dehydrogenase
Direct electron transfer
Gold nanoparticles
Silver nanoparticles
Biphenyl-4,4′-dithiol
Lactose

ABSTRACT

Efficient direct electron transfer (DET) between cellobiose dehydrogenase from *Corynascus thermophilus* (*Ct*CDH) and a novel gold electrode platform, obtained by covalent linking of green AuNPs and AgNPs modified with a dithiol self-assembled monolayer, consisting of biphenyl-4,4′-dithiol (BPDT), was presented. The green AuNPs and AgNPs were synthesized using quercetin as reducing agent at room temperature. TEM experiments showed that the AuNPs and AgNPs were circular in shape with an average diameter of 5 and 8 nm, respectively. Cyclic voltammetry of *Ct*CDH immobilized onto the AuNPs/BPDT/AuE and the AgNPs/BPDT/AuE electrode platforms were carried out and compared with naked AuE, BPDT/AuE, AuNPs/AuE, and AgNPs/AuE. A pair of well-defined redox waves in neutral pH solution due to efficient DET of CtCDH was present with both MNPs/BPDT/AuE platforms. No DET communication was found with platforms without MNPs linked to BPDT. The apparent heterogeneous electron transfer rate constants (k_S) of *Ct*CDH were calculated to be $21.5 \pm 0.8\ s^{-1}$ and $10.3 \pm 0.7\ s^{-1}$, for the AuNPs/BPDT/AuE and the AgNPs/BPDT/AuE platforms, respectively.

The modified electrodes were successively used to develop an eco-friendly biosensor for lactose detection. The *Ct*CDH/AuNPs/BPDT/AuE based biosensor showed the best analytical performances with an excellent stability, a detection limit of 3 μM, a linear range between 5 and 400 μM and a sensitivity of $27.5 \pm 2.5\ \mu A\ cm^{-2}\ mM^{-1}$. Such performances were favorably compared with other lactose biosensors reported in literature.

The biosensor was successively tested to quantify lactose content in real milk and cream samples. No significant interference present in the sample matrices was observed.

1. Introduction

Studies of direct electron transfer (DET) between redox enzymes and electrodes represent an area of extensive research for developing bioelectronic devices such as biosensors and biofuel cells. However, it is well known in the literature that most redox enzymes are not able to reveal DET, because the active site of the enzyme is usually deeply buried within the protein structure (Ghindilis et al., 1997). Nanomaterial based electrodes are able to promote efficient DET reactions because of their large surface area for protein loading as well as their excellent biocompatibility (Pumera et al., 2007; Jianrong et al., 2004; Bollella et al., 2016).

Several approaches of electrode nanostructuration have been developed in order to increase the electroactive area of the electrode (Minteer et al., 2012; Wang et al., 2012; Mazzei et al., 2015; Taurino et al., 2016), including single- and multi-walled carbon nanotubes (Liu et al., 2005; Favero et al., 2015), graphene (Pumera, 2011; Carbone et al., 2015) and metal nanoparticles (Wang et al., 2004; Pingarron et al., 2008).

Among all kind of nanomaterials, metal nanoparticles (MNPs) play an important role in making electrode modifications, because of their high surface area-to-volume ratios and high surface energy, which facilitate the immobilization of several kinds of proteins, allowing to act as electron conducting pathways between the prosthetic groups of the enzymes and the electrode surface (Yañez-Sedeño et al., 2005; Ludwig et al., 2010; Loo et al., 2012; Katz and Willner, 2004; Chen et al., 2012). Another advantage of the use of MNPs is the improved stability of enzyme based electrodes. This can be due to a reduced enzyme

* Corresponding author.
E-mail address: riccarda.antiochia@uniroma1.it (R. Antiochia).

http://dx.doi.org/10.1016/j.bios.2016.08.027
Received 13 June 2016; Received in revised form 9 August 2016; Accepted 10 August 2016
Available online 24 August 2016
0956-5663/

leaching from the electrode because of the strong adsorption of proteins onto the uncoated nanometer-sized colloidal MNPs allowing the protein to retain its biological activity (Baudhuin et al., 1989).

Green synthesis of MNPs has recently become a cheep alternative way for a sustainable and safe production of MNPs (Shah et al., 2015; Cinelli et al., 2015). Several approaches have been reported in the literature, which employ extracts from a variety of different plant species in combination with a variety of acids and metal salts (Ghoreishi et al., 2011; Elia et al., 2014; Makarov et al., 2014). The principal biomolecules present in plant extracts utilized as reducing agents to form MNPs are proteins, polyphenols, vitamins and sugars, such as L-ascorbic acid, gallic acid and quercetin (Wang et al., 2007; Nune et al., 2009; Iravani, 2011). However, most synthesis methods utilizing these biomolecules require high temperatures such as the synthesis using starch and glucose as reducing agents at high temperature for 20 h (Raveendran et al., 2003) or the synthesis using L-ascorbic acid at 80 °C (Mat Zain et al., 2014; Xiong et al., 2011) or the need of microwave assistance (Valodkar et al., 2011; Singh et al., 2016). Moreover these methods are influenced by several variables which are difficult to control and can affect the method reproducibility (Nadagouda and Varma, 2008; Philip, 2010; Zargar et al., 2011).

MNPs can be deposited onto an electrode surface by different approaches: drop-casting (Krueger et al., 2011), covalent linkage (Yang et al., 2006) or electrodeposition directly from the metal precursor (Saha et al., 2012). One of the easiest ways to perform electrode modification is the covalent linkage by using the self-assembled monolayer (SAM) technique (Chaki and Vijayamohanan, 2002; Arya et al., 2009). In recent years, MNPs were self-assembled into two-dimensional or three-dimensional superstructures by using several cross-linkers such as dithiols, diamines, thiolsiloxanes etc. (Wink et al., 1997; Wang et al., 2004). It has been recently demonstrated that aromatic dithiols work better than alkanedithiols because of their enhanced conductivity and low suppleness. In particular it has been found that biphenyl 4,4′-dithiol (BPDT), compared with alkanethiol molecules, is more conductive and forms a monolayer with a vertical molecular configuration, probably because of the rigid structure of the phenyl rings and the π stacking of the molecule (Liang et al., 2007; Matei et al., 2012).

Cellobiose dehydrogenase (CDH) is receiving great attention in recent years in the development of biosensors and biofuel cells (Ludwig et al., 2010; Ludwig et al., 2013) because of its ability to show DET (Lindgren et al., 2001; Schulz et al., 2016; Matsumura et al., 2012; Tasca et al., 2011) for a large number of substrates including sugars, such as glucose and lactose (Tasca et al., 2013; Harreither et al., 2007). CDH is an extracellular flavocytochrome secreted by wood degrading fungi (Zamocky et al., 2006). It consists of a catalytically active flavin adenine dinucleotide (FAD) containing dehydrogenase domain (DH_{CDH}) connected via a flexible linker region to an electron mediating, heme *b* containing cytochrome domain (CYT_{CDH}). The oxidation of the natural substrate cellobiose fully reduces FAD and the electrons are successively transferred by an internal electron transfer mechanism (IET) to the CYT_{CDH} domain resulting in reduced heme *b* (Schulz et al., 2014). CYT_{CDH} acts as a built-in mediator, which shuttles the electrons to suitable electrodes (Schulz et al., 2016). CHDs are expressed by fungi from the dikariotic phyla Basidiomycota (class I CDHs) and Ascomycota (class II CDHs) with different protein sequences (Ludwig et al., 2013; Zamocky et al., 2008). All CDHs accept cellodextrines, cellobiose and lactose as substrates, some class II CHDs also show activity for glucose (Harreither et al., 2011). CDH obtained from the ascomycete *Corynascus thermophilus* (*Ct*CDH) belongs to class II CDHs (Zafar et al., 2012). Unlike CDHs from basidiomycetes and most class II CDHs that show more efficient DET at acidic pHs, CtCDH catalyzes the oxidation of the mono- and disaccharides at neutral pHs, thus allowing DET at physiological conditions.

The aim of this work was to improve the DET efficiency between *Ct*CDH and a novel gold electrode platform, obtained by covalent linking of green AuNPs and AgNPs with a dithiol self-assembled monolayer, biphenyl-4,4′-dithiol (BPDT). The AuNPs and AgNPs were synthesized using quercetin as reducing agent in aqueous solution at room temperature. The novelty of this approach is the use of green MNPs together with BPDT, which allowed an ordered linkage of MNPs because of the low suppleness of its molecule. The so modified electrode was used to develop an eco-friendly biosensor for lactose detection. To the best of our knowledge this is the very first time that BPDT has been used with MNPs for the development of a lactose biosensor. The modified electrode platforms, *Ct*CDH/AuNPs/BPDT/AuE and *Ct*CDH/AgNPs/BPDT/AuE, shown in Scheme 1, were compared with naked gold electrode, BPDT/AuE and MNPs/AuE in absence and in presence of lactose. The study aimed at investigating the effects of the different electrode modifications on DET between *Ct*CDH and the electrode surface. The electrochemical characterization and optimization of the lactose biosensor obtained with the *Ct*CDH/AuNPs/BPDT/AuE platform is also presented in this work. Finally the applicability of the developed biosensor was tested for lactose detection in real milk and cream samples.

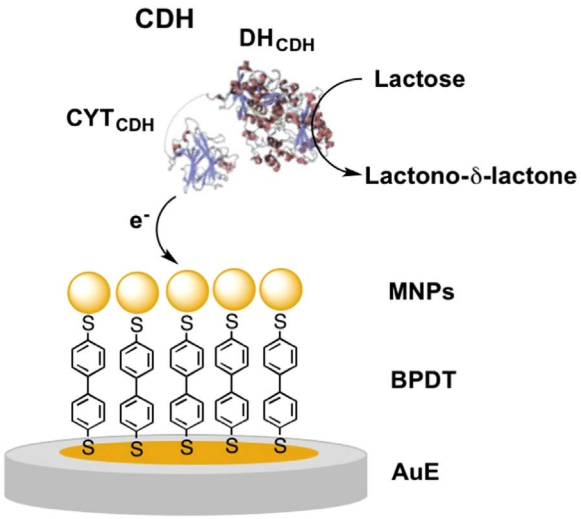

Scheme 1. *Ct*CDH/MNPs/BPDT/AuE platform and DET between *Ct*CDH and the modified electrode.

2. Experimental

2.1. Chemicals and reagents

3-(N-morpholino)propanesulfonic acid (MOPS), β-lactose, sulfuric acid (H_2SO_4), hydrogen peroxide (H_2O_2), D-glucose, D-cellobiose, biphenyl-4,4′-dithiol (BPDT), chloroauric acid ($HAuCl_4{\cdot}3H_2O$), quercetin (QUC), silver nitrate ($AgNO_3$), sodium phosphate monobasic (NaH_2PO_4), sodium phosphate dibasic (Na_2HPO_4) and potassium chloride (KCl) were obtained from Sigma Aldrich (St. Louis, MO, USA), calcium chloride ($CaCl_2$) was purchased from Merck KgaA (Darmstadt, Germany), dialysis membranes (Spectrapor, MWCO 12–14 kDa) were purchased from Spectrum Medical Industires (CA, USA). *Ct*CDH (E.C. 1.1.99.18) (volumetric activity with cytochrome *c* at pH 7.5=53 U ml^{-1}, protein concentration=8.4 mg ml^{-1}) was used for electrode modification. *Ct*CDH was purified from the culture supernatant of the ascomycete *Corynascus thermophilus* (CBS 405.69) obtained from the Centralbureau voor Schimmelcultures (Baarn, The Netherlands). Cultivation and purification of the enzyme were similar to previously reported protocols for *Myriococcum thermophilum* CDH (Zamocky et al., 2008). The enzyme was stored in a 50 mM acetate buffer (pH 5.5 at −80 °C).

Real samples (2% lowfat milk, light cream, whipped cream and 80% lactose-reduced milk) were bought in a local supermarket and carefully

diluted in 50 mM MOPS buffer at pH 7.4 in a ratio 1:250, before analysis. All solutions were prepared using Milli-Q water (18.2 MΩ cm, Millipore, Bedford, MA, USA).

2.2. Synthesis of green AuNPs and AgNPs

The synthesis of AuNPs and AgNPs was carried out using quercetin (QUC) to reduce $HAuCl_4$ and $AgNO_3$, respectively. $HAuCl_4$ and $AgNO_3$ were solubilized in 50 mM PBS buffer at pH 7; quercetin was solubilized in a 1 M NaOH solution with a final concentration of 1 mM, then diluted in 50 PBS buffer at pH 7, and adjusting the pH of the final solution to pH 7.0. The synthesis was performed by mixing a 50 μM solution of QUC with a 300 μM solution of $HAuCl_4$ or $AgNO_3$, in a total reaction batch volume of 10 ml, at room temperature in 50 PBS buffer at pH 7. In both cases the mixture changed color from orange to deep purple for AuNPs and to yellow for AgNPs within a few seconds, because of the formation of the MNPs colloidal solutions. A complete characterization of the synthetized NPs was carried out and reported completely in our previous paper (Bollella et al., submitted).

2.3. TEM experiments

Transmission electron microscopy (TEM) was undertaken with a Philips/FEI BioTwin CM120 TEM microscopy (Hillsboro, OR, USA). Two drops of the synthesized colloidal samples were deposited on a polymer thin copper grid followed by solvent evaporation under vacuum.

2.4. Electrode preparation and modification

Polycrystalline gold electrodes (diameter=1.6 mm, BASi, West Lafayette, IN, USA) were cleaned by incubation in Piranha solution for 2 min (1:3 mixture of conc·H_2O_2 with H_2SO_4, *CAUTION: Piranha solution is especially dangerous, corrosive and may explode if contained in a closed vessel, it should be handled with special care*), then with polishing cloths with deagglomerated alumina slurry of 1 μm diameter (Struers, Ballerup, Denmark), successively sonicated in ultrapure water for 5 min and finally electrochemically cleaned in 0.5 M H_2SO_4 by cycling 20 times between −0.3 and 1.7 V vs. $Ag|AgCl_{sat\ KCl}$ at a scan rate of 300 mV/s.

The electrode modification was carried out by immersing the electrodes in a 10 mM ethanolic solution of biphenyl-4,4′-dithiol (BPDT) overnight at room temperature. The electrodes were successively gently rinsed with ultrapure water and dried under a stream of N_2. MNPs colloidal solutions were drop-cast onto the top of gold electrodes and left to dry at room temperature for 20 min, then gently rinsed with water to avoid any excess of MNPs unreacted with the SAM. Finally, 3 μL of the *Ct*CDH solution were drop-cast onto the so modified surface, left to dry, and then entrapped by covering it with a pre-soaked dialysis membrane, which was fixed with a plastic holder (Haladjian et al., 1994).

AuNPs/AuE and AgNPs/AuE electrodes were obtained following the same procedure described above without the step of BPDT immobilization. Figure SM1 (Supplementary material) shows the SEM images of AuNPs/AuE and AgNPs/AuE electrodes before and after washing, thus confirming that the MNPs remain onto the electrode surface after the washing procedure.

2.5. Electrochemical measurements and electrochemical apparatus

Cyclic voltammetry experiments were carried out using a PalmSens potentiostat (model Emstat^2, Palm Instruments BV, Utrecht, The Netherlands) equipped with PSTrace, version 4.5. A conventional three-electrode electrochemical cell was used for all experiments performed with an Ag|AgCl (sat. KCl) as reference electrode, a platinum wire as counter electrode and a modified gold electrode as working electrode.

Flow injection experiments were performed with a three electrode potentiostat (Zäta Elektronik, Höör, Sweden). The enzyme-modified gold electrode, inserted into a wall-jet flow-through amperometric cell and positioned at a constant distance (1–2 mm) from the inlet nozzle (Appelqvist et al., 1985), was used as working electrode, an $Ag|AgCl_{0.1\ KCl}$ electrode as reference electrode and a platinum wire as counter electrode. The electrochemical cell was connected to a flow injection system consisting of a peristaltic pump (Gilson, Villier-le-Bel, France) and a six-port valve electrical injector (Rheodyne, Cotati, CA, USA). A 50-ll aliquot of the substrate was applied by a loop mounted onto the injector. The resulting electrical current was recorded on a strip chart recorder (Kipp & Zonen, Utrecht, The Netherlands). All measurements were performed at room temperature.

3. Results and discussion

3.1. Green synthesis and characterization of AuNPs and AgNPs

Both AuNPs and AgNPs were synthesized at room temperature using QUC as reducing agent and $HAuCl_4$ and $AgNO_3$ as metal precursors, respectively, according to the reactions shown in Figure SM2 (see Supplementary material). The solution turned from orange to purple and yellow color, indicating the formation of AuNPs and AgNPs, respectively. The most important reaction parameters, reaction time and metal precursor concentration, have been optimized with UV–Vis spectrophotometry, as already described in a previous paper (Bollella et al., submitted). The reaction time was very short (20 min for AgNPs and 30 min for AuNPs) and the synthesis showed a high reaction yield and great reproducibility. MNPs were characterized by transmission electron microscopy (TEM), in order to study their shape, dimensions and size distributions and the results are shown in Fig. 1. Both AuNPs and AgNPs show an almost homogeneous size distribution, spherical form and crystalline structure without aggregates and clusters. The real diameter of the AuNPs and AgNPs resulted in 5.5 ± 0.6 and 8.4 ± 0.3 nm, respectively. A more detailed characterization of the MNPs (EDS spectroscopy, dynamic light scattering, zeta potential) is reported in our previous work (Bollella et al., submitted).

3.2. Electrochemistry of CtCDH on modified MNPs/BPDT/Au electrodes

In order to demonstrate the influence of an ordered nanostructuration on the efficiency of DET communication between *Ct*CDH and the electrode surface, CVs experiments were initially carried out with CDH immobilized onto a bare Au electrode. As shown in Fig. 2a (black curve), no redox waves relative to DET communication between the CYT_{CDH} domain and the electrode surface are visible. The AuE surface was then modified by self-assembling biphenyl-4,4′-dithiol, in order to allow a proper orientation of the enzyme onto the electrode surface. However, once again, no clear redox waves were obtained, as shown in Fig. 2b (black curve). The modification with a bifunctional reagent generally largely enhances the analytical response as the SAM molecule links the enzyme facilitating a DET reaction with the electrode surface (Ludwig et al., 2010). This unexpected result can be ascribed to the fact that BPDT has a terminal -SH group instead of the terminal alcohol or acid groups of most SAMs, which can covalently link only a very small amount of enzyme; moreover at the working pH (7.4) the -SH groups of BPDT are negatively charged (pK_a=6.6) and create an electrostatic repulsion with CtCDH, which is in its anionic form (pI=3.8), thus not favoring the electron transfer from CtCDH to the electrode surface.

Fig. 2(c and d, black curves) shows the CVs of the *Ct*CDH/AuNPs/AuE (C) and *Ct*CDH/AgNPs/AuE (D). With the modification of the electrode with MNPs without SAM a pair of redox waves start to become visible, indicating DET communication of *Ct*CDH, favored by the MNPs. The efficiency of DET is increased with the nanostructura-

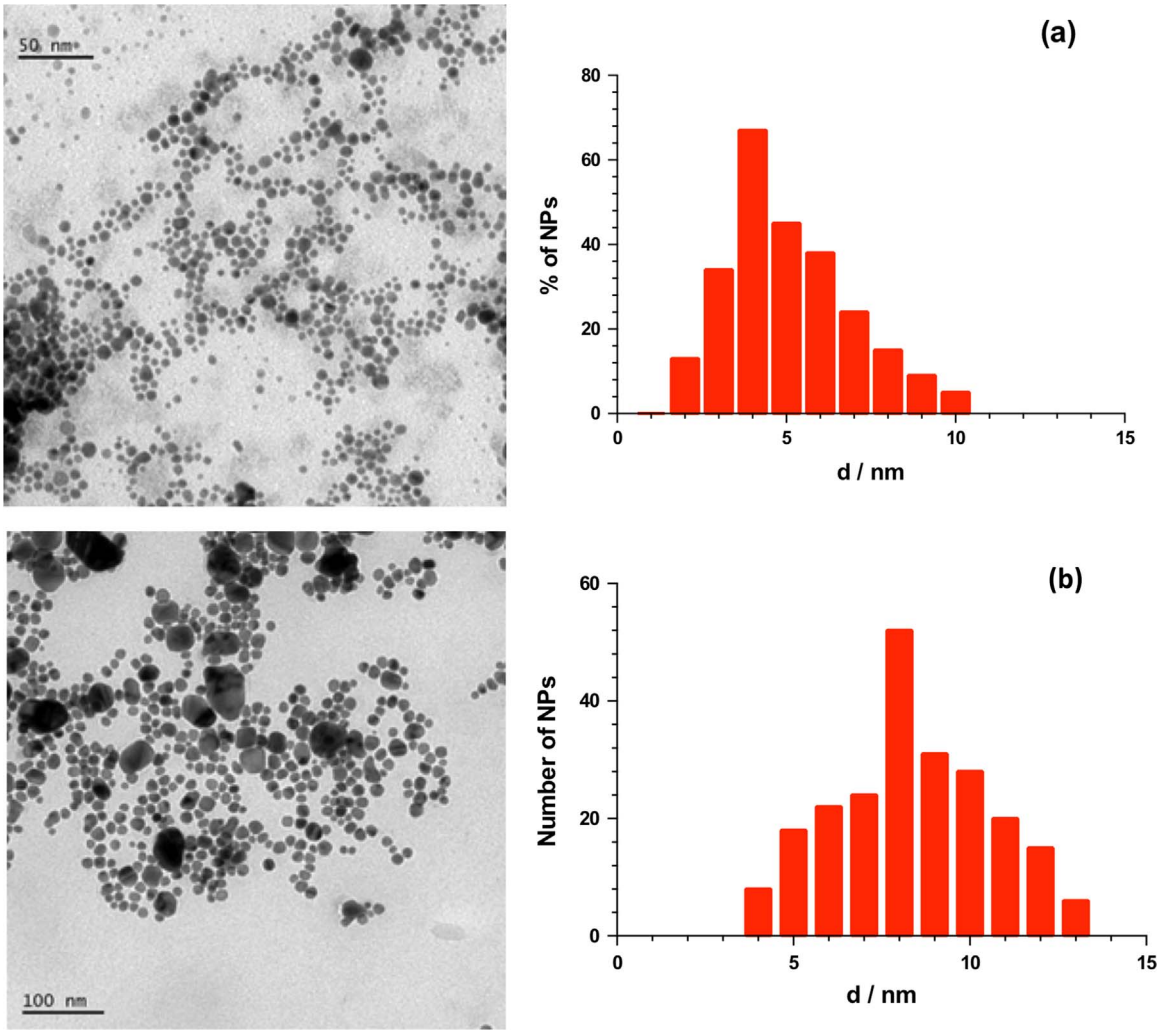

Fig. 1. (a) TEM image of a colloidal solution of AuNPs formed by reduction of Au^{3+} ions using quercetin (left) and size distribution (right); (b) TEM image of a colloidal solution of AgNPs formed by reduction of Ag^{+} ions using quercetin (left) and size distribution (right).

tion of the electrode surface, because there is a higher probability that the enzyme is immobilized in the correct orientation for DET.

Successively, AgNPs and AuNPs were drop-cast onto the BPDT modified electrode. Fig. 2(e and f, black curves) shows CVs relative to CtCDH/BPDT/Au electrodes modified with AgNPs (Fig. 2e) and AuNPs (Fig. 2f). As expected, a pair of well-defined high redox waves, originating from the oxidation and reduction of the heme *b* cofactor located in the CYT_{CDH}, are visible in both cases. DET is now favored by a combined effect of a higher fraction of immobilized *Ct*CDH molecules in DET orientation and a larger number of CtCDH molecules immobilized, due to the presence of the MNPs linked to the SAM, which allow an ordered nanostructuration of the electrode surface. The formal potential (E°′) of the heme *b* group of CYT_{CDH}, evaluated as the midpoint of the oxidation and reduction peak potentials, resulted to be approximately −96 mV and −114 mV vs. $Ag|AgCl_{sat\ KCl}$ for AuNPs and AgNPs, respectively, close to literature values for *Ct*CDH immobilized onto gold electrodes (Harreither et al., 2012a, 2012b). The peak separation between the anodic and cathodic peak potentials were 44 mV and 50 mV at ν=1 mV s^{-1} for AuNPs and AgNPs, respectively, in good agreement with the typical values of a surface confined redox process (Haladjian et al., 1994; Laviron, 1979).

It should be noted that with AuNPs modified electrodes the redox peak currents are almost ten times higher than those with AgNPs modified electrodes. This result may be ascribed to the fact that the AuNPs are smaller and slightly more positively charged than the AgNPs at pH 7.4 (zeta potential values −28.5 ± 1.4 mV and −39.0 ± 1.3 mV for the AuNPs and the AgNPs, respectively) (Bollella et al., submitted). A less electrostatic repulsive environment for the CYT_{CDH} (pI 3.8) is created with AuNPs, thus enhancing DET and allowing a larger enzyme loading onto the electrode surface without influencing the electrochemical behavior of the enzyme.

The electroactive area (A_{EA}) and the roughness factor of the electrode surface of the different platforms were studied. Both parameters exhibited to be largely enhanced with the MNPs/BPDT/AuE platforms, thanks to the ordered nanostructuration Table SM1, (see Supplementary material). Even though the geometrical surface areas are identical, the electrode modified with MNPs linked to BPDT shows a higher real surface area for CDH immobilization compared to naked Au electrodes and to the electrodes modified with the cross-linker agent BPDT or MNPs, separately (Ward et al., 2013).

The scan rate effect was investigated on the DET reaction of the immobilized CtCDH at the MNPs/BPDT/Au electrodes. The CVs at the AuNPs/BPDT/AuE and AgNPs/BPDT/AuE are presented in Fig. SM3a and b (see Supplementary material). It is possible to see that the anodic and cathodic peak currents were linearly proportional versus the scan rate in the range 5–300 mV s^{-1} (Fig. SM3c), indicating a surface controlled electrochemical process.

Further analysis of the CVs allowed calculating the apparent heterogeneous electron transfer rate constants (k_s) for the redox reaction between CtCDH and AuNPs/BPDT/AuE and AgNPs/BPDT/AuE electrodes using the Laviron's method (Laviron, 1979). From the slopes of the linear part of the trumpet plot reported in Fig. SM4d the

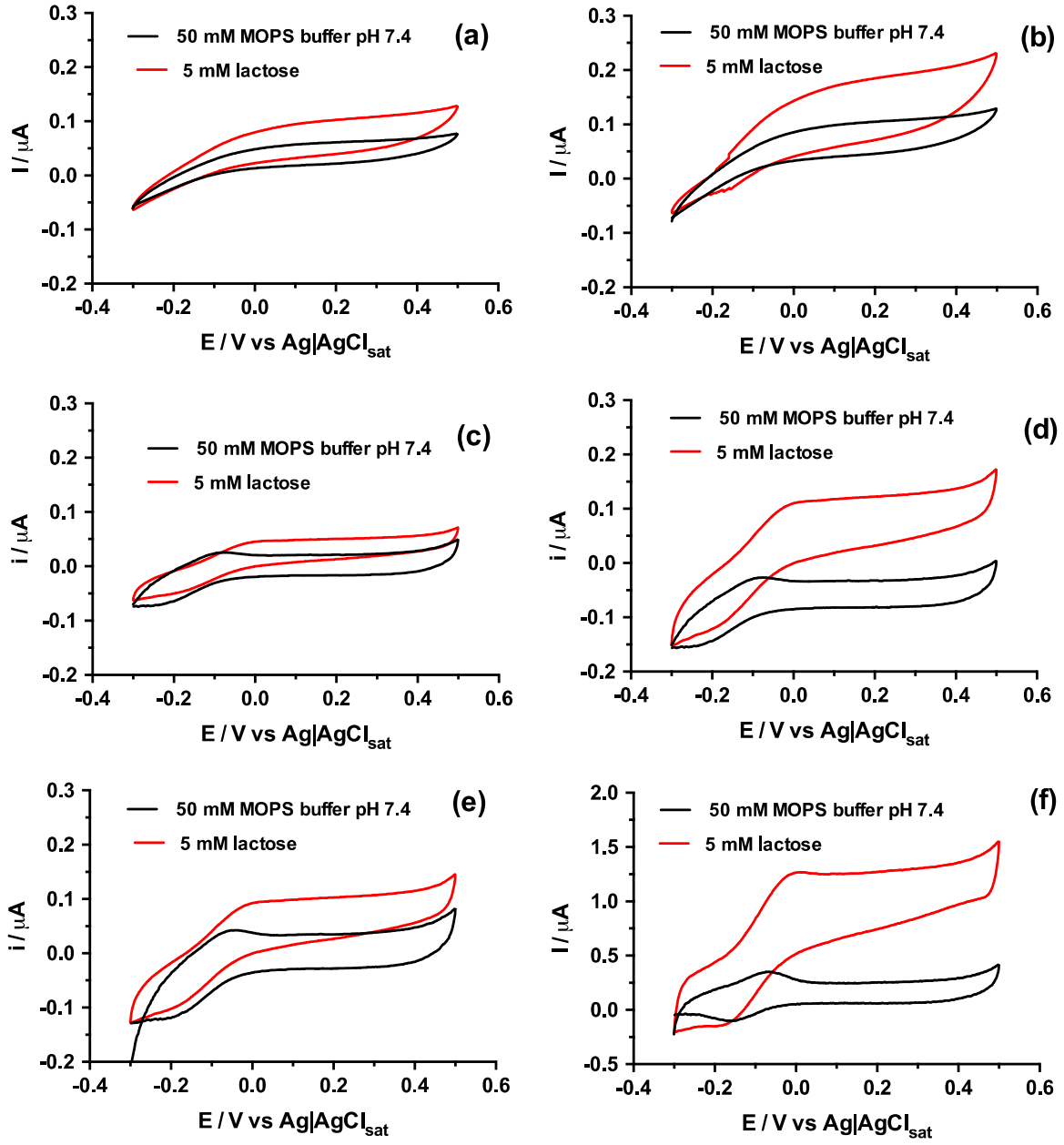

Fig. 2. CVs of *Ct*CDH immobilized onto AuE (a), DPDB/AuE (b) AgNPs/AuE (c), AuNPs/AuE (d), AgNPs/DBDP/AuE (e), AuNPs/DBDP/AuE (f) in absence (black curves) and in presence (red curves) of 5 mM lactose in 50 mM MOPS buffer pH 7.4. Scan rate 1 mV/s. (For interpretation of the references to color in this figure legend, the reader is referred to the web version of this article.).

values can be determined to be 0.49 and 0.47 for the AuNPs and the AgNPs modified electrodes, respectively. Thereafter, the k_s values were calculated according to Laviron's derivation of the Butler-Volmer theory (Eq. (1)) (Laviron, 1979) for a two-electron reaction of a surface confined electroactive species and resulted in 21.5 ± 0.8 s^{-1} and 10.3 ± 0.7 s^{-1} for the AuNPs and the AgNPs modified electrodes, respectively (ν between 5 and 300 mV s^{-1}):

$$\log k_s = \alpha \log(1-\alpha) + (1-\alpha)\log(RT/nF\nu) - \alpha(1-\alpha)nF\Delta E_p/2.3RT \quad (1)$$

where α is the electron transfer coefficient, n is the number of electron, ΔE_p is the separation of the redox peak potentials, ν the scan rate and F, T and R have their usual meanings (F=96.493 C mol^{-1}; T=298 K; R=8.31 J mol^{-1} K^{-1}).

3.3. Electrocatalytic behavior of CtCDH on modified Au electrodes

The electrocatalytic behavior of *Ct*CDH modified electrodes was studied by performing CV experiments in the presence of lactose (Fig. 2, red curves) with the different electrode platforms: AuE (Fig. 2a), BPDT/AuE (Fig. 2b), AgNPs/AuE (Fig. 2c), AuNPs/AuE (Fig. 2d), AgNPs/BPDT/AuE, (Fig. 2e) and AuNPs/BPDT/AuE (Fig. 2f). The CVs clearly show the effects of different electrode modifications towards the electrocatalytic current recorded in the presence of substrate and perfectly agree with the results obtained for DET of CtCDH in the absence of substrate.

With the bare AuE no significant electrocatalytic current is observed, probably because the *Ct*CDH molecules are not properly orientation for DET (Fig. 2a, red curve). With the BPDT/AuE platform a small electrocatalytic current is noted after the addition of substrate (Fig. 2b, red curve) as expected when a cross-linking agent is used, although the current is very low, possibly because of the strong

repulsion between the enzyme and the self-assembled monolayer, both negatively charged at pH 7.4 (Gadogbe et al., 2015). With the modification of the electrode with MNPs the electrocatalytic current for lactose can be observed with a maximum at around 0 V vs. Ag|AgCl, due to the effect of the nanostructuration of the electrode surface (Fig. 2c and d, red curves). AuNPs modified electrodes showed a definitely higher electrocatalytic current probably because at pH 7.4 the AgNPs are less negatively charged than the AgNPs and therefore create a less electrostatic repulsive effect for CtCDH. With the BPDT/MNPs modified electrodes the catalytic currents were higher than with the other electrode platforms (Fig. 2e and f), in accordance with the observations reported in the previous paragraph. These excellent performances can be ascribed to the synergistic effect of nanostructuration and cross-linking, which create a highly packed and ordered nanostructured surface responsible for the enhanced electron transfer. AgNPs and AuNPs are linked through strong covalent bonds with the -SH groups of the SAM, which favor the electron transfer to the electrode thanks to its two aromatic rings. The rigid structure of the molecule, which does not allow any bending onto the electrode surface is another factor that might promote the fast electron transfer from the enzyme. It is easily noted that the AuNPs modified electrode exhibited an electrocatalytic current more than 10 times higher (Fig. 2f, red curve) than that obtained with AgNPs modified electrodes, always probably because the AuNPs are smaller and less negatively charged than the AgNPs.

The results showed that the best electrode platform was shown to be the *Ct*CDH/AuNPs/DBDP/AuE and therefore this platform was used for further experiments.

3.4. Lactose biosensor development

In order to investigate the electroanalytical and kinetic parameters of the *Ct*CDH/AuNPs/BPDT/AuE and *Ct*CDH/AgNPs/BPDT/AuE platforms, the amperometric response to lactose was studied with flow injection analysis (FIA) by successively injecting lactose solutions into the neutral MOPS buffer solution. The fastest peak response was obtained with the AuNPs/BPDT/AuE (3 s), compared to the AgNPs/BPDT/AuE (5 s), probably due to the better electrochemical communication between CtCDH and the electrode surface. Calibration curves for the *Ct*CDH/AuNPs/BPDT/AuE and the *Ct*CDH/AgNPs/BPDT/AuE platforms showed linear response ranges from 5 to 400 μM and from 10 to 400 μM for AuNPs/BPDT/AuE and AgNPs/BPDT/AuE, respectively (R^2=0.99 for both). At higher concentrations the response is no longer linear, thus indicating enzyme saturation (Fig. 3a). The inset in Fig. 3a shows the strict linear response of the biosensor versus lactose concentration. The detection limit was found to be 3 μM for AuNPs/BPDT/AuE and 7.5 μM for AgNPs/BPDT/AuE (S/N=3). The sensitivity for lactose was 27.5 μA mM^{-1} cm^{-2} with the AuNPs/BPDT/AuE platform, almost three times higher than that obtained with the AgNPs modified electrode (10 μA mM^{-1} cm^{-2}).

The characteristics of the lactose biosensor are presented in Table 1. The apparent kinetic parameters (I_{max}, K_M^{app}), obtained by fitting the calibration curves, show a sensible reduction of the apparent Michaelis-Menten constant (K_M^{app}) obtained with AuNPs (844.2 μM) compared to AgNPs ordered nanostructuration (2553.3 μM), suggesting an enhanced enzymatic affinity for the substrate when AuNPs are used. This result can also be explained taking into account that the modification of the electrode with AuNPs creates a more favorable environment for CtCDH compared to AgNPs, allowing the enzyme to correctly orientate its redox centers for an efficient DET.

To date, only a few lactose biosensors have been reported in the literature based on various CDHs (Table SM2) (see Supplementary material) while most other lactose biosensors are based on a cascade of two or three different enzymes (Stoica et al., 2006). In Table SM2 are reported the main analytical characteristics of lactose biosensors based on different types of CDHs. It is interesting to note that the proposed AuNPs/BPDST/AuE biosensor shows a clear extension of the linear range, an enhanced sensitivity and a lower response time compared to other lactose biosensors reported in the literature.

3.5. Stability measurements, interferences evaluation and real samples analysis

The stability and lifetime of the *Ct*CDH/AuNPs/BPDST/AuE biosensor was studied by FIA by measuring the decrease in the electrocatalytic currents after successive injections of lactose. It is possible to observe in Fig. 3b a decrease in the response signal of only 24.3% during continuous injections for 20 days. This result can be due to the ordered nanostructuration of the electrode surface achieved with the concomitant use of BPDT and AuNPs and also to the very small AuNPs dimensions, which can prevent the leaching/detaching of the immobilized enzyme from the electrode surface thus allowing a long term stability of the biosensor.

In order to evaluate the performance of the proposed biosensor for the detection of lactose in real samples, the selectivity of the biosensor was studied by comparing the signal obtained adding equal quantities of interfering compounds (Ca^{2+}, D-cellobiose and D-glucose) and lactose (Harreither et al., 2007). The results are reported in Fig. 3c. It can be observed that the amperometric signal of Ca^{2+} is less than 20% of the response of lactose, while D-cellobiose about 75% and glucose about 15%. As cellobiose and glucose are not present in milk samples, the proposed biosensor can be utilized for lactose detection in real samples with no significant interference. Table 2 shows the results obtained on four different real samples (2% lowfat milk, light cream, whipping cream and 80% lactose-reduced milk). The biosensor *Ct*CDH/AuNPs/BPDT/AuE biosensor allowed the detection of lactose in all samples analyzed with a satisfactory recovery in the range 90–98% (RSD values lower than 4.7%).

4. Conclusions

This work demonstrates the feasible achievement of an efficient DET of a CDH thanks to the ordered electrode nanostructuration realized with a gold electrode modified with a self-assembled monolayer and MNPs. This is the very first time, to the best of our knowledge, that BPDT has been used with AuNPs and AgNPs for the development of a lactose biosensor. The best performances were obtained with the *Ct*CDH/AuNPs/BPDT/AuE platform because AuNPs are smaller and less negatively charged than AgNPs, thus allowing a better orientation and wiring of the enzyme onto the electrode surface. The proposed lactose biosensor can be prepared by a simple and eco-friendly procedure as the MNPs were synthesized according to a green reaction pathway using quercetin as reducing agent which allowed a synthesis at room temperature with a short reaction time, without harmful and expensive reagents, and with high reproducibility. The lactose biosensor was fast-responding and showed a very good stability, excellent sensitivity and a broad linear range. Milk and dairy product matrices did not affect the performance of the biosensor. It can be operated at neutral pH and, unlike lactose biosensors based on class I CDHs, it can also detect glucose. For this reason, the proposed biosensor holds great promises for possible applications as a biofuel cell bioanode suitable to work at human blood conditions.

Acknowledgments

The authors thank the following agencies for financial support: The Swedish Research Council (Vetenskapsradet project 2014-5908), the European Commission (project “Bioenergy” FP7-PEOPLE-2013-ITN-607793).

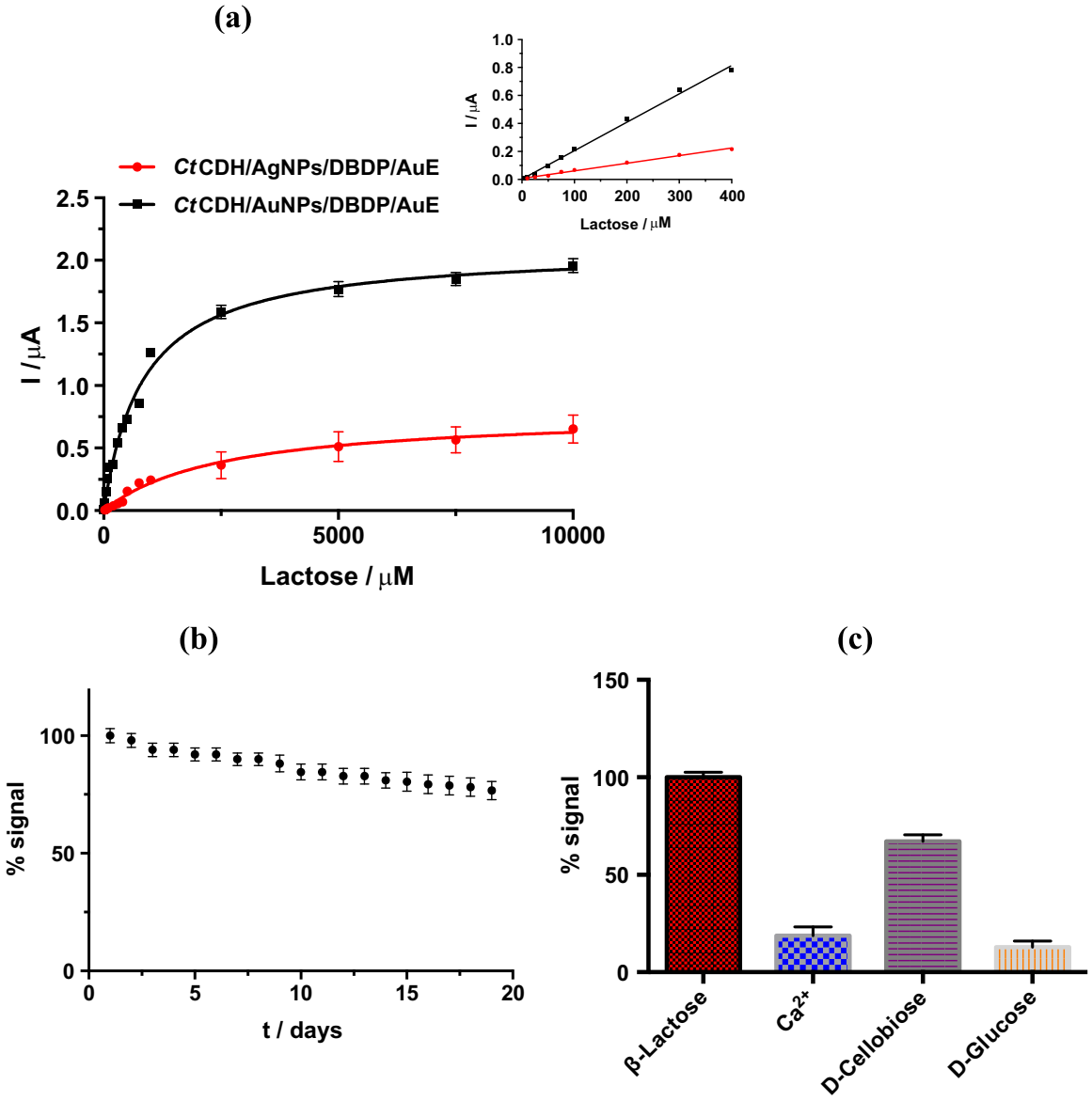

Fig. 3. Calibration graphs for lactose **(a)**; in the inset, the biosensor response in the low-micromolar range; lifetime of *Ct*CDH/AuNPs/DBDP/AuE biosensor in the presence of 200 μM lactose solution in 50 mM MOPS buffer pH 7.4 **(b)**; influence of interfering compounds on lactose response: 1 mM lactose solution (red), 1 mM Ca^{2+} solution (blue), 1 mM D-cellobiose (purple) and 1 mM D-glucose (pink) **(c)**. Buffer: 50 mM MOPS, pH 7.4; applied potential: +0.250 V vs. Ag|$AgCl_{sat}$. (For interpretation of the references to color in this figure legend, the reader is referred to the web version of this article.).

Table 1
Electroanalytical and kinetic parameters of *Ct*CDH biosensors employing different electrochemical platforms obtained by FIA amperometry in 50 mM MOPS buffer, pH 7.4. Applied potential: +0.250 V vs. Ag|$AgCl_{sat}$.

	AuNPs/BPDT/AuE	AgNPs/BPDT/AuE
E_{app}/(V vs Ag|$AgCl_{sat}$)	0.250	0.250
K_M^{app}/(μM)	844 ± 30	2553 ± 39
I_{max}/(μA)	2.1 ± 0.05	0.8 ± 0.04
LOD/(μM)	3	7.5
Linearity range/(μM)	5–400	10–400
Sensitivity/(μA mM^{-1} cm^{-2})	27.5 ± 2.5	10 ± 1
R^2	0.990	0.991

Table 2
Measurements of lactose in real samples diluted 1:250. Experimental conditions: 50 mM MOPS buffer pH 7.4; applied potential: +0.250 V vs. Ag|$AgCl_{sat}$.

Samples	Found value (μM)	Nominal value (μM)	Recovery (%)
2% Lowfat milk	368.6 ± 14.5	384.3 ± 29.2	95.91
Light Cream	440.7 ± 36.9	478.8 ± 53.1	92.04
Whipping Cream	535.3 ± 34.8	594.2 ± 21.6	90.08
80% Lactose-reduced Milk	114.9 ± 12.5	117.3 ± 15.7	97.95

Appendix A. Supplementary material

Supplementary data associated with this article can be found in the online version at doi:10.1016/j.bios.2016.08.027.

References

Appelqvist, R., Marko-Varga, G., Gorton, L., Torstensson, A., Johansson, G., 1985. Anal. Chim. Acta 169, 237–247.
Arya, S.K., Solanki, P.R., Datta, M., Malhotra, B.D., 2009. Biosens. Bioelectron. 24, 2810–2817.
Baudhuin, P., Van der Smissen, P., Beauvois, S., Courtoy, P.J., 1989. Molecular interactions between colloidal gold, proteins, and living cells. In: Hayat, M.A. (Ed.), Colloidal Gold: Principles, Methods, and Applications 2. Academic Press, San Diego,

2–34.
Bollella, P., Fusco, G., Tortolini, C., Sanzò, G., Favero, G., Gorton, L., Antiochia, R., 2016. Biosens. Bioelectron.. http://dx.doi.org/10.1016/j.bios.2016.03.068.
Bollella, P., Schulz, C., Favero, G., Mazzei, F., Ludwig, R., Gorton, L., Antiochia, R., Electroanalysis, accepted for publication
Carbone, M., Gorton, L., Antiochia, R., 2015. Electroanalysis 27, 16–31.
Chaki, N.K., Vijayamohanan, K., 2002. Biosens. Bioelectron. 17, 1–12.
Chen, J.I., Zheng, X.L., Miao, F.J., Zhang, J.N., Cui, X.Q., Zheng, W.T., 2012. J. Appl. Electrochem. 42, 875–881.
Cinelli, M., Coles, S.R., Nadagouda, M.N., Btaszczyński, J., Słowiński, R., Varma, R.S., Kirman, K., 2015. Green Chem. 17, 2825–2839.
Elia, P., Zach, R., Hazan, S., Kolusheva, S., Porat, Z., Zeiri, Y., 2014. Int. J. Nanomed. 9, 4007–4021.
Favero, G., Fusco, G., Mazzei, F., Tasca, F., Antiochia, R., 2015. Nanomaterials 5, 1995–2006.
Gadogbe, M., Chen, M., Zhao, X., Saebo, S., Beard, D.J., Zhang, D., 2015. J. Phys. Chem. C 119, 6626–6633.
Ghindilis, A.L., Atanasov, P., Wilkins, E., 1997. Electroanalysis 9, 661–674.
Ghoreishi, S., Behpour, M., Khayatkashani, M., 2011. Physica E 44, 97–104.
Haladjian, J., Bianco, P., Nunzi, F., Bruschi, M., 1994. Anal. Chim. Acta 289, 15–20.
Harreither, W., Coman, V., Ludwig, R., Haltrich, D., Gorton, L., 2007. Electroanalysis 19, 172–180.
Harreither, W., Sygmund, C., Augustin, M., Narciso, M., Rabinovich, M.L., Gorton, L., Haltrich, D., Ludwig, R., 2011. Appl. Environ. Microbiol. 77, 1804–1815.
Harreither, W., Felice, A.K.G., Paukner, R., Gorton, L., Ludwig, R., Sygmund, C., 2012a. Biotechnol. J. 7, 1359–1366.
Harreither, W., Nicholls, P., Sygmund, C., Gorton, L., Ludwig, R., 2012b. Langmuir 28, 6714–6723.
Iravani, S., 2011. Green Chem. 13, 2638–2650.
Jianrong, C., Yuqing, M., Nongyue, H., Xiaohua, W., Sijiao, L., 2004. Biotechnol. Adv. 22, 505–518.
Katz, E., Willner, I., 2004. Angew. Chem. Int. Ed. 43, 6042–6108.
Krueger, M., Berg, S., Stone, D., Strelcov, E., Dikin, D.A., Kim, J., Cote, L.J., Huang, U., Kolmakov, A., 2011. ACS Nano 5, 10047–10054.
Laviron, E., 1979. J. Electroanal. Chem. 101, 19–28.
Liang, J., Rosa, L.G., Scoles, G., 2007. J. Phys. Chem. C 111, 17275–17284.
Lindgren, A., Gorton, L., Ruzgas, T., Baminger, U., Haltrich, D., Schülein, M., 2001. J. Electroanal. Chem. 496, 76–81.
Liu, Y., Wang, M., Zhao, F., Xu, Z., Dong, S., 2005. Biosens. Bioelectron. 21, 984–988.
Loo, A.H., Bonanni, A., Ambrosi, A., Poh, H.L., Pumera, M., 2012. Nanoscale 4, 921–925.
Ludwig, R., Harreither, W., Tasca, F., Gorton, L., 2010. ChemPhysChem 11, 2674–2697.
Ludwig, R., Ortiz, R., Schulz, C., Harreither, W., Sygmund, C., Gorton, L., 2013. Anal. Bioanal. Chem. 405, 3637–3658.
Makarov, V.V., Love, A.J., Sinitsyna, O.V., Makarova, S.S., Yaminsky, I.V., Taliansky, M.E., Kalinina, N.O., 2014. Acta Nat. 6, 35–44.
Matei, D.G., Mukik, H., Golzhauser, A., Turchanin, A., 2012. Langmuir 28, 13905–13911.
Matsumura, H., Ortiz, R., Ludwig, R., Igarashi, K., Samejima, M., Gorton, L., 2012. Langmuir 28, 10925–10933.
Mat Zain, N., Stapley, A.G.F., Shama, G., 2014. Carbohydr. Polym. 112, 195–202.
Mazzei, F., Favero, G., Bollella, P., Tortolini, C., Mannina, L., Antiochia, R., 2015. Int. J. Environ. Health Res. 7, 267–291.
Minteer, S.D., Atanassov, H.R., Luckarift, G.R., Johnson, G.R., 2012. Mater. Today 15, 166–173.
Nadagouda, M.N., Varma, R.S., 2008. Green. Chem. 10, 859–862.
Nune, S.K., Chanda, N., Shukla, R., Katti, K., Kulkarni, R.R., Thilakavathy, S., Mekapothula, S., Kannan, R., Katti, K.V., 2009. J. Mater. Chem. 19, 2912–2920.
Pingarron, J., Yanez-Sedeno, P., Gonzalez-Cortes, A., 2008. Electrochim. Acta 53, 5848–5866.
Philip, D., 2010. Physica E: Low.-Dim. Syst. Nanostr 42, 1417–1424.
Pumera, M., 2011. Mater. Today 14, 308–315.
Pumera, M., Sanchez, S., Ichinose, I., Tang, J., 2007. Sens. Actuat. B 123, 1195–1205.
Raveendran, P., Fu, J., Wallen, S.L., 2003. J. Am. Chem. Soc. 125, 13940–13941.
Saha, K., Agasti, S.S., Kim, C., Li, X., Rotello, V.M., 2012. Chem. Rev. 112, 2739–2779.
Schulz, C., Kittl, R., Ludwig, R., Gorton, L., 2016. ACS Catal. 6, 555–563.
Schulz, C., Ludwig, R., Gorton, L., 2014. Anal. Chem. 86, 4256–4263.
Shah, A.T., Din, M.I., Bashir, S., Qadir, M.A., Rashid, F., 2015. Anal. Lett. 48, 1180–1189.
Singh, D., Rawat, D., Isha, 2016. Bioresour. Bioprocess. 3, 14–21.
Stoica, L., Ludwig, R., Haltich, D., Gorton, L., 2006. Anal. Chem. 78, 393–398.
Tasca, F., Harreither, W., Ludwig, R., Gooding, J.J., Gorton, L., 2011. Anal. Chem. 83, 2042–3049.
Tasca, F., Ludwig, R., Gorton, L., Antiochia, R., 2013. Sens. Actuat. B 177, 64–69.
Taurino, I., Sanzò, G., Antiochia, R., Tortolini, C., Mazzei, F., Favero, G., De Micheli, G., Carrara, S., 2016. Trends Anal. Chem. 79, 151–159.
Valodkar, M., Modi, S., Pal, A., Thakore, S., 2011. Mat. Res. Bull. 46, 384–389.
Wang, L., Wang, E., 2004. Electrochem. Commun. 6, 49–54.
Wang, W., Chen, Q., Jiang, C., Yang, D., Liu, X., Xu, S., 2007. Colloid Surf. A: Physicochem. Eng. ASP 301, 73–79.
Wang, X.J., Falk, M., Ortiz, R., Matsumura, H., Bobacka, J., Ludwig, R., Bergelin, M., Gorton, L., Shleev, S., 2012. Biosens. Bioelectron. 31, 251–256.
Ward, K., Gara, M., Lawrence, N.S., Hartshome, R.S., Compton, R.G., 2013. J. Electroanal. Chem. 695, 1–9.
Wink, T., van Zuilen, S.J., Bult, A., van Bennekom, W.P., 1997. Analyst 122, 43R–50R.
Xiong, J., Wang, Y., Xue, Q., Wu, X., 2011. Green. Chem. 13, 900–904.
Yañez-Sedeño, P., Pingarron, J.M., 2005. Anal. Bioanal. Chem. 382, 884–886.
Yang, W., Wang, J., Zhao, S., Sun, Y., Sun, C., 2006. Electrochem. Commun. 8, 665–672.
Zafar, M.N., Safina, G., Ludwig, R., Gorton, L., 2012. Anal. Biochem. 425, 36–42.
Zamocky, M., Ludwig, R., Peterbauer, C., Hallberg, B.M., Divne, C., Nicholls, P., Haltrich, D., 2006. Curr. Protein Pept. Sci. 7, 255–280.
Zamocky, M., Schumann, C., Sygmund, C., O'Callaghan, J., Dobson, A.D.W., Ludwig, R., Haltrich, D., Peterbauer, C.K., 2008. Prot. Expres Purif. 59, 258–265.
Zargar, M., Amid, A.A., Bakar, F.A., Shamsudin, M.N., Shameli, K., Jahanshiri, F., Farahani, F., 2011. Molecules 16, 6667–6676.

Supplementary Material

Improved DET communication between cellobiose dehydrogenase and a gold electrode modified with a rigid self-assembled monolayer and green metal nanoparticles: the role of an ordered nanostructuration

P. Bollella[a], F. Mazzei[a], G. Favero[a], G. Fusco[a], R. Ludwig[c], L. Gorton[b], R. Antiochia [a]*

[a]*Department of Chemistry and Drug Technologies, Sapienza University of Rome, P.le Aldo Moro 5, 00185 - Rome, Italy*

[b]*Department of Analytical Chemistry/Biochemistry and Structural Biology, Lund University, P.O.Box 124, SE-221 00 Lund, Sweden*

[c]*Food Biotechnology Laboratory, Department of Food Science and Technology, BOKU – University of Natural Resources and Life Sciences, Muthgasse 18, A-1190 Vienna, Austria*

*Corresponding author.

Email address: riccarda.antiochia@uniroma1.it

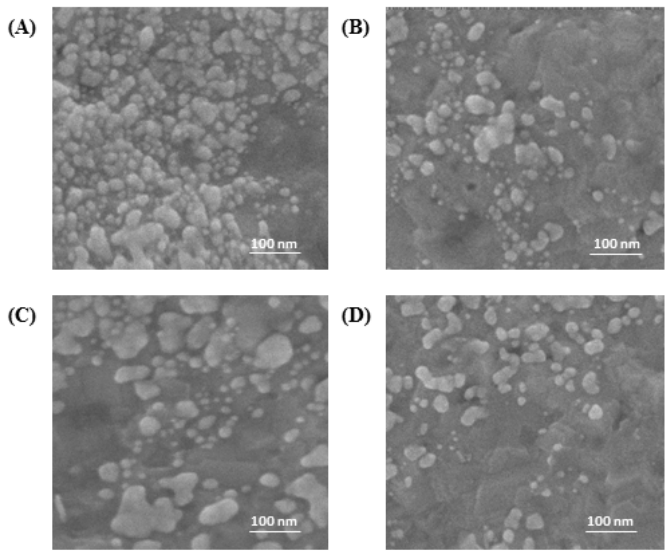

Fig. SM1. SEM images of (A) AuNPs/AuE before washing, (B) AgNPs/AuE before washing, (C) AuNPs/AuE after washing and (D) AgNPs/AuE after washing.

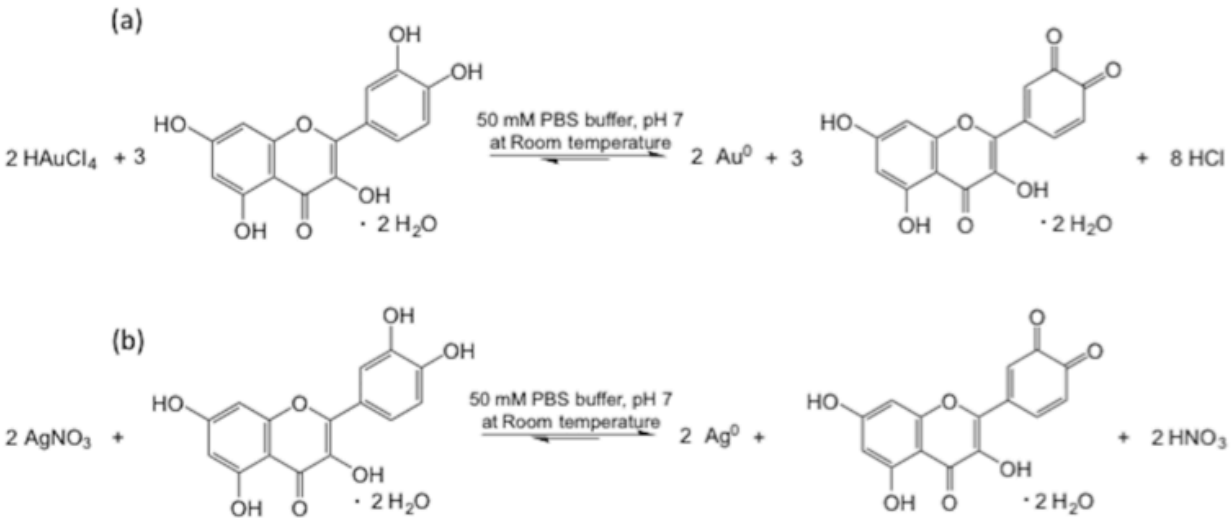

Fig. SM2. Green synthesis of metal nanoparticles through reduction of metal cations by quercetin: (a) $HAuCl_4$ and (b) $AgNO_3$.

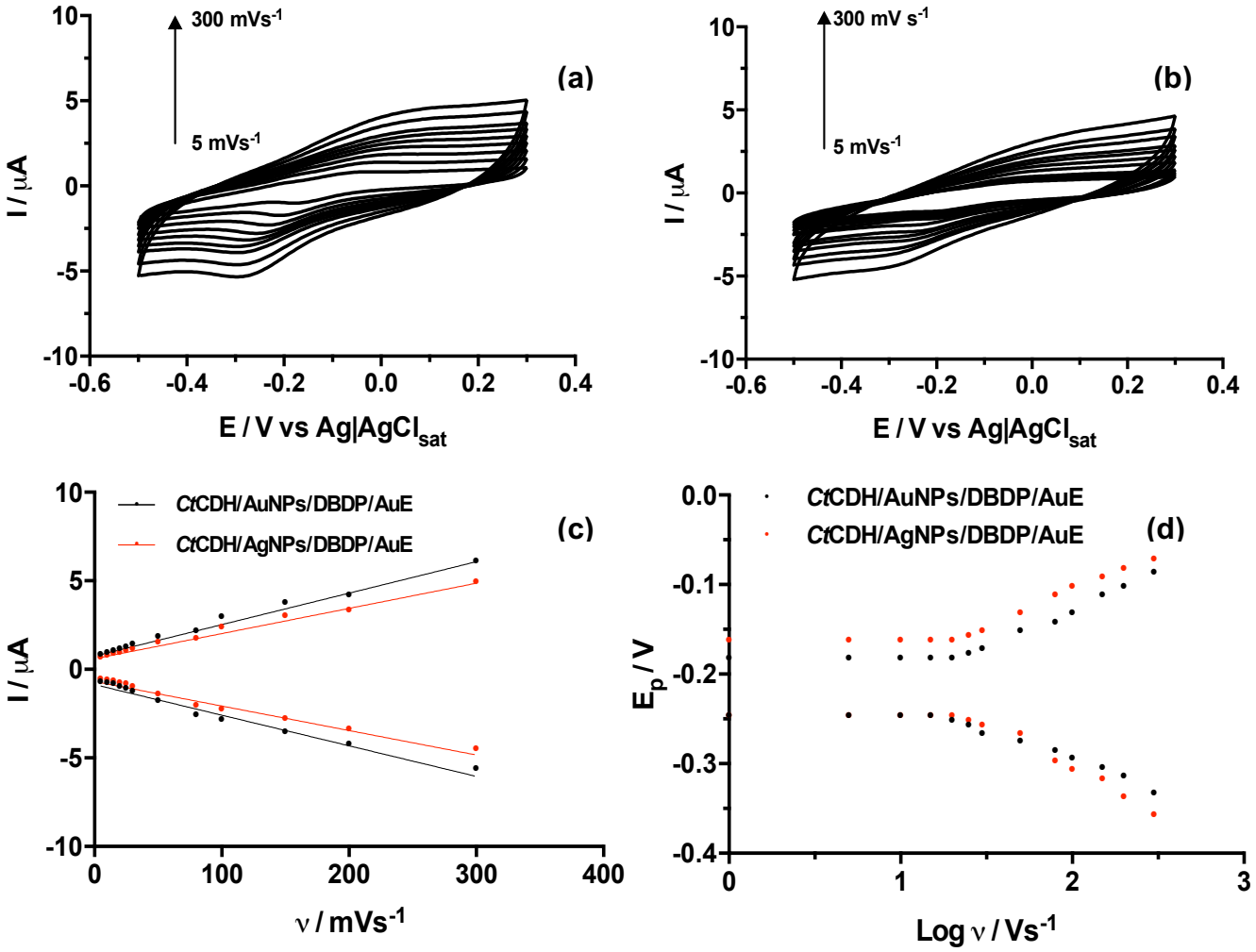

Fig. SM3. CVs of *Ct*CDH immobilized onto AuNPs/DBDP/AuE **(a)** and AgNPs/DBDP/AuE **(b)** in 50 mM MOPS buffer pH 7.4 at different scan rates ranging from 1 to 300 mV s^{-1}. **(c)** Plot of the peak current (I_p) versus scan rate (v). **(d)** Variations of E_p versus log v for *Ct*CDH modified electrodes.

Table SM1.
Electroactive area (A_{EA}) and roughness factor (ρ) values of different electrochemical platforms with 5 mM $Fe(CN)_6^{3-/4-}$ in 50 mM PBS buffer pH 7.4.

	A_{EA} (cm^2)	ρ
AuE	0.036 ± 0.013	1.80
AuE/BPDT	0.042 ± 0.018	2.10
AuE/AuNPs	0.054 ± 0.016	2.70
AuE/AgNPs	0.039 ± 0.010	1.95
AuE/BPDT/AuNPs	0.078 ± 0.026	3.90
AuE/BPDT/AgNPs	0.045 ± 0.014	2.25

Table SM2.
Comparisons between the main analytical parameters of lactose biosensors based on different CDH enzymes.
List of abbreviations: AuE, solid gold electrode; GC, glassy carbon electrode; MWCNTs, multi-walled carbon nanotubes; MUDOH, 11-mercaptoundecanol; NH_2-PD, *p*-phenylenediamine; SPCE, screen printed carbon electrode; SWCNTs, single-walled carbon nanotubes; GA-Tri, glutaraldehyde-Triton; *Ps*CDH, cellobiose dehydrogenase from *Phanerochaete sordida*; *Tv*CDH, cellobiose dehydrogenase from *Trametes villosa*.

Biosensor Platform	Linear Range/ (μM)	LOD/ (μM)	Sensitivity/ (μA mM^{-1} cm^{-2})	Response Time/ (s)	E/(V vs. Ag/AgCl)	Reference
***Ps*CDH/MWCNTs/SPCEs** ***Tv*CDH/MWCNTs/SPCEs**	0.5-100 0.5-200	0.2	-	65	0.10	Safina et al., 2010
***Ps*CDH/NH_2-PD/SWCNTs/GC**	1-100	0.5	4.8	4	0.10	Tasca et al., 2013
***Ps*CDH/MUDOH/AuE**	1-100	1	17.8	4	0.30	Stoica et al., 2006
***Ps*CDH/GA/Tri/MWCNTs/SPCEs**	2-200	2	-	-	-	Glithero et al., 2013
***Ct*CDH/AuNPs/BPDT/AuE**	5-400	3	27.5	3	0.25	this work

Paper III

Sensors and Actuators B xxx (2017) xxx–xxx

Contents lists available at ScienceDirect

Sensors and Actuators B: Chemical

journal homepage: www.elsevier.com/locate/snb

Research Paper

A Glucose/Oxygen Enzymatic Fuel Cell based on Gold Nanoparticles modified Graphene Screen-Printed Electrode. Proof-of-Concept in Human Saliva

Paolo Bollella[a], Giovanni Fusco[b], Daniela Stevar[a], Lo Gorton[c], Roland Ludwig[d], Su Ma[d], Harry Boer[e], Anu Koivula[e], Cristina Tortolini[a], Gabriele Favero[a], Riccarda Antiochia[a,*], Franco Mazzei[a,*]

[a] Department of Chemistry and Drug Technologies, Sapienza University of Rome, P.le Aldo Moro, 5 00185 Rome, Italy
[b] Department of Chemistry, Sapienza University of Rome, P.le Aldo Moro, 5 00185 Rome, Italy
[c] Department of Analytical Chemistry/Biochemistry and Structural Biology, Lund University, P.O. Box 124, SE-221 00 Lund, Sweden
[d] Food Biotechnology Laboratory, Department of Food Science and Technology, BOKU – University of Natural Resources and Life Sciences, Muthgasse 18, A-1190 Vienna, Austria
[e] VTT Technical Research Centre of Finland, P.O. Box 1000, FI-02044 VTT, Finland

ARTICLE INFO

Article history:
Received 12 April 2017
Received in revised form
29 September 2017
Accepted 4 October 2017
Available online xxx

Keywords:
Enzymatic fuel cells (EFCs)
Cellobiose dehydrogenase
Laccase
Direct electron transfer
AuNPs
Human saliva

ABSTRACT

This paper presents a new direct electron transfer based-miniaturized glucose/oxygen enzymatic fuel cell (EFC) whose operating ability has been tested in real saliva samples. The bioanode and biocathode are a graphene working electrode and a graphite counter electrode localized on the same screen printed electrode (SPE) modified with poly(vinyl alcohol) *N*-methyl-4(4′-formylstyryl)pyridinium methosulfate acetal (PVA-SbQ)/cellobiose dehydrogenase from *Corynascus Thermophilus* (*Ct*CDH) C291Y/AuNPs and with *Trametes Hirsuta* laccase (*Th*Lac)/AuNPs, respectively.

In order to optimize the bioanode, several CDH immobilization procedures were adopted, such as drop-casting, use of Nafion membrane or PVA-SbQ photopolymer. The photopolymer showed the best performance in terms of stability and reliability. As biocathode a partially optimized laccase electrode was employed with the variant that the used nanomaterials allowed to reduce the overpotential of O_2/H_2O redox reaction catalyzed by *Trametes Hirsuta* Laccase (*Th*Lac), drop-casted onto the gold nanoparticles (AuNPs) modified SPE.

The performances of bioanode and biocathode were tested separately, initially immobilizing the two enzymes onto separated graphene SPEs. An efficient direct electron transfer was achieved for both elements, obtaining an apparent heterogeneous electron transfer rate constant (k_s) of $0.99 \pm 0.05\ s^{-1}$ for *Ct*CDH C291Y and $5.60 \pm 0.05\ s^{-1}$ for *Th*Lac. Both electrodes were then assembled in a two compartment EFC obtaining a maximal power output of $5.16 \pm 0.15\ \mu W\ cm^{-2}$ at a cell voltage of 0.58 V and an open circuit voltage (OCV) of 0.74 V. Successively, the bioanode and biocathode were assembled in a non-compartmentalized EFC and a remarkable 50% decrease of the maximum power output at the value of $2.15 \pm 0.12\ \mu W\ cm^{-2}$ at cell voltage of 0.48 V and an OCV of 0.62 V at pH 6.5 was registered. In order to reduce the cell dimensions in view of its possible integration in biomedical devices, the bioanode and biocaythode were realized by immobilization of both enzymes onto the same SPE. The so miniaturized EFC delivered a maximal power output of $1.57 \pm 0.07\ \mu W\ cm^2$ and $1.10 \pm 0.12\ \mu W\ cm^{-2}$ with an OCV of 0.58 V and 0.41 V in a 100 μM glucose solution and in human saliva, respectively.

1. Introduction

Over the past two decades there was a growing demand for energy along with a need to have increasing "green" and sustainable energy resources [1–3]. Furthermore, the exponential growth in the use of miniaturized and portable computing and communi-

* Corresponding authors.
E-mail addresses: riccarda.antiochia@uniroma1.it (R. Antiochia), franco.mazzei@uniroma1.it (F. Mazzei).

https://doi.org/10.1016/j.snb.2017.10.025
0925-4005/

cations devices [4] has determined the development of a number of technologies addressed to implement space-saving power sources, more preferentially "environmentally friendly" [5,6]. Among the various technologies, the realization of biological fuel cells (BCFs) appears to be particularly interesting for some of their peculiar characteristics such as small dimensions, lightweight and sustainable power sources by using renewable fuels (e.g., alcohols, sugars). These devices have three main advantages: high conversion efficiency, operability at room temperature and the possibility to scale down. The most effective advantage is the scalability as evidenced by the recent progresses in medical sciences, with an increasing development of implantable electrically operated devices (e.g., pacemakers), which need a small power sources that can supply energy over a long period of time, avoiding any maintenance and replacement issues that would require a surgery [7–9].

BFCs can be classified on the basis of the different biological entities used in the anodic part: enzymatic fuel cells (EFCs) based on redox enzymes and microbial fuel cells (MFCs) based on whole microbial cells, both catalysing the fuel oxidation [10–13]. MFCs require continuous maintenance of whole living cells to sustain physiological process, severely limiting the possibility to produce an adequate power output [14]. Interesting results can be achieved by using EFCs, based on redox enzymes, obtained through extraction and purification from living organisms, and directly applied as a biocatalysts in a BFCs [15,16].

The EFCs can be divided into two main groups: (a) mediated electron transfer (MET) devices, in which redox species are used to transport the electrons between enzyme and electrode surface; (b) direct electron transfer (DET) based biodevices, where the enzyme is able to communicate directly with the electrode. In order to enhance the overall performances of EFCs, several nanomaterials, such as carbon nanotubes (single- or multi-walled) [17,18], metal nanoparticles (gold-, silver- or platinum-NPs) [19,20] and graphene [21,22], have been employed taking advantage from the high surface/volume ratio improving the enzyme loading as well as the electron transfer at the electrode surface. Most EFCs reported in the literature employ redox mediators to establish a fast electron transfer between enzymes and electrodes [16]. However, the immobilization of a mediator showed a decrease of the theoretical open-circuit potential (OCP) of the biofuel cell. Hence, great attention has recently been given to EFCs based on direct electron transfer (DET) [16].

In this context graphene is considered an ideal material for electrode modification mainly due to its high electron conductivity in the 2D-plane and for its simple and low cost fabrication [23,24]. These extraordinary properties could be improved through coupling graphene with gold nanoparticles (AuNPs), to considerably increase the real surface area, thus stabilizing the protein layer immobilized according to different procedures such as drop-casting, physical entrapment with a polymer membrane or chemical cross-linking [25,26]. Moreover, the combination of graphene and AuNPs could act as electron shuttles of electrons from the prosthetic group of redox proteins to the electrode surface [27–30].

DET-based devices have several advantages over MET-based devices, preventing the voltage losses arising from the potential difference between the active site of the enzyme and the mediator, as well as, allowing a simplification in the EFCs development thus making miniaturization easier. Among the enzymes able to perform DET with the electrode surface as bioanode electrode in the development of biofuel cells, cellobiose dehydrogenase (CDH) is receiving great attention [30,31] thanks to its ability to show DET [32–35] with many substrates including sugars, such as glucose and lactose [36,37]. CDH is an extracellular flavocytochrome secreted by wood-degrading fungi [38]. It consists of a catalytically active flavin adenine dinucleotide (FAD) containing dehydrogenase domain (DH_{CDH}) connected via a flexible linker region to an electron mediating, heme *b*-containing cytochrome domain (CYT_{CDH}). The oxidation of the natural substrate cellobiose fully reduces FAD and the electrons are successively transferred by an internal electron transfer mechanism (IET) to the CYT_{CDH} domain resulting in reduced heme *b* [39].

In the case of biocathode development using enzymes, such as laccases or bilirubin oxidase, the crucial point is the achievement of a low overpotential for the four proton/four electron reduction of oxygen into the water at pH = 7. In the neutral pH range, considering the thermodynamic O_2/H_2O redox potential of +0.93 V NHE, it is required to have overpotential values within the range 30–70 mV to obtain an efficient electron transfer (ET) [40–45].

In the last twenty years, screen-printed electrodes (SPEs) have received great attention for the on-site monitoring as a good compromise between high-volume and low-cost electrodes production, although not yet highly reproducible and reliable single-use sensors. Therefore, the use of screen-printing technology in the serial production of disposable low-cost electrodes for the electrochemical determination of a wide range of substances is currently undergoing widespread growth [46,47].

The aim of this work is to realize a miniaturized high-power biofuel cell based on efficient DETs between *Ct*CDH C291Y mutant and *Trametes Hirsuta* Laccase, respectively, using the same screen-printed electrode modified with "green" AuNPs. The electrodes were characterized separately by calculating all the parameters concerning the direct electron transfer, in order to optimize the construction of the enzymatic fuel cell. The device was studied in three different configurations: i) by using two separate SPEs as bioanode and biocathode in a two separate compartments cell; ii) by using two separate SPEs as bioanode and biocathode in a membrane-less one-compartment EFC; iii) by using one SPE for both bioanode and biocathode in a membrane-less one-compartment EFC. Finally, the single-SPE EFC was tested in human saliva samples.

2. Materials and methods

2.1. Chemicals and reagents

Catechol, 2,2′-azino-bis-(3-ethylbenzotiazoline-6-solfonate) (ABTS), potassium ferricyanide ($K_3[Fe(CN)_6]$), potassium chloride (KCl), sodium phosphate monobasic (NaH_2PO_4), sodium phosphate dibasic (Na_2HPO_4), sodium citrate monobasic ($C_6H_7NaO_7$), sulfuric acid (H_2SO_4), D-glucose 99,8%, β-lactose 99%, quercetin ~95%, tetrachloroauric acid ($HAuCl_4$), gold nanoparticles (AuNPs, d = 5 nm stabilized with 0.1 mM PBS, reactant free), Nafion® 117 (~5% in a mixture of lower aliphatic alcohols and water) were purchased from Sigma-Aldrich (Buchs, Switzerland).

Poly(vinyl alcohol) *N*-methyl-4(4′-formylstyryl)pyridinium methosulfate acetal (PVA-SbQ) was purchased from Polysciences Inc. (Warrington PA,USA).

Orthophosphoric acid ~85% (H_3PO_4), boric acid (H_3BO_3), acetic acid (CH_3COOH), sodium hydroxyde (NaOH) were purchased from Merck (Darmstadt, Germany).

*Ct*CDH (E.C. 1.1.99.18) (volumetric activity with cytochrome *c* at pH 7.5 = 53 U ml^{-1}, protein concentration = 8.4 mg ml^{-1}) solution was used for electrode modification. *Ct*CDH was purified from the culture supernatant of the ascomycete *Corynascus thermophilus* (CBS 405.69) obtained from the Central bureau voor Schimmelcultures (Baarn, The Netherlands). Cultivation and purification of the enzyme were similar to previously reported protocols for *Myriococcum thermophilum* CDH [48]. The enzyme was stored in a 50 mM acetate buffer (pH 5.5 at −80 °C).

Please cite this article in press as: P. Bollella, et al., A Glucose/Oxygen Enzymatic Fuel Cell based on Gold Nanoparticles modified Graphene Screen-Printed Electrode. Proof-of-Concept in Human Saliva, Sens. Actuators B: Chem. (2017), https://doi.org/10.1016/j.snb.2017.10.025

*Th*Lac (E.C. 1.10.3.2) (volumetric activity with ABTS at pH 4.5 = 421 U ml^{-1}, protein concentration = 3.9 mg ml^{-1}) produced in its native host was purified in two chromatographic steps basically as described [49]. The concentrated and buffer exchanged culture filtrate from *Trametes hirsuta* strain VTT D-95443 was applied to a DEAE Sepharose Fast Flow anion exchange column equilibrated with 15 mM sodium acetate pH 5.0. Proteins were eluted with a linear 50–150 mM NaCl gradient. Laccase-positive fractions (on ABTS) were pooled and Na_2SO_4 was added to the sample to a final concentration of 0.5 M. The sample was applied to a Phenyl Sepharose Fast Flow hydrophobic interaction column equilibrated with 20 mM citrate buffer pH 5.0 containing 0.5 M Na_2SO_4. Proteins were eluted with a linear decreasing Na_2SO_4 gradient (500–50 mM). Laccase containing fractions were pooled and concentrated (Millipore; PM10 membrane) [50].

All solutions were prepared using Milli-Q water (ρ = 18.2 MΩ cm a 25 °C; TOC < 10 μg L^{-1}, Millipore, Molsheim, France).

2.2. Synthesis of gold nanoparticles (AuNPs)

The synthesis of AuNPs was carried out by using quercetin (QUC), as reducing agent, to reduce the metal precursor, $HAuCl_4$. The metal precursor was solubilized in 50 mM PBS at pH 7; quercetin was solubilized in a 1 M NaOH solution with a final concentration of 1 mM, then diluted in 50 mM PBS buffer at pH 7, adjusting the pH to pH 7.0 by using 6 M HCl/NaOH solutions. The reaction was performed by mixing a 50 μM solution of QUC with a 300 μM solution of $HAuCl_4$ in a total reaction batch volume of 10 mL, at room temperature in 50 mM PBS buffer at pH 7, the solution changed color from orange to deep purple within a few seconds, for the formation of the AuNPs colloidal solutions. A detailed characterization of the synthesized AuNPs was carried out and reported in our previous paper [51].

2.3. Electrochemical measurements

Cyclic voltammetry, linear sweep voltammetry and chronoamperometry experiments were performed by using a μAutolab III potentiostat (Eco Chemie, The Netherlands) controlled by GPES Manager program (Eco Chemie, The Netherlands) with a conventional three electrodes configuration. Screen-printed working electrodes (DropSens, Oviedo, Spain) with a surface diameter of 4 mm, formed of the following materials, graphite (G) Cat. DRP-110, gold (Au) Cat. DRP-220AT and graphene (GPH) Cat. DRP-110GPH were used. A saturated calomel electrode (SCE, 244 mV vs. NHE, Cat. 303/SCG/12, AMEL, Milano, Italy) and a glassy carbon rod electrode (d = 2 mm, Cat. 6.1241.020, Metrohm, Herisau, Switzerland) were used as reference and counter electrodes, respectively. The polarization curves have been recorded by running linear sweep voltammetry (LSV) at 1 mV s^{-1} from the open circuit potential (OCV) to 0 connencting the bioanode namely PVA-SbQ/*Ct*CDH/AuNPs/GPH as working electrode and *Th*Lac/AuNPs/GPH (in the first two steps of enzymatic fuel cell assembly, below reported) or *Th*Lac/AuNPs/G (in the third step when a single-SPE EFC was assembled) as a combined reference and counter electrode. In the first step the measurements have been carried out in U-glass tube equipped with a proton-exchange membrane, placing in one compartment the bioanode (5 mM glucose, 50 mM PBS buffer pH 7.4 + 150 mM NaCl) while in the others the biocathode (air-satured 50 mM Britton–Robinson buffer pH 5.5). After a careful pH optimization carried out in air-saturated 50 mM citrate-phosphate + 150 mM NaCl at different pH values ranging between 4.5 and 7.5, the proton-exchange membrane has been removed placing both electrodes in a becker containing 50 mM citrate-phosphate buffer pH 6.5 (5 mM glucose). Finally, the measurements with the single-SPE EFC were carried out placing 50 μL of fuel solution onto the so modified SPE (100 μM glucose, 50 mM citrate-phosphate pH 6.5 + 150 mM NaCl).

2.4. Electrodes modification

For either bioanode and biocathode preparation, graphene (GPH) screen printed electrodes (SPE) Cat. DRP-110GPH from DropSens (Oviedo, Spain) were used. In the bioanode development the following different procedures for the immobilization of the *Ct*CDH C291Y were used and compared:

- *Method 1) drop-casting (CtCDH C291Y/AuNPs/GPH):* 5 μL of AuNPs colloidal suspension (50% v/v diluted in 50 mM PBS buffer pH 7.4) were drop-casted onto the SPE electrode surface through a layer by layer deposition method (4 layers) and left to dry at room temperature for 20 min after each deposition. After that, 5 μL of *Ct*CDH 291Y were spread onto the SPE and left to dry at room temperature for 20 min and then in an desiccator for about 2 h before use.
- *Method 2) nafion (Nafion/CtCDH C291Y/AuNPs/GPH):* a Nafion 117 solution (5%, w/v) was diluted with ethanol and NaOH solution to give a stock solution of 1%, pH 5.0. 10 μL of the Nafion solution was mixed with 5 μL of AuNPs colloidal suspension (50% v/v diluted in 50 mM PBS buffer pH 7.4) and 5 μL of *Ct*CDH C291Y. 5 μL of the resulting solution were drop-casted onto the electrode surface and left to dry at room temperature over 2 h.
- *Method 3) PVA-SbQ (PVA-SbQ/CtCDH C291Y/AuNPs/GPH):* 5 μL of a *Ct*CDH C291Y enzymatic solution with 8 μL of PVA-SbQ solution (50 mg of PVA-SbQ solubilized in 400 μL of AuNPs colloidal suspension 50% v/v diluted in 50 mM PBS buffer pH 7.4) were drop-casted onto the electrode surface. The modified SPEs were exposed for 20 min under a UV lamp (λ = 365 nm) at room temperature to allow the physical immobilization of the enzyme by photopolymerization.

In the biocathode development the drop-casting method was employed to immobilize *Trametes Hirsuta* Laccase (*Th*Lac) thanks to the strong interaction between the enzyme and the carbon based electrode as previously described [52].

All the modified electrodes were stored at 4 °C before use.

2.5. Enzymatic fuel cell assembly

EFC has been assembled and studied in different configurations eventually leading to a compact space-saving single-SPE EFC, in particular the EFC was obtained by using GPH SPEs as follows:

- two separate SPEs as bioanode and biocathode in a two separate compartments cell;
- two separate SPEs as bioanode and biocathode in a membraneless one-compartment EFC;
- one SPE for both bioanode and biocathode in a membrane-less one-compartment EFC. Finally, the single-SPE EFC was tested in human saliva samples.

While in the first two cases the electrodes were prepared separately as already described in previous section, in the latter one a single SPE was used for biofuel cell assembly using the working electrode as bioanode and the counter electrode as biocathode; both electrodes have different geometries but the same electroactive area as experimentally verified (data not reported). 5 μL of diluted AuNPs suspension were drop-cast onto the graphene working electrode and graphite counter electrode surfaces and let to dry, the procedure was repeated depositing 4 layers for each electrode (working and counter). Afterwards, 5 μL of a *Ct*CDH C291Y

Please cite this article in press as: P. Bollella, et al., A Glucose/Oxygen Enzymatic Fuel Cell based on Gold Nanoparticles modified Graphene Screen-Printed Electrode. Proof-of-Concept in Human Saliva, Sens. Actuators B: Chem. (2017), https://doi.org/10.1016/j.snb.2017.10.025

Table 1
Electrochemical parameters: electroactive area (A_{EA}, mm^2), electron transfer rate constant (k^0, $cm\,s^{-1}$) and roughness factor for different modified and unmodified electrodes. List of abbreviations: "green" gold nanoparticles (AuNPs), gold SPE (Au), graphene SPE (GPH), graphite SPE (G), sigma gold nanoparticles ($AuNPs_{sigma}$).

Electrodes	k^0_{app} ($cm\,s^{-1}$)	A_{EA} (mm^2)	ρ
G	1.1 ± 0.1	5.4 ± 0.8	0.4 ± 0.2
G + AuNPs	1.3 ± 0.1	6.4 ± 0.5	0.5 ± 0.1
Au	0.1 ± 0.1	6.2 ± 0.4	0.5 ± 0.1
Au + AuNPs	0.2 ± 0.1	7.6 ± 0.5	0.6 ± 0.1
GPH	1.5 ± 0.1	8.0 ± 0.7	0.6 ± 0.2
GPH + AuNPs	3.5 ± 0.1	9.8 ± 0.8	0.7 ± 0.2
GPH + $AuNPs_{(Sigma)}$	0.8 ± 0.1	8.4 ± 0.8	0.7 ± 0.2

enzymatic solution with 8 μL of PVA-SbQ solution (50 mg of PVA-SbQ solubilized in 400 μL distilled water) were drop-cast onto the working electrode surface, and further exposed for 20 min under a UV lamp (λ = 365 nm) at room temperature to allow the physical immobilization of the enzyme by photopolymerization. Successively, the biocathode was modified by drop-casting 5 μL of *Th*Lac solution onto the electrode surface by simple adsorption. The pseudo-reference electrode of SPE was not connected to the potentiostat.

2.6. Analysis on saliva samples

Saliva samples collection was performed at 8.30 a.m. from one healthy female patient refrained from eating, drinking and oral hygiene procedures (at least for 1 h before). The patient was given drinking bottled water and asked to rinse well her mouth. After 5 min, the patient was asked to spit whole saliva (WS) into a 50 mL sterile Falcon® tube, once a minute for up to 10 min until sampling 5 mL of WS [53]. Measurement on real sample was repeated three times.

3. Results and discussion

3.1. Electrochemical characterization of AuNPs modified SPEs

AuNPs modified screen-printed electrodes were characterized by cyclic voltammetry experiments at different scan rates in a solution of 1.1 mM $Fe(CN)_6^{3-}$, calculating the electroactive area (A_{EA}), the electron transfer rate constant (k^0) and the roughness factor (electroactive/geometrical area ratio, ρ) taking into account that the higher is the roughness factor the higher is the electrocatalytic activity and consequently the electron transfer rate [54,55]. Screen-printed electrodes (SPEs) of different materials (graphite, gold and graphene) were tested before and after the modification with four layer of "green" AuNPs and the results are shown in Table 1. The A_{EA} was calculated by plotting the peak current vs. square root of the scan rate ($\upsilon^{1/2}$) and inserting the slope obtained into the Randles-Sevcik equation [56]. The k^0 was evaluated by plotting the peak potential (E_p) vs. log $\upsilon^{1/2}$, for both anodic and cathodic peaks by using a method that merges Klingler & Kochi and Nicholson & Shain methods, as previously reported [57]. From Table 1 it is possible to observe that the best performance is achieved with the GPH + AuNPs electrode (A_{EA} = 9.8 ± 0.9 mm^2, k^0 = 3.5 ± 0.1 10^{-3} $cm\,s^{-1}$ and ρ = 0.7 ±n0.2) taking into account that as the roughness factor increases also the nanostructuration increases thus enhancing electrochemical activity. For further comparison, GPH electrodes were modified also with a AuNPs commercial colloidal suspension ($AuNPs_{(Sigma)}$) (same diameter, d = 5 nm) instead of self-prepared ones. The results (k^0 = 3.5 ± 0.1 vs. 0.8 ± 0.1) demonstrated that the NPs synthesized according to the procedure reported in our previous paper [51] gave the best results, possibly due to the presence of quercetin as stabilizing agent, which prevents the natural AuNPs aggregation onto the electrode surface, after drop-casting. This is also confirmed by the results obtained using a different number of layers (either of "green" or commercial AuNPs) as reported in Fig. 1(A) SM: although up to three layers no particular differences can be evidenced, when the number of layers increases the "green" AuNPs appear to aggregate less than the commercial ones being four layers the optimal modification condition.

Successively, the dilution effect of the colloidal suspension was also studied. The A_{EA} values were calculated and reported in Fig. 1(B) SM; the best results were obtained with the 50% v/v diluted AuNPs suspension.

3.2. Electrochemical characterization of bioanode CtCDH C291Y/AuNPs/GPH modified SPEs with different immobilization methods

In order to assess the synergic effect of nanostructured materials (graphene and AuNPs) on the DET efficiency between *Ct*CDH C291Y and SPE electrode, several CVs experiments were carried out in pH 7.4 phosphate buffer solution (PBS) containing 150 mM NaCl to evaluate the three different enzymatic immobilization methods: drop-casting (Method 1), Nafion (Method 2) and PVA-SbQ (Method 3). Moreover, also the electrocatalytical behaviour of the aforementioned modified electrode platforms have been investigated by performing CV experiments in pH 7.4 phosphate buffer solution (PBS) containing 150 mM NaCl in presence of 10 mM lactose, as substrate.

Method 1: In Fig. 2A SM (black curve) in the nonturnover CV no redox waves relative to DET communication between the CYT_{CDH} domain and the electrode surface are visible, while a couple of peaks with E^{0}' about 0.450 V vs. NHE are clearly observed, probably due to some impurities in the graphene layer of the SPE. In presence of substrate, it was observed a slight catalytic wave, probably due to the weak immobilization method (Fig. 2A SM, red curve).

Method 2: As shown in Fig. 2B SM (black curve), in the nonturnover CV, a couple of peaks relative to DET communication between the CYT_{CDH} domain and the electrode surface are now clearly visible with E^{0}' of 0.090 V vs. NHE. A small enhancement of the catalytic wave was observed with Nafion membrane (Fig. 2B SM, red curve) probably due both to the slow substrate diffusion through the membrane and to the hindering of internal electron transfer (IET) of the enzyme after immobilization occurred.

Method 3: The immobilization through the photopolymer PVA-SbQ showed the best results (Fig. 1A, black curve) in the nonturnover conditions, with a well-defined couple of redox peaks of the heme *b* cofactor located in the CYT_{CDH} with E^{0}' of 0.100 vs. NHE, which is consistent with the values reported in the literature [19,58]. When adding lactose (Fig. 1A, red curve), the PVA-SbQ modified electrode showed a clearly visible catalytic wave relative to the sugar oxidation, approximately estimated to be 20 μA cm^{-2}, mainly due to the mobility of the enzyme into the PVA-SbQ layer as well as to a correct orientation through the interaction between *Ct*CDH C291Y and AuNPs. Since the CtCDH C291Y mutant has an enhanced turnover for glucose as substrate, the electrocatalytic behaviour study with PVA-SbQ/*Ct*CDH C291Y/AuNPs/GPH platform (Fig. 1A, blue curve) has been carried out also with 10 mM glucose solution, showing a clear catalytic wave for glucose oxidation. Therefore, a kinetic characterization of the PVA-SbQ/*Ct*CDH C291Y/AuNPs/GPH has been performed with these two different substrates, lactose in the range 0.1–10 mM and glucose in the range 0.1–100 mM by applying a potential E = + 0.450 V *vs.* NHE with an injection time of 60 s. The apparent kinetic parameters, the maximum current density and the apparent Michaelis-Menten constant (I_{max}, K_M^{app}), obtained by fitting the calibration curves of lactose and glucose (Fig.

Please cite this article in press as: P. Bollella, et al., A Glucose/Oxygen Enzymatic Fuel Cell based on Gold Nanoparticles modified Graphene Screen-Printed Electrode. Proof-of-Concept in Human Saliva, Sens. Actuators B: Chem. (2017), https://doi.org/10.1016/j.snb.2017.10.025

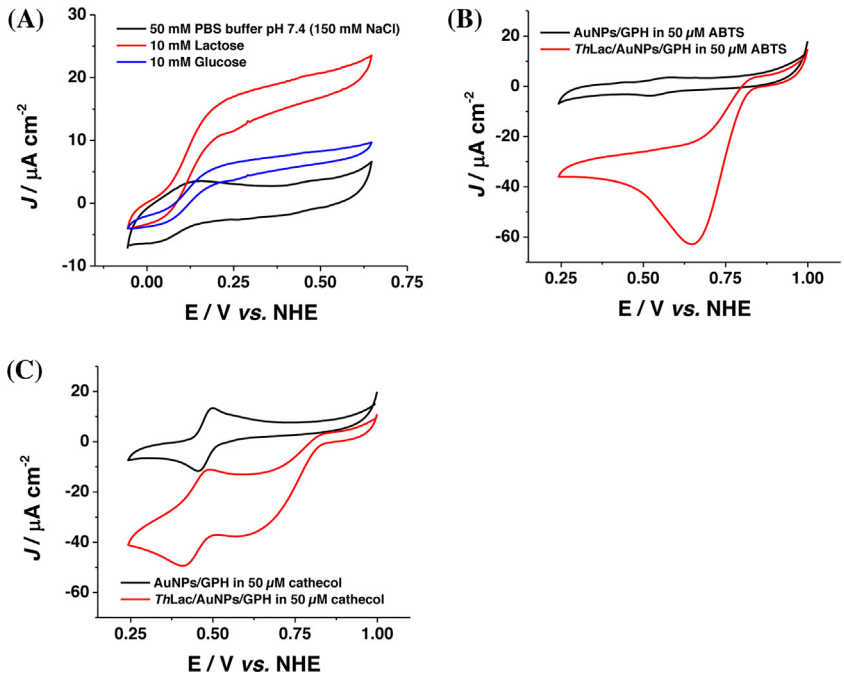

Fig. 1. (A) CVs of *Ct*CDH C291Y immobilized onto PVA-SbQ/AuNPs/GPH in absence (black curve), in presence of 10 mM lactose (red curve) and 10 mM glucose (blue curve), in 50 mM PBS buffer pH 7.4 + 150 mM NaCl. Scan rate 5 mV s^{-1}; (B) CVs of AuNPs/GPH (black curve) and *Th*Lac/AuNPs/GPH (red curve) in presence of 50 µM ABTS in 50 mM B-R buffer pH 5.5. Scan rate 5 mV s^{-1}; (C) CVs of AuNPs/GPH (black curve) and *Th*Lac/AuNPs/GPH (red curve) in presence of 50 µM catechol in 50 mM B-R buffer pH 5.5. Scan rate 5 mV s^{-1}. (For interpretation of the references to colour in this figure legend, the reader is referred to the web version of this article.)

4 A and B SM), for PVA-SbQ/*Ct*CDH C291Y/AuNPs/GPH platform are presented in Table 1 SM.

In both latter cases, namely with Nafion and PVA-SbQ, the DET is favored by a combined effect of (i) a higher fraction of immobilized *Ct*CDH C291Y molecules, due to the physical entrapment of the enzyme, and (ii) a favorable orientation of the enzyme onto the electrode surface ascribable to the AuNPs. In fact, the so prepared AuNPs present an isoelectric point (pI) of 6.4, measured and reported previously [19,51], whose value is much more positive if compared to the pI of *Ct*CDH C291Y (pI = 3.8) and it is well documented in literature that, upon these conditions, a suitable electrostatic interaction positively affects the enzyme orientation [20,35]. With the PVA-SbQ immobilization method, it was also possible to observe higher current densities for the CYT_{CDH} compared to the Nafion immobilization method. Thereafter, the integration of the redox peaks relative to DET of CYT_{CDH}, allowed to evaluate the enzyme surface coverage for both immobilization methods by using the Faraday's law (Eq. (1)):

$$\Gamma_T = \frac{Q}{nFA} \quad (1)$$

where Γ_T is the total surface concentration of electroactive protein in mol cm^{-2}, A is electrode area in cm^2, F is Faraday's constant (96 485.34C mol^{-1} of electrons), Q is the charge underlying the redox wave and n is the number of electrons transferred in the reaction [59]. Γ_T resulted to be 312 ± 21 pmol cm^{-2} and 433 ± 27 pmol cm^{-2} for Nafion/CtCDH C291Y/AuNPs/GPH and PVA-SbQ/CtCDH C291Y/AuNPs/GPH, respectively.

The effect of the scan rate for the PVA-SbQ/*Ct*CDH C291Y/AuNPs/GPH platform is reported in Fig. 2A. The results allowed to calculate the apparent heterogeneous electron transfer rate constants (k_s) for the redox reaction between *Ct*CDH C291Y and AuNPs/GPH SPE by using the Laviron's method (Laviron, 1979). From the slopes of the linear part of the trumpet plot it was possible to determine the electron transfer coefficient $\alpha = 0.47 \pm 0.07$. The k_s value was calculated according to Laviron's derivation of the Butler–Volmer theory [60] for a two-electron reaction of a surface confined electroactive species (Eq. (2)) and resulted to be 0.99 ± 0.05 s^{-1} (ν between 5 and 100 mVs^{-1}):

$$\log \quad k_s = \alpha \log(1-\alpha) + (1-\alpha)\log\left(RT/nF\upsilon\right) - \alpha(1-\alpha)$$
$$nF\Delta E_p/2.3RT \quad (2)$$

where α is the electron transfer coefficient, n is the number of electrons, ΔE_p is the separation of the redox peak potentials, ν the scan rate and F, T and R have their usual meanings (F = 96 485.34C mol^{-1}; T = 298 K; R=8.31 J $mol^{-1}K^{-1}$).

With the aforementioned results, it was possible to demonstrate that the modified electrode is a potential candidate as bioanode element for EFC if compared to other electrode platforms reported in literature [61,62], mainly due to the proper electrode modification and to the enhanced turnover towards glucose for *Ct*CDH C291Y mutant.

3.3. Electrochemical characterization of biocathode ThLac/AuNPs/GPH

The characterization of the biocathode element *Th*Lac/AuNPs/GPH was performed by studying the electron transfer in nonturnover conditions and in mediated electron transfer conditions, for comparison, by using ABTS and catechol as electron donors. CVs experiments carried out in 50 mM PBS pH 6.5 with *Th*Lac/GPH (Fig. 6 SM, black curve) and *Th*Lac/AuNPs/GPH (Fig. 6 SM, red curve) clearly demonstrated the synergic contribution of both nanomaterials towards the electron transfer in nonturnover conditions (absence of O_2), as it is possible to observe the presence of a couple of peaks only when the GPH electrode is modified with AuNPs. No redox peaks were observed for *Th*Lac/GPH (Fig. 6 SM, black curve), probably due to the insufficient nanostructuration of the electrode surface.

Therefore, CVs experiments were realized to evaluate DET rate constant for *Th*Lac/AuNPs/GPH, as reported in Fig. 2B; k_s values were calculated by using the Laviron's method, as reported in Eq. (2). From the slopes of the linear part of the trumpet plot, it was pos-

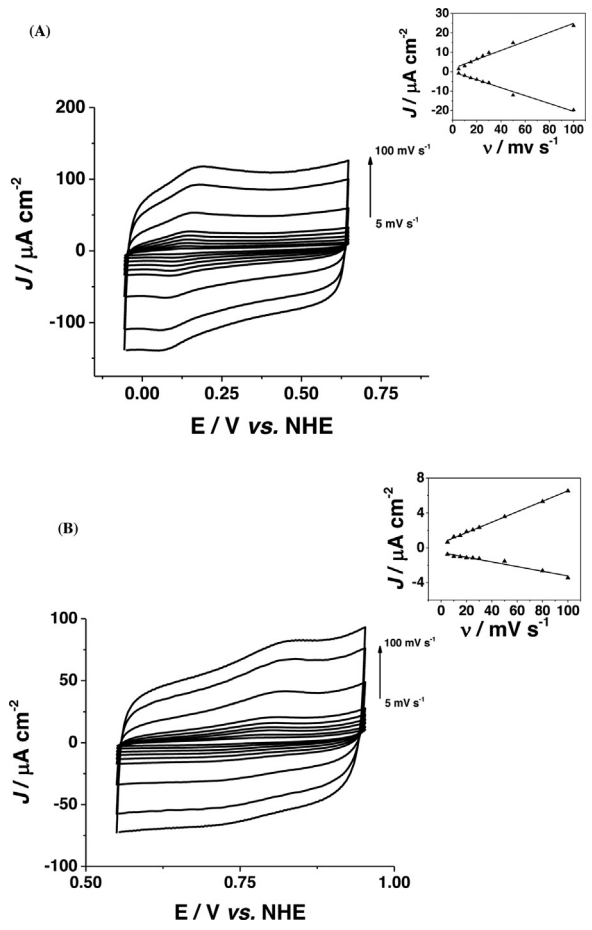

Fig. 2. (A) CVs of *Ct*CDH C291Y immobilized onto PVA-SbQ/AuNPs/GPH in 50 mM PBS buffer pH 7.4 + 150 mM NaCl, varying scan rates from 5 mV s^{-1} to 100 mV s^{-1}, Inset: linear dependence of current density (*J*, μA cm^{-2}) upon scan rates (*ν*, mV s^{-1}); (B) CVs of *Th*Lac immobilized onto AuNPs/GPH (T1 site) in 50 mM PBS buffer pH 6.5, varying scan rates from 5 mV s^{-1} to 100 mV s^{-1}, Inset: linear dependence of current density (*J*, μA cm^{-2}) upon scan rates (*ν*, mV s^{-1}).

sible to determine the electron transfer coefficient α = 0.51 ± 0.06, thus allowing to assess a k_s of 5.6 ± 0.05 s^{-1} (*ν* between 5 and 100 mVs^{-1}).

The electrocatalytic behaviour of *Th*Lac/AuNPs/GPH was studied in 50 mM Britton-Robinson buffer pH 5.5, by using ABTS and catechol, as shown by red curves in Fig. 1B and C, respectively. From both experiments, it was possible to observe an efficient electrocatalysis even in the presence of small amounts of both electron donors, starting both at E_{onset} = 0.800 V vs. NHE.

The electroanalytical and kinetic parameters for *Th*Lac/AuNPs/GPH were evaluated performing chronoamperometric experiments in the presence of ABTS and catechol in the range 0.1–2.5 mM by applying E = +0.1 V *vs.* NHE with an injection time of 60 s. The apparent kinetic parameters, the maximum current density and the apparent Michaelis-Menten constant (I_{max}, K_M^{app}), obtained by fitting the calibration curves in the presence of ABTS and catechol (Fig. 4 SM) for *Th*Lac/AuNPs/GPH platform are presented in Table 1 SM. With the above-mentioned results, it was possible to demonstrate that the so modified electrode is a valid candidate as biocathode element to be coupled to previously characterized CtCDH-based bioanode for EFC assembly.

In sum, it should be pointed out that in order to assemble an efficient cell, the obtainable maximum current density (J_{max}) from both anode and cathode should be comparable as for instance occurs in this case (compare the numerical values of J_{max} reported in Table 1 SM that are always comprised in the range 7–16 μA cm^{-2} for both bioanode and biocathode and the substrates considered); otherwise, should one of them display different order of magnitude in J_{max}, the worst behaving electrode would the limiting factor of the fuel cell [63,64].

3.4. Assembling, optimization and characterization of the EFC: PVA-SbQ/CtCDH C291Y/AuNPs/GPH and ThLac/AuNPs/GPH

The selected bioelectrodes, PVA-SbQ/*Ct*CDH C291Y/AuNPs/GPH and *Th*Lac/AuNPs/GPH were assembled as bioanode and biocahode to obtain an enzymatic fuel cell, in a U-tube two compartments cell separated by a proton-exchange membrane. As first approach, the solutions contained in the two compartments were different, due to the different optimization conditions found for the two enzymes: the PVA-SbQ/*Ct*CDH C291Y/AuNPs/GPH bioanode, was immersed in a 50 mM PBS pH 7.4 ± 150 mM NaCl solution containing 5 mM glucose while the *Th*Lac/AuNPs/GPH biocathode was dipped in air-saturated 50 mM B-R buffer pH 5.5. In the conditions reported above, the OCV was found to be about 0.74 V, close to the potential difference between bioanode and biocathode, as shown in Fig. 3A. A maximum power density of 5.16 ± 0.15 μW cm^{-2} at a cell voltage of 0.58 V was obtained in the above reported experimental conditions. The stability of the EFC was further evaluated by running polarization curves in the same experimental conditions every hour, upon a range of 8 h, as shown in Fig. 3B and C. It is possible to observe a performances decrease in terms of either OCV (30%) and maximum power output (90%), respectively, achieving a constant maximum power density of 0.67 ± 0.08 μW cm^{-2} after 8 h (Fig. 3C). This behaviour can be mainly attributed to the progressive reduction of the enzymes activity and partially also to the fact that the two elements were working in different compartments separated by a proton-exchange membrane [65].

As further step towards EFC thorough development, both electrodes were dipped in the same electrochemical cell (without the proton-exchange membrane) containing 5 mM glucose solution and several polarization curves were recorded varying the pH range between 4.5–7.5 in 50 mM citrate-phosphate buffer containing 150 mM NaCl (Fig. 5B SM). From the graph reported in Fig. 5A SM, it was possible to observe that the highest maximum power output of 2.15 ± 0.12 μW cm^{-2}, obtained at cell voltage of 0.51 V and an OCV of 0.66 V, was registered at a pH value of 6.5. It must be noted that pH 6.5 is not the optimum pH for the bioanode and therefore this could be reasonably taken as the reason of the loss of performances of about 50% compared to the EFC working with two different solution separated by the proton exchange membrane; anyway, the need to optimize the operating conditions in a single-compartment cells thus employing the enzyme selectivity to separate reduction and oxidation reactions, is mandatory in view of the possible application of the EFC to real cases, even at the cost of an obvious contraction in performance.

3.5. Single-SPE EFC: characterization and application in human saliva

In order to obtain a compact version of the developed EFC, a new configuration of the bioelectrodes has been realized (see Section 2.5) by placing both bioanode and biocathode onto the same SPE [56]. The resulting | PVA-SbQ/*Ct*CDH C291Y/AuNPs/GPH || *Th*Lac/AuNPs/G| device was dipped in air-saturated 100 μM glucose solution that corresponds to physiological glucose concentration in human saliva (50 mM citrate-phosphate buffer pH 6.5 + 150 mM NaCl) and the polarization curves were recorded. The maximum power density obtained in a 100 μM glucose solution was 1.57 ± 0.07 μW cm^{-2} with an OCV of 0.58 V (Fig. 4A), i.e. above the voltage of 0.4 V, a crucial value for practical applications because of the requirements for modern electronics [66]. The power output

Please cite this article in press as: P. Bollella, et al., A Glucose/Oxygen Enzymatic Fuel Cell based on Gold Nanoparticles modified Graphene Screen-Printed Electrode. Proof-of-Concept in Human Saliva, Sens. Actuators B: Chem. (2017), https://doi.org/10.1016/j.snb.2017.10.025

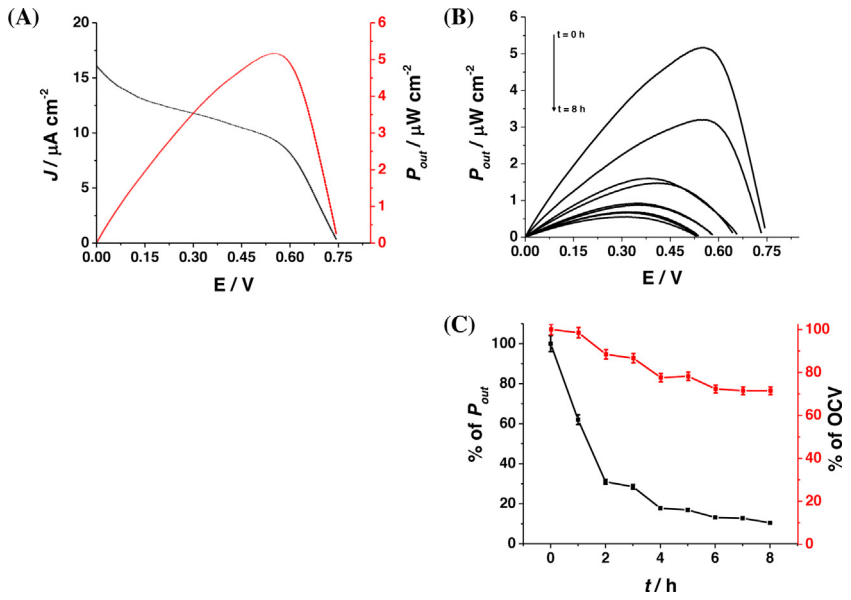

Fig. 3. (A) Polarization curve recorded for glucose/oxygen EFC in 5 mM glucose solution (50 mM PBS buffer pH 7.4 + 150 mM NaCl, left part bioanode) and 50 mM B-R buffer pH 5.5 (air saturated). The plot was obtained from linear sweep voltammetry at 1 mV s^{-1}; (B) Power output profiles recorded for two-compartment glucose/oxygen EFC in 5 mM glucose solution (50 mM PBS buffer pH 7.4 + 150 mM NaCl, left part bioanode) and 50 mM B-R buffer pH 5.5 (air saturated), during 8 h. The plots were obtained from linear sweep voltammetry at 1 mV s^{-1}; (C) Power output trend (black line) and OCV trend (red line) upon 8 working hours. (For interpretation of the references to colour in this figure legend, the reader is referred to the web version of this article.)

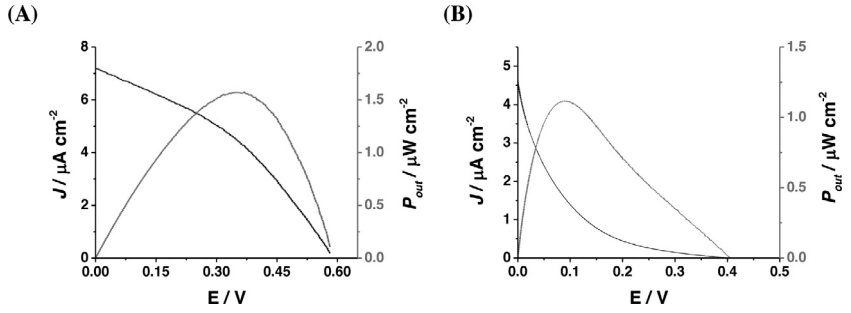

Fig. 4. (A) Polarization curve recorded for SPE-miniaturized glucose/oxygen EFC in 100 μM glucose solution (50 mM citrate-phosphate buffer pH 6.5 + 150 mM NaCl); (B) Polarization curve recorded for SPE-miniaturized glucose/oxygen EFC in human saliva. The plots were obtained from linear sweep voltammetry at 1 mV s^{-1}.

decrease obtained with the single-SPE EFC compared to the EFC with separated SPEs is possibly ascribable not only to the lower glucose concentration but also to the fact that the biocathode is in this case made of graphite instead of graphene, since this type of commercial SPEs have graphene electrodes as working electrodes and graphite electrodes as counter electrodes.

Finally, the so obtained single-SPE EFC was tested in human saliva samples containing low amounts of glucose from 30 to 100 μM. Many factors should be taken into account when saliva is used as real sample, because of the extremely variable amounts of glucose, depending on health and diet conditions, as well as the presence of interfering compounds, such as other carbohydrates, urea, amino acids, peptides, proteins and lipids [67]. Moreover, the pH value in human saliva is ranging between 6.5 and 7.5 [68,69]. Fig. 4B reports the polarization curve recorded in a saliva sample, kindly provided by a female volunteer, showing a maximal power output of 1.10 ± 0.12 μW cm^{-2} at cell voltage of 0.095 V and an OCV of 0.41 V.

A comparison of the results with others obtained with EFCs based on DET of *Ct*CDH as bioanode and *Myrothecium verrucaria* bilirubine oxidase (*Mv*BOD) as biocathode has been reported in Table 2 [58,67,70,71]. It can be observed that the power density output and the OCV values are always higher compared to the other ones even exceeding, in the case of power output, up to ten times the values reported in literature; the only exception is an EFC operating in lactose [58]. The loss of performances detected once the EFC is assembled using a single SPE leads anyway to values comparable with the similar examples reported in literature and operating in biological fluids.

4. Conclusions

In this work we have demonstrated the feasible achievement of an efficient DET of *Ct*CDH C291Y and *Th*Lac thanks to the synergic effect of graphene and AuNPs as nanostructured materials. Two modified enzymatic electrodes were optimized and characterized in order to achieve the best results and then coupled to assemble an enzymatic fuel cell (EFC). To the best of our knowledge, this is the really first time that an EFC is assembled by using screen printed electrodes (SPE) and further miniaturized onto the same SPE containing both bioanode and biocathode. The biodevice was finally tested in real saliva samples showing good performances (power output of 1.10 ± 0.12 μW cm^{-2} at cell voltage of 0.095 V and an OCV of 0.41 V), where the maximal power output was mainly influenced by the amount of glucose in the specific sample. This kind of biode-

Please cite this article in press as: P. Bollella, et al., A Glucose/Oxygen Enzymatic Fuel Cell based on Gold Nanoparticles modified Graphene Screen-Printed Electrode. Proof-of-Concept in Human Saliva, Sens. Actuators B: Chem. (2017), https://doi.org/10.1016/j.snb.2017.10.025

Table 2
Comparison of potentially implantable DET-based glucose/oxygen EFCs. Abbreviations: *Corynascus thermophilus* cellobiose dehydrogenase (CtCDH), flexible transparent polymer electrode (FTPE), gold electrode (AuE), gold microwires electrode (AuMWs), gold nanoparticles (AuNPs),graphene based screen-printed electrode (GPH), graphite based screen-printed electrode (G), graphite electrode (SPGE), *Myrothecium verrucaria* bilirubine oxidase (*Mv*BOD), poly(vinyl alcohol) N-methyl-4(4′-formylstyryl)pyridinium methosulfate acetal (PVA-SbQ), *Trametes hirsuta* laccase (ThLac).

BFC	Conditions	OCV (V)	Power output	Operational stability	References
*Ct*CDH/*Mv*BOD AuNPs/FTPE-based	50 mM PBS buffer pH 7.4 containing 5 mM glucose and 150 mM NaCl	0.63	0.6 μW cm^{-2} at 0.35 V	Half-life > 12 h	[70]
*Ct*CDH/*Mv*BOD SPGE-based	50 mM PBS buffer pH 7.4 containing 5 mM glucose and 150 mM NaCl	0.62	~3 μW cm^{-2} at 0.37 V	Half-life > 6 h	[71]
	Human serum	0.58	~4 μW cm^{-2} at 0.19 V	Half-life < 2 h	
*Ct*CDH/*Mv*BOD AuNPs/AuE-based	50 mM PBS buffer pH 7.4 containing 5 mM glucose and 150 mM NaCl	0.68	3.3 μW cm^{-2} at 0.52 V	~20%drop in 12 h of continuous operation	[58]
	50 mM PBS buffer pH 7.4 containing 5 mM lactose	0.68	14.9 μW cm^{-2} at 0.52 V	Half-life > 12 h	
	Human blood	0.66	2.8 μW cm^{-2} at 0.45 V	Half-life < 3 h	
	Human plasma	0.63	3 μW cm^{-2} at 0.47 V	Half-life < 8 h	
*Ct*CDH/*Mv*BOD AuNPs/AuMWs-based	Sweat	0.58	0.26 μW cm^{-2} at 0.5 V	Half-life > 10 h	[67]
	Sweat + 500 μM glucose	0.61	0.47 μW cm^{-2} at 0.5 V	–	
	Saliva before lunch	0.56	0.1 μW cm^{-2} at 0.5 V	–	
	Saliva after lunch	0.56	0.2 μW cm^{-2} at 0.5 V	–	
	Saliva after lunch + 500 μM glucose	0.60	0.46 μW cm^{-2} at 0.5 V	–	
PVA-SbQ/*Ct*CDH/*Th*Lac AuNPs/GPH-based	Compartimented: 50 mM PBS buffer pH 7.4 containing 5 mM glucose and 150 mM NaCl (anode); 50 mM B-R buffer pH 5.5 (cathode)	0.74	5.16 μW cm^{-2} at 0.58 V	Half-life > 8 h	This work
	Non-compartimented: 50 mM PBS buffer pH 6.5 containing 5 mM glucose and 150 mM NaCl	0.66	2.15 μW cm^{-2} at 0.51 V	–	
PVA-SbQ/*Ct*CDH/AuNPs/GPH|| *Th*Lac/AuNPs/G (on a single SPE)	Single SPE: 50 mM PBS buffer pH 6.5 containing 100 μM glucose and 150 mM NaCl	0.58	1.57 μW cm^{-2} at 0.31 V	–	This work
	Saliva	0.41	1.10 μW cm^{-2} at 0.10 V	–	

vice could be used as non-invasive autonomous biodevice, possibly providing great benefits for several biomedical applications.

Author contributions

P.B. and R.A. wrote the manuscript. D.A.S. run all the measurements during her master degree's project. P.B., G.Fu. and C.T. directly supervised D.A.S. during the project. R.L. and S.M. kindly provided *Ct*CDH C291Y mutant, while H.B. and A.K. kindly provided *Th*Lac. R.A., L.G., G.F. and F.M. revised the manuscript. All the authors have read and approved the final version.

Acknowledgements

The authors would like to thank the Italian Research Council and Unipharma-Graduates Project for financial support.

Appendix A. Supplementary data

Supplementary data associated with this article can be found, in the online version, at https://doi.org/10.1016/j.snb.2017.10.025.

References

[1] J.B. Goodenough, Electrochemical energy storage in a sustainable modern society, Energy Environ. Sci. 7 (2014) 14–18.
[2] D.P. Ho, H.H. Ngo, W. Guo, A mini review on renewable sources for biofuel, Bioresour. Technol. 169 (2014) 742–749.
[3] M. Rasmussen, S. Abdellaoui, S.D. Minteer, Enzymatic biofuel cells: 30 years of critical advancements, Biosens. Bioelectron. 76 (2016) 91–102.
[4] T. Zeng, D. Pankratov, M. Falk, S. Leimkuhler, S. Shleev, U. Wollenberger, Miniature direct electron transfer based sulphite/oxygen enzymatic fuel cells, Biosens. Bioelectron. 66 (2015) 39–42.
[5] T. Miyake, M. Nishizawa, Miniature Enzymatic Fuel Cells Enzymatic, Fuel Cells, 2014, pp. 361–373.
[6] S. Shleev, A. Bergel, L. Gorton, Biological fuel cells: divergence of opinion, Bioelectrochemistry 106 (2015) 1–2.
[7] S. Cosnier, A. Le Goff, M. Holzinger, Towards glucose biofuel cells implanted in human body for powering artificial organs: review, Electrochem. Commun. 38 (2014) 19–23.
[8] A.J. Bandodkar, J. Wang, Wearable biofuel cells: a review, Electroanalysis 28 (2016) 1188–1200.
[9] A. Zebda, S. Cosnier, J.P. Alcaraz, M. Holzinger, A. Le Goff, C. Gondran, et al., Single glucose biofuel cells implanted in rats power electronic devices, Sci. Rep. 3 (2013).
[10] N.L. Akers, C.M. Moore, S.D. Minteer, Development of alcohol/O 2 biofuel cells using salt-extracted tetrabutylammonium bromide/nafion membranes to immobilize dehydrogenase enzymes, Electrochim. Acta 50 (2005) 2521–2525.
[11] F. Barriere, P. Kavanagh, D. Leech, A laccase-glucose oxidase biofuel cell prototype operating in a physiological buffer, Electrochim. Acta 51 (2006) 5187–5192.
[12] R.M. Allen, H.P. Bennetto, Microbial fuel-cells – electricity production from carbohydrates, Appl. Biochem. Biotech. 39 (1993) 27–40.
[13] H. Wang, J.-D. Park, Z.J. Ren, Practical energy harvesting for microbial fuel cells: a review, Environ. Sci. Technol. 49 (2015) 3267–3277.
[14] B.E. Logan, Scaling up microbial fuel cells and other bioelectrochemical systems, Appl. Microbiol. Biotechnol. 85 (2010) 1665–1671.
[15] D. Leech, P. Kavanagh, W. Schuhmann, Enzymatic fuel cells: recent progress, Electrochim. Acta 84 (2012) 223–234.
[16] M. Falk, Z. Blum, S. Shleev, Direct electron transfer based enzymatic fuel cells, Electrochim. Acta 82 (2012) 191–202.
[17] G. Favero, G. Fusco, F. Mazzei, F. Tasca, R. Antiochia, Electrochemical characterization of graphene and MWCNT screen-printed electrodes modified with AuNPs for laccase biosensor development, Nanomaterials-Basel 5 (2015) 1995–2006.
[18] F. Mazzei, G. Favero, P. Bollella, C. Tortolini, L. Mannina, M.E. Conti, et al., Recent trends in electrochemical nanobiosensors for environmental analysis, Int. J. Environ. Health 7 (2015) 267–291.
[19] P. Bollella, F. Mazzei, G. Favero, G. Fusco, R. Ludwig, L. Gorton, et al., Improved DET communication between cellobiose dehydrogenase and a gold electrode modified with a rigid self-assembled monolayer and green metal nanoparticles: the role of an ordered nanostructuration, Biosens. Bioelectron. 88 (2017) 196–203.
[20] M. Tavahodi, R. Ortiz, C. Schulz, A. Ekhtiari, R. Ludwig, B. Haghighi, et al., Direct electron transfer of cellobiose dehydrogenase on positively charged polyethyleneimine gold nanoparticles, ChemPlusChem 82 (2017) 546–552.
[21] M. Carbone, L. Gorton, R. Antiochia, An overview of the latest graphene-based sensors for glucose detection: the effects of graphene defects, Electroanalysis 27 (2015) 16–31.

[22] P. Bollella, G. Fusco, C. Tortolini, G. Sanzo, G. Favero, L. Gorton, et al., Beyond graphene: electrochemical sensors and biosensors for biomarkers detection, Biosens. Bioelectron. 89 (2017) 152–166.
[23] M. Pumera, Graphene in biosensing, Mater. Today 14 (2011) 308–315.
[24] M. Pumera, S. Sanchez, I. Ichinose, J. Tang, Electrochemical nanobiosensors, Sens. Actuators B-Chem. 123 (2007) 1195–1205.
[25] J.M. Pingarron, P. Yanez-Sedeno, A. Gonzalez-Cortes, Gold nanoparticle-based electrochemical biosensors, Electrochim. Acta 53 (2008) 5848–5866.
[26] M. Holzinger, A. Le Goff, S. Cosnier, Nanomaterials for biosensing applications: a review, Front. Chem. 2 (2014).
[27] B. Zhang, Y.L. Cui, H.F. Chen, B.Q. Liu, G.N. Chen, D.P. Tang, A new electrochemical biosensor for determination of hydrogen peroxide in food based on well-dispersive gold nanoparticles on graphene oxide, Electroanalysis 23 (2011) 1821–1829.
[28] S.A.V. Eremia, I. Vasilescu, A. Radoi, S.C. Litescu, G.L. Radu, Disposable biosensor based on platinum nanoparticles-reduced graphene oxide-laccase biocomposite for the determination of total polyphenolic content, Talanta 110 (2013) 164–170.
[29] Y.H. Song, H.Y. Liu, L.L. Wan, Y. Wang, H.Q. Hou, L. Wang, Direct electrochemistry of cytochrome c based on poly(diallyldimethylammonium chloride)- graphene nanosheets/gold nanoparticles hybrid nanocomposites and its biosensing, Electroanalysis 25 (2013) 1400–1409.
[30] R. Ludwig, W. Harreither, F. Tasca, L. Gorton, Cellobiose dehydrogenase a versatile catalyst for electrochemical applications, Chemphyschem 11 (2010) 2674–2697.
[31] R. Ludwig, R. Ortiz, C. Schulz, W. Harreither, C. Sygmund, L. Gorton, Cellobiose dehydrogenase modified electrodes: advances by materials science and biochemical engineering, Anal. Bioanal. Chem. 405 (2013) 3637–3658.
[32] A. Lindgren, L. Gorton, T. Ruzgas, U. Baminger, D. Haltrich, M. Schulein, Direct electron transfer of cellobiose dehydrogenase from various biological origins at gold and graphite electrodes, J. Electroanal. Chem. 496 (2001) 76–81.
[33] C. Schulz, R. Kittl, R. Ludwig, L. Gorton, Direct electron transfer from the FAD cofactor of cellobiose dehydrogenase to electrodes, ACS Catal. 6 (2016) 555–563.
[34] H. Matsumura, R. Ortiz, R. Ludwig, K. Igarashi, M. Samejima, L. Gorton, Direct electrochemistry of phanerochaete chrysosporium cellobiose dehydrogenase covalently attached onto gold nanoparticle modified solid gold electrodes, Langmuir 28 (2012) 10925–10933.
[35] F. Tasca, W. Harreither, R. Ludwig, J.J. Gooding, L. Gorton, Cellobiose dehydrogenase aryl diazonium modified single walled carbon nanotubes: enhanced direct electron transfer through a positively charged surface, Anal. Chem. 83 (2011) 3042–3049.
[36] F. Tasca, R. Ludwig, L. Gorton, R. Antiochia, Determination of lactose by a novel third generation biosensor based on a cellobiose dehydrogenase and aryl diazonium modified single wall carbon nanotubes electrode, Sens. Actuators B-Chem. 177 (2013) 64–69.
[37] W. Harreither, V. Coman, R. Ludwig, D. Haltrich, L. Gorton, Investigation of graphite electrodes modified with cellobiose dehydrogenase from the ascomycete Myriococcum thermophilum, Electroanalysis 19 (2007) 172–180.
[38] M. Zamocky, R. Ludwig, C. Peterbauer, B.M. Hallberg, C. Divne, P. Nicholls, et al., Cellobiose dehydrogenase-a flavocytochrome from wood-degrading, phytopathogenic and saprotropic fungi, Curr. Protein Pept. Sci. 7 (2006) 255–280.
[39] C. Schulz, R. Ludwig, L. Gorton, Polyethyleneimine as a promoter layer for the immobilization of cellobiose dehydrogenase from myriococcum thermophilum on graphite electrodes, Anal. Chem. 86 (2014) 4256–4263.
[40] B. Reuillard, A. Le Goff, C. Agnes, M. Holzinger, A. Zebda, C. Gondran, et al., High power enzymatic biofuel cell based on naphthoquinone-mediated oxidation of glucose by glucose oxidase in a carbon nanotube 3D matrix, Phys. Chem. Chem. Phys. 15 (2013) 4892–4896.
[41] C. Gutierrez-Sanchez, M. Pita, C. Vaz-Dominguez, S. Shleev, A.L. De Lacey, Gold nanoparticles as electronic bridges for laccase-based biocathodes, J. Am. Chem. Soc. 134 (2012) 17212–17220.
[42] N. Lalaoui, K. Elouarzaki, A. Le Goff, M. Holzinger, S. Cosnier, Efficient direct oxygen reduction by laccases attached and oriented on pyrene-functionalized polypyrrole/carbon nanotube electrodes, Chem. Commun. 49 (2013) 9281–9283.
[43] S. Shleev, J. Tkac, A. Christenson, T. Ruzgas, A.I. Yaropolov, J.W. Whittaker, et al., Direct electron transfer between copper-containing proteins and electrodes, Biosens. Bioelectron. 20 (2005) 2517–2554.
[44] S. Shleev, A. Jarosz-Wilkolazka, A. Khalunina, O. Morozova, A. Yaropolov, T. Ruzgas, et al., Direct electron transfer reactions of laccases from different origins on carbon electrodes, Bioelectrochemistry 67 (2005) 115–124.
[45] A. Le Goff, M. Holzinger, S. Cosnier, Recent progress in oxygen-reducing laccase biocathodes for enzymatic biofuel cells, Cell. Mol. Life Sci. 72 (2015) 941–952.
[46] J. Wang, Decentralized electrochemical monitoring of trace metals: from disposable strips to remote electrodes. Plenary lecture, Analyst 119 (1994) 763–766.
[47] O.D. Renedo, M.A. Alonso-Lomillo, M.J.A. Martinez, Recent developments in the field of screen-printed electrodes and their related applications, Talanta 73 (2007) 202–219.
[48] M. Zamocky, C. Schumann, C. Sygmund, J. O'Callaghan, A.D.W. Dobson, R. Ludwig, et al., Cloning, sequence analysis and heterologous expression in Pichia pastoris of a gene encoding a thermostable cellobiose dehydrogenase from Myriococcum thermophilum, Protein Exp. Purif. 59 (2008) 258–265.
[49] K. Rittstieg, A. Suurnakki, T. Suortti, K. Kruus, G. Guebitz, J. Buchert, Investigations on the laccase-catalyzed polymerization of lignin model compounds using size-exclusion HPLC, Enzyme Microb. Technol. 31 (2002) 403–410.
[50] M. Frasconi, G. Favero, H. Boer, A. Koivula, F. Mazzei, Kinetic and biochemical properties of high and low redox potential laccases from fungal and plant origin, BBA-Proteins Proteom. 1804 (2010) 899–908.
[51] P. Bollella, C. Schulz, G. Favero, F. Mazzei, R. Ludwig, L. Gorton, et al., Green synthesis and characterization of gold and silver nanoparticles and their application for development of a third generation lactose biosensor, Electroanalysis 29 (2017) 77–86.
[52] A. Christenson, N. Dimcheva, E.E. Ferapontova, L. Gorton, T. Ruzgas, L. Stoica, et al., Direct electron transfer between ligninolytic redox enzymes and electrodes, Electroanalysis 16 (2004) 1074–1092.
[53] B.S. Henson, D.T. Wong, Collection, storage, and processing of saliva samples for downstream molecular applications, Oral Biol.: Mol. Tech. Appl. (2010) 21–30.
[54] Y. Xiao, F. Patolsky, E. Katz, J.F. Hainfeld, I. Willner, Plugging into enzymes: nanowiring of redox enzymes by a gold nanoparticle, Science 299 (2003) 1877–1881.
[55] A. De Poulpiquet, A. Ciaccafava, E. Lojou, New trends in enzyme immobilization at nanostructured interfaces for efficient electrocatalysis in biofuel cells, Electrochim. Acta 126 (2014) 104–114.
[56] K.B. Oldham, Analytical expressions for the reversible Randles-Sevcik function, J. Electroanal. Chem. Interfacial Electrochem. 105 (1979) 373–375.
[57] I. Lavagnini, R. Antiochia, F. Magno, An extended method for the practical evaluation of the standard rate constant from cyclic voltammetric data, Electroanalysis 16 (2004) 505–506.
[58] X. Wang, M. Falk, R. Ortiz, H. Matsumura, J. Bobacka, R. Ludwig, et al., Mediatorless sugar/oxygen enzymatic fuel cells based on gold nanoparticle-modified electrodes, Biosens. Bioelectron. 31 (2012) 219–225.
[59] J.F. Rusling, Z. Zhang, Thin films on electrodes for direct protein electron transfer Handbook of Surfaces and Interfaces of Materials, 5, 2001, pp. 33–71.
[60] E. Laviron, General expression of the linear potential sweep voltammogram in the case of diffusionless electrochemical systems, J. Electroanal. Chem. Interfacial Electrochem. 101 (1979) 19–28.
[61] R. Ortiz, R. Ludwig, L. Gorton, Highly efficient membraneless glucose bioanode based on corynascus thermophilus cellobiose dehydrogenase on aryl diazonium-activated single-walled carbon nanotubes, ChemElectroChem 1 (2014) 1948–1956.
[62] V. Krikstolaityte, P. Lamberg, M.D. Toscano, M. Silow, O. Eicher-Lorka, A. Ramanavicius, et al., Mediatorless carbohydrate/oxygen biofuel cells with improved cellobiose dehydrogenase based bioanode, Fuel Cells 14 (2014) 792–800.
[63] M.H. Osman, A.A. Shah, F.C. Walsh, Recent progress and continuing challenges in bio-fuel cells, Part I: Enzym. Cells Biosens. Bioelectron. 26 (2011) 3087–3102.
[64] V. Soukharev, N. Mano, A. Heller, A four-electron O2-electroreduction biocatalyst superior to platinum and a biofuel cell operating at 0.88 V, J. Am. Chem. Soc. 126 (2004) 8368–8369.
[65] P. Pinyou, F. Conzuelo, K. Sliozberg, J. Vivekananthan, A. Contin, S. Pöller, et al., Coupling of an enzymatic biofuel cell to an electrochemical cell for self-powered glucose sensing with optical readout, Bioelectrochemistry 106 (2015) 22–27.
[66] M. Falk, V. Andoralov, M. Silow, M.D. Toscano, S. Shleev, Miniature biofuel cell as a potential power source for glucose-sensing contact lenses, Anal. Chem. 85 (2013) 6342–6348.
[67] M. Falk, D. Pankratov, L. Lindh, T. Arnebrant, S. Shleev, Miniature direct electron transfer based enzymatic fuel cell operating in human sweat and saliva, Fuel Cells 14 (2014) 1050–1056.
[68] J.K.M. Aps, L.C. Martens, Review: the physiology of saliva and transfer of drugs into saliva, Forensic Sci. Int. 150 (2005) 119–131.
[69] W.M. Edgar, D.M. O'Mullane, C. Dawes, Saliva and Oral Health, British Dental Association London, 2004.
[70] D. Pankratov, R. Sundberg, J. Sotres, I. Maximov, M. Graczyk, D.B. Suyatin, et al., Transparent and flexible, nanostructured and mediatorless glucose/oxygen enzymatic fuel cells, J. Power Sources 294 (2015) 501–506.
[71] V. Coman, R. Ludwig, W. Harreither, D. Haltrich, L. Gorton, T. Ruzgas, et al., A direct electron transfer-based glucose/oxygen biofuel cell operating in human serum, Fuel cells 10 (2010) 9–16.

Biographies

Cristina Tortolini received her degree in Industrial Chemistry from Sapienza – University of Rome in 2005. Her work concerned the decomposition of N_2O over supported metal zirconia and sulfated zirconia catalysts. Subsequently, she got a training funded by Lazio region, by means of she focused on characterization of branched host-guest supramolecular polymers at the Dept. of Chemistry, Sapienza – University of Rome. Since 2008, she joined to Prof. Mazzei's Biosensors Laboratory, at the Dept. of Chemistry and Drug Technologies, Sapienza – University of Rome. Currently is a PhD student in the Department of Chemistry Sapienza – University of Rome and her research efforts are on the development of electrochemical and optical biosensors.

Please cite this article in press as: P. Bollella, et al., A Glucose/Oxygen Enzymatic Fuel Cell based on Gold Nanoparticles modified Graphene Screen-Printed Electrode. Proof-of-Concept in Human Saliva, Sens. Actuators B: Chem. (2017), https://doi.org/10.1016/j.snb.2017.10.025

Gabriele Favero is an Assistant Professor of Analytical Chemistry at the Department of Chemistry and Drug Technologies of Sapienza University of Rome. His research activity is mainly focused on the study, development and application of sensors and biosensors to pharmaceutical, biomedical and food analysis, ranging from whole cell biosensors to enzymatic biosensors operating either in aqueous solution or in organic solvent and the use of reconstituted biological membranes as sensing elements for amplified-response sensors. He has participated to various national and international research projects (in the Sixth Framework Programme and the Eurostars Programme 2010). He is author of 1 patent, 2 book chapters, 65 papers including 58 on peer-reviewed international journals, 27 long abstracts and almost 200 oral or poster contributions to national and international congresses; H-index = 20; Hc-index = 12; Number of citations = 955. He is a member of SCI – Italian Chemical Society, ECS – The Electrochemical Society, ISE – International Society of Electrochemistry and the Order of Chemists of Lazio.

Riccarda Antiochia received her MSc degree in Chemistry in 1997 and a MSc degree in Pharmacy in 2009, both at Sapienza, University of Rome. In 1996 received a PhD in Analytical Chemistry and since 2000 is researcher at Sapienza University of Rome. Her field of research are biosensors, studies on electrode kinetics, liquid chromatography and their use for determination and analysis of analytes of food, environmental and biomedical interest.

Franco Mazzei is an Associate Professor of Physical Chemistry at the Department of Chemistry and Drug Technologies, Sapienza –University of Rome, and is responsible for the Biosensor Laboratory. He has published over 80 papers on various aspects of electrochemical sensors and biosensors in national and international journals. His research activity for the last 10–15 years has focused on solving different problems in clinical, toxicological and pharmacological fields, often as an alternative to more complex analytical procedures, as well as evaluating the potential use of electrochemical and optical biosensors for the detection of doping substances and methods.

Please cite this article in press as: P. Bollella, et al., A Glucose/Oxygen Enzymatic Fuel Cell based on Gold Nanoparticles modified Graphene Screen-Printed Electrode. Proof-of-Concept in Human Saliva, Sens. Actuators B: Chem. (2017), https://doi.org/10.1016/j.snb.2017.10.025

Supporting Material

A glucose/oxygen enzymatic fuel cell based on gold nanoparticles modified graphene screen-printed electrode. Proof-of-concept in human saliva

Paolo Bollella[a], Giovanni Fusco[b], Daniela Stevar[a], Lo Gorton[c], Roland Ludwig[d], Su Ma[d], Harry Boer[e], Anu Koivula[e], Cristina Tortolini[a], Gabriele Favero[a], Riccarda Antiochia[a]*, Franco Mazzei[a]*

[a]*Department of Chemistry and Drug Technologies, Sapienza University of Rome, P.le Aldo Moro, 5 00185 Rome, Italy*

[b]*Department of Chemistry, Sapienza University of Rome, P.le Aldo Moro, 5 00185 Rome, Italy*

[c]*Department of Analytical Chemistry/Biochemistry and Structural Biology, Lund University, P.O. Box 124, SE-221 00 Lund, Sweden*

[d]*Food Biotechnology Laboratory, Department of Food Science and Technology, BOKU – University of Natural Resources and Life Sciences, Muthgasse 18, A-1190 Vienna, Austria*

[e]*VTT Technical Research Centre of Finland, P.O. Box 1000, FI-02044 VTT, Finland*

* corresponding authors

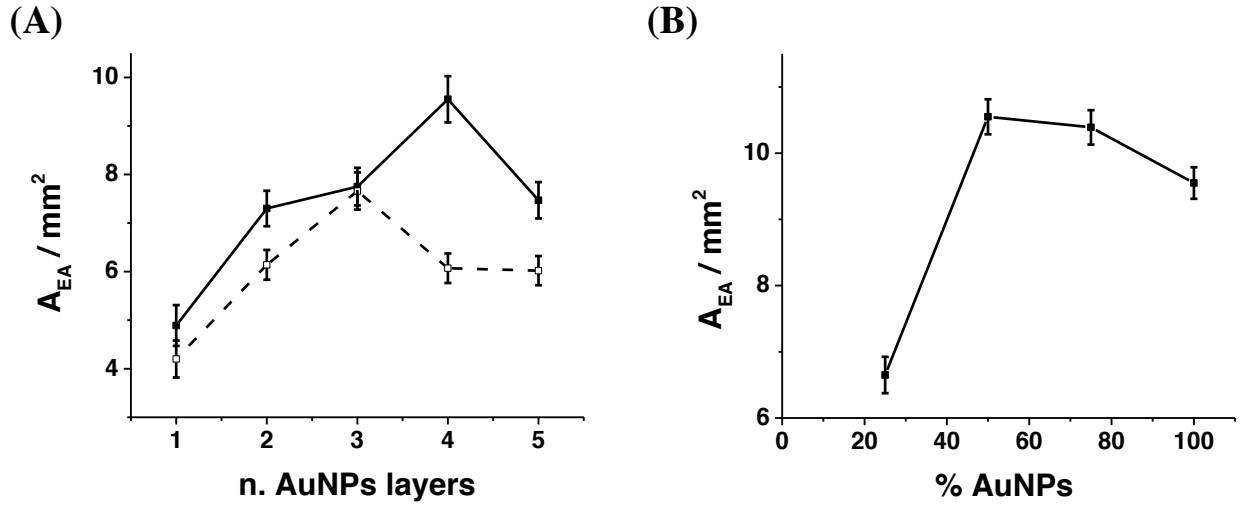

Fig. 1 SM (A) Electroactive area (A_{EA}) trend upon different numbers of AuNPs layer drop-casted for AuNPs green (filled square, solid line) and AuNPs sigma (empty square, dashed line); **(B)** Electroactive area (A_{EA}) trend upon different dilution factor. The plots were obtained recording CVs in 1.1 mM $Fe(CN)_6^{3-}$ (100 mM PBS buffer pH 7.4 + 100 mM KCl) varying scan rates from 5 mV s^{-1} to 1000 mV s^{-1}.

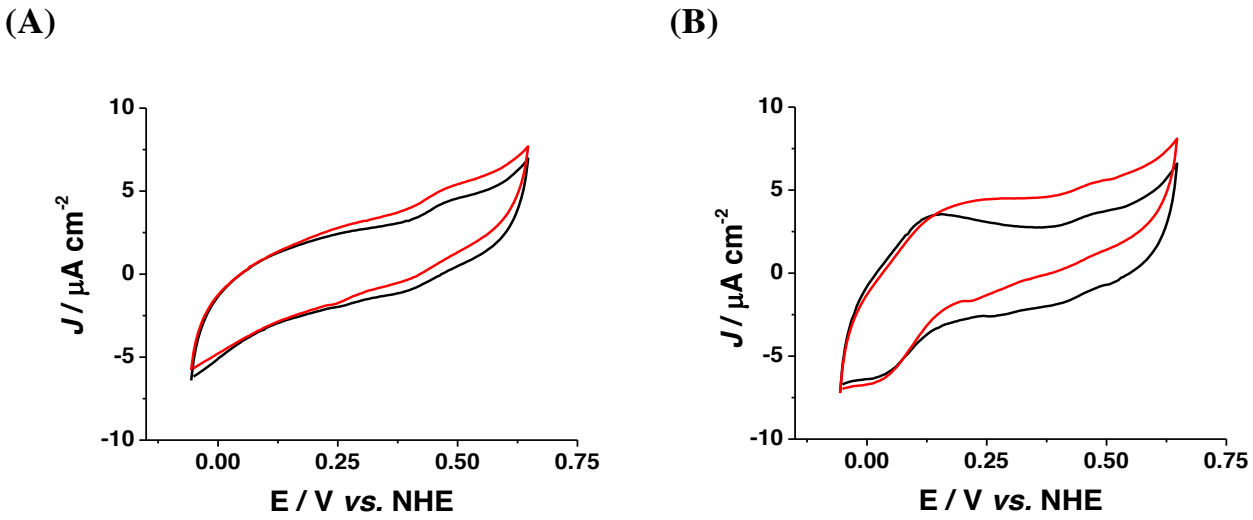

Fig. 2 SM (A) CVs of *Ct*CDH C291Y immobilized onto AuNPs/GPH in absence (black curve) and in presence (red curve) of 10 mM lactose in 50 mM PBS buffer pH 7.4 + 150 mM NaCl. Scan rate 5 mV s^{-1}; **(B)** CVs of *Ct*CDH C291Y immobilized onto Nafion/AuNPs/GPH in absence (black curve) and in presence (red curve) of 10 mM lactose in 50 mM PBS buffer pH 7.4 + 150 mM NaCl. Scan rate 5 mV s^{-1}.

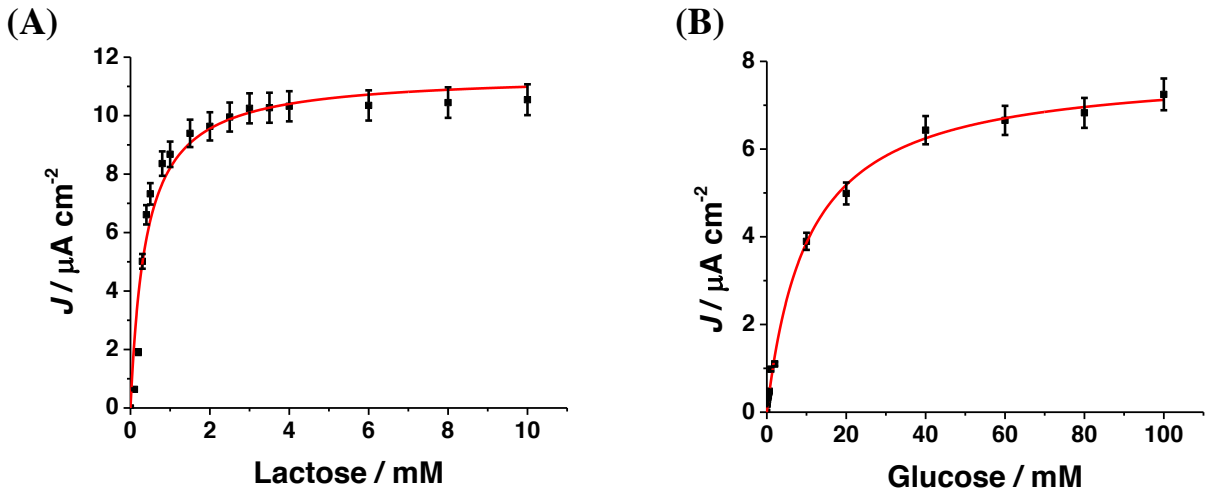

Fig. 3 SM Calibration curves for lactose **(A)** and glucose **(B)** in 50 mM PBS buffer pH 7.4 + 150 mM NaCl. The graphs were obtained by recording CVs in presence of different substrate concentrations, 0.1-10 mM for lactose and 0.1-100 mM for glucose, respectively. E_{app}= +0.450 V *vs.* NHE with an injection time of 60 s, (n=3).

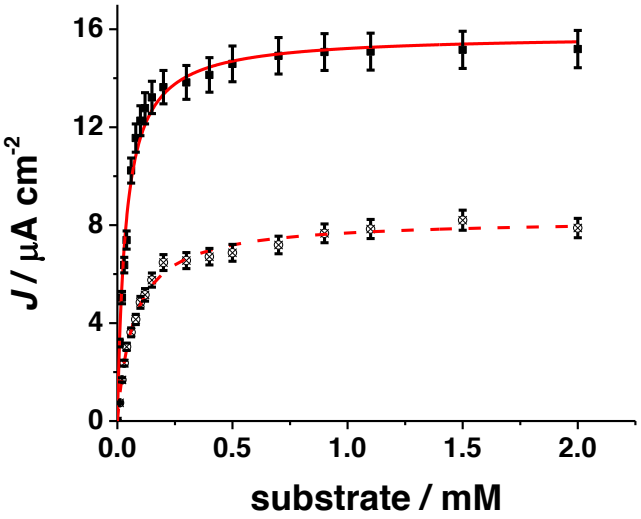

Fig. 4 SM Calibration curves for ABTS (filled square, solid line) and catechol (empty square, dashed line) in 50 mM B-R buffer pH 5.5. The graph was obrained by recording chronoaperograms in presence of different substrate concentration, 0.1-2.5 mM for both ABTS and catechol. E_{app}= +0.100 V *vs.* NHE with an injection time of 60 s, (n=3).

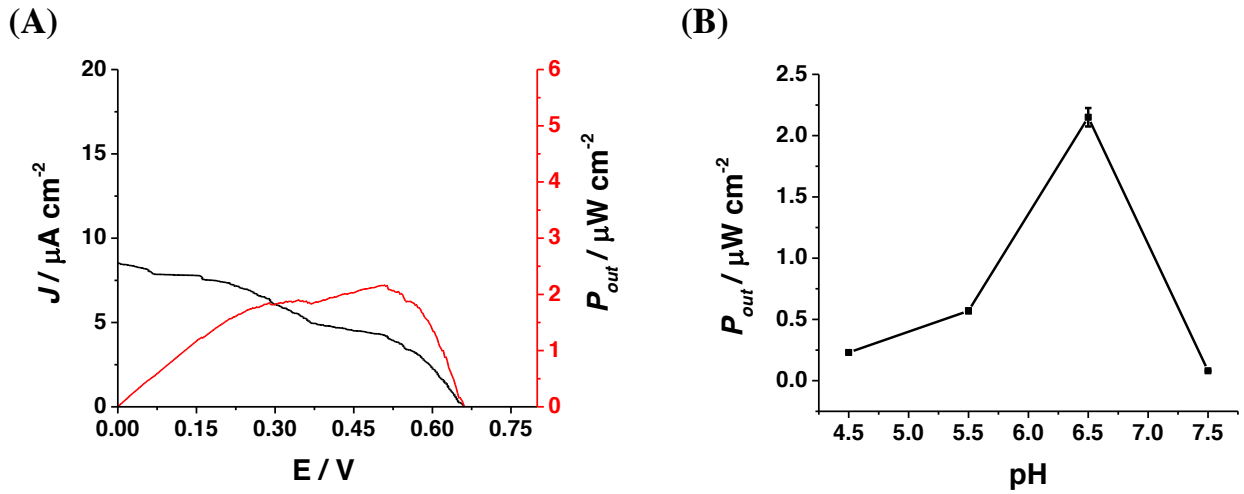

Fig. 5 SM (A) Polarization curve recorded for membrane-less glucose/oxygen EFC in 5 mM glucose solution (50 mM citrate-phosphate buffer pH 6.5 + 150 mM NaCl). The plot was obtained from linear sweep voltammetry at 1 mV s^{-1}. The distance between the electrodes was kept constant throught all experiments (1 cm); **(B)** Power output trend upon pH.

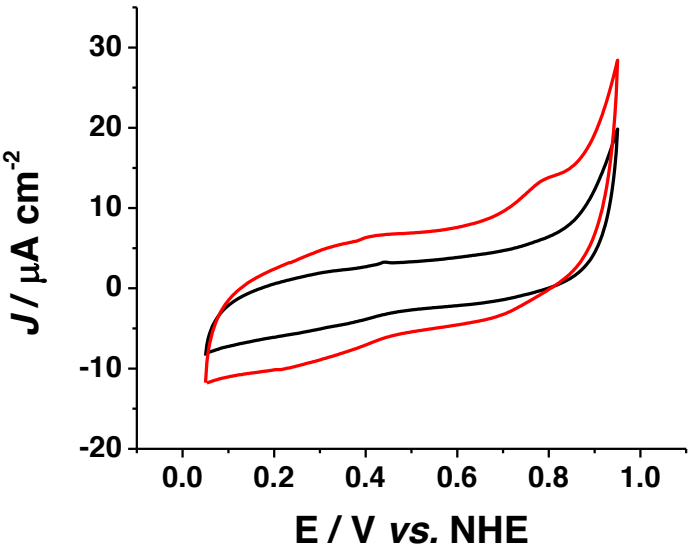

Fig. 6 CVs of *Th*Lac/GPH (black curve) and *Th*Lac/AuNPs/GPH (red curve) in 50 mM PBS buffer pH 6.5. Scan rate 5 mV s^{-1}.

Substrate	J_{max} (µA cm^{-2})	K_M^{app} (mM)	J_{max}/K_M^{app} (µA mM^{-1} cm^{-2})	
Lactose	11.9 ± 1.0	0.4 ± 0.1	27.6 ± 0.3	*Corynascus thermophilus* cellobiose dehydrogenase (*Ct*CDH)
Glucose	7.9 ± 0.6	10.3 ± 0.8	0.8 ± 0.2	
Substrate	J_{max} (µA cm^{-2})	K_M^{app} (µM)	J_{max}/K_M^{app} (µA mM^{-1} cm^{-2})	
ABTS	15.8 ± 1.7	40 ± 10	39.4 ± 0.4	*Trametes hirsuta* laccase (*Th*Lac)
Catechol	7.9 ± 0.7	40 ± 10	19.7 ± 0.3	

Tab. 1 SM Electroanalytical parameters for PVA-SbQ/*Ct*CDH C291Y/AuNPs/GPH for lactose and glucose and the electroanalytical parameters for *Th*Lac/AuNPs/GPH for ABTS and catechol.

Paper IV

sensors

MDPI

Article

A Third Generation Glucose Biosensor Based on Cellobiose Dehydrogenase Immobilized on a Glassy Carbon Electrode Decorated with Electrodeposited Gold Nanoparticles: Characterization and Application in Human Saliva

Paolo Bollella [1], Lo Gorton [2], Roland Ludwig [3] and Riccarda Antiochia [1,*]

[1] Department of Chemistry and Drug Technologies, Sapienza University of Rome, P.le Aldo Moro. 5, 00185 Rome, Italy; paolo.bollella@uniroma1.it

[2] Department of Analytical Chemistry/Biochemistry and Structural Biology, Lund University, P.O. Box 124, SE-221 00 Lund, Sweden; lo.gorton@biochemistry.lu.se

[3] Food Biotechnology Laboratory, Department of Food Science and Technology, BOKU—University of Natural Resources and Life Sciences, Muthgasse 18, A-1190 Vienna, Austria; roland.ludwig@boku.ac.at

* Correspondence: riccarda.antiochia@uniroma1.it

Received: 4 July 2017; Accepted: 16 August 2017; Published: 18 August 2017

Abstract: Efficient direct electron transfer (DET) between a cellobiose dehydrogenase mutant from *Corynascus thermophilus* (*Ct*CDH C291Y) and a novel glassy carbon (GC)-modified electrode, obtained by direct electrodeposition of gold nanoparticles (AuNPs) was realized. The electrode was further modified with a mixed self-assembled monolayer of 4-aminothiophenol (4-APh) and 4-mercaptobenzoic acid (4-MBA), by using glutaraldehyde (GA) as cross-linking agent. The *Ct*CDH C291Y/GA/4-APh,4-MBA/AuNPs/GC platform showed an apparent heterogeneous electron transfer rate constant (k_s) of 19.4 ± 0.6 s^{-1}, with an enhanced theoretical and real enzyme surface coverage (Γ_{theor} and Γ_{real}) of 5287 ± 152 pmol cm^{-2} and 27 ± 2 pmol cm^{-2}, respectively. The modified electrode was successively used as glucose biosensor exhibiting a detection limit of 6.2 μM, an extended linear range from 0.02 to 30 mM, a sensitivity of 3.1 ± 0.1 μA mM^{-1} cm^{-2} (R^2 = 0.995), excellent stability and good selectivity. These performances compared favourably with other glucose biosensors reported in the literature. Finally, the biosensor was tested to quantify the glucose content in human saliva samples with successful results in terms of both recovery and correlation with glucose blood levels, allowing further considerations on the development of non-invasive glucose monitoring devices.

Keywords: cellobiose dehydrogenase; gold nanoparticles; electrodeposition; glucose biosensor; human saliva

1. Introduction

Glucose monitoring has attracted great attention in several fields, ranging from biomedical applications to ecological fields [1]. In particular, for clinical trials, glucose monitoring has been considered one of the key factor in early diagnosis of diabetes mellitus, which is a main cause of death or other diseases around the world. Diabetes is a metabolic disease generally related to non-/under-production of insulin in the pancreas and hyperglycemia, reflected by blood glucose concentrations higher or lower than the normal range of 80–120 mg dL^{-1} [2]. It is possible to distinguish between three types of diabetes: (i) type 1, which most affects young people, with non-production of insulin in the pancreas and involves about 10% of diabetic people [3]; (ii) type 2, which occurs in

middle-age or old people, with low production of insulin or when the body does not use the insulin produced and involves about 90% of diabetic people [4]; (iii) gestational diabetes, which occurs during the pregnancy, with a connected risk of diabetes development for both mother and child [5].

In the last century, several approaches for early diagnosis of diabetes mellitus mainly focused on glucose monitoring have been developed such as capillary zone electrophoresis (CZE) [6], gas chromatography (GC) mainly coupled with mass spectrometry (MS) [7], high performance liquid chromatography/mass spectrometry (HPLC-MS) [8], enzymatic spectrophotometric assays [9], Fourier transform near-infrared spectroscopy (FT-NIR) [10] and proton NMR.

However, these methods require expensive equipment and complicated operations and therefore they cannot be applied to home-based care [11]. Most diabetic patients need to test their blood glucose levels periodically, even several times a day. Biosensors may represent a valid alternative as they allow time-saving, accurate, repeatable and cost-effective determination of glucose in blood [12]. Typically, a blood test for analysis is realized through a finger prick, which may cause physical and mental stress to patients, especially to young children and elderly people. Therefore, there is a great need for the developing of a point-of-care non-invasive glucose monitoring system [2]. A positive correlation between blood glucose (80–120 mg dL^{-1}) and salivary glucose (0.6–1.8 mg dL^{-1}) has been revealed in many studies [4].

Saliva shows great advantages compared to other biological fluids such as blood, tears, urine, etc. because its sampling is not invasive and it is recognized as the most sensitive one, containing also other disease biomarkers in a concentration larger than in blood. Moreover saliva sampling involves a simple collection method that allows easy storage and transport.

It is well known that electrochemical enzymatic glucose biosensors are divided into three classes depending on the electrochemical communication between the enzyme and the electrode: (i) first generation biosensors, where glucose is considered as co-substrate of glucose oxidase (GOx) with a subsequent generation of hydrogen peroxide (H_2O_2), which is oxidised at the electrode surface at quite high redox potential (e.g., 0.6 V vs. Ag | $AgCl_{sat}$ for carbon modified electrodes, 0.4 V Ag | $AgCl_{sat}$ for gold electrodes and 0.7 V vs. Ag | $AgCl_{sat}$ for platinum electrode; (ii) second generation biosensors, where oxygen was replaced with a non-physiological electron acceptor (mediator) able to shuttle the electrons from the enzyme redox center to the surface of the electrode; (iii) third generation biosensors, where the mediator was eliminated to develop a reagentless glucose biosensor transferring the electrons from glucose to the electrode through the active site of the enzyme, with a low operating potential, close to that of the redox potential of the enzyme itself [13]. The electrode nanostructure plays a key role, particularly for third generation biosensors, thanks to the increased electroactive area and roughness factor [13]. Among the various nanostructured materials, carbon nanotubes, graphene [14] and metal nanoparticles (MNPs) showed very promising results [15], because of their high surface/volume ratio, thus allowing a better communication between the electrode and the prosthetic group of the enzyme [16]. Recently, several MNPs deposition approaches have been developed to modify the electrode surface, such as drop-casting [17,18], covalent linkage [19,20] or direct electrodeposition [21]. Among these methods, the electrodeposition allows a fast and easy MNPs synthesis with the possibility to monitor the MNPs geometry and size [22], especially by sweeping the potential [23] instead of applying a fixed potential [24]. Moreover, MNPs can grow directly onto the electrode surface without the need of further sample preparation, being surfactant-free and cost-effective and allowing to tune the nature of the nanoclusters by changing electrolyte composition and deposition parameters [24].

Unfortunately, despite the electrode nanostructure, only a few enzymes are able to directly transfer electrons from their active sites to the electrode [25,26]. Cellobiose dehydrogenase (CDH) has received great attention for biosensors [27] and biofuel cell development [28] because of its ability to show DET. CDH is a flavocytochrome oxidoreductase expressed by the dikaryotic phyla of Basidiomycota (Class I) and Ascomycota (Class II and Class III), consisting of two domains [29]. The first domain, called dehydrogenase domain (DH_{CDH}), contains a flavin adenine dinucleotide (FAD) cofactor, connected through a flexible linker to a second subunit containing a *heme-b* cofactor, called cytochrome domain

(CYT_{CDH}) [30]. DH_{CDH} domain is structurally similar to the FAD domain of most GMC-oxidoreductase enzymes and is fully reduced by di-/mono- saccharides, transferring the electrons through internal electron transfer (IET) to the CYT_{CDH}, which finally shuttles the electrons to properly modified electrodes [31]. Among II class CDHs, *Corynascus thermophilus* CDH (*Ct*CDH) was genetically mutated in its active site (*Ct*CDH C291Y mutant) to enhance its sensitivity toward glucose and reduce the maltose cross-reactivity [32].

In this work, we report an improved DET efficiency between *Ct*CDH C291Y and a novel GC modified electrode, obtained through direct electrodeposition of gold nanoparticles (AuNPs) on the GC electrode, further modified with a mixed self-assembled monolayer of 4-aminothiophenol (4-APh) and 4-mercaptobenzoic acid (4-MBA) using glutaraldehyde as cross-linking agent, as shown in Scheme 1. The proposed electrodeposition method allowed to monitor the nanoparticles surface coverage as well as the surface area available for the biomodification, which is directly related to the biosensor sensitivity. The so modified AuNPs/GC electrode was used to develop a third generation biosensor for glucose detection. The performances of the proposed biosensor were investigated in human saliva samples, demonstrating that the constructed AuNPs/GC biosensor has great potentials to realize electrochemical devices for non-invasive diabetes mellitus monitoring.

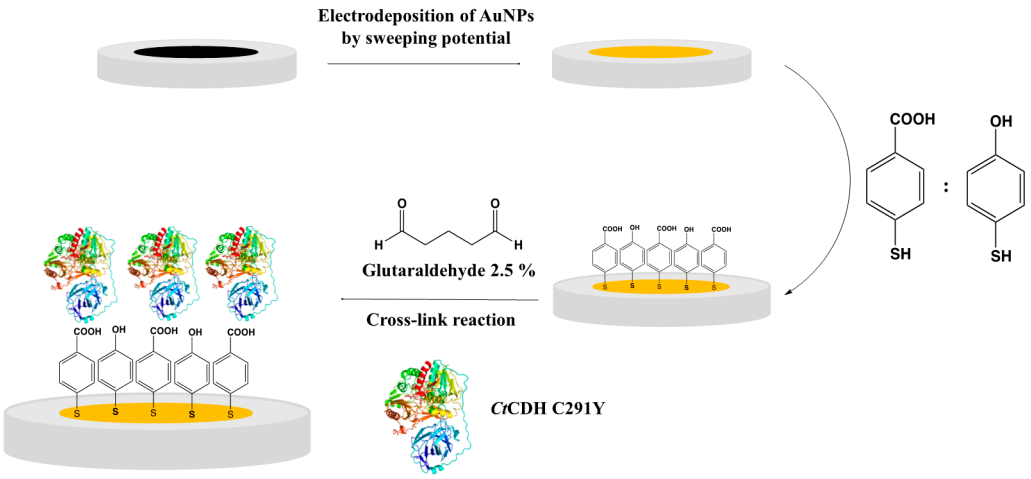

Scheme 1. The electrode modification pathway for *Ct*CDH C291Y/GA/4-APh,4-MBA/AuNPs/GC platform has been reported. Initially, AuNPs were directly electrodeposited onto cleaned GC electrode by sweeping the potential. Afterward, the electrode was incubated in a thiol mixture (1:1 *v*/*v* 4-APh and 4-MBA) overnight, followed by cross-linking reaction (glutaraldehyde GA: cross-linking agent) to covalently link the enzyme (*Ct*CDH C291Y) to the so modified electrode surface.

2. Experimental Section

2.1. Chemicals

Sulfuric acid (H_2SO_4), D-glucose, D-(+)-maltose monohydrate, ascorbic acid, calcium chloride ($CaCl_2$), chloroauric acid ($HAuCl_4 \cdot 3H_2O$), potassium ferricyanide ($K_3[Fe(CN)_6]$), potassium ferrocyanide ($K_4[Fe(CN)_6]$), sodium acetate (CH_3COOH), 3-(*N*-morpholino)propanesulfonic acid (MOPS), tris(hydroxymethyl)aminomethane (TRIS), urea, cortisol, 4-aminothiophenol (4-APh), 4-mercaptobenzoic acid (4-MBA), glutaraldehyde (GA), potassium chloride (KCl) and Glucose (GO) Assay Kit were purchased from Sigma Aldrich (St. Louis, MO, USA).

*Ct*CDH C291Y (E.C. 1.1.99.18) was purified from the culture supernatant of the ascomycete *Corynascus thermophilus* (CBS 405.69) obtained from the Centralbureau voor Schimmelcultures (Baarn, The Netherlands) (volumetric activity with cytochrome *c* at pH 7.5 = 54 U mL^{-1}, protein

concentration = 16 mg mL^{-1}). All solutions were prepared using Milli-Q water (R = 18.2 MΩ cm at 25 °C; TOC < 10 μg L^{-1}, Millipore, Molsheim, France).

2.2. Electrode Preparation and Modification

GC electrodes (Bioanalytical Systems Inc., West Lafayette, IN, USA, d = 3 mm) were polished with alumina slurries (Al_2O_3, particle size of 1 and 0.1 μm) on cloth pads wet with Milli-Q water (Struers ApS, Ballerup, Denmark), thoroughly rinsed with Milli-Q water and further sonicated for 5 min between each polishing step. GC electrodes were successively modified by electrodeposition of gold nanoparticles (AuNPs) by sweeping the potential between 1.1 and −0.1 V vs. $Ag|AgCl_{sat}$ for a given number of scans (5, 10, 15, 20, 25, 30, 35 scans) in 10 mM $HAuCl_4$ [33]. Then, the modified electrodes were activated in 0.5 M H_2SO_4 by running 25 scans between 0 and +1.7 vs. $Ag|AgCl_{sat}$ at a scan rate of 0.1 V s^{-1} until a well-defined cyclic voltammogram (CV) was obtained. The best modified electrode was selected on the basis of the electroactive and real surface area, heterogeneous electron transfer rate constant (k^0, cm s^{-1}) and roughness factor (ρ), calculated from CV measurements carried out in 10 mM $Fe(CN)_6^{3-/4-}$ (50 mM TRIS buffer pH 7.4). It was further dipped into a volumetric 1:1 mixture of 1 mM 4-APh/4-MBA ethanol solution. Then, the electrode was thoroughly rinsed with ethanol and dried under N_2 stream. For the biomodification, 1 μL of GA solution (2.5% v/v in distilled water) and 3 μL of *Ct*CDH C291Y solution (16 mg mL^{-1}) were drop-cast, gently mixed on the top of thiol-modified AuNPs/GC electrode and allowed to react in a moisturised atmosphere for 2 h to avoid evaporation of the reactants. Finally, the so modified electrode was gently rinsed with 50 mM TRIS buffer (pH 7.4) in order to remove any possible unbounded enzyme molecule [34].

2.3. Whole Saliva and Blood Samples Collection and Analysis

Saliva samples collection was performed at 8.30 a.m. from three healthy male and female patients refrained from eating, drinking and oral hygiene procedures (at least for 1 h before). The patients were given drinking bottled water and asked to rinse well their mouths. After 5 min, the patients were asked to spit whole saliva (WS) into a 50 mL sterile Falcon® tube, once a minute for up to 10 min until sampling 5 mL of WS [35]. At the same time the patients were punched on their fingers to collect a drop of blood sufficient to measure glucose with the commercial GlucoContour XT (Bayer, Leverkusen, Germany) used by diabetic patients for self-monitoring and with the glucose oxidase-peroxidase method [36,37] by using the Glucose (GO) Assay Kit, which is the standard reference method for WS samples [38].

2.4. SEM Experiments

Scanned electron microscopy (SEM) measurements were performed with a JSM-7600F Schottky Field Emission Scanning Electron Microscope (JEOL Nordic AB, Sollentuna, Sweden). All samples were prepared according to the electrodeposition protocol, reported in Section 2.2, using glassy carbon plates (25 × 25 × 1 mm, ALS Co. Ltd., Tokyo, Japan) instead of GC electrodes. The samples were paced on a clip SEM sample holder (JEOL Nordic AB).

2.5. Electrochemical Measurements and Electrochemical Apparatus

Cyclic voltammograms (CVs) were recorded by using a PGSTAT 30 potentiostat (equipped with GPES 4.9, Autolab, Utrecht, The Netherlands). CVs were performed in a three-electrode electrochemical cell containing a standard silver chloride electrode (Ag | AgCl, sat. KCl), a platinum wire counter electrode and a modified glassy carbon (GC) electrode as working electrode. The temperature controlled experiments were carried out by using a cryostatic bath (T ± 0.01 °C, LAUDA RM6, Delran, NJ, USA). Flow injection analysis (FIA) data have been collected by using an analogic potentiostat (Zäta Elektronik, Höör, Sweden) connected with a strip chart recorder (Kipp & Zonen, Utrecht, The Netherlands). The modified GC electrode, an Ag | AgCl (0.1 M KCl) reference electrode and a platinum wire counter electrode were fitted into a wall-jet cell. The electrochemical system was

equipped with a flow system consisting of a peristaltic pump (Gilson, Villier-le-Bel, France) and a six-port valve electrical injector (Rheodyne, Cotati, CA, USA).

3. Results and Discussion

3.1. SEM and Electrochemical Characterization of AuNPs Modified GC Electrodes

SEMs were used to evaluate the physical appearance and surface characteristics of the AuNPs on the electrode surfaces for a given number of scans. Figure 1a–g show the SEM images relative to increasing number of scans. It is clearly visible that the surface coverage of the AuNPs increases with increasing number of scans until 25 scans, when the electrode surface is completely covered by a single layer of AuNPs. For electrodes prepared with 30 and 35 scans (Figure 1f,g), it is possible to observe multiple layers of AuNPs with possible formation of AuNPs agglomerates.

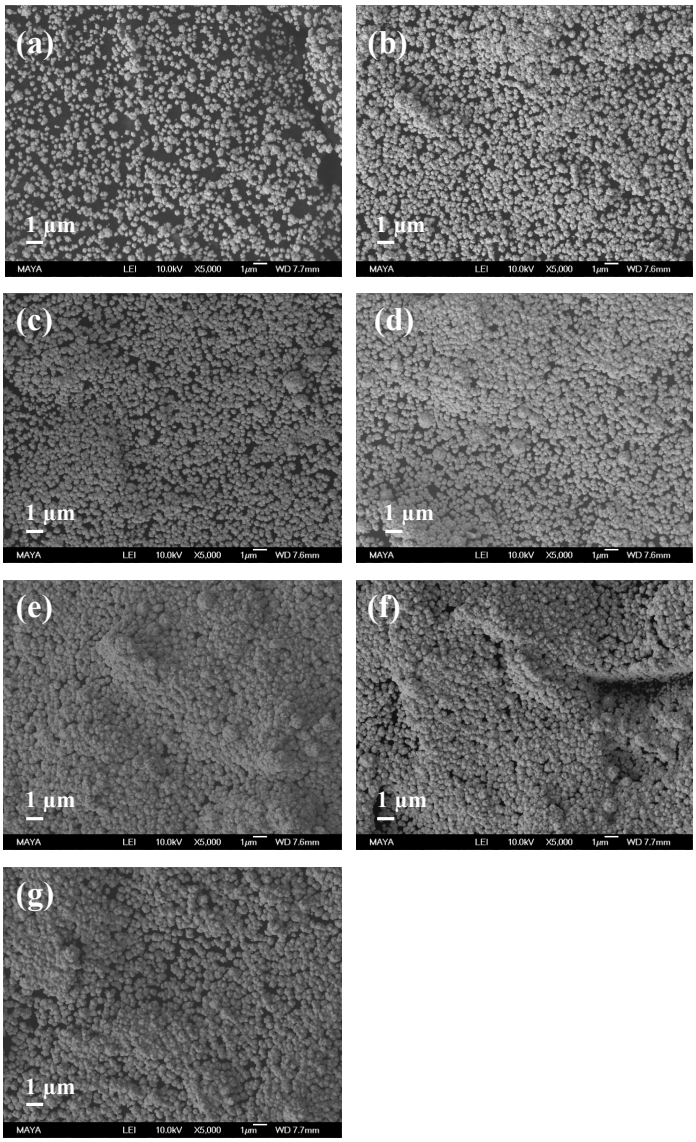

Figure 1. SEM images of AuNPs-modified GCEs obtained by sweeping the potential between 1.1 and −0.1 V vs. $Ag|AgCl_{sat}$ for a given number of scans in 10 mM $HAuCl_4$ (0.5 M H_2SO_4): (**a**) 5, (**b**) 10, (**c**) 15, (**d**) 20, (**e**) 25, (**f**) 30 and (**g**) 35.

All AuNP-modified electrodes were successively characterized by cyclic voltammetry (CV) experiments in a solution of $Fe(CN)_6^{3-/4-}$ (data not shown) in order to calculate the electroactive area (A_{EA}, cm^2), the heterogeneous electron transfer rate constant (k^0, cm s^{-1}) and the roughness factor (electroactive/geometrical area ratio, ρ) and in 0.5 M H_2SO_4 (Figure 2) in order to calculate the real surface area (A_{real}). All data are shown in Table 1. The A_{EA} has been evaluated using the Randles-Sevcik equation by the slope of the peak current vs. square root of scan rate ($v^{1/2}$) [39], whereas the real surface area (A_{real}) was calculated by integration of the peak current related to the gold oxide reduction process occurring by running CVs in 0.5 M H_2SO_4 [40,41]. The theoretical charge density considered for gold oxide reduction is 390 ± 10 μC cm^{-2} [42]. k^0 was calculated using the extended method which merges the Klingler-Kochi and Nicholson-Shain methods for totally irreversible and reversible systems, respectively [43,44]. It is possible to observe in Table 1 that all the electrochemical parameters are highly influenced by the number of scans, showing the best results after 25 scans with an A_{EA} of 12.96 ± 0.18 cm^2 and a roughness factor of 183.6 ± 1.2, probably related to the increase in AuNPs surface coverage with the scan number. With electrodes prepared with 30 and 35 scans the decrease in the electrochemical parameters reported in Table 1 might be due to the presence of multiple layers and possible AuNPs agglomeration (Figure 1f,g).

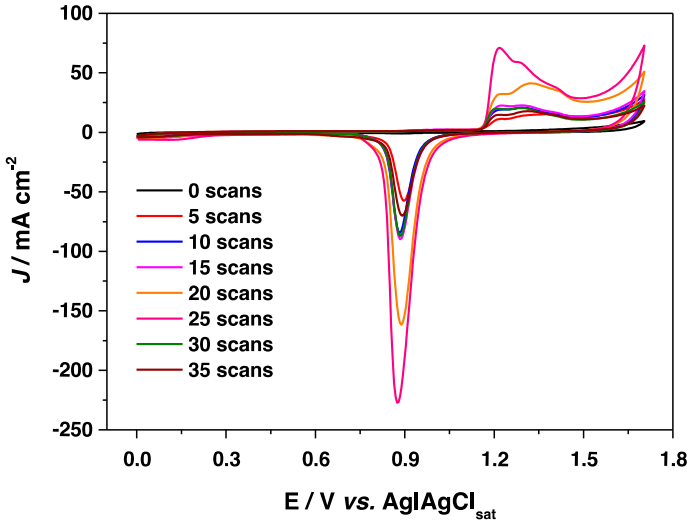

Figure 2. Cyclic voltammograms of AuNPs modified GCE electrodes with different number of scans (from 0 scans to 35 scans) in 0.5 M H_2SO_4. Scan rate 100 mV s^{-1}. T = 25 °C.

Table 1. Characterization of AuNPs on GC modified electrodes for different numbers of cyclic scans (N) during the electrodeposition step. Experimental conditions: 10 mM $Fe(CN)_6^{3-/4-}$ in 50 mM TRIS buffer pH 7.4 with 0.1 M KCl for electroactive area (A_{EA}), real surface area (A_{real}), electron transfer rate constant (k^0) and roughness factor (ρ) determination; 0.5 M H_2SO_4 at a scan rate of 100 mV s^{-1}, for A_{real} determination.

Scan Numbers (N)	A_{EA}/cm^2	A_{real}/cm^2	$k^0{}_{app}$/10^{-2} cm s^{-1}	Roughness Factor (ρ)
0	0.09 ± 0.01	-	4.6 ± 0.1	1.3 ± 0.1
5	2.72 ± 0.21	2.93 ± 0.07	5.2 ± 0.3	38.5 ± 0.3
10	3.92 ± 0.12	4.13 ± 0.06	7.9 ± 0.4	55.5 ± 0.3
15	4.13 ± 0.19	4.46 ± 0.06	13.4 ± 0.6	58.5 ± 0.5
20	8.74 ± 0.25	9.26 ± 0.04	18.2 ± 0.7	123.8 ± 0.8
25	12.96 ± 0.18	13.83 ± 0.04	26.8 ± 0.3	183.6 ± 1.2
30	4.18 ± 0.06	4.39 ± 0.08	15.3 ± 0.8	59.2 ± 0.7
35	3.26 ± 0.12	3.99 ± 0.06	10.6 ± 0.5	46.2 ± 1.3

3.2. Electrochemistry of CtCDH C291Y on Modified GA/4-APh,4-MBA/AuNPs/GC Electrode

After preliminary characterization, the modified AuNPs/GC electrode obtained after 25 scans of electrodeposition was further modified with *Ct*CDH C291Y covalently linked through GA with a mixed SAM consisting of 4-APh and 4-MBA. Figure 3a depicts the typical CVs of the enzyme electrode at different scan rates, showing an increased peak-to-peak separation (ΔE_p) between the anodic and cathodic peak potentials. The modified electrode exhibited a clear linear dependence of both anodic and cathodic peak current densities versus the scan rate over the range 2–500 mV s^{-1}, as shown in the inset of Figure 3a. The presented results fitted with thin-layer electrochemical behaviour, as generally reported for immobilized systems.

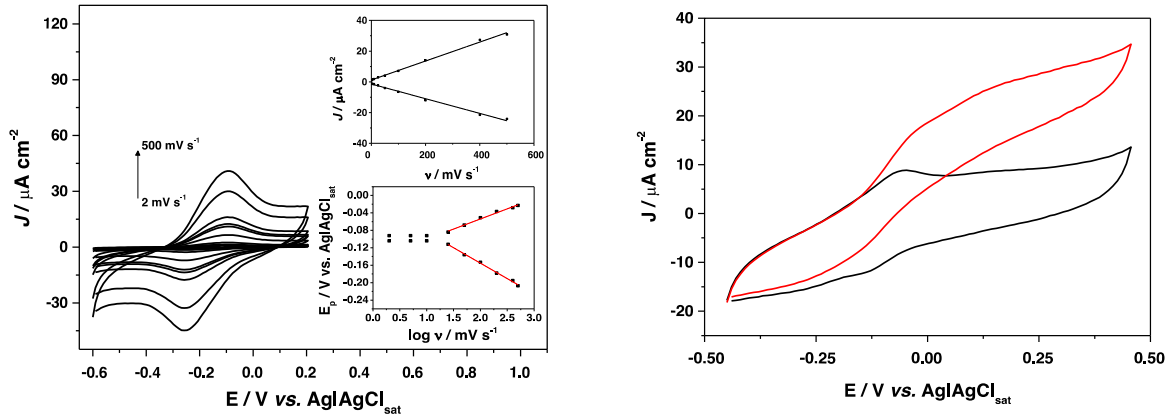

(**a**) (**b**)

Figure 3. (**a**) CVs of *Ct*CDH C291Y/GA/4-APh,4-MBA/AuNPs/GC in pH 7.4, 50 mM TRIS (0.1 M KCl) in the potential range of −0.6 V to 0.35 V, scan rates from 2 mV s^{-1} to 500 mV s^{-1}. Inset: linear part of cathodic (J_{pc}) and anodic peak current densities (J_{pa}) vs. scan rate (v). (**b**) CVs of *Ct*CDH C291Y/GA/4-APh, 4-MBA/AuNPs/GC in absence (black) and in presence of 5 mM glucose (red) in 50 mM TRIS buffer, pH 7.4 (0.1 M KCl) at a scan rate of 5 mV s^{-1}. T = 25 °C.

It is possible to observe in Figure 3b (black curve) a couple of peaks related to DET of CDH through the CYT_{CDH} subunit containing the *heme b*, which displayed a midpoint potential ($E^{0\prime}$) of −98 mV vs. Ag | $AgCl_{sat}$, close to the values reported in the literature for Ascomycota CDHs immobilized on gold electrodes [19]. The apparent heterogeneous electron transfer rate constant (k_s) was calculated by considering an electron transfer coefficient of 0.53, obtained by fitting the linear part of the trumpet plot, as shown in the inset of Figure 3a. Therefore, the k_s value was estimated to be 19.4 ± 0.6 s^{-1}, according to Laviron's equation [45] reported below:

$$\log k_s = \alpha \log(1-\alpha) + (1-\alpha)\log(RT/nFv) - \alpha(1-\alpha)nF\Delta E_p/2.3RT \quad (1)$$

where α is the electron transfer coefficient, n the number of electrons, ΔE_p the separation of the redox peak potentials and v the scan rate (F = 96.495 C mol^{-1}, T = 298 K, R = 8.31 J mol^{-1} K^{-1}).

By integration of the redox peaks relative to the DET of CYT_{CDH} it was possible to evaluate the enzyme surface coverage using the Faraday's law below reported in Equation (2):

$$\Gamma_T = \frac{Q}{nFA} \quad (2)$$

where Γ_T is the total surface concentration of electroactive protein (mol cm^{-2}), A the electrode area (cm^2), F the Faraday's constant (96 495 C mol^{-1} of electrons), Q the charge underlying the redox wave and n the number of electrons [46]. The theoretical surface coverage (Γ_{theor}) was estimated to be 5287 ± 152 pmol cm^{-2} (A_{geom} = 0.073 cm^2), while the real surface coverage (Γ_{real}) resulted to be 27 ± 2 pmol cm^{-2} (A_{real} = 13.83 ± 0.04 cm^2, as shown in Table 1). Afterwards, the electrocatalytic behaviour of the *Ct*CDH C291Y/GA/4-APh,4-MBA/AuNPs/GC electrode was studied by performing CVs in the presence of 5 mM glucose as substrate (Figure 3b, red curve), showing excellent performances with a current density of about 30 µA cm^{-2}, probably due to the high nanostructuration of the electrode surface and the covalent immobilization of the enzyme.

3.3. Glucose Biosensor Development

The amperometric response to glucose was studied by injecting glucose solutions at different concentrations by using the flow injection analysis (FIA) system, in order to investigate the electroanalytical and kinetic parameters of the modified *Ct*CDH C291Y/GA/4-APh, 4-MBA/AuNPs/GC electrode. The biosensor showed a fast peak response (5 s), probably due to the enlarged surface area related to the electrodeposition of the AuNPs and the cross-linking of the enzyme, which ensure high number of immobilized enzyme molecules and stable enzyme layer.

The calibration curve displayed a linear response range between 0.02 and 30 mM (R^2 = 0.995, n = 5) with a sensitivity of 3.1 ± 0.1 µA mM^{-1} cm^{-2}, as shown in the inset of Figure 4a. At higher concentrations the amperometric response is no longer linear due to the saturation of the enzyme active site. The detection limit for *Ct*CDH C291Y/GA/4-APh,4-MBA/AuNPs/GC biosensor was found to be 6.2 µM, calculated using the relation 3σ/S, where σ is the absolute standard deviation of the intercept and S is the slope of the calibration curve [47]. The analytical performances of the glucose biosensor and the kinetic parameters are listed in Table 2. The apparent kinetic parameters (I_{max}, K_M^{app}) are in good agreement with the values reported in the literature for nanostructured electrodes [48]. It is interesting to underline that today very few third generation glucose biosensors based on Ascomycota CDHs have been reported in the literature while most other glucose biosensors are based on first and second generation electron transfer mechanism of other GMC oxidoreductase enzymes (e.g., GOx).

Table 2. Electroanalytical and kinetic parameters of the *Ct*CDH C291Y/GA/4-APh,4-MBA/AuNPs/GC biosensor obtained by FIA amperometry in 50 mM TRIS buffer, pH 7.4. Applied potential: +0.250 V vs. Ag | $AgCl_{sat}$.

	***Ct*CDH C291Y/GA/4-APh,4-MBA/AuNPs/GC**
E_{app}/(V vs. Ag | $AgCl_{sat}$)	+0.250
K_M^{app}/mM	11.7 ± 1.2
J_{max}/µA cm^{-2}	126.9 ± 3.0
LOD/µM	6.2
Linear range/mM	0.02–30
Sensitivity/µA mM^{-1} cm^{-2}	3.1 ± 0.1
R^2	0.99

The proposed *Ct*CDH C291Y/GA/4-APh,4-MBA/AuNPs/GC biosensor shows a clear increase in terms of sensitivity, selectivity, stability, extended linear range and lower detection limit compared to other second and third generation glucose biosensors reported in the literature, as shown in Table 3.

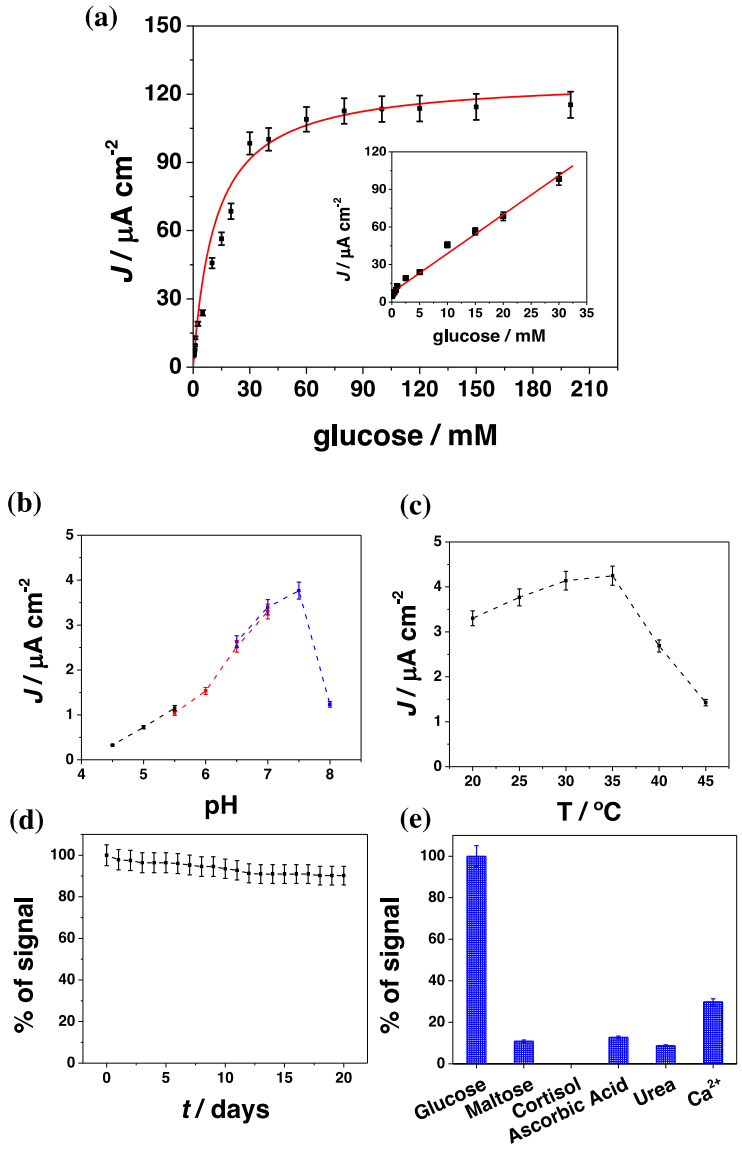

Figure 4. (**a**) Glucose biosensor calibration graph of *Ct*CDH C291Y/GA/4-APh,4-MBA/AuNPs/GC in 50 TRIS buffer pH 7.4 (0.1 M KCl); E_{app} = 0.250 vs. Ag | $AgCl_{sat}$; flow rate 0.5 mL min^{-1}; inset: linear part of the calibration curve; (**b**) biosensor response over the pH range (4.5–8): 50 mM acetate buffer (black), 50 mM MOPS buffer (red) and in 50 mM TRIS buffer (blue), with E_{app} = 0.250 vs. Ag | $AgCl_{sat}$; flow rate 0.5 mL min^{-1}; (**c**) biosensor response over the T range (20–45 °C) in TRIS buffer; (**d**) lifetime of *Ct*CDH C291Y/GA/4-APh,4-MBA/AuNPs/GC biosensor in presence of 750 µM glucose solution; (**e**) influence of interfering compounds on glucose response in presence of 750 µM glucose, maltose, cortisol, ascorbic acid, Ca^{2+}. Experimental conditions (**c**–**e**): 50 TRIS buffer pH 7.4 (0.1 M KCl), E_{app} = 0.250 vs. Ag | $AgCl_{sat}$; flow rate 0.5 mL min^{-1}; injection volume 50 µL; T = 25 °C.

Nevertheless, it exhibits a lower sensitivity compared to the first generation glucose biosensors, probably because of some issues related to the DET [49–55]. On the other hand, first and second generation biosensors have known drawbacks, such as their instability and the toxicity of the mediator layer.

Table 3. Comparison between glucose biosensors based on mediated (MET) and direct electron transfer (DET). List of abbreviations: 1,1′-dimethylferrocene (DMFc), 1,2-diaminobenzene (p-DAB), 4-aminophenol (4-APh), 4-mercaptobenzoic acid (4-MBA), *Corynascus thermophilus* cellobiose dehydrogenase (*Ct*CDH), *Corynascus thermophilus* cellobiose dehydrogenase C291Y mutant (*Ct*CDH C291Y), ferrocene-COOH (Fc-COOH), glassy carbon electrode (GC), glucose oxidase (GOx), glutaraldehyde (GA), gold (Au), gold nanoparticles (AuNPs), osmium $(bpy)_2$poly (1-vinylimidazole) (PVI-Os), Prussian Blue (PB), screen-printed carbon electrode (SPCE), single walled carbon nanotubes (SWCNTs), titanium nanotubes (TiNTs).

Modified Electrode	E_{app}/V vs. $Ag\,|\,AgCl_{sat}$	Linear Range/mM	LOD/μM	Sensitivity/μA mM^{-1} cm^{-2}	Stability	Reference
(GOx/Au/pDAB)-PB/ AuNPs/TiNTs (1st generation)	−0.35	0.01–0.70	3.2	248.0	>90% after 1 month	[49]
GOx-GA/PB/Pt (1st generation)	−0.05	0.01–1	5	80.0	83.3% after 23 days	[50]
GOx/PB/SPCE (1st generation)	−0.30	0.25–2	10.0	17.0	72% after 45 days	[51]
GOx/Fc-COOH/SPCE (2nd generation)	+0.25	1–5	180.0	2.0	~80% after 3 weeks	[52]
GOx/DMFc/G (2nd generation)	+0.16	1–30	300	-	-	[53]
GOx-SWCNTs-PVI-Os/SPCE (2nd generation)	+0.30	0.2–7.5	0.07	32	~90% after 30 days	[54]
*Ct*CDH/GA/SWCNTs/SPCE (3rd generation)	+0.10	0.1–30	10.0	-	~90% after 7.5 h	[55]
*Ct*CDH C291Y/GA/4-APh, 4-MBA/AuNPs/GC (3rd generation)	+0.25	0.02–30	6.2	3.1	~90% after 20 days	this work

3.4. Effect of pH and Temperature, Interferences and Stability Studies

The effects of pH and temperature on the proposed glucose biosensor were evaluated and the results are reported in Figure 4b. The optimum pH resulted to be pH 7 in TRIS buffer at a temperature of 35 °C. A significant decrease in the current densities occurs below pH 5.5 and above 8, in perfect agreement with the data reported in the literature about the optimum pH of the free CDH [56]. The dependence on the temperature is shown in Figure 4c where it is possible to see that the amperometric response increased from 20 to 30–35 °C and drastically decreased above 37 °C, due to a possible inactivation of the enzyme caused by the temperature.

The stability and lifetime of the *Ct*CDH C291Y/GA/4-APh,4-MBA/AuNPs/GC biosensor was evaluated using the FIA system by monitoring the signal decrease within 20 days when the biosensor is used for one measurement per day, as reported in Figure 4d. The modified biosensor seems to retain about 90% of its initial activity after 20 days, probably due to the stability of the enzyme layer directly related to the nanostructuration of the electrode surface.

Finally, the selectivity of the proposed biosensor was studied in order to see the influence of possible interfering compounds generally present in human saliva such as maltose, cortisol, ascorbic acid, urea and calcium ions (Ca^{2+}). The signal obtained for a fixed concentration of glucose (750 μM) was compared to that obtained with a sample containing the same glucose concentration plus equal amounts of the possible interfering compounds. The amperometric signal is lower than 10% for all compounds tested with the exception of Ca^{2+} ions, which potentially may interfere in real measurements (30% of glucose signal), probably because of its interaction with some amino acid residues present between the DH_{CDH} and CYT_{CDH} domains [56].

3.5. Glucose Detection in Human Saliva

In order to demonstrate the feasibility of the modified electrode for the non-invasive detection of glucose, the proposed biosensor was used to detect the concentration of glucose in human saliva samples. The samples were collected according to the procedure reported in Section 2.3, referred to literature on saliva analysis. The reliability of the amperometric biosensor platform *Ct*CDH

C291Y/GA/4-APh,4-MBA/AuNPs/GC was evaluated by comparing the results with those obtained with the glucose oxidase-peroxidase method. The proposed biosensor showed satisfactory results in all samples tested with a recovery between 95.0 and 97.4% (RSD values lower than 4%), as reported in Table 4.

Table 4. Glucose measurements in human saliva with the *Ct*CDH C291Y/GA/4-APh, 4-MBA/AuNPs/GC biosensor and with the glucose oxidase-peroxidase kit (GlucoContour XT), as reference method. Experimental conditions: 50 mM TRIS buffer pH 7.4, E_{app} = +0.250 V vs. Ag | $AgCl_{sat}$.

	Biosensor/mg dL^{-1}	Reference Method/mg dL^{-1}	Recovery/%
Sample 1 (male)	0.77 ± 0.03	0.79 ± 0.03	97.4
Sample 2 (male)	0.96 ± 0.02	1.00 ± 0.04	95.7
Sample 3 (male)	0.89 ± 0.03	0.92 ± 0.05	96.9
Sample 1 (female)	0.74 ± 0.03	0.75 ± 0.03	98.8
Sample 2 (female)	0.71 ± 0.01	0.74 ± 0.02	95.0
Sample 3 (female)	0.77 ± 0.02	0.80 ± 0.01	96.5

The glucose content was measured also in blood samples collected from the same healthy patients with a commercial self-monitoring system (GlucoContour XT) in order to evaluate the correlation between glucose saliva and blood levels, for future potential development of devices for non-invasive glucose monitoring [57]. Figure 5 shows a good correlation between salivary and blood glucose concentration, opening the doors to the development of possible self-non invasive glucose monitoring devices.

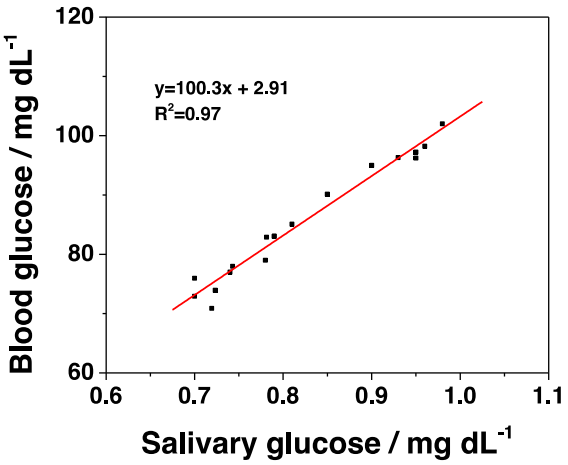

Figure 5. Correlation between glucose blood and saliva glucose concentration in 6 healthy patients at fasting state. Salivary glucose was detected with the *Ct*CDH C291Y/GA/4-APh,4-MBA/AuNPs/GC biosensor, blood glucose was detected with the commercial GlucoContour XT.

4. Conclusions

We have demonstrated the possibility to carefully monitor the surface coverage of AuNPs on the electrode surface through a direct electrochemical deposition method of AuNPs onto a glassy carbon electrode which allows to achieve an efficient DET thanks to the effective nanostructure and the cross-linking of CDH molecules. AuNPs resulted to be very efficient for retaining the enzyme activity and promoting the electron transfer. The *Ct*CDH C291Y/GA/4-APh,4-MBA/AuNPs/GC biosensor showed great performances in terms of extended linear range and higher sensitivity, selectivity and stability compared to other glucose biosensors. The promising platform allowed the detection of glucose in human saliva with results in very good agreement with those obtained with the standard spectrophotometric method showing also a good correlation with glucose blood levels. For these

reasons, the proposed biosensor may represent the basis for the development of a portable non-invasive device for glucose monitoring in diabetes mellitus patients.

Acknowledgments: A particular acknowledgment to Daniel Jacobsson for the SEM characterization of the AuNPs modified GC electrodes. The authors would like to thank for financial funding the Swedish Research Council (Vetenskapsrådet project 2014-5908), the European Commission (project "Bioenergy" FP7-PEOPLE-2013-ITN-607793) and a scholarship of the Erasmus+ Project Unipharma-Graduates, promoted by a Consortium of Italian Universities and coordinated by Sapienza University of Rome.

Author Contributions: P.B. and R.A. conceived and designed the experiments; P.B. performed the experiments and analyzed the data. L.G. and R.A. revised the manuscript and R.L. kindly provided *Ct*CDH C291Y mutant.

Conflicts of Interest: The authors declare no conflicts of interest. All authors have revised and approved the final version.

References

1. Heller, A.; Feldman, B. Electrochemical glucose sensors and their applications in diabetes management. *Chem. Rev.* **2008**, *108*, 2482–2505. [CrossRef] [PubMed]
2. Wang, J. Electrochemical glucose biosensors. *Chem. Rev.* **2008**, *108*, 814–825. [CrossRef] [PubMed]
3. American Diabetes Association. Diagnosis and classification of diabetes mellitus. *Diabetes Care* **2014**, *37*, S81–S90.
4. Janghorbani, M.; Van Dam, R.M.; Willett, W.C.; Hu, F.B. Systematic review of type 1 and type 2 diabetes mellitus and risk of fracture. *Am. J. Epidemiol.* **2007**, *166*, 495–505. [CrossRef] [PubMed]
5. Newman, J.D.; Turner, A.P.F. Home blood glucose biosensors: A commercial perspective. *Biosens. Bioelectron.* **2005**, *20*, 2435–2453. [CrossRef] [PubMed]
6. Lehmann, R.; Huber, M.; Beck, A.; Schindera, T.; Rinkler, T.; Houdali, B.; Weigert, C.; Häring, H.U.; Voelter, W.; Schleicher, E.D. Simultaneous, quantitative analysis of UDP-N-acetylglucosamine, UDP-N-acetylgalactosamine, UDP-glucose and UDP-galactose in human peripheral blood cells, muscle biopsies and cultured mesangial cells by capillary zone electrophoresis. *Electrophoresis* **2000**, *21*, 3010–3015. [CrossRef]
7. Orata, F. *Derivatization Reactions and Reagents for Gas Chromatography Analysis*; Mohd, M.A., Ed.; InTech Open Access Publisher: Rijeka, Croatia, 2012; pp. 83–108. ISBN 978-953-0298-4. [CrossRef]
8. Wang, C.; Kong, H.; Guan, Y.; Yang, J.; Gu, J.; Yang, S.; Xu, G. Plasma phospholipid metabolic profiling and biomarkers of type 2 diabetes mellitus based on high-performance liquid chromatography/electrospray mass spectRometry and multivariate statistical analysis. *Anal. Chem.* **2005**, *77*, 4108–4116. [CrossRef] [PubMed]
9. Srinivasan, V.; Pamula, V.K.; Fair, R.B. Droplet-based microfluidic lab-on-a-chip for glucose detection. *Anal. Chim. Acta* **2004**, *507*, 145–150. [CrossRef]
10. Chen, S.-F.; Danao, M.-G.C.; Singh, V.; Brown, P.J. Determining sucrose and glucose levels in dual-purpose sorghum stalks by Fourier transform near infrared (FT-NIR) spectroscopy. *J. Sci. Food Agric.* **2014**, *94*, 2569–2576. [CrossRef] [PubMed]
11. Scheller, F.W.; Schubert, F.; Neumann, B.; Pfeiffer, D.; Hintsche, R.; Dransfeld, I.; Wollenberger, U.; Renneberg, R.; Warsinke, A.; Johansson, G. Second generation biosensors. *Biosens. Bioelectron.* **1991**, *6*, 245–253. [CrossRef]
12. Antiochia, R.; Vinci, G.; Gorton, L. Rapid and direct determination of fructose in food: A new osmium-polymer mediated biosensor. *Food Chem.* **2013**, *140*, 742–747. [CrossRef] [PubMed]
13. Mazzei, F.; Favero, G.; Bollella, P.; Tortolini, C.; Mannina, L.; Conti, M.E.; Antiochia, R. Recent trends in electrochemical nanobiosensors for environmental analysis. *Int. J. Environ. Health* **2015**, *7*, 267–291. [CrossRef]
14. Bollella, P.; Fusco, G.; Tortolini, C.; Sanzò, G.; Favero, G.; Gorton, L.; Antiochia, R. Beyond graphene: Electrochemical sensors and biosensors for biomarkers detection. *Biosens. Bioelectron.* **2017**, *89*, 152–166. [CrossRef] [PubMed]
15. Bollella, P.; Schulz, C.; Favero, G.; Mazzei, F.; Ludwig, R.; Gorton, L.; Antiochia, R. Green Synthesis and Characterization of Gold and Silver Nanoparticles and Their Application for Development of a Third Generation Lactose Biosensor. *Electroanalysis* **2017**, *29*, 77–86. [CrossRef]
16. Favero, G.; Fusco, G.; Mazzei, F.; Tasca, F.; Antiochia, R. Electrochemical characterization of graphene and MWCNT screen-printed electrodes modified with AuNPs for laccase biosensor development. *Nanomaterials* **2015**, *5*, 1995–2006. [CrossRef] [PubMed]

17. Katz, E.; Willner, I. Integrated nanoparticle–biomolecule hybrid systems: Synthesis, properties, and applications. *Angew. Chem. Int. Ed.* **2004**, *43*, 6042–6108. [CrossRef] [PubMed]
18. Krueger, M.; Berg, S.; Stone, D.A.; Strelcov, E.; Dikin, D.A.; Kim, J.; Cote, L.J.; Huang, J.; Kolmakov, A. Drop-casted self-assembling graphene oxide membranes for scanning electron microscopy on wet and dense gaseous samples. *ACS Nano* **2011**, *5*, 10047–10054. [CrossRef] [PubMed]
19. Bollella, P.; Mazzei, F.; Favero, G.; Fusco, G.; Ludwig, R.; Gorton, L.; Antiochia, R. Improved DET communication between cellobiose dehydrogenase and a gold electrode modified with a rigid self-assembled monolayer and green metal nanoparticles: The role of an ordered nanostructuration. *Biosens. Bioelectron.* **2017**, *88*, 196–203. [CrossRef] [PubMed]
20. Shah, A.T.; Din, M.I.; Bashir, S.; Qadir, M.A.; Rashid, F. Green synthesis and characterization of silver nanoparticles using *Ferocactus echidne* extract as a reducing agent. *Anal. Lett.* **2015**, *48*, 1180–1189. [CrossRef]
21. El-Deab, M.S.; Sotomura, T.; Ohsaka, T. Size and crystallographic orientation controls of gold nanoparticles electrodeposited on GC electrodes. *J. Electrochem. Soc.* **2005**, *152*, C1–C6. [CrossRef]
22. Hezard, T.; Fajerwerg, K.; Evrard, D.; Collière, V.; Behra, P.; Gros, P. Gold nanoparticles electrodeposited on glassy carbon using cyclic voltammetry: Application to Hg(II) trace analysis. *J. Electroanal. Chem.* **2012**, *664*, 46–52. [CrossRef]
23. Luo, X.-L.; Xu, J.-J.; Du, Y.; Chen, H.-Y. A glucose biosensor based on chitosan–glucose oxidase–gold nanoparticles biocomposite formed by one-step electrodeposition. *Anal. Biochem.* **2004**, *334*, 284–289. [CrossRef] [PubMed]
24. Ustarroz, J.; Ke, X.; Hubin, A.; Bals, S.; Terryn, H. New insights into the early stages of nanoparticle electrodeposition. *J. Phys. Chem. C* **2012**, *116*, 2322–2329. [CrossRef]
25. Matsumura, H.; Ortiz, R.; Ludwig, R.; Igarashi, K.; Samejima, M.; Gorton, L. Direct electrochemistry of *Phanerochaete chrysosporium* cellobiose dehydrogenase covalently attached onto gold nanoparticle modified solid gold electrodes. *Langmuir* **2012**, *28*, 10925–10933. [CrossRef] [PubMed]
26. Ludwig, R.; Ortiz, R.; Schulz, C.; Harreither, W.; Sygmund, C.; Gorton, L. Cellobiose dehydrogenase modified electrodes: Advances by materials science and biochemical engineering. *Anal. Bioanal. Chem.* **2013**, *405*, 3637–3658. [CrossRef] [PubMed]
27. Cipri, A.; Schulz, C.; Ludwig, R.; Gorton, L.; Del Valle, M. A novel bio-electronic tongue using different cellobiose dehydrogenases to resolve mixtures of various sugars and interfering analytes. *Biosens. Bioelectron.* **2016**, *79*, 515–521. [CrossRef] [PubMed]
28. Falk, M.; Pankratov, D.; Lindh, L.; Arnebrant, T.; Shleev, S. Miniature direct electron transfer based enzymatic fuel cell operating in human sweat and saliva. *Fuel Cells* **2014**, *14*, 1050–1056. [CrossRef]
29. Zamocky, M.; Ludwig, R.; Peterbauer, C.; Hallberg, B.M.; Divne, C.; Nicholls, P.; Haltrich, D. Cellobiose dehydrogenase-a flavocytochRome from wood-degrading, phytopathogenic and saprotropic fungi. *Curr. Protein. Pept. Sci.* **2006**, *7*, 255–280. [CrossRef] [PubMed]
30. Schulz, C.; Ludwig, R.; Gorton, L. Polyethyleneimine as a promoter layer for the immobilization of cellobiose dehydrogenase from *Myriococcum thermophilum* on graphite electrodes. *Anal. Chem.* **2014**, *86*, 4256–4263. [CrossRef] [PubMed]
31. Tavahodi, M.; Ortiz, R.; Schulz, C.; Ekhtiari, A.; Ludwig, R.; Haghighi, B.; Gorton, L. Direct Electron Transfer of Cellobiose Dehydrogenase on Positively Charged Polyethyleneimine Gold Nanoparticles. *ChemPlusChem* **2017**, *82*, 546–552. [CrossRef]
32. Ortiz, R.; Rahman, M.; Zangrilli, B.; Sygmund, C.; Micheelsen, P.O.; Silow, M.; Toscano, M.D.; Ludwig, R.; Gorton, L. Engineering of Cellobiose Dehydrogenases for Improved Glucose Sensitivity and Reduced Maltose Affinity. *ChemElectroChem* **2017**, *4*, 846–855. [CrossRef]
33. Dai, X.; Nekrassova, O.; Hyde, M.E.; Compton, R.G. Anodic stripping voltammetry of arsenic(III) using gold nanoparticle-modified electrodes. *Anal. Chem.* **2004**, *76*, 5924–5929. [CrossRef] [PubMed]
34. Wang, X.; Falk, M.; Ortiz, R.; Matsumura, H.; Bobacka, J.; Ludwig, R.; Bergelin, M.; Gorton, L.; Shleev, S. Mediatorless sugar/oxygen enzymatic fuel cells based on gold nanoparticle-modified electrodes. *Biosens. Bioelectron.* **2012**, *31*, 219–225. [CrossRef] [PubMed]
35. Henson, B.S.; Wong, D.T. Collection, storage, and processing of saliva samples for downstream molecular applications. *Oral Biol. Mol. Technol. Appl.* **2010**, *666*, 21–30.
36. Mehta, Y.P.; Munde, B.P. Study of blood sugar levels in high risk neonates using glucometer method and laboratory glucose oxidase peroxidase method. *Int. J. Contemp. Pediatr.* **2017**, *4*, 1185–1192. [CrossRef]

37. Trinder, P. Determination of glucose in blood using glucose oxidase with an alternative oxygen acceptor. *Ann. Clin. Biochem.* **1969**, *6*, 24–27. [CrossRef]
38. Wilkins, E.; Atanasov, P. Glucose monitoring: State of the art and future possibilities. *Med. Eng. Phys.* **1996**, *18*, 273–288. [CrossRef]
39. Oldham, K.B. Analytical expressions for the reversible Randles-Sevcik function. *J. Electroanal. Chem. Interfacial Electrochem.* **1979**, *105*, 373–375. [CrossRef]
40. Daglia, M.; Antiochia, R.; Sobolev, A.P.; Mannina, L. Untargeted and targeted methodologies in the study of tea (*Camellia sinensis* L.). *Food Res. Int.* **2014**, *63*, 275–289. [CrossRef]
41. Murata, K.; Kajiya, K.; Nukaga, M.; Suga, Y.; Watanabe, T.; Nakamura, N.; Ohno, H. A Simple Fabrication Method for Three-Dimensional Gold Nanoparticle Electrodes and Their Application to the Study of the Direct Electrochemistry of Cytochrome c. *Electroanalysis* **2010**, *22*, 185–190. [CrossRef]
42. Trasatti, S.; Petrii, O.A. Real surface area measurements in electrochemistry. *Pure Appl. Chem.* **1991**, *63*, 711–734. [CrossRef]
43. Lavagnini, I.; Antiochia, R.; Magno, F. An extended method for the practical evaluation of the standard rate constant from cyclic voltammetric data. *Electroanalysis* **2004**, *16*, 505–506. [CrossRef]
44. Lavagnini, I.; Antiochia, R.; Magno, F. A calibration-base method for the evaluation of the detection limit of an electrochemical biosensor. *Electroanalysis* **2007**, *19*, 1127–1230. [CrossRef]
45. Laviron, E. General expression of the linear potential sweep voltammogram in the case of diffusionless electrochemical systems. *J. Electroanal. Chem. Interfacial Electrochem.* **1979**, *101*, 19–28. [CrossRef]
46. Rusling, J.F.; Zhang, Z. Thin films on electrodes for direct protein electron transfer. In *Handbook of Surfaces and Interfaces of Materials*; Elsevier: Amsterdam, The Netherlands, 2001; pp. 33–71.
47. Shrivastava, A.; Gupta, V.B. Methods for the determination of limit of detection and limit of quantitation of the analytical methods. *Chron. Young Sci.* **2011**, *2*, 21–25. [CrossRef]
48. Tasca, F.; Zafar, M.N.; Harreither, W.; Nöll, G.; Ludwig, R.; Gorton, L. A third generation glucose biosensor based on cellobiose dehydrogenase from *Corynascus thermophilus* and single-walled carbon nanotubes. *Analyst* **2011**, *136*, 2033–2036. [CrossRef] [PubMed]
49. Gao, Z.-D.; Qu, Y.; Li, T.; Shrestha, N.K.; Song, Y.-Y. Development of amperometric glucose biosensor based on Prussian Blue functionlized TiO_2 nanotube arrays. *Sci. Rep.* **2014**, *4*, 6891. [CrossRef] [PubMed]
50. Liu, Y.; Chu, Z.; Zhang, Y.; Jin, W. Amperometric glucose biosensor with high sensitivity based on self-assembled Prussian Blue modified electrode. *Electrochim. Acta* **2009**, *54*, 7490–7494. [CrossRef]
51. Sekar, N.C.; Shaegh, S.A.M.; Ng, S.H.; Ge, L.; Tan, S.N. A paper-based amperometric glucose biosensor developed with Prussian Blue-modified screen-printed electrodes. *Sens. Actuators B Chem.* **2014**, *204*, 414–420. [CrossRef]
52. Lawrence, C.S.K.; Tan, S.N.; Floresca, C.Z. A "green" cellulose paper based glucose amperometric biosensor. *Sens. Actuators B Chem.* **2014**, *193*, 536–541. [CrossRef]
53. Cass, A.E.G.; Davis, G.; Francis, G.D.; Hill, H.A.O.; Aston, W.J.; Higgins, I.J.; Plotkin, E.V.; Scott, L.D.L.; Turner, A.P.F. Ferrocene-mediated enzyme electrode for amperometric determination of glucose. *Anal. Chem.* **1984**, *56*, 667–671. [CrossRef] [PubMed]
54. Gao, Q.; Guo, Y.; Zhang, W.; Qi, H.; Zhang, C. An amperometric glucose biosensor based on layer-by-layer GOx-SWCNT conjugate/redox polymer multilayer on a screen-printed carbon electrode. *Sens. Actuators B Chem.* **2011**, *153*, 219–225. [CrossRef]
55. Zafar, M.N.; Safina, G.; Ludwig, R.; Gorton, L. Characteristics of third-generation glucose biosensors based on *Corynascus thermophilus* cellobiose dehydrogenase immobilized on commercially available screen-printed electrodes working under physiological conditions. *Anal. Biochem.* **2012**, *425*, 36–42. [CrossRef] [PubMed]
56. Harreither, W.; COman, V.; Ludwig, R.; Haltrich, D.; Gorton, L. Investigation of graphite electrodes modified with cellobiose dehydrogenase from the ascomycete *Myriococcum thermophilum*. *Electroanalysis* **2007**, *19*, 172–180. [CrossRef]
57. Zhang, W.; Du, Y.; Wang, M.L. Noninvasive glucose monitoring using saliva nano-biosensor. *Sens. Biol. Sens. Res.* **2015**, *4*, 23–29. [CrossRef]

Paper V

Applied Materials Today 9 (2017) 319–332

Contents lists available at ScienceDirect

Applied Materials Today

journal homepage: www.elsevier.com/locate/apmt

Cellobiose dehydrogenase: Insights on the nanostructuration of electrodes for improved development of biosensors and biofuel cells

Paolo Bollella[a,b], Roland Ludwig[c], Lo Gorton[b,*]

[a] Department of Chemistry and Drug Technologies, Sapienza University of Rome, P.le Aldo Moro, 500185 Rome, Italy
[b] Department of Analytical Chemistry/Biochemistry and Structural Biology, Lund University, PO Box 124, SE-22100 Lund, Sweden
[c] Department of Food Sciences and Technology, BOKU University of Natural Resources and Life Sciences, A-1190 Vienna, Austria

ARTICLE INFO

Article history:
Received 11 August 2017
Accepted 23 August 2017

Keywords:
Cellobiose dehydrogenase (CDH)
Carbon nanomaterials
Metal nanomaterials
Electrochemical biosensors
Enzymatic fuel cells (EFCs)

ABSTRACT

Cellobiose dehydrogenase (CDH) is a versatile bioelectrocatalyst lately at focus due to its sugar oxidising properties in combination with its inherent ability for direct electron transfer communication with electrodes making it possible to be used in bioanodes in the enzymatic fuel cells (EFCs), self-powered biosensors, and biosupercapacitors. During the last 20 years, many new nanomaterials and hybrid nanocomposites have been developed and employed in combination with various oxidoreductases, such as CDH, to increase the overall performance of electrical devices (e.g. biosensors, EFCs etc.). It has also been shown that nanomaterials can be further chemically modified to facilitate electron transfer pathways between the biocomponent and electrodes. Both carbon and metal based nanomaterials and combinations thereof have been used together with CDH to improve the performance. In this review, we resume all the findings related to the influence of effective nanostructuration to improve the electron transfer communication with electrodes yielding higher sensitivity of biosensors or increasing the power output of EFC based on CDH from different sources.

Contents

1. Introduction

CDH [(cellobiose:acceptor) 1-oxidoreductase, EC 1.1.99.18] is an extracellular flavocytochrome oxidoreductase expressed by the dikaryotic phyla Basidiomycota (Class I CDH) and Ascomycota (Class II and Class III CDH) essential for the degradation of lignocellulose in nature [1]. All CDHs consist of two domains [2–5], a larger catalytic dehydrogenase domain (DH_{CDH}) containing one strongly but not covalently bound flavin adenine dinucleotide (FAD) molecule as cofactor [4] and connected through a flexible linker region to a second smaller cytochrome domain containing *heme b* as cofactor (CYT_{CDH}) [3] as displayed by the crystal structure of CDH seen in Fig. 1a [5]. The DH_{CDH} is structurally similar to the FAD containing domain of most other GMC-oxidoreductase enzymes [6,7] and is fully reduced by di-/mono-saccharides. In a following step the electrons are transferred through an internal electron transfer (IET) mechanism to the CYT_{CDH}, which in

* Corresponding author.
E-mail address: lo.gorton@biochemistry.lu.se (L. Gorton).

http://dx.doi.org/10.1016/j.apmt.2017.08.009
2352-9407/

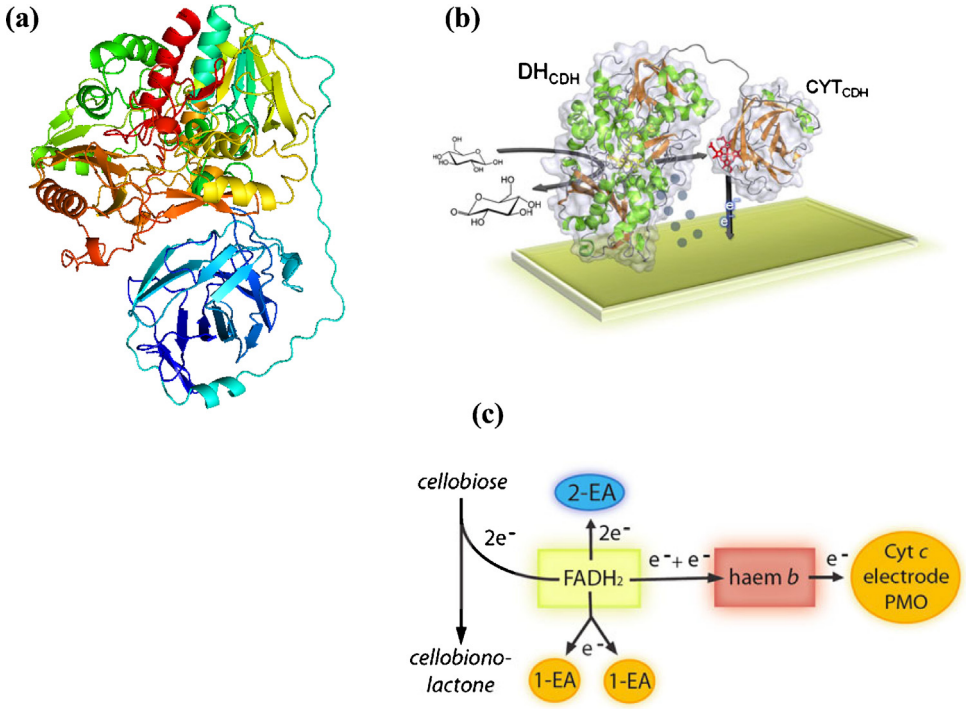

Fig. 1. (a) Crystal structure of *Corynascous thermophilus* CDH; (b) electron transfer through the two CDH domains and onto the terminal electron acceptor. DET depends on CYT_{CDH} as an electron shuttle, whereas MET (blue spheres indicate soluble mediators or polymeric redox centres) transfers electrons from DH_{CDH} to the electrode surface through the help of a redox mediator; (c) Electron transfer pathways from the substrate through CDH to various electron acceptors. One- and two-electron acceptors (EA) can be reduced directly by the $FADH_2$ in the DH_{CDH}. Alternatively, electrons can be transferred by IET to the haem *b* in the CYT_{CDH}, which works as a relay for the reduction of macromolecular electron acceptors like PMO, cyt *c* or an electrode. 1 b and c reproduced from [10] with permission of Springer-Verlag. (For interpretation of the references to color in this figure legend, the reader is referred to the web version of this article.)

turn finally shuttles the electrons to its recently discovered natural electron acceptor, lytic polysaccharide monooxygenase (LPMO) [8]. When CDH is immobilised on an electrode, the electrode can serve as the electron acceptor taking the electrons sequentially from CYT_{CDH}, which was first shown already in 1996 [9]. The possible electron transfer pathways through CDH to the electrode are illustrated in Fig. 1b and c.

In the last decades, cellobiose dehydrogenase (CDH) from different origins has been widely used as a bioelectrocatalyst for development of both biosensors and biofuel cells mainly due to its inherent ability for direct electron transfer (DET) communication with electrodes [10,11]. A large number of various carbon or metal nanomaterials (e.g. single walled carbon nanotubes SWCNTs, multi walled carbon nanotubes MWCNTs, gold nanoparticles AuNPs, highly porous gold hPG) [12–16] have been used to improve current density by increasing the surface area of electrodes and also possibly by increasing the percentage of the immobilised enzyme molecules orientated for DET. However, also mediated electron transfer (MET) approaches by means of redox or conductive polymers [17,18] have been used as in most cases MET still results in improved current densities compared with any approach based on DET [12,19–24]. CDH has been applied in the development of biosensors for detection of a variety of substrates such as cellobiose, cellodextrins, maltose, lactose, diphenolic compounds and catecholamines [25–27], as well as for development of biofuel cells using lactose, glucose or cellobiose as fuels [28–35].

2. Direct electron transfer (DET)

The most commonly used sugar oxidising enzyme in bioelectrochemistry/bioelectronics, glucose oxidase, GOx, from *Aspergillus niger* is a homodimer, where each mer contains an FAD molecule located in the active site, however, with a distance to the surface of the enzyme of more than 17 Å thereby making DET communication with electrodes not possible even though authors of a very large number of papers claim DET with GOx [36–38]. In contrast to GOx, as mentioned above, all CDHs also contain a CYT_{CDH} domain, connected through a highly flexible linker to the DH_{CDH} [2]. Through this CYT_{CDH} acting like a "built in mediator" [39] CDH has the ability for efficient DET communication with electrodes and thus makes it special among the sugar oxidising enzymes. Among all other sugar oxidising enzymes possibly only fructose dehydrogenase, FDH, shows similar efficient DET communication with electrodes as CDH and that is also due to that FDH contains not only an FAD containing DH_{FDH} but additionally another domain containing three hemes and where at least two of those are involved in the ET pathway from the DH_{FDH} to an electrode [40]. However, with the recent focus on LPMO, the natural electron acceptor for CDH, and on the importance of sugar oxidising enzymes in the carbohydrate metabolism in general and lignocellulose breakdown in nature in particular [1], it is expected that a series of new and very interesting sugar oxidising enzymes will be discovered and with possible DET such as the recently found PQQ-dependent quinohemoprotein pyranose dehydrogenase from *Coprinopsis cinerea* [41].

The electron transfer reaction between the DH_{CDH} domain and an electrode can occur mainly according to three different routes. In a first reaction the sugar substrate, an aldose, is oxidised at the C1 position (only the β-anomer is a substrate for CDH) into its corresponding lactone and concurrently the FAD in the active site of the DH_{CDH} is fully reduced to $FADH_2$–DH_{CDH}, Reaction (1):

$$\text{Aldose} + \text{FAD–DH}_{\text{CDH}} \rightarrow \text{lactone} + \text{FADH}_2\text{–DH}_{\text{CDH}} \quad (1)$$

The reoxidation of $FADH_2$–DH_{CDH} can be accomplished by a $2e^-$, $2H^+$ acceptor such as quinone (Q) or an equivalent aromatic redox compound according to Reaction (2):

$$FADH_2\text{–}DH_{CDH} + Q \rightarrow FAD\text{–}DH_{CDH} + QH_2 \quad (2)$$

the reduced quinone, QH_2, will be reoxidised at the electrode if the applied potential (E_{app}) is set higher than the formal potential of the Q/QH_2 redox couple, $E^{\circ'}_{Q/QH_2}$, Reaction (3);

$$QH_2 \overset{E_{app} > E^{\circ'}_{Q/QH_2}}{\longrightarrow} Q + 2H^+ + 2e^- \quad (3)$$

alternatively, a $1e^-$, non-H^+ acceptor, e.g., an Os^{3+}-complex (Os^{3+}), accepts the electrons sequentially from the $FADH_2$–DH_{CDH}, whereby Os^{2+}-complex (Os^{2+}) and the enzyme stabilised semiquinone of the bound FAD, FADH•–DH_{CDH}, are formed in Reaction (4);

$$FADH_2 - DH_{CDH} + Os^{3+} \rightarrow FADH\bullet - DH_{CDH} + Os^{2+} + H^+ \quad (4)$$

this reaction is then followed by the second electron transfer to a second Os^{3+}, whereby the fully oxidised DH_{CDH} is regained, Reaction (5);

$$FADH\bullet - DH_{CDH} + Os^{3+} \rightarrow FA - DH_{CDH} + Os^{2+} + H^+ \quad (5)$$

The two Os^{2+} formed will be reoxidised at the electrode if E_{app} is set higher than the formal potential of the $Os^{3+/2+}$ redox couple, $E^{\circ'}_{Os^{3+/2+}}$, Reaction (6);

$$2Os^{2+} \overset{E_{app} > E^{\circ'}_{Os^{3+/2+}}}{\longrightarrow} 2Os^{3+} + 2e^- \quad (6)$$

the electrons can also be transferred from $FADH_2$-DH_{CDH} to the CYT_{CDH} sequentially in an internal electron transfer, IET, process according to Reaction (7);

$$FADH_2 - DH_{CDH} - CYT_{CDH} \overset{IET}{\longrightarrow} FADH\bullet - DH_{CDH} - CYT_{CDH}\bullet^- + H^+ \quad (7)$$

this first electron transfer step is followed by reoxidation of the reduced CYT_{CDH}, $CYT_{CDH}\bullet^-$, by an e^- acceptor such as Os^{3+} or cytochrome *c* (or by the electrode, see below), however, the second electron from the DH_{CDH} will then be transferred to the CYT_{CDH} simultaneously, Reaction (8);

$$FADH\bullet - DH_{CDH} - CYT_{CDH}\bullet^- + Os^{3+} \rightarrow FADH - DH_{CDH} - CYT_{CDH}\bullet^- + Os^{2+} \quad (8)$$

Finally the last electron will be transferred from the CYT_{CDH} to a second 1 e^- acceptor molecule, Reaction (9),

$$FADH\bullet - DH_{CDH} - CYT_{CDH}\bullet^- + Os^{3+} \rightarrow FADH - DH_{CDH} - CYT_{CDH} + Os^{2+} \quad (9)$$

When CDH is immobilised on the electrode surface and in the absence of any competing e^- acceptors, the reoxidation of the reduced enzyme can be summarised as follows [42–46], Reaction (10);

$$FADH - DH_{CDH} - CYT_{CDH} \overset{1st\ IET\ setp}{\longrightarrow} FAD\bullet - DH_{CDH} - CYT\bullet^- \quad (10)$$

this step is followed by a first electron transfer (ET) step to the electrode, which is immediately followed by a second IET step delivering the second electron from the DH_{CDH} to the CYT_{CDH}, Reaction (11);

$$FAD\bullet - DH_{CDH} - CYT_{CDH}\bullet^- \overset{1st\ ET\ to\ electrode\ 2nd\ IET setp}{\longrightarrow} FAD - DH_{CDH} - CYT_{CDH}\bullet^- + (electrode) \quad (11)$$

finally the second electron is then delivered to the electrode, Reaction (12).

$$FAD - DH_{CDH} - CYT_{CDH}\bullet^- \overset{2st\ ET\ to\ electrode}{\longrightarrow} FAD - DH_{CDH} - CYT_{CDH} + e^- + (electrode) \quad (12)$$

As mentioned above, CDH is produced by both basiomycete (class I CDH) and ascomycete (class II CDH) fungi [2]. Apart from some basic major structural differences, such as class I CDHs have shorter sequences, highly conserved linker region, and no carbohydrate binding motive, from a biosensor–biofuel cell perspective class I CDHs are all acidic enzymes and only oxidise cellodextrins and lactose very efficiently, whereas class II CDHs may have pH optima in the neutral pH region and they are much less selective for cellodextrins and lactose and some of them are quite good glucose oxidising enzymes [47]. In general it seems as though class I CDHs have better DET properties compared to class II CDHs [27,28]. Recently it was even found that under acidic conditions DET between the DH_{CDH} of some class I CDHs and mercaptoundecanol modified gold electrodes could be accomplished [48].

One can say that bioelectrochemical research on CDH has been driven by both fundamental aspects on how to accomplish most efficient DET but also by its possible applications in biosensors and BFCs. The research has accordingly been directed in different and separate lines. There is a great demand for a sensitive and selective lactose biosensor, especially in conjunction with the diary industry but also in the pharmaceutical industry as lactose is a common compound in pharmaceutical formulations [49]. Conventional analytical protocols neither fulfil the demands for sensitivity nor selectivity for lactose in dairy products. Because of the strict selectivity of class I CDHs from basidiomycete for cellodextrins and lactose, these CDHs would fulfil the demands as these are excellent lactose oxidising enzymes [50–52] and in dairy products other possible sugar substrates for class I CDH are non-present or in very low concentrations [25,53–56]. Most bioelectrochemical investigations of class I CDHs have been performed with the following three enzymes, *Phanerochaete chrysosporium* CDH (*Pc*CDH) [28,57–62], *Phanerochaete sordida* CDH (*Ps*CDH) [12,27,48,56,63,64], and *Trametes villosa* CDH (*Tv*CDH) [27,28,48].

Even though there are a number of well functioning glucose biosensors on the market, there is still no commercial glucose biosensor based on DET, and therefore there has been quite some interest in the emerging class II CDHs from ascomycetes [47,65,66], which are able to oxidise also glucose and such CDHs especially those from *Myriococcum thermophilum*, *Mt*CDH [27,61,67–70], *Corynascus thermophilus*, *Ct*CDH [29,34,71], and *Humicola insolens*, *Hi*CDH [58,61], have been considered for use in both glucose biosensing and EFCs applications [29,34,35,72]. To improve the glucose oxidising properties and at the same time decrease the maltose oxidising properties (essential for glucose determination in diabetic patients) by blocking the binding of disaccharides in the active site of both *Ct*CDH and *Hi*CDH have been engineered by a single cysteine to tyrosine substitution in the active sites of *Ct*CDH (position 291) and *Hi*CDH (position 285), which resulted in improved kinetic constants with glucose while decreasing the activity with several disaccharides, including maltose [66]. Such engineering also points out the possibility to obtain a "real" 3rd generation biosensor [36,37] to increase the selectivity when detecting glucose [71]. Recently it was also shown that a combination of various CDHs could be used in an electronic tongue application [73]

The production of the original fungi gives low productivity of CDH and therefore new expression systems to be able to "mass produce" the enzyme has mainly been overexpressed in *Pichia pastoris* or *A. niger* [71,74]. However, especially overexpression in *Pichia* leads to a even higher degree of glycosylation and thus less

efficient DET as the distance between the bound cofactor in the enzyme and the electrode surface increases and moreover, the sugars of the glycosylation shell are more insulating than the pure protein.

To improve the DET properties of CDH mainly two directions have been taken; i.e., deglycosylation of the enzyme [75] and surface modification of electrode surfaces. As deglycosylation seems to make the enzyme more fragile e.g., by loosing the bound FAD [75] most work on how to improve current density has been through the use of nanostructured electrodes. However, it has also been noticed that the rate of the IET (Reactions (10) and (11)) for both class I and II CDHs is sensitive to ionic strength and increases with concentration of the buffer [61] and that the IET of class II CDHs seems to be specifically influenced by divalent ions in the buffer [43,45,46,61] and also when immobilised onto positively charged surfaces [44,49,68].

3. Electrode nanostructuration: A useful tool to optimize the direct electron transfer

The nanostructuration of electrode surfaces has become one of the key subjects to optimize DET reactions of several enzymes by increasing the effective surface area available to bind the enzyme [14,76–79]. In the family of nanomaterials, one can sort them into carbon nanomaterials (e.g. single walled carbon nanotubes, SWCNTs, multiwalled carbon nanotubes, MWCNTs, graphene, GPH, graphene oxide, GO etc.) [80–82] and metal nanoparticles (e.g. gold nanoparticles, AuNPs, silver nanoparticles, AgNPs, etc.) [83–85]. In general using NP modified electrodes leads to an increase in the current density of the bioelectrodes based on DET reactions. However, even though an increased current density is obtained when using nanostructured electrode surfaces compared with conventional electrodes for DET based systems, it is not clear whether the increase is only due to an increased electrode surface [14] or due to an increased percentage of the immobilised enzyme molecules orientated in a position facilitating DET as was recently shown for horseradish peroxidase (HRP) immobilised on three different screen printed electrode materials based on graphite, MWCNT, and SWCNT and where the nanostructured electrode surfaces showed a higher percentage of the immobilised HRP molecules orientated for DET [79]. Using further chemical modification of the electrode surface it is possible to orient properly the enzyme onto the electrode surface. Thus the combination of both nanostructuration and further chemical modification has shown very promising results [68,86–89].

In particular, carbon nanotubes (CNTs) have received considerable attention because of their unique properties, including their remarkable electrical, chemical, mechanical and structural properties [15]. CNTs can show metallic, semiconducting and superconducting electron transport, possess a hollow core suitable for storing guest molecules and have the largest elastic modulus of any known material [15,90–95]. Nevertheless, also 2D carbon nanomaterials help the ET of redox enzymes through different functionalization pathways. Graphene presents as single- or double-layer of carbon atoms linked by sp^2 bonds in a honeycomb lattice. The different graphene layers are held together by weak van der Waals interactions along the distance of 3.35 Å. However, graphene displays peculiar properties mainly due to the chemical structure, where each carbon atoms is sp^2 covalently linked with other 3 carbon atoms in the 2D-plane, so that one electron is freely moving in the third dimension generating high electronic conduction [96–99].

On the other hand, also metal nanoparticles, MNPs, offer different possibilities of electrode modification through different techniques such as drop-casting, covalent binding, self assembling monolayers (SAM), which pursuit the aim of an efficient nanostructuration of the electrode surface in order to enhance the DET communication with redox enzymes [14,100,101]. MNPs exhibit high surface area-to-volume ratios and high surface energy, which facilitate the immobilization of several kinds of proteins, allowing to act as electron conducting pathways between the prosthetic groups of the enzymes and the electrode surface [102]. Another advantage of the use of MNPs is the improved stability of enzyme based electrodes. This can be due to a reduced enzyme leaching from the electrode, because of the strong adsorption of proteins onto the uncoated nanometre-sized colloidal MNPs allowing the protein to retain its biological activity [103].

In this review, we would like to resume all findings related to electrode modification with CDHs as bioelectrocatalyst and different nanostructuration strategies, which have been used to develop CDH based bioelectrodes both for biosensors and biofuel cells during the last 20 years.

4. Effect of carbon nanomaterials for biosensor development

Among the carbon nanomaterials that were used in conjunction with CDH, the most used were SWCNTs and MWCNTs due to their high surface area to volume ratio and better electrical, mechanical, and chemical properties [15,90–95]. The first reports on using such material with CDH was to optimize the direct DET between various CDHs and graphite electrodes modified with SWCNTs work done by Tasca et al. in the period 2008–2011 [12,63,64,67]. SWCNTs were initially oxidatively shortened in a mixture of sulfuric and nitric acid and sonicated for 6 h at 40 °C followed by chromatographic separation in a column filled with controlled pore glass with water and 1 wt% Triton-X as the mobile phase [104]. SWCNTs from one of the separated fractions were placed onto the surface of a graphite electrode by drop-casting and allowed to dry. Next a solution of CDH was applied and further cross-linked with polyethyleneglycol diglycidyl lether (PEGDGE). Only after modification with the SWCNTs a clear couple of redox waves in the cyclic voltammograms could be observed with an $E^{\circ\prime}$ of about +100 mV vs. NHE reflecting the $1e^-$ redox process of the heme in the CYT_{CDH}, In the anodic scan additionally another wave was observed roughly about −40 mV vs. NHE attributed probably to a denaturation process occurred to DH_{CDH} domain. The use of SWCNTs allowed the immobilization of a larger number of CDH molecules, which is beneficial both for basic investigations of the potential window, where the redox processes occur close/onto the electrode surface, and also for increasing the current density and thus also for increasing the sensitivity for the sugar substrate whether lactose or glucose based on class I (*Ps*CDH or *Tv*CDH) [53,55,56,64] or class II CDH, respectively (*Ct*CDH) [105,106].

In order to develop a portable device, Safina et al. realized a lactose biosensor based on class I CDHs (*Tv*CDH and *Ps*CDH) [53]. In this paper, they used different commercial screen-printed carbon electrode (SPCEs) made of graphite and MWCNTs, where *Tv*CDH and *Ps*CDH were cross-linked to the so modified electrode surface by using polyethyleneglycol diglycidyl ether (PEGDGE) or glutaraldehyde (GA) through different reaction pathways forming an amino bond and an imino bond, respectively. The biosensors based on PEGDGE/MWCNTs/SPCEs were able to detect lactose in a concentration range between 0.5–200 μM and 0.5–100 μM employing *Tv*CDH and *Ps*CDH, respectively, with a limit of detection of 250 nM for both. Thus, it was confirmed the importance of nanomaterials to optimize the sensitivity and linear range of the modified biosensors.

Further, Zafar et al. developed a 3rd generation portable glucose biosensor based on a class II *Ct*CDH [106]. Concerning the nanostructuration procedures, the same strategy was adopted using

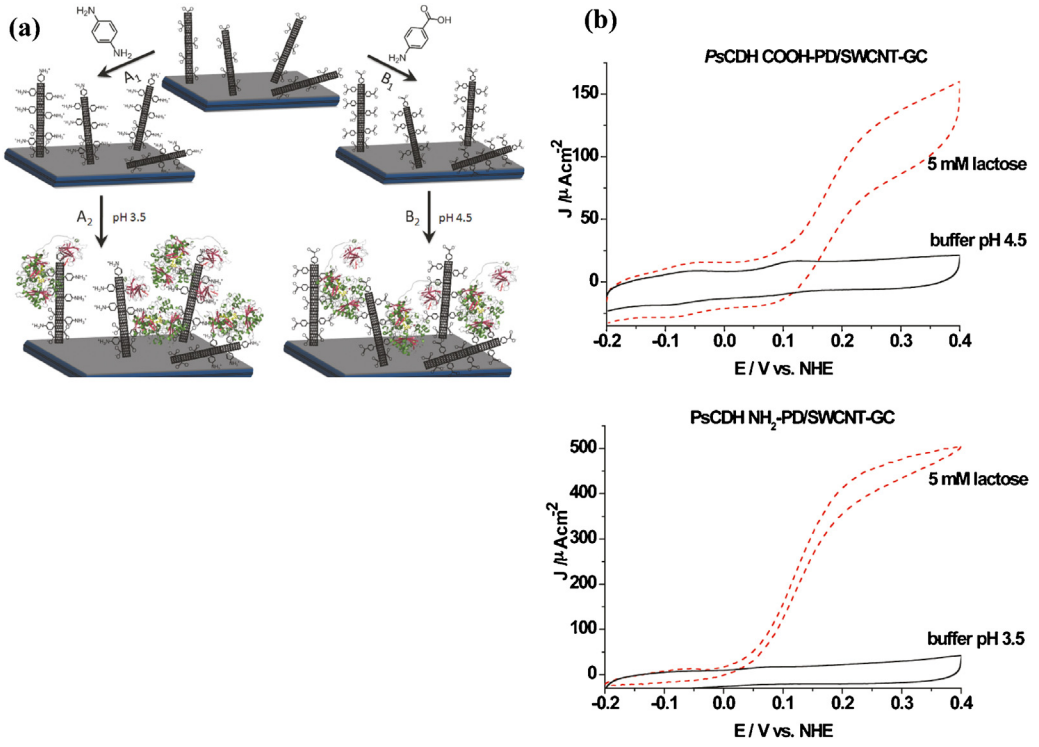

Fig. 2. (a) Schematic representation of SWCNTs-GC electrodes modified with (A_1) *p*-phenylenediamine or (B_1) *p*-aminobenzoic acid. After modification, PsCDH is added and will adsorb onto the SWCNTs exhibiting either (A_2) aniline moieties or (B_2) benzoic acid moieties. The orientation of *Ps*CDH is very likely influenced by the charged surfaces, with the highly negatively charged CYT_{CDH} attracted by the positive charges of A_2 or repulsed by the negative charges on B_2. (b) Cyclic voltammogram of a *Ps*CDH/*p*-ABA/SWCNTs/GC electrode in the presence of 5 mM lactose (red, dashed) and in the absence of substrate (black, solid). 0.1 M acetate buffer, pH 4.5. Scan rate 1 mV s^{-1}. Cyclic voltammogram of a PsCDH NH2-PD/SWCNTs-GC electrode in the presence of 5 mM lactose (red, dashed) and in the absence of substrate (black, solid). 0.1 M acetate buffer, pH 3.5. Scan rate 1 mV s^{-1}. Reproduce from [65] with permission of the American Chemical Society. (For interpretation of the references to color in this figure legend, the reader is referred to the web version of this article.)

SPCEs made of graphite, SWCNTs and MWCNTs. By considering the electrocatalytic current, *Ct*CDH modified electrodes generally exhibited better performance when the enzyme was cross-linked with PEGDGE than with GA (5 times higher current) probably due to the high reactivity of the epoxy-terminal group of PEGDGE and the NH_2 groups easily available on the enzyme surface. Moreover, it was possible to observe a better performance when using SWCNTs instead of MWCNTs probably due to a larger surface area to volume ratio and better electrical, mechanical, and chemical properties than electrodes based on MWCNTs. Finally, the best electrode platform was realized through using *Ct*CDH/PEGDGE/SWCNTs/SPCEs, which displayed a low limit of detection for glucose (10 μM), with a good linear range (0.025–30 mM) and a high selectivity, sufficient for glucose self-monitoring in human blood. The development of SPEs has been very rapid [107–110] and graphene and ordered mesoporous carbon appear as promising new materials for electrochemical biosensors, because they have large surface-to-volume ratio due to a huge porous cavity, an extraordinary carrier mobility and high compatibility with biological element. Kanso et al. entrapped *Ct*CDH in a photocrosslinkable PVA-based polymer on graphene based SPCEs [111,112]. The calibration curve for lactose using optimized parameters shows a wide linear measurement range between 0.25 and 5 mM. A good operational stability of the *Ct*CDH-PVA-modified graphene electrode was obtained and the initial activity was kept constant for 8 h and exhibited a good storage stability with a decrease of only 9% in analytical response after 3 months storage at 4 °C.

One of the challenges in biosensors and biofuel cells field is the possibility to orient the enzyme onto the electrode surface in order to shorten the ET pathway, which is one of the key issues to increase the ET rate constant according to Marcus equation [113,114]. To investigate the effect of surface charges, Tasca et al. [64] chemically modified SWCNTs deposited on glassy carbon electrodes (GCEs) through diazonium coupling using *p*-phenylenediamine (*p*-PD) and *p*-aminobenzoic acid (*p*-ABA), respectively, in order to obtain one positively and one negatively charged surface, as exhibited in Fig. 2. The novelty of this approach is the *in-situ* generation of diazonium salts from the aryl amines followed by direct electro-grafting of SWCNTs modified GCE. The authors were able to observe for *Ps*CDH/*p*-ABA/SWCNTs/GCE two redox waves, one at −50 mV vs. NHE referred to FAD from DH_{CDH}, while the second one at a more positive potential (+100 mV vs. NHE), assigned to the heme *b* in CYT_{CDH}.

In this case, the electrocatalytic wave observed in presence of 5 mM lactose as substrate, had an onset potential close to +70 mV vs. NHE, so that the redox couple observed at −50 mV is related to FAD released from the protein or a denatured domain, since no electrocatalytic wave was observed from the DH_{CDH}. By considering the other electrode platform; *Ps*CDH/*p*-PD/SWCNTs/GCE, it was possible to observe a catalytic anodic wave for lactose oxidation with an onset potential around 50 mV lower compared with that of the *p*-ABA/SWCNTs/GCE (70 mV) and previously for the unmodified SWCNTs (75 mV at pH 3.5). The reason for the lower onset of the anodic wave for lactose oxidation and for the heme *b* midpoint potential might be the obvious extremely good DET communication between CYT_{CDH} and the *p*-PD/SWCNTs/GCE layer. The low isoelectric point of CYT_{PsCDH} (pI < 3.5) and the high surface concentration of negatively charged amino acid residues already at pH 3.5 can explain why a NH_2-PD modification (together with the already existing COOH groups) can create a less electrostatic repulsive

environment for CYT_{PsCDH} and enhance DET. This latter electrode platform was then used to develop a *Ps*CDH based biosensor for lactose detection showing a linear range between 1 and 150 μM, with a LOD of 0.5 μM and an enhanced sensitivity (476.8 nA μM cm^{-2}) compare to previous works [56].

Basically the same approach has been used through testing several other types of aryl amines through diazonium coupling (e.g. *p*-ABA, p-PD, *N*,*N*-diethyl-*p*-phenylenediamine (DEPD), *N*,*N*-dimethyl-*p*-phenylenediamine (DMPD), aniline (AN), *p*-aminophenol (APh)) in order to investigate the effect of a series of functional groups, viz. negative (—COOH), neutral, (—OH), and positive ($—NH_2$) charges on the orientation of *Ct*CDH and possible substitution on the $—NH_2$ groups (i.e., *N*,*N*-diethyl and *N*,*N*-dimethyl group) [115]. In this case the authors generally observed a decrease with around 60 mV on the onset potential compared to the non-grafted SWCNTs/GCE electrodes (+50 mV vs. NHE). By comparing the current densities at a certain set potential for two investigated substrates, viz. lactose and glucose, it was possible to observe a trend based upon the functional groups available on the electrode surface. Contrary to the results with class I *Ps*CDH referred to above [64] the highest current densities for class II *Ct*CDH [115] were obtained in presence of —COOH groups (e.g. *p*-ABA as diazonium salt). When shifting the superficial charge to uncharged (e.g. APh) the current densities were decreased and further with positive charges (e.g. *p*-PD). However, for electrodes modified with *p*-PD it was also observed an increase in terms of current densities once using GA as cross-linking agent. Moreover, the substitution effect on the $—NH_2$ group did not give any particular trend, because the current densities were increasing when used *N*,*N*-dimethyl groups while decreasing with *N*,*N*-diethyl groups. Finally, the best modified electrode platform *Ct*CDH/*p*-ABA/SWCNTs/GCE was selected to investigate the analytical performance (data not reported) and the stability by considering both usage perspectives as biosensors and bioanode for biofuel cells development. Tanne et al. used carboxylated or aminated polyaniline MWCNT nanohybrids for immobilization of class I *Ps*CDH on Au electrodes [116] and they found similar to previous investigations [64] that a positively charged surface promoted DET.

One way to even further increase the efficiency of DET would be to be able to fully control the orientation of CDH on the electrode surface. Recently two *Mt*CDH mutants, E522 and T701, with single cysteine residues on the surface of the DH_{MtCDH} were covalently immobilised onto glassy carbon electrodes modified with MWCNT using a "linker", a "spacer", a "reactive group" type click chemistry resulting in improved catalytic currents and prolonged life time compared with just adsorbed enzyme [86].

Recently, a new carbon based nanomaterial, carbon aerogel (CA), has been developed by using the sol–gel technique in order to obtain an effective nanostructuration and a favourable environment to improve DET between class I *Pc*CDH and the surface of a GCE. CA is a new carbon based nanomaterial with interesting features for construction of biosensors and in energy harvesting applications due to its unusual properties, such as low density, continuous porosity, high specific surface area, electrical conductivity, good chemical stability, as well as environmental compatibility and easy preparation [117,118]. In this work, several CA suspensions have been prepared by considering chitosan as medium and dissolving different amounts of CA, providing different degrees of nanostructuration directly correlated with the amounts of CA and the electroactive area [119]. From the CVs, it is possible to see a proportional increase in the capacitive current with the amount of CA, which is responsible for the enhanced enzyme loading on the electrode surface. The best modified electrode for lactose detection (15 μL of CA-Chi suspension containing 150 μg of CA) was further investigated through chronoamperometry to obtain analytical parameters (e.g. linear range, LOD, pH etc.), which are in good agreement with previous electrode platforms based on carbon and metal nanomaterials.

5. Effect of metal nanoparticles for biosensor development

To date several synthesis methods to prepare MNPs have been developed through the use of toxic reducing agents (e.g., sodium borohydride, dendrimer, citrate), physical agents (e.g., laser ablation) or electrochemical methods [120,121]. 3rd generation lactose biosensors based on AuNPs synthesized according to the citrate procedure and further modified with a variety of SAMs have been developed (e.g., 4-aminothiophenol 4-ATP, 4-mercaptobenzoic acid 4-MBA, 4-mercaptophenol 4-MP, 11-mercapto-1-undecanamine $MUNH_2$, 11-mercapto-1-undecanoic acid MUCOOH, and 11-mercapto-1-undecanol MUOH) [29,62,75,122,123]. After preliminary experiments carried out with class I *Ps*CDH in combination with several SAMs based only on one type of thiol, several mixed SAMs based on e.g., mixtures of 4-MP/4-ATP, 4-MBA/4-ATP, MUOH/$MUNH_2$, or MUCOOH/$MUNH_2$ were used by optimizing the concentration of each component and using GA as cross-linking agent [62]. For all SAMs based on mixed combinations, a $—NH_2$ terminated thiol acted as a binder between GA and an amino group in the enzyme. The other thiol helped both orientate the enzyme and facilitate the ET to the electrode. By considering the dependence of ΔE_p on the log ν according to Laviron's equation [124], the k_s values were unexpectedly increasing with MUOH/$MUNH_2$ probably due to Van der Waals interactions between the long carbon chains, which create a more stable SAM for the enzyme immobilization. The standard ET rate constant (k_s) was estimated for the first time for any CDH and was found to be 52.1, 59.8, 112, and 154 s^{-1} for 4-ATP/4-MBA, 4-ATP/4-MP, $MUNH_2$/MUCOOH, and $MUNH_2$/MUOH modified electrodes, respectively.

Although the chemical modification to form a SAM of nanostructured electrode surface already provides for an efficient ET, other chemical modifications have been adopted such as polymer coating with different charges (e.g. polyethyleneimine (PEI), polystyrenesulfonate (PSS) and citrate). Recently, Tavahodi et al. synthesized AuNPs by using the citrate protocol and final resuspending the AuNPs pellet in a diluted solution of the highly positively charged PEI [85]. In this work *Ps*CDH was orientated onto the surface of the NPs due to a strong electrostatic attraction between the enzyme (negatively charged, pI 3.8) and the AuNPs (positive charged ζ = +30 mV) at the investigated pH 4.5 as working pH. The modified electrode *Ps*CDH/PEI@AuNPs/AuE showed a couple of peaks in the non-turnover cyclic voltammograms (CV) corresponding in terms of $E^{\circ\prime}$ to the CYT_{CDH} domain. In the *Ps*CDH/PEI@AuNPs/AuE platform the enzyme was favourably orientated on the modified electrode surface, so far increasing the ET rate to around 40 s^{-1}, which is a key issue to enhance the biosensor sensitivity reaching a linear range between 1 and 100 μM.

Conversely, in the last few years, a lot of efforts have been addressed on the development of highly reproducible eco-friendly synthesis method for MNPs in order to produce these catalysts with non-alterate properties compared with using conventional but possibly toxic methods and at the same time avoiding any kind of toxic chemicals both during synthesis and for the stabilization of the colloidal suspension. In a recent paper, Bollella et al. demonstrated the advantages of this new method for synthesising MNPs employing quercetin, a polyphenolic compound acting as reducing agent for gold and silver salts with a high reaction yield [83]. Interestingly, quercetin showed a different behaviour towards gold and silver, where in the case of gold quercetin acts only as reducing agent while for silver it acts also as chelating agent preventing further aggregation phenomena. This conclusion could be

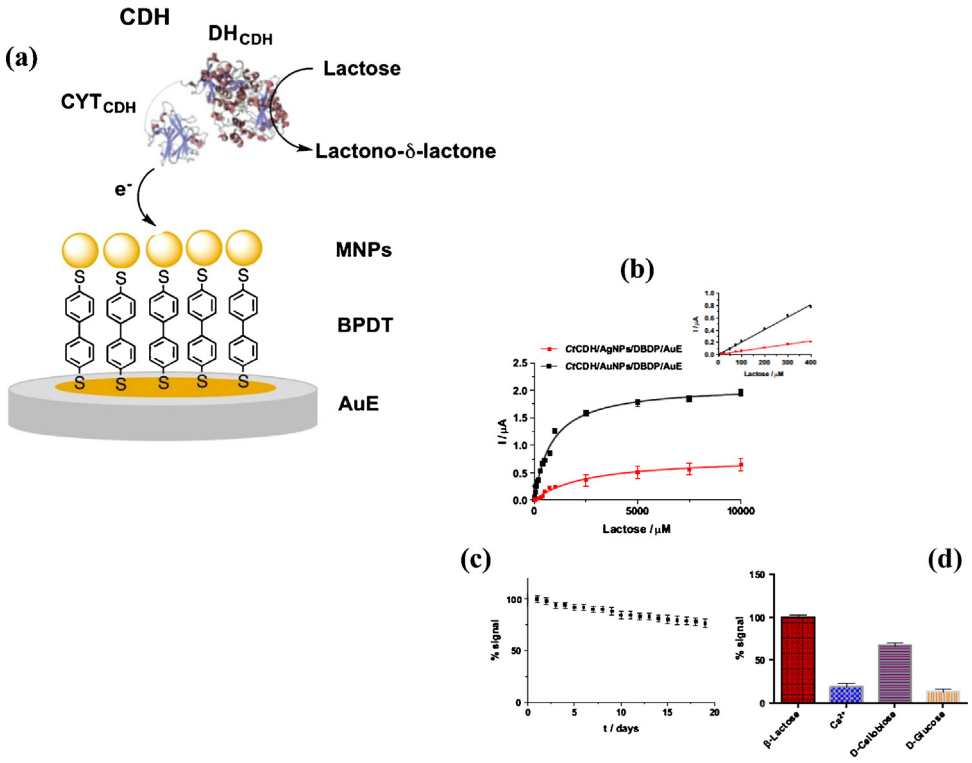

Fig. 3. (a) *Ct*CDH/MNPs/BPDT/AuE platform and DET between *Ct*CDH and the modified electrode. (b) Calibration graphs for lactose; in the inset, the biosensor response in the low-micromolar range; (c) lifetime of *Ct*CDH/AuNPs/DBDP/AuE biosensor in the presence of 200 μM lactose solution in 50 mM MOPS buffer pH 7.4; (d) influence of interfering compounds on lactose response: 1 mM lactose solution (red), 1 mM Ca^{2+} solution (blue), 1 mM D-cellobiose (purple) and 1 mM D-glucose (pink). Buffer: 50 mM MOPS, pH 7.4; applied potential: +0.250 V vs. $Ag|AgCl_{sat}$. Reproduced from [47] with permission of Elsevier Ltd. (For interpretation of the references to color in this figure legend, the reader is referred to the web version of this article.)

drawn from the fact that the AgNPs, in contrast to the AuNPs, when deposited on a solid graphite electrode drastically reduced the large overvoltage for electrocatalytic NADH oxidation. These synthesized NPs were further used to fabricate electrochemical biosensors for lactose detection based on a simply drop-casting technique. Preliminary investigations have been performed to demonstrate the effect of the electrostatic interactions between CDH and MNPs on the enzyme orientation, which would enhance the electron transfer rate, the enzyme loading and stability. Finally, class I *Tv*CDH showed promising results on the AuNPs/graphite platform with a LOD of 3.5 μM for lactose detection and an extended linear range (10–300 μM), which could be further increased by considering the chemical electrode modification approach to obtain an ordered nanostructuration.

In order to improve the DET efficiency between CDH and the electrode platform, an ordered electrode nanostructuration have been performed by covalently linking AuNPs or AgNPs onto an solid Au electrode [84]. In this work, it was proven that the ordered packaging of MNPs on the electrode surface could positively contribute to increase the ET rate constant, which would be beneficial for both biosensors and biofuel cells development. The novelty of this approach is related to the possibility to bind the NPs on a rigid SAM made up of 4,4'-biphenyl-dithiol (BPDT), which has a very high rigidity as it can only rotate around the σ-bond connecting the two phenyl units (see Fig. 3) and a high conductivity as the system is highly conjugated. After preliminary investigations on the different electrode platforms (with values of the apparent heterogeneous electron transfer rate constants (k_s) for *Ct*CDH of $21.5 \pm 0.8\ s^{-1}$ and $10.3 \pm 0.7\ s^{-1}$, for the AuNPs/BPDT/AuE and the AgNPs/BPDT/AuE platforms, respectively) it was possible to obtain the best analytical results for lactose detection with *Ct*CDH/AuNPs/BPDT/AuE modified electrodes with a LOD of 3 μM lactose, a wide linear range (5–400 μM) and an enhanced sensitivity of $27.5\ \mu A\ mM^{-1}\ cm^{-2}$. These results are mainly related to the organized packaging of the AuNPs, the high conductivity of BPDT and the electrostatic interactions between *Ct*CDH and the AuNPs responsible for a correct orientation of the enzyme molecules, which in turn also influences the ET rate.

Besides AuNPs, also other kinds of MNPs (e.g. platinum nanoparticles, PtNPs and palladium nanoparticles, PdNPs) have been used in combination with MWCNTs to prepare hybrid nanocomposites. The prepared nanocomposite was drop-cast onto a graphite electrode and further modified through a layer-by-layer construction with *Pc*CDH [88]. The electrochemical platform was characterized in non-turnover conditions showing no waves related to CYT_{CDH} probably due to the increased double-layer capacitance, while considering the electrocatalytic current in turnover conditions it was possible to observe an increasing up to 4 and 2 times with PtNPs-MWCNTs and PdNPs-MWCNTs, respectively. Both electrode platforms showed an improved analytical performance. The sensitivity towards lactose was 3.07 and $3.28\ \mu A\ mM^{-1}$ at the *Pc*CDH/PtNPs–MWCNTs/SPGE and *Pc*CDH/PdNPs–MWCNTs/SPGE electrodes, respectively, which were higher than those measured at the *Pc*CDH/MWCNTs/SPGE ($2.60\ \mu A\ mM^{-1}$) and *Pc*CDH/SPGE ($0.92\ \mu A\ mM^{-1}$), values indicating to be helpful for biosensor and biofuel cell construction using lactose as fuel.

6. Others nanostructuration pathways for biosensor development

As an alternative for electrode nanostructuration, the layer-by-layer technique (LbL) could represent a good candidate to increase the DET between CDH and electrodes. Feifel et al. took advantage of a supramolecular architecture with embedded *Tv*CDH, cyt *c*,

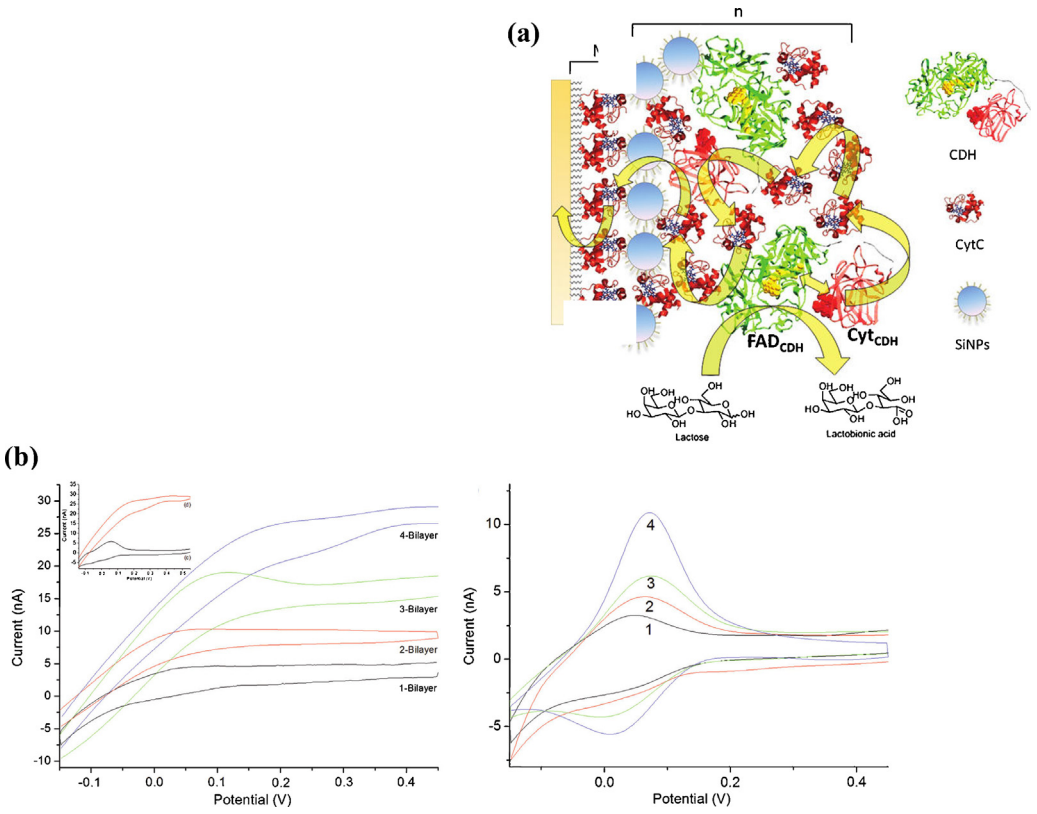

Fig. 4. (a) Schematic representation of a supramolecular [SiNP/CDH·cyt *c*] architecture prepared on a cyt *c* monolayer electrode (M). The cyt *c* monolayer is assembled on a mixed thiol layer (MU/MUA). The layer structure is [SiNP's/CDH·cyt *c*]*n* (*n* = 1, 2, 3, 4). (b, left) Cyclic voltammograms of Au-MUA/MU-cyt *c*-[SiNP-CDH·cyt *c*]*n* nanobiomolecular electrodes. Catalytic currents of d*Tv*CDH-based multilayer electrodes (*n* = 1, 2, 3, 4) in the presence of lactose (5 mM) at a scan rate of 5 mV/s. (Inset) Four-bilayer electrode (c) without and (d) with lactose. (b, right) Increase in the cyt *c* concentration with the number of bilayers (1, 2, 3, 4) measured at a scan rate of 100 mV/s. CV is performed in 20 mM phosphate–citrate buffer at pH 4.5. Reproduced from [76] with permission of the American Chemical Society.

and carboxy-terminated silica nanoparticles (SiNPs) as an artificial matrix. An electrode modification was assembled by alternating incubation steps in solutions of SiNPs and a CDH·cyt *c* mixture to coimmobilize *Tv*CDH and cyt *c* [125], as displayed in Fig. 4, and where cyt *c* acts as mediator. The inner monolayer consists of cyt *c* adsorbed on a mixed thiol layer of MUCOOH and MUOH known to facilitate the ET between the electrode and cyt *c*. In this paper, two different forms of *Tv*CDHs have been used; the wild-type fully glycosylated *Tv*CDH (wt*Tv*CDH) and the deglygosylated one (d*Tv*CDH) showing a remarkable increase in efficiency with d*Tv*CDH when comparing otherwise equally constructed 4 bilayer electrodes. This means that by increasing the number of catalytic sites by using the smaller d*Tv*CDH compared with the bigger wt*Tv*CDH within the LbL structure on the electrode surface in combination with an expected higher intramolecular ET between d*Tv*CDH and cyt *c* compared with that between wt*Tv*CDH and cyt *c* the specific bioelectrocatalytic conversion of lactose can be much enhanced. By considering that a large portion of the enzyme molecules are immobilized rather far away from the electrode surface, they conclude that the catalytic oxidation reaction at either d*Tv*CDH or wt*Tv*CDH provides the electrons for the catalytic current, which are in turn transferred by cyt *c*–cyt *c* interprotein electron transfer toward the electrode [126]. Additionally, the effect of dimensions of the SiNPs (5, 15, 20, 40 nm) within the LbL architecture was investigated showing the best performance with 20 nm SiNPs probably due to highest amount of electroactive cyt *c* available to shuttle the electrons through a hip-hop mechanism from *Tv*CDH to the electrode surface. The so modified electrode displayed a wide linear range for lactose (0.010–1 mM) with enhanced sensitivity and a low limit of detection.

This strategy was further compared by using an alternative element in the building block constructions, i.e, double-stranded DNA (dsDNA) [127]. In this work, it was possible to observe a remarkable increase in the surface coverage of cyt *c* compared to the previous LbL architecture, considering 4 bilayers as a fixed parameter. The d*Tv*CDH/cyt *c*-dsDNA/AuE showed a smaller linear range (10–200 μM) probably due to the higher amounts of cyt *c* accumulated, which results in a longer ET pathways and thus a lower electron transfer rates. Compared to dsDNA the surface-modified SiNPs seem to provide a more suitable artificial matrix for the construction of fully catalytically active CDH assemblies. Increasing the numbers of bi-protein layers for SiNPs-based systems result in a linear increase in both the amount of electro-active cyt *c* and catalytic response. This significant improvement is very likely due to a more defined and ordered structure, a higher amount of d*Tv*CDH and fast ET between the protein molecules compared to the DNA-based ones. Later these authors took the system further and established a supramolecular multicomponent protein architecture on electrodes that allows the establishment of bidirectional ET cascades based on interprotein electron exchange [128]. The architecture was formed by embedding laccase and *Ct*CDH and cyt *c* by means of carboxy-modified SiNPs in a multiple layer format. The construct is designed as a switchable dual analyte detection device allowing the measurement of lactose and oxygen, respectively. The applied potential of the electrode was used as switching force ensuring control of the redox state of cyt *c*. The two signal chains are operating in a non-separated matrix and are not disturbed by the other biocatalyst.

7. Carbon and metal nanomaterials for development of biofuel cells and biosupercapacitors

In order to enhance the overall performance of EFCs, several nanomaterials [129,130], such as SWCNTs and MWCNTs [80,81], MNPs (Au-, Ag- or Pt-NPs) [84,85] and graphene [82,96], have been employed taking advantage from the high surface/volume ratio improving the enzyme loading as well as the ET at the electrode surface [33]. Most EFCs reported in the literature employ redox mediators to establish a fast ET between enzymes and electrodes [131–136]. However, with the use and immobilization of a mediator usually follows a decrease in the theoretical open-circuit potential (OCV) of the biofuel cell lost because of the necessary potential difference between the enzyme and mediator to drive the ET between the electrode and enzyme. Hence, great attention has recently been given to EFCs based on DET [34,35,137,138].

For this purpose, one of the first reports on the possible use of CDH as the enzyme in a potential bioanode highlighted the usage of SWCNTs as support for the enzyme [63]. In the presence of SWCNTs, the electrocatalytic current for substrate oxidation based on DET between *Ps*CDH and electrode was significantly increased. Furthermore, the onset of the electrocatalytic current was at lower potential than in the absence of SWCNTs. The highest electrocatalytic activity toward oxidation of lactose was found for the three investigated class I CDHs, (*Ps*CDH > *Pc*CDH > *Tv*CDH), followed by two class II CDHs (*Mt*CDH> a CDH from the plantpathogen fungus *Sclerotium rolfsii* (SrCDH)). The *Ps*CDH/PEGDGE/SWCNTs/graphite electrode was further connected with a Pt black electrode as cathode to measure the polarization curve in the presence of 5 mM lactose as fuel exhibiting a maximum voltage of 590 mV, a maximum current density of 112 $\mu A\,cm^{-2}$, and a maximum power density of 32 $\mu W\,cm^{-2}$ at an operating voltage of 430 mV (under oxygen purging/non-quiescent conditions). Aiming at the construction of membrane-less biofuel cells based on DET, in which also oxygen reduction is catalyzed by redox enzymes such as laccase or bilirubin oxidase, additional improvements of the electrode architecture will be needed in order to increase the stability and the power density of the anode.

However, the same approach has been used for making BFC anode prototypes based on both class I and class II CDHs cross-linked through PEGDGE to SWCNTs both in DET mode [63] and in the MET mode in combination with a cross-linking agent, an Os polymer with a $E^{\circ\prime}$ close to the $E^{\circ\prime}$ of CYT_{CDH} domain [67]. At the beginning, the activity towards different mono- and disaccharides (e.g. lactose, cellobiose and glucose) was carefully evaluated by varying the pH. *Mt*CDH showed its optimum in terms of electrocatalytic oxidation of lactose at pH 4.5 when in DET configuration, while at pH 8 in MET mode. Also glucose exhibited good performance at physiological pH with *Mt*CDH/PEGDGE/Os-polymer/SWCNTs/GCE allowing further considerations on a possible usage as bioanode in combination with laccase (Lac) or bilirubine oxidase (BOD) as biocathode. As a model for a membraneless biofuel cell, a *Mt*CDH-modified electrode was applied as the anode together with a Pt black electrode as the cathode in a 0.1 M solution of glucose in PBS buffer at 37 °C. This cell exhibited an OCV of 500 mV, a maximum current density (J_{max}) of almost 700 $\mu A\,cm^{-2}$, and a maximum power density (P_{max}) of 157 $\mu W\,cm^{-2}$ at an operating voltage of 280 mV (under oxygen purging/nonquiescent conditions).

Also AuNPs have been largely employed for EFCs based on CDH/BOD combination in DET. In one paper [29], 20 nm-AuNPs were used after being synthesized through the classical citrate protocol and further drop-cast many times onto a solid AuE surface in order to obtain an effective nanostructuration for both the anode and cathode EFC elements. Afterwards, the modified electrode was incubated into a volumetric 1:1 mixture of 1 mM 4-mercaptophenol/4-mercaptobenzoic acid ethanol solution. Thus for the biomodification, 3 μL of a *Ct*CDH solution and 1 μL of a GA solution were drop-cast, gently mixed on the top of the thiol-modified AuNPs/AuE electrode and allowed to react in a moisturised atmosphere for 2 h to avoid evaporation of the reactants. The modified bioanode exhibited an $E^{\circ\prime}$ for the CYT_{CDH} domain around 75 mV vs. NHE, a real surface coverage of 0.65 $pmol\,cm^{-2}$ corresponding to a sub-monolayer coverage of the thiol-modified AuNPs by the enzyme, a good turnover number *ca.* 0.5 s^{-1}, and a maximal current density around 40 $\mu A\,cm^{-2}$ being a good candidate for EFC construction. Finally, a mediator-, separator- and membrane-less EFC have been developed by connecting the *Ct*CDH modified anode with a BOD modified cathode exhibiting good performance for both lactose and glucose in human physiological buffer at pH 7. So far, the implemented device was tested also in a few biological fluids (e.g. human blood and serum) with a maximum power density (P_{max}) of 3 $\mu W\,cm^{-2}$ at a cell voltage of 0.45 V, assuming the latter as a first step toward an extensive miniaturization and as a future implantable device.

Essentially the same electrode modification protocol was applied by using a microelectrode for making both the anode and cathode exploiting the possibility to implant such microelectrodes in a rat brain [139] and as a device serving as a power source for electronic contact lenses [140]. After a series of preliminary experiments, the EFC was tested in human lachrymal liquid (tears) [141]. In this work, Falk et al. performed calculations on the maximum recoverable electrical energy, extractable from the biofuel, glucose, and the biooxidant, molecular oxygen, in human tears [138]. Contrary to the concentration in a biofuel cell for blood, the concentration of the biooxidant in lachrymal liquid is very high (*ca.* 0.25 mM), since human tears are air saturated during wake hours [142]. Thus, the availability of glucose would limit the total power output from the eyes. They concluded that the minimal and maximal electric power from a glucose/O_2 EFC operating in tears is 0.02–22 μW. In the real application the device exhibited an OCV of 0.57, about 1 $\mu W\,cm^{-2}$ as maximum power density at a cell voltage of 0.5 V, and more than 20 h of operational half-life.

Moreover, the same device was tested in human saliva and sweat to investigate whether in these biological fluids there are the same limiting factors [143]. So far, the main problem in the last application was related to the half-life, because the device retained only 50% of the initial power output probably due to the presence of many different organic and inorganic compounds that can affect the bioelectrocatalytic activity of both the bioanode and especially the biocathode, such as chloride ions, uric and ascorbic acids, cells, and a multitude of proteins. According to theoretical calculations, also in this case the limiting factor is the fuel in particular for sweat compare to saliva, where it is possible to observe a one-order difference in magnitude. A similar device following the same modification procedure but using as support electrodes made of a biocompatible flexible polymer (Fig. 5) was realized by Pankratov et al., looking forward for some real implantable device [140].

Recently, Shleev et al. showed the possibility for making miniature, self-contained biodevices powered by BFCs based on a CDH anode and a BOD cathode to enable a new generation of implantable, wireless, minimally invasive neural interfaces for neurophysiological in vivo studies and for clinical applications [133,139]. Extensive studies using electrochemical impedance spectroscopy (EIS) was carried out to demonstrate the inductive coupling between the device and the neurons of the rat brain. Here, they showed that AuNPs led to aggregates responsible for the effective 3D nanostructuration, which would be beneficial in the perspective to get connected to neuronal activity. Considering limitations, one could expect that the performance of the EFC would be clearly limited by the anodic bioelectrocatalytic reactions at least when the EFC is operating in vitro using simple glucose

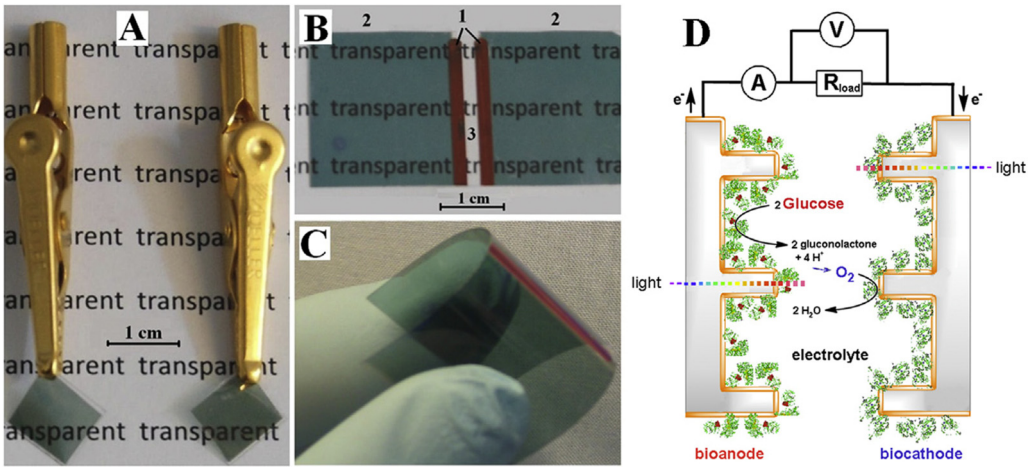

Fig. 5. Photographic images of separate electrodes (a) connected to alligator clips along with a complete transparent flexible device. (b and c) 1-biocompatible transparent polymer, 2-current collectors (metallised thick (opaque) layer of Au on the polymer), 3-transparent electrodes (metallised thin layer of Au on the polymer). (d) A principal scheme of a compartment- and mediator-less, flexible and transparent glucose/oxygen enzymatic fuel cell based on nanostructured electrodes. Reproduced from [89] with permission of Elsevier.

containing solutions. Moving to physiological situations, e.g., from simple buffers to cerebrospinal fluid (CSF), the BOD based cathodes would definitely be responsible for a lowering of the voltage of the EFCs because of their depolarization in CSF. Moreover, one could also expect a significant decrease in current densities obtained from micro-biocathodes operating in vivo, because of the significantly lower concentration of available O_2 in both brain tissue and CSF in the living organism, around 50 μM, compared to air saturated solutions used in in vitro studies, ca. 250 μM. The obtained results unequivocally show an electric connection between nanostructured Au surfaces and neurons, evidenced by the appearance of inductive loops in the impedance spectra of the bioelectrodes, a consequence of the inductive properties of neuronal membranes. These are very interesting and practically applicable findings in the field of implantable nanostructure based neural interfaces especially by considering the first extensive EIS study on EFCs.

Today, other aspects of crucial interest are self-contained, i.e., wireless and self-powered, bioelectronics as self-sustaining implantable medical devices, and in environmental, and biocomputing applications. In particular, Falk et al. demonstrated the operation of self-sustained carbohydrate and oxygen sensitive biodevices based on a CDH anode and a BOD cathode, consisting of a wireless electronic unit, radio transmitter and separate sensing bioelectrodes, supplied with electrical energy from a combined multi-enzyme fuel cell generating sufficient current at required voltage to power the electronics [144]. A carbohydrate/oxygen enzymatic fuel cell was assembled by comparing the performance of a range of different bioelectrodes followed by selection of the most suitable, stable combination. Besides the possibility to use it as power source, the device was also tested to monitor the variation of lactose as substrate/fuel and molecular oxygen as substrate/oxidant being finally assembled a real wireless self-powered biosensor. Another recent BFC accomplishment was the fabrication of transparent and nanostructured electrodes based on chemically modified indium tin oxide (ITO) NPs substantially increasing the active surface area without significantly compromising transparency [145]. The ITO NPs were spray-coated or drop-coated followed chemical modification with silanes, and then by immobilisation of either *Ct*CDH on the anode and *Myrothecium verrucaria* BOD on the cathode.

Since the EFCs are not able to produce enough energy to power real devices (e.g. pacemakers), one of the main solutions exploited recently is represented by biosupercapacitors [146],

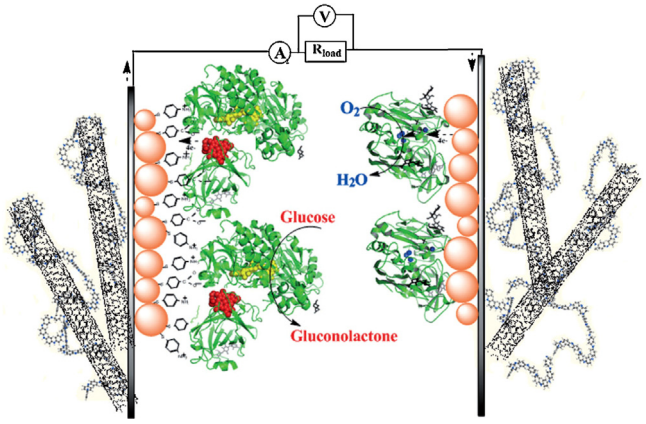

Fig. 6. Schematic representation of a self-charging biological supercapacitor. The electrochemical capacitor is built using a graphite foil modified with a polyaniline/CNTs composite on one side (the capacitive side/face), and the enzymatic fuel cell is designed from three-dimensional gold NPs based nanobiostructures on the other (the charging side/face). Gold NPs: pink-orange spheres; thiol layer: black sticks. The structure of BOD was taken from the known crystal structure (PDB 2XLL) and CDH was rendered using the cytochrome and the FAD domains of the enzyme from *Phanerochaete chrysosporium* (PDB 1D7D and 1NAA, respectively). Protein globule: green ribbons; copper ions: blue spheres; heme: red spheres; FAD: yellow spheres; carbohydrates: black sticks. Reproduced from [96] with permission of Wiley. (For interpretation of the references to color in this figure legend, the reader is referred to the web version of this article.)

which are a combination of EFCs and capacitors [147]. In this field, the nanomaterials play a key role on increasing the double-layer capacitance, which is directly correlated with the amount of energy accumulated and finally the power output generated [148]. Recently, Pankratov et al. [149] reported on the first biosupercapacitor based on *Ct*CDH/BOD electrodes in DET communication. In this work both parts, capacitive and charging part, were prepared on the two faces of a discrete electrode based on different kinds of nanomaterials. For the capacitive part, a polyaniline/CNT composite was prepared by drop-cast a suspension of nanotubes and electrodepositing a polyaniline film onto the electrode surface, as shown in Fig. 6. Whereas the charging part has been prepared according to a previous protocol [29], without any optimization on the protocol. The so prepared biosupercapacitor provided a maximum of 1.2 mW cm^{-2} at 0.38 V. Thus, the power output was improved by a factor of 170 in comparison to state-of-the-art EFCs albeit operating

biosupercapacitors in a pulsed power mode. The AuNPs/CF EFC was also able to operate in pulse power mode, delivering about 50 times less specific electric charge, compared to the biosupercapacitor.

8. Conclusions and outlook

Several combinations between several nanomaterials (e.g. nanotubes and nanoparticles), polymers (e.g. polyaniline, osmium polymers) and a really efficient bioelectrocatalytic anodic based on CDH have been extensively exploited in the last 20 years, mainly displaying the advantages provided by the usage of carbon and metal based nanomaterials. Nanomaterials played the key role on increasing of electroactive area while the right orientation of the bioelectrocatalyst produced by chemical modification increased also the electrocatalytic efficiency in presence of substrates. Based on these concepts, the nanostructured electrodes were used to obtain real devices as biosensors for both lactose and glucose according to the different CDH classes, EFCs as key topic for the implantable and self-powered devices, and finally one of the hot topics these days, the biosupercapacitors. Apart from what was explored during the last 20 years, we strongly believe in investigating new ET mechanisms and pathways in order to be able to catch the electrons directly from the DH_{CDH} or equivalent domains in other sugar oxidising enzymes to be able to reach a lower onset potential for the bioelectrocatalytic oxidation of the sugar substrate, new nanocomposites as potential support for the redox enzyme in order to ensure an improved long-term stability of the enzyme layer, and finally the possibility to arrange new devices according to human needs.

Acknowledgments

The authors would like to thank the following agencies for financial support: The Swedish Research Council (Vetenskapsrådet project 2014-5908), the European Commission (project "Bioenergy" FP7-PEOPLE-2013-ITN-607793), and a scholarship of the Erasmus+ Project Unipharma-Graduates, promoted by a Consortium of Italian Universities and coordinated by Sapienza University of Rome.

References

[1] D. Kracher, R. Ludwig, Cellobiose dehydrogenase: an essential enzyme for lignocellulose degradation in nature—a review/Cellobiosedehydrogenase (Ein essentielles Enzym für den Lignozelluloseabbau in der Natur—Eine Übersicht), Bodenkultur 67 (2016) 145–163.
[2] M. Zamocky, R. Ludwig, C. Peterbauer, B.M. Hallberg, C. Divne, P. Nicholls, D. Haltrich, Cellobiose dehydrogenase—a flavocytochrome from wood-degrading, phytopathogenic and saprotropic fungi, Curr, Protein Pept. Sci. 7 (2006) 255–280.
[3] B.M. Hallberg, T. Bergfors, K. Backbro, G. Pettersson, G. Henriksson, C. Divne, A new scaffold for binding haem in the cytochrome domain of the extracellular flavocytochrome cellobiose dehydrogenase, Structure 8 (2000) 79–88.
[4] B.M. Hallberg, G. Henriksson, G. Pettersson, C. Divne, Crystal structure of the flavoprotein domain of the extracellular flavocytochrome cellobiose dehydrogenase, J. Mol. Biol. 315 (2002) 421–434.
[5] T.-C. Tan, D. Kracher, R. Gandini, C. Sygmund, R. Kittl, D. Haltrich, B.M. Hallberg, R. Ludwig, C. Divne, Structural basis for cellobiose dehydrogenase action during oxidative cellulose degradation, Nat. Commun. 6 (2015), http://dx.doi.org/10.1038/ncomms8542.
[6] D.R. Cavener, GMC oxidoreductases: a newly defined family of homologous proteins with diverse catalytic activities, J. Mol. Biol. 223 (1992) 811–814.
[7] G. Henriksson, G. Johansson, G. Pettersson, A critical review of cellobiose dehydrogenases, J. Biotechnol. 78 (2000) 93–113.
[8] D. Kracher, S. Scheiblbrandner, A.K.G. Felice, E. Breslmayr, M. Preims, K. Ludwicka, D. Haltrich, V.G.H. Eijsink, R. Ludwig, Extracellular electron transfer systems fuel cellulose oxidative degradation, Science 352 (2016) 1098–1101.
[9] T. Larsson, M. Elmgren, S.E. Lindquist, M. Tessema, L. Gorton, G. Henriksson, Electron transfer between cellobiose dehydrogenase and graphite electrodes, Anal. Chim. Acta 331 (1996) 207–215.
[10] R. Ludwig, R. Ortiz, C. Schulz, W. Harreither, C. Sygmund, L. Gorton, Cellobiose dehydrogenase modified electrodes: advances by materials science and biochemical engineering, Anal. Bioanal. Chem. 405 (2013) 3637–3658.
[11] R. Ludwig, W. Harreither, F. Tasca, L. Gorton, Cellobiose dehydrogenase: a versatile catalyst for electrochemical applications, ChemPhysChem 11 (2010) 2674–2697.
[12] F. Tasca, L. Gorton, W. Harreither, D. Haltrich, R. Ludwig, G. Nöll, Comparison of direct and mediated electron transfer for cellobiose dehydrogenase from *Phanerochaete sordida*, Anal. Chem. 81 (2009) 2791–2798.
[13] M. Holzinger, A. Le Goff, S. Cosnier, Nanomaterials for biosensing applications: a review, Front. Chem. 2 (2014) 63.
[14] D. Pankratov, R. Sundberg, D.B. Suyatin, J. Sotres, A. Barrantes, T. Ruzgas, I. Maximov, L. Montelius, S. Shleev, The influence of nanoparticles on enzymatic bioelectrocatalysis, RSC Adv. 4 (2014) 38164–38168.
[15] J. Wang, Carbon-nanotube based electrochemical biosensors: a review, Electroanalysis 17 (2005) 7–14.
[16] E. Malel, R. Ludwig, L. Gorton, D. Mandler, Localized deposition of Au nanoparticles by direct electron transfer through cellobiose dehydrogenase, Chem. Eur. J. 16 (2010) 11697–11706.
[17] A. Heller, Electrical connection of enzyme redox centers to electrodes, J. Phys. Chem. 96 (1992) 3579–3587.
[18] A. Heller, B. Feldman, Electrochemical glucose sensors and their applications in diabetes management, Chem. Rev. 108 (2008) 2482–2505.
[19] P. Kavanagh, D. Leech, Mediated electron transfer in glucose oxidising enzyme electrodes for application to biofuel cells: recent progress and perspectives, Phys. Chem. Chem. Phys. 15 (2013) 4859–4869.
[20] M. Shao, D.A. Guschin, Z. Kawah, Y. Beyl, L. Stoica, R. Ludwig, W. Schuhmann, X. Chen, Cellobiose dehydrogenase entrapped within specifically designed Os-complex modified electrodeposition polymers as potential anodes for biofuel cells, Electrochim. Acta 128 (2014) 318–325.
[21] M. Shao, S. Pöller, C. Sygmund, R. Ludwig, W. Schuhmann, A low-potential glucose biofuel cell anode based on a toluidine blue modified redox polymer and the flavodehydrogenase domain of cellobiose dehydrogenase, Electrochem. Commun. 29 (2013) 59–62.
[22] U. Salaj-Kosla, M.D. Scanlon, T. Baumeister, K. Zahma, R. Ludwig, P. Ó Conghaile, D. MacAodha, D. Leech, E. Magner, Mediated electron transfer of cellobiose dehydrogenase and glucose oxidase at osmium polymer-modified nanoporous gold electrodes, Anal. Bioanal. Chem. 405 (2013) 3823–3830.
[23] M. Shao, M.N. Zafar, M. Falk, R. Ludwig, C. Sygmund, C.K. Peterbauer, D.A. Guschin, D. MacAodha, P. Ó Conghaile, D. Leech, M.D. Toscano, S. Shleev, W. Schuhmann, L. Gorton, Optimization of a membraneless glucose/oxygen enzymatic fuel cell based on a bioanode with high coulombic efficiency and current density, ChemPhysChem 14 (2013) 2260–2269.
[24] M. Shao, M.N. Zafar, C. Sygmund, D.A. Guschin, R. Ludwig, C.K. Peterbauer, W. Schuhmann, L. Gorton, Mutual enhancement of the current density and the coulombic efficiency for a bioanode by entrapping bi-enzymes with Os-complex modified electrodeposition paints, Biosens. Bioelectron. 40 (2013) 308–314.
[25] L. Stoica, R. Ludwig, D. Haltrich, L. Gorton, Third-generation biosensor for lactose based on newly discovered cellobiose dehydrogenase, Anal. Chem. 78 (2006) 393–398.
[26] L. Stoica, A. Lindgren-Sjölander, T. Ruzgas, L. Gorton, Biosensor based on cellobiose dehydrogenase for detection of catecholamines, Anal. Chem. 76 (2004) 4690–4696.
[27] L. Stoica, N. Dimcheva, D. Haltrich, T. Ruzgas, L. Gorton, Electrochemical investigation of cellobiose dehydrogenase from new fungal sources on Au electrodes, Biosens. Bioelectron. 20 (2005) 2010–2018.
[28] L. Stoica, T. Ruzgas, R. Ludwig, D. Haltrich, L. Gorton, Direct electron transfer—a favorite electron route for cellobiose dehydrogenase (CDH) from *Trametes villosa.* Comparison with CDH from Phanerochaete chrysosporium, Langmuir 22 (2006) 10801–10806.
[29] X. Wang, M. Falk, R. Ortiz, H. Matsumura, J. Bobacka, R. Ludwig, M. Bergelin, L. Gorton, S. Shleev, Mediatorless sugar/oxygen enzymatic fuel cells based on gold nanoparticle-modified electrodes, Biosens. Bioelectron. 31 (2012) 219–225.
[30] S. Shleev, Quo vadis, implanted fuel cell? ChemPlusChem 82 (2017) 522–539.
[31] J. Vivekananthan, R.A. Rincon, V. Kuznetsov, S. Poeller, W. Schuhmann, Biofuel-cell cathodes based on bilirubin oxidase immobilized through organic linkers on 3d hierarchically structured carbon electrodes, ChemElectroChem 1 (2014) 1901–1908.
[32] S. Sane, C. Heilemann, P. Salavei, S. Rubenwolf, C. Jolivalt, C. Madzak, R. Zengerle, P.J. Nielsen, S. Kerzenmacher, Enzymatic fuel cells solely supplied with unpurified cellobiose dehydrogenase and laccase in microorganism's culture supernatants, ChemElectroChem 1 (2014) 1886–1894.
[33] P. Lamberg, S. Shleev, R. Ludwig, T. Arnebrant, T. Ruzgas, Performance of enzymatic fuel cell in cell culture, Biosens. Bioelectron. 55 (2014) 168–173.
[34] V. Coman, R. Ludwig, W. Harreither, D. Haltrich, L. Gorton, T. Ruzgas, S. Shleev, A direct electron transfer-based glucose/oxygen biofuel cell operating in human serum, Fuel Cells 10 (2010) 9–16.
[35] V. Coman, C. Vaz-Dominguez, R. Ludwig, W. Herreither, D. Haltrich, A.L. De Lacey, T. Ruzgas, L. Gorton, S. Shleev, A membrane-, mediator-, cofactor-less glucose/oxygen biofuel cell, Phys. Chem. Chem. Phys. 10 (2008) 6093–6096.

[36] P.N. Bartlett, F.A. Al-Lolage, There is no evidence to support literature claims of direct electron transfer (DET) for native glucose oxidase (GOx) at carbon nanotubes or graphene, J. Electroanal. Chem. (2017) (in press).
[37] G.S. Wilson, Native glucose oxidase does not undergo direct electron transfer, Biosens. Bioelectron. 82 (2016) vii–viii.
[38] R.D. Milton, S.D. Minteer, Direct enzymatic bioelectrocatalysis: differentiating between myth and reality, J. Roy. Soc. Interf. 14 (2017).
[39] T. Ikeda, D. Kobayashi, F. Matsushita, T. Sagara, K. Niki, Bioelectrocatalysis at electrodes coated with alcohol-dehydrogenase, a quinohemoprotein with heme-c serving as a built-in mediator, J. Electroanal. Chem. 361 (1993) 221–228.
[40] S. Kawai, T. Yakushi, K. Matsushita, Y. Kitazumi, O. Shirai, K. Kano, The electron transfer pathway in direct electrochemical communication of fructose dehydrogenase with electrodes, Electrochem. Commun. 38 (2014) 28–31.
[41] K. Takeda, H. Matsumura, T. Ishida, M. Samejima, H. Ohno, M. Yoshida, K. Igarashi, N. Nakamura, Characterization of a novel PQQ-dependent quinohemoprotein pyranose dehydrogenase from *Coprinopsis cinerea* classified into auxiliary activities family 12 in carbohydrate-active enzymes, PLoS ONE 10 (2015), e0115722/0115721-e0115722/115722.
[42] K. Igarashi, I. Momohara, T. Nishino, M. Samejima, Kinetics of inter-domain electron transfer in flavocytochrome cellobiose dehydrogenase from the white-rot fungus *Phanerochaete chrysosporium*, Biochem. J. 365 (2002) 521–526.
[43] A. Kadek, D. Kavan, A.K. Felice, R. Ludwig, P. Halada, P. Man, Structural insight into the calcium ion modulated interdomain electron transfer in cellobiose dehydrogenase, FEBS Lett. 589 (2015) 1194–1199.
[44] A. Kadek, D. Kavan, J. Marcoux, J. Stojko, A.K. Felice, S. Cianferani, R. Ludwig, P. Halada, P. Man, Interdomain electron transfer in cellobiose dehydrogenase is governed by surface electrostatics, Biochim. Biophys. Acta 1861 (2017) 157–167.
[45] P. Kielb, M. Sezer, S. Katz, F. Lopez, C. Schulz, L. Gorton, R. Ludwig, U. Wollenberger, I. Zebger, I.M. Weidinger, Spectroscopic observation of calcium-induced reorientation of cellobiose dehydrogenase immobilized on electrodes and its effect on electrocatalytic activity, ChemPhysChem 16 (2015) 1960–1968.
[46] D. Kracher, K. Zahma, C. Schulz, C. Sygmund, L. Gorton, R. Ludwig, Inter-domain electron transfer in cellobiose dehydrogenase: modulation by pH and divalent cations, FEBS J. 282 (2015) 3136–3148.
[47] W. Harreither, C. Sygmund, M. Augustin, M. Narciso, M.L. Rabinovich, L. Gorton, D. Haltrich, R. Ludwig, Catalytic properties and classification of cellobiose dehydrogenases from ascomycetes, Appl. Environ. Microbiol. 77 (2011) 1804–1815.
[48] C. Schulz, R. Kittl, R. Ludwig, L. Gorton, Direct electron transfer from the FAD cofactor of cellobiose dehydrogenase to electrodes, ACS Catal. 6 (2016) 555–563.
[49] P. Knöös, C. Schulz, L. Piculell, R. Ludwig, L. Gorton, M. Wahlgren, Quantifying the release of lactose from polymer matrix tablets with an amperometric biosensor utilizing cellobiose dehydrogenase, Int. J. Pharm. 468 (2014) 121–132.
[50] W. Harreither, C. Sygmund, E. Dunhofen, R. Vicuna, D. Haltrich, R. Ludwig, Cellobiose dehydrogenase from the ligninolytic basidiomycete *Ceriporiopsis subvermispora*, Appl. Environ. Microbiol. 75 (2009) 2750–2757.
[51] G. Henriksson, V. Sild, I.J. Szabo, G. Pettersson, G. Johansson, Substrate specificity of cellobiose dehydrogenase from *Phanerochaete chrysosporium*, Biochim. Biophys. Acta 1383 (1998) 48–54.
[52] K. Igarashi, M. Yoshida, H. Matsumura, N. Nakamura, H. Ohno, M. Samejima, T. Nishino, Electron transfer chain reaction of the extracellular flavocytochrome cellobiose dehydrogenase from the basidiomycete *Phanerochaete chrysosporium*, FEBS J. 272 (2005) 2869–2877.
[53] G. Safina, R. Ludwig, L. Gorton, A simple and sensitive method for lactose detection based on direct electron transfer between immobilised cellobiose dehydrogenase and screen-printed carbon electrodes, Electrochim. Acta 55 (2010) 7690–7695.
[54] M. Yakovleva, O. Buzas, H. Matsumura, M. Samejima, K. Igarashi, P.O. Larsson, L. Gorton, B. Danielsson, A novel combined thermometric and amperometric biosensor for lactose determination based on immobilised cellobiose dehydrogenase, Biosens. Bioelectron. 31 (2012) 251–256.
[55] N. Glithero, C. Clark, L. Gorton, W. Schuhmann, N. Pasco, At-line measurement of lactose in dairy-processing plants, Anal. Bioanal. Chem. 405 (2013) 3791–3799.
[56] F. Tasca, R. Ludwig, L. Gorton, R. Antiochia, Determination of lactose by a novel third generation biosensor based on a cellobiose dehydrogenase and aryl diazonium modified single wall carbon nanotubes electrode, Sens. Actuat. B 177 (2013) 64–69.
[57] L. Gorton, A. Lindgren, T. Larsson, F.D. Munteanu, T. Ruzgas, I. Gazaryan, Direct electron transfer between heme-containing enzymes and electrodes as basis for third generation biosensors, Anal. Chim. Acta 400 (1999) 91–108.
[58] A. Lindgren, L. Gorton, T. Ruzgas, U. Baminger, D. Haltrich, M. Schülein, Direct electron transfer of cellobiose dehydrogenase from various biological origins at gold and graphite electrodes, J. Electroanal. Chem. 496 (2001) 76–81.
[59] A. Lindgren, T. Larsson, T. Ruzgas, L. Gorton, Direct electron transfer between the heme of cellobiose dehydrogenase and thiol modified gold electrodes, J. Electroanal. Chem. 494 (2000) 105–113.
[60] L. Stoica, T. Ruzgas, L. Gorton, Electrochemical evidence of self-substrate inhibition as functions regulation for cellobiose dehydrogenase from *Phanerochaete chrysosporium*, Bioelectrochemistry 76 (2009) 42–52.
[61] C. Schulz, R. Ludwig, P.O. Micheelsen, M. Silow, M.D. Toscano, L. Gorton, Enhancement of enzymatic activity and catalytic current of cellobiose dehydrogenase by calcium ions, Electrochem. Commun. 17 (2012) 71–74.
[62] H. Matsumura, R. Ortiz, R. Ludwig, K. Igarashi, M. Samejima, L. Gorton, Direct electrochemistry of *Phanerochaete chrysosporium* cellobiose dehydrogenase covalently attached onto gold nanoparticle modified solid gold electrodes, Langmuir 28 (2012) 10925–10933.
[63] F. Tasca, L. Gorton, W. Harreither, D. Haltrich, R. Ludwig, G. Nöll, Direct electron transfer at cellobiose dehydrogenase modified anodes for biofuel cells, J. Phys. Chem. C 112 (2008) 9956–9961.
[64] F. Tasca, W. Harreither, R. Ludwig, J.J. Gooding, L. Gorton, Cellobiose dehydrogenase aryl diazonium modified single walled carbon nanotubes: enhanced direct electron transfer through a positively charged surface, Anal. Chem. 83 (2011) 3042–3049.
[65] W. Harreither, P. Nicholls, C. Sygmund, L. Gorton, R. Ludwig, Investigation of the pH-dependent electron transfer mechanism of ascomycetous class II cellobiose dehydrogenases on electrodes, Langmuir 28 (2012) 6714–6723.
[66] R. Ortiz, M. Rahman, B. Zangrilli, C. Sygmund, P.O. Micheelsen, M. Silow, M.D. Toscano, R. Ludwig, L. Gorton, Engineering of cellobiose dehydrogenases for improved glucose sensitivity and reduced maltose affinity, ChemElectroChem 4 (2017) 846–855.
[67] F. Tasca, L. Gorton, W. Harreither, D. Haltrich, R. Ludwig, G. Nöll, Highly efficient and versatile anodes for biofuel cells based on cellobiose dehydrogenase from Myriococcum thermophilum, J. Phys. Chem. C 112 (2008) 13668–13673.
[68] C. Schulz, R. Ludwig, L. Gorton, Polyethyleneimine as a promoter layer for the immobilization of cellobiose dehydrogenase from *Myriococcum thermophilum* on graphite electrodes, Anal. Chem. 86 (2014) 4256–4263.
[69] V. Coman, W. Harreither, R. Ludwig, D. Haltrich, L. Gorton, Investigation of electron transfer between cellobiose dehydrogenase from *Myriococcum Thermophilum* and gold electrodes, Chem. Anal. 52 (2007) 945–960.
[70] W. Harreither, V. Coman, R. Ludwig, D. Haltrich, L. Gorton, Investigation of graphite electrodes modified with cellobiose dehydrogenase from the ascomycete *Myriococcum thermophilum*, Electroanalysis 19 (2007) 172–180.
[71] W. Harreither, A.K. Felice, R. Paukner, L. Gorton, R. Ludwig, C. Sygmund, Recombinantly produced cellobiose dehydrogenase from *Corynascus thermophilus* for glucose biosensors and biofuel cells, Biotechnol. J. 7 (2012) 1359–1366.
[72] V. Krikstolaityte, P. Lamberg, M.D. Toscano, M. Silow, O. Eicher-Lorka, A. Ramanavicius, G. Niaura, L. Abariute, T. Ruzgas, S. Shleev, Mediatorless carbohydrate/oxygen biofuel cells with improved cellobiose dehydrogenase based bioanode, Fuel Cells 14 (2014) 792–800.
[73] A. Cipri, C. Schulz, R. Ludwig, L. Gorton, M. del Valle, A novel bio-electronic tongue using different cellobiose dehydrogenases to resolve mixtures of various sugars and interfering analytes, Biosens. Bioelectron. 79 (2016) 515–521.
[74] S. Ma, M. Preims, F. Piumi, L. Kappel, B. Seiboth, E. Record, D. Kracher, R. Ludwig, Molecular and catalytic properties of fungal extracellular cellobiose dehydrogenase produced in prokaryotic and eukaryotic expression systems, Microb. Cell Factor. 16 (2017), http://dx.doi.org/10.1186/s12934-017-0653-5.
[75] R. Ortiz, H. Matsumura, F. Tasca, K. Zahma, M. Samejima, K. Igarashi, R. Ludwig, L. Gorton, Effect of deglycosylation of cellobiose dehydrogenases on the enhancement of direct electron transfer with electrodes, Anal. Chem. 84 (2012) 10315–10323.
[76] K. Scida, P.W. Stege, G. Haby, G.A. Messina, C.D. García, Recent applications of carbon-based nanomaterials in analytical chemistry: critical review, Anal. Chim. Acta 691 (2011) 6–17.
[77] X.-Y. Yang, G. Tian, N. Jiang, B.-L. Su, Immobilization technology: a sustainable solution for biofuel cell design, Energy Environ. Sci. 5 (2012) 5540–5563.
[78] M.T. Meredith, S.D. Minteer, Biofuel cells: enhanced enzymatic bioelectrocatalysis, Ann. Rev. Anal. Chem. 5 (2012) 157–179.
[79] F. Chekin, L. Gorton, I. Tapsobea, Direct and mediated electrochemistry of peroxidase and its electrocatalysis on a variety of screen-printed carbon electrodes: amperometric hydrogen peroxide and phenols biosensor, Anal. Bioanal. Chem. 407 (2015) 439–446.
[80] F. Mazzei, G. Favero, P. Bollella, C. Tortolini, L. Mannina, M.E. Conti, R. Antiochia, Recent trends in electrochemical nanobiosensors for environmental analysis, Int. J. Environ. Health 7 (2015) 267–291.
[81] G. Favero, G. Fusco, F. Mazzei, F. Tasca, R. Antiochia, Electrochemical characterization of graphene and MWCNT screen-printed electrodes modified with AuNPs for laccase biosensor development, Nanomaterials 5 (2015) 1995–2006.
[82] P. Bollella, G. Fusco, C. Tortolini, G. Sanzo, G. Favero, L. Gorton, R. Antiochia, Beyond graphene: electrochemical sensors and biosensors for biomarkers detection, Biosens. Bioelectron. 89 (2017) 152–166.
[83] P. Bollella, C. Schulz, G. Favero, F. Mazzei, R. Ludwig, L. Gorton, R. Antiochia, Green synthesis and characterization of gold and silver nanoparticles and their application for development of a third generation lactose biosensor, Electroanalysis 29 (2017) 77–86.
[84] P. Bollella, F. Mazzei, G. Favero, G. Fusco, R. Ludwig, L. Gorton, R. Antiochia, Improved DET communication between cellobiose dehydrogenase and a

gold electrode modified with a rigid self-assembled monolayer and green metal nanoparticles: the role of an ordered nanostructuration, Biosens. Bioelectron. 88 (2017) 196–203.
[85] M. Tavahodi, R. Ortiz, C. Schulz, A. Ekhtiari, R. Ludwig, B. Haghighi, L. Gorton, Direct electron transfer of cellobiose dehydrogenase on positively charged polyethyleneimine gold nanoparticles, ChemPlusChem 82 (2017) 546–552.
[86] F.A. Al-Lolage, M. Meneghello, S. Ma, R. Ludwig, P.N. Bartlett, A flexible method for the stable, covalent immobilization of enzymes at electrode surfaces, ChemElectroChem 4 (2017) 1528–1534.
[87] S.A. Trashin, D. Haltrich, R. Ludwig, L. Gorton, A.A. Karyakin, Improvement of direct bioelectrocatalysis by cellobiose dehydrogenase on screen printed graphite electrodes using polyaniline modification, Bioelectrochemistry 76 (2009) 87–92.
[88] S. Bozorgzadeh, H. Hamidi, R. Ortiz, R. Ludwig, L. Gorton, Direct electron transfer of *Phanerochaete chrysosporium* cellobiose dehydrogenase at platinum and palladium nanoparticles decorated carbon nanotubes modified electrodes, Phys. Chem. Chem. Phys. 17 (2015) 24157–24165.
[89] K. Balasubramanian, M. Burghard, Chemically functionalized carbon nanotubes, Small 1 (2005) 180–192.
[90] J.J. Gooding, Nanostructuring electrodes with carbon nanotubes: a review on electrochemistry and applications for sensing, Electrochim. Acta 50 (2005) 3049–3060.
[91] J.J. Gooding, R. Wibowo, J. Liu, W. Yang, D. Losic, S. Orbons, F.J. Mearns, J.G. Shapter, D.B. Hibbert, Protein electrochemistry using aligned carbon nanotube arrays, J. Am. Chem. Soc. 125 (2003) 9006–9007.
[92] D. Vairavapandian, P. Vichchulada, M.D. Lay, Preparation and modification of carbon nanotubes: review of recent advances and applications in catalysis and sensing, Anal. Chim. Acta 626 (2008) 119–129.
[93] A. Merkoci, M. Pumera, X. Llopis, B. Perez, M. del Valle, S. Alegret, New materials for electrochemical sensing VI: carbon nanotubes, Trends Anal. Chem. 24 (2005) 826–838.
[94] E.T. Thostenson, Z.F. Ren, T.W. Chou, Advances in the science and technology of carbon nanotubes and their composites: a review, Composites Sci. Technol. 61 (2001) 1899–1912.
[95] G. Wang, L. Zhang, J. Zhang, A review of electrode materials for electrochemical supercapacitors, Chem. Soc. Rev. 41 (2012) 797–828.
[96] M. Carbone, L. Gorton, R. Antiochia, An overview of the latest graphene-based sensors for glucose detection: the effects of graphene defects, Electroanalysis 27 (2015) 16–31.
[97] M. Pumera, A. Ambrosi, A. Bonanni, E.L.K. Chng, H.L. Poh, Graphene for electrochemical sensing and biosensing, Trends Anal. Chem. 29 (2010) 954–965.
[98] W. Yang, K.R. Ratinac, S.P. Ringer, P. Thordarson, J.J. Gooding, F. Braet, Carbon nanomaterials in biosensors: should you use nanotubes or graphene? Angew. Chem. Int. Ed. 49 (2010) 2114–2138.
[99] Y. Shao, J. Wang, M. Engelhard, C. Wang, Y. Lin, Facile and controllable electrochemical reduction of graphene oxide and its applications, J. Mater. Chem. 20 (2010) 743–748.
[100] J.M. Pingarrón, P. Yáñez-Sedeño, A. González-Cortés, Gold nanoparticle-based electrochemical biosensors, Electrochim. Acta 53 (2008) 5848–5866.
[101] F.N. Crespilho, M.E. Ghica, M. Florescu, F.C. Nart, O.N. Oliveira, C.M.A. Brett, A strategy for enzyme immobilization on layer-by-layer dendrimer–gold nanoparticle electrocatalytic membrane incorporating redox mediator, Electrochem. Commun. 8 (2006) 1665–1670.
[102] M.A. Hayat, Colloidal gold: principles, methods, and applications, Elsevier, Amsterdam, 2012.
[103] Y. Xiao, F. Patolsky, E. Katz, J.F. Hainfeld, I. Willner, Plugging into enzymes: nanowiring of redox enzymes by a gold nanoparticle, Science 299 (2003) 1877–1880.
[104] F. Tasca, L. Gorton, J.B. Wagner, G. Nöll, Increasing amperometric biosensor sensitivity by length fractionated single-walled carbon nanotubes, Biosen. Bioelectron. 24 (2008) 272–278.
[105] F. Tasca, M.N. Zafar, W. Harreither, G. Nöll, R. Ludwig, L. Gorton, A third generation glucose biosensor based on cellobiose dehydrogenase from *Corynascus thermophilus* and single-walled carbon nanotubes, Analyst 136 (2011) 2033–2036.
[106] M.N. Zafar, G. Safina, R. Ludwig, L. Gorton, Characteristics of third-generation glucose biosensors based on *Corynascus thermophilus* cellobiose dehydrogenase immobilized on commercially available screen-printed electrodes working under physiological conditions, Anal. Biochem. 425 (2012) 36–42.
[107] F. Arduini, L. Micheli, D. Moscone, G. Palleschi, S. Piermarini, F. Ricci, G. Volpe, Electrochemical biosensors based on nanomodified screen-printed electrodes: recent applications in clinical analysis, Trends Anal. Chem. 79 (2016) 114–126.
[108] S. Fletcher, Screen-printed carbon electrodes, Adv. Electrochem. Sci. Eng. 16 (2015) 425–443.
[109] N. Jaiswal, I. Tiwari, Recent build outs in electroanalytical biosensors based on carbon-nanomaterial modified screen printed electrode platforms, Anal. Meth. 9 (2017) 3895–3907.
[110] W. Zhang, S. Zhu, R. Luque, S. Han, L. Hu, G. Xu, Recent development of carbon electrode materials and their bioanalytical and environmental applications, Chem. Soc. Rev. 45 (2016) 715–752.
[111] H. Kanso, M.B.G. García, L.F. Llano, S. Ma, R. Ludwig, P.F. Bolado, D.H. Santos, Novel thin layer flow-cell screen-printed graphene electrode for enzymatic sensors, Biosens. Bioelectron. 93 (2017) 298–304.
[112] H. Kanso, M. Begona Gonzalez Garcia, S. Ma, R. Ludwig, P. Fanjul Bolado, D. Hernandez Santos, Dual biosensor for simultaneous monitoring of lactate and glucose based on thin-layer flow cell screen-printed electrode, Electroanalysis 29 (2017) 87–92.
[113] R.A. Marcus, J. Chem. Phys. 43 (1965) 679–701.
[114] R.A. Marcus, N. Sutin, Biochim. Biophys. Acta Rev. Bioenerg. 811 (1985) 265–322.
[115] R. Ortiz, R. Ludwig, L. Gorton, Highly efficient membraneless glucose bioanode based on *Corynascus thermophilus* cellobiose dehydrogenase on aryl diazonium-activated single-walled carbon nanotubes, ChemElectroChem 1 (2014) 1948–1956.
[116] J. Tanne, D. Kracher, B. Dietzel, B. Schulz, R. Ludwig, F. Lisdat, F.W. Scheller, F.F. Bier, Carboxylated or aminated polyaniline-multiwalled carbon nanotubes nanohybrids for immobilization of cellobiose dehydrogenase on gold electrodes, Biosensors 4 (2014) 370–386.
[117] J. Wang, S.Q. Zhang, J. Shen, Y.Z. Guo, S.M. Attia, B. Zhou, Z.Q. Lai, G.Z. Zheng, Y.S. Gui, Electrical transport properties of carbon aerogels, J. Porous Mater. 8 (2001) 167–170.
[118] J. Biener, M. Stadermann, M. Suss, M.A. Worsley, M.M. Biener, K.A. Rose, T.F. Baumann, Advanced carbon aerogels for energy applications, Energ. Environ. Sci 4 (2011) 656–667.
[119] C.I. Fort, R. Ortiz, L.C. Cotet, V. Danciu, I.C. Popescu, L. Gorton, Carbon aerogel as electrode material for improved direct electron transfer in biosensors incorporating cellobiose dehydrogenase, Electroanalysis 28 (2016) 2311–2319.
[120] S. Kumar, K.S. Gandhi, R. Kumar, Modeling of formation of gold nanoparticles by citrate method, Indust. Engin. Chem. Res. 46 (2007) 3128–3136.
[121] F. Mafuné, J.-y. Kohno, Y. Takeda, T. Kondow, H. Sawabe, Formation of gold nanoparticles by laser ablation in aqueous solution of surfactant, J. Phys. Chem. B 105 (2001) 5114–5120.
[122] P. Lamberg, J. Hamit-Eminovski, M.D. Toscano, O. Eicher-Lorka, G. Niaura, T. Arnebrant, S. Shleev, T. Ruzgas, Electrical activity of cellobiose dehydrogenase adsorbed on thiols: influence of charge and hydrophobicity, Bioelectrochemistry 115 (2017) 26–32.
[123] G. Kovacs, R. Ortiz, V. Coman, W. Harreither, I.C. Popescu, R. Ludwig, L. Gorton, Influence of sam structure on direct electron transfer at au electrodes modified with cellobiose dehydrogenase from *Neurospora crassa*, Rev. Roum. Chim. 57 (2012) 361–368.
[124] E. Laviron, General expression of the linear potential sweep voltammogram in the case of diffusionless electrochemical systems, J. Electroanal. Chem. 101 (1979) 19–28.
[125] S.C. Feifel, R. Ludwig, L. Gorton, F. Lisdat, Catalytically active silica nanoparticle-based supramolecular architectures of two proteins—cellobiose dehydrogenase and cytochrome *c* on electrodes, Langmuir 28 (2012) 9189–9194.
[126] D. Sarauli, R. Ludwig, D. Haltrich, L. Gorton, F. Lisdat, Investigation of the mediated electron transfer mechanism of cellobiose dehydrogenase at cytochrome *c*-modified gold electrodes, Bioelectrochemistry 87 (2012) 9–14.
[127] S.C. Feifel, A. Kapp, R. Ludwig, L. Gorton, F. Lisdat, Electrocatalytically active multi-protein assemblies using nanoscaled building blocks, RSC Adv. 3 (2013) 3428–3437.
[128] S.C. Feifel, A. Kapp, R. Ludwig, F. Lisdat, Nanobiomolecular multiprotein clusters on electrodes for the formation of a switchable cascadic reaction scheme, Angew. Chem. Int. Ed. 53 (2014) 5676–5679.
[129] A. Walcarius, S.D. Minteer, J. Wang, Y.H. Lin, A. Merkoci, Nanomaterials for bio-functionalized electrodes: recent trends, J. Mater. Chem. B 1 (2013) 4878–4908.
[130] S.D. Minteer, P. Atanassov, H.R. Luckarift, G.R. Johnson, New materials for biological fuel cells, Mater. Today 15 (2012) 166–173.
[131] S.C. Barton, J. Gallaway, P. Atanassov, Enzymatic biofuel cells for Implantable and microscale devices, Chem. Rev. 104 (2004) 4867–4886.
[132] D. Leech, P. Kavanagh, W. Schuhmann, Enzymatic fuel cells: recent progress, Electrochim. Acta 84 (2012) 223–234.
[133] M. Falk, C.W. Narváez Villarrubia, S. Babanova, P. Atanassov, S. Shleev, Biofuel cells for biomedical applications: colonizing the animal kingdom, ChemPhysChem 14 (2013) 2045–2058.
[134] M.J. Cooney, V. Svoboda, C. Lau, G. Martin, S.D. Minteer, Enzyme catalysed biofuel cells, Energy Environ. Sci. 1 (2008) 320–337.
[135] S.D. Minteer, B.Y. Liaw, M.J. Cooney, Enzyme-based biofuel cells, Curr. Opin. Biotechnol. 18 (2007) 228–234.
[136] M. Rasmussen, S. Abdellaoui, S.D. Minteer, Enzymatic biofuel cells: 30 years of critical advancements, Biosens. Bioelectron. 76 (2016) 91–102.
[137] M. Falk, Z. Blum, S. Shleev, Direct electron transfer based enzymatic fuel cells, Electrochim. Acta 82 (2012) 191–202.
[138] M. Falk, V. Andoralov, Z. Blum, J. Sotres, D.B. Suyatin, T. Ruzgas, T. Arnebrant, S. Shleev, Biofuel cell as a power source for electronic contact lenses, Biosens. Bioelectron. 37 (2012) 38–45.
[139] V. Andoralov, M. Falk, D.B. Suyatin, M. Granmo, J. Sotres, R. Ludwig, V.O. Popov, J. Schouenborg, Z. Blum, S. Shleev, Biofuel cell based on microscale nanostructured electrodes with inductive coupling to rat brain neurons, Sci. Rep. 3 (2013), http://dx.doi.org/10.1038/srep03270.

[140] D. Pankratov, R. Sundberg, J. Sotres, I. Maximov, M. Graczyk, D.B. Suyatin, E. Gonzalez-Arribas, A. Lipkin, L. Montelius, S. Shleev, Transparent and flexible, nanostructured and mediatorless glucose/oxygen enzymatic fuel cells, J. Power Sources 294 (2015) 501–506.
[141] D. Pankratov, E. Gonzalez-Arribas, Z. Blum, S. Shleev, Tear based bioelectronics, Electroanalysis 28 (2016) 1250–1266.
[142] N. Efron, Contact Lens Practice E-Book, Elsevier Health Sciences, Amsterdam, The Netherlands, 2016.
[143] M. Falk, D. Pankratov, L. Lindh, T. Arnebrant, S. Shleev, Miniature direct electron transfer based enzymatic fuel cell operating in human sweat and saliva, Fuel Cells 14 (2014) 1050–1056.
[144] M. Falk, M. Alcalde, P.N. Bartlett, A.L. De Lacey, L. Gorton, C. Gutierrez-Sanchez, R. Haddad, J. Kilburn, D. Leech, R. Ludwig, E. Magner, D.M. Mate, P. Ó Conghaile, R. Ortiz, M. Pita, S. Pöller, T. Ruzgas, U. Salaj-Kosla, W. Schuhmann, F. Sebelius, M. Shao, L. Stoica, C. Sygmund, J. Tilly, M.D. Toscano, J. Vivekananthan, E. Wright, S. Shleev, Self-powered wireless carbohydrate/oxygen sensitive biodevice based on radio signal transmission, PLoS ONE 9 (2014) e109104.
[145] E. Gonzalez-Arribas, T. Bobrowski, C. Di Bari, K. Sliozberg, R. Ludwig, M.D. Toscano, A.L. De Lacey, M. Pita, W. Schuhmann, S. Shleev, Transparent, mediator- and membrane-free enzymatic fuel cell based on nanostructured chemically modified indium tin oxide electrodes, Biosens. Bioelectron. 97 (2017) 46–52.
[146] X. Xiao, P. Ó Conghaile, D. Leech, R. Ludwig, E. Magner, A symmetric supercapacitor/biofuel cell hybrid device based on enzyme-modified nanoporous gold: an autonomous pulse generator, Biosens. Bioelectron. 90 (2017) 96–102.
[147] D. Pankratov, Z. Blum, S. Shleev, Hybrid electric power biodevices, ChemElectroChem 1 (2014) 1798–1807.
[148] P. Simon, Y. Gogotsi, Materials for electrochemical capacitors, Nat. Mater. 7 (2008) 845–854.
[149] D. Pankratov, Z. Blum, D.B. Suyatin, V.O. Popov, S. Shleev, Self-charging electrochemical biocapacitor, ChemElectroChem 1 (2014) 343–346.

Paper VI

The Influence of pH and Divalent/Monovalent Cations on the Internal Electron Transfer (IET), Enzymatic Activity and Structure of Fructose Dehydrogenase

Paolo Bollella[a,b], Yuya Hibino[c], Kenji Kano[c], Lo Gorton[b]*, Riccarda Antiochia[a,]*

[a]Department of Chemistry and Drug Technologies, Sapienza University of Rome P.le Aldo Moro 5, 00185 – Rome, Italy

[b]Department of Analytical Chemistry/Biochemistry, Lund University, P.O. Box 124, 221 00 – Lund, Sweden

[c]Division of Applied Life Sciences, Graduate School of Agriculture, Kyoto University, Sakyo, Kyoto 606-8502, Japan

Abstract

In this paper we report on the influence of pH and monovalent/divalent cations on the catalytic current response, internal electron transfer (IET) and structure of fructose dehydrogenase (FDH) by using amperometry, spectrophotometry and circular dichroism (CD). Amperometric measurements were performed on graphite electrodes, onto which FDH was adsorbed and the effect on the response current to fructose was investigated when varying the pH and the concentrations of divalent/monovalent cations in the contacting buffer. In the presence of 10 mM $CaCl_2$, a current increase of up to ≈ 240% was observed, probably due to an intra-complexation reaction between Ca^{2+} and the aspartate/glutamate residues found at the interface between the dehydrogenase domain and the cytochrome domain of FDH. Contrary to $CaCl_2$, addition of $MgCl_2$ did not show any particular influence, while addition of monovalent cations (Na^+ or K^+) led to a slight linear increase in the maximum response current. To complement the amperometric investigations, spectrophotometric assays were carried out under homogeneous conditions in the presence of either a 1-electron non-proton-acceptor, cytochrome *c,* or a 2-electron-proton acceptor, 2,6-dichloroindophenol (DCIP), respectively. In the case of cytochrome *c*, it was possible to observe a remarkable increase in the absorbance up to 200% when 10 mM $CaCl_2$ was added. However, by further increasing the concentration of $CaCl_2$ up to 50 mM and 100 mM, a decrease in the absorbance with a slight inhibition effect was observed for the highest $CaCl_2$ concentration. Addition of $MgCl_2$ or of the monovalent cations shows surprisingly no effect on the electron transfer to the electron acceptor. Contrary to the case of cytochrome *c*, with DCIP none of the cations tested seem to affect the rate of catalysis. In order to correlate the results obtained by

amperometric and spectrophotometric measurements, CD experiments have been performed showing a great structural change of FDH when increasing the concentration $CaCl_2$ up to 50 mM at which the enzyme molecules start to agglomerate hindering the substrate access to the active site probably due to a chelation reaction occurring at the enzyme surface with the glutamate/aspartate residues.

Keywords: fructose dehydrogenase (FDH), calcium chloride, direct electron transfer (DET), enzyme activity, enzyme structure

* Corresponding Authors:
Riccarda.Antiochia@uniroma1.it
Lo.Gorton@biochemistry.lu.se

1. Introduction

In the last 30 years, studies of direct electron transfer (DET) reactions between redox enzymes and electrodes has attracted a lot of interest both to understand the background reaction mechanism [1-3] and thus gain sufficient basic knowledge to be able to found the basis and to improve the performance of third generation biosensors and enzymatic fuel cells (EFCs) [4-7]. DET based reactions have been explored for a number of redox proteins [8] such as cytochrome *c* (cyt *c*) [9-12], ferredoxin [13,14], azurin [15,16], and redox enzymes [17] such as peroxidases [18-24], hydrogenases [25], "blue" multi-copper oxidases (BMCO) [26-29], sulfite oxidase (SOx) [30,31], alcohol PQQ dehydrogenase (ADH) [32,33], cellobiose dehydrogenase (CDH) [34-38], D-fructose dehydrogenase (FDH) [39-42], etc. Several of the redox enzymes mentioned above, such as SOx, ADH, CDH and FDH are composed of at least two different domains, where one domain is the catalytically active domain containing a bound cofactor such as FAD, PQQ or MOCO and a second domain, a cytochrome containing heme *c* or heme *b*, acting as an electron transfer domain or in other words "as a built in mediator" [32] connecting the redox enzyme to its natural electron acceptor or when immobilized onto the surface of an electrode to the electrode if the enzyme is properly orientated on its surface. The electron transfer (ET) reaction between the catalytic and the cytochrome domain, the internal electron transfer (IET) reaction, can be very much dependent on pH, ion strength and buffer constituents [43]. Studies to be able to understand what determines and limits the ET reactions are fundamental to increase the knowledge about protein structure, mechanisms of redox transformations of protein molecules, and metabolic processes involving

redox transformations [44]. DET is the key issue to develop "reagentless" electrochemical biosensors [45,8,7,4,2,3,5,6,1]. Among the flavocytochrome oxidoreductases, the DET mechanism for membrane bound FDH has not been yet elucidated [46] and therefore FDH has attracted a growing interest also regarding all factors that can influence on the DET reaction (e.g. pH, cations, ionic strength etc.) [47-49].

D-Fructose dehydrogenase (FDH; EC 1.1.99.11) from *Gluconobacter japonicus* NCBR 3260 is a heterotrimeric membrane-bound enzyme complex with a molecular mass of 146.4 kDa, consisting of three subunits/domains [46]: subunit I, which is the catalytic dehydrogenase domain (DH_{FDH}) with a covalently bound flavin adenine dinucleotide (FAD) cofactor, where D-(-)-fructose is involved in a $2H^+/2e^-$ oxidation reaction to form 5-dehydro-D-(-)-fructose; subunit II, which is equivalent to the cytochrome domain (CYT_{FDH}) acts as electron acceptor to subunit I and contains three *heme c* moieties covalently bound to the enzyme scaffold and two of them are involved in the one-by-one ET pathway [46]; subunit III, which is not involved in the ET but rather plays a key role for the stability of the enzyme complex [50,51,39,46]. FDH exhibits a strict substrate specificity to D-(-)-fructose and therefore it has been used as bioelectrocatalyst for biosensor development both in direct and mediated ET (DET and MET) modes [52-55].

Unfortunately, the crystal structure of FDH is not yet available, because of the difficulties involved with crystallization of a membrane bound protein with a high molecular weight (ca. 146 kDa). Despite these obvious difficulties, in the last few years a lot of efforts have been addressed with regards to considering new crystallization methods [56]. The crystal structure would be of fundamental importance to clarify the ET mechanism of this enzyme with particular attention on the co-factor involved.

The suggested ET pathway for FDH when immobilised on the electrode surface and in the absence of any competing e^- acceptors [39], is assumed to occur according to Scheme 1:

1. Oxidation of D-(-)-fructose to 5-keto-D-(-)-fructose involving $2e^-/2H^+$ with the reduction of FAD to $FADH_2$;
2. $FADH_2$ is sequentially reoxidized in two separate 1 ET steps. In the first $FADH_2$ is partially reoxidized to $FADH^\bullet$ through the IET pathway between the DH_{FDH} and CYT_{FDH} domains, whereby one of the three heme *c* (heme c_1) is reduced. Next, the electron is transferred from heme c_1 to a second heme *c* (heme c_2) of the two hemes involved in the ET pathway and then to a final electron acceptor, which is the electrode when FDH is adsorbed onto the electrode surface;
3. $FADH^\bullet$ is finally reoxidized to FAD by heme c_1 and the electron is then transferred to heme c_2 (which gives the second internal electron transfer (IET) step), which in turn is reoxidized

by the electrode whereby FDH is returned to its fully oxidized state.

The influence of ionic strength as well as various cationic and anionic species on enzymes has been already proved to modulate enzymatic activity or stability in different ways [57,58]. E.g., CDH has two redox domains connected through a flexible linker [59-61], with an ET mechanism similar to FDH but with only one heme in its cytochrome domain as electron acceptor. Moreover, Sezer et al. showed an increase in terms of catalytic current of SOx by increasing the ionic strength of the buffer solution [62], while Feng et al. reported on the influence of the viscosity on the rate of the IET [63]. Nevertheless, each of these enzymes has its own and different dependency on pH and ionic strength, due to the amino acids residues at the interface between the subunits connecting each other through linker regions.

The aim of this paper was to investigate whether there is any influence of pH and the concentration of various divalent/monovalent cations on the rate of the IET and the activity and the structure of FDH. First, FDH was immobilized onto graphite electrodes by a drop-casting procedure and amperometric measurements were carried out when shifting the pH and in presence of various concentrations of divalent cations ($CaCl_2$ and $MgCl_2$) or monovalent cations (KCl and NaCl). Furthermore, the influence of pH on the rate of the IET was investigated also in the presence of that $CaCl_2$ concentration that yielded the highest current density for fructose. These results were compared with those obtained with the spectrophotometric assays carried out in the presence of 2,6-dichloroindophenol (DCIP, bielectronic acceptor) or of cytochrome *c* (cyt *c*, monoelectronic acceptor). Finally, circular dichoism (CD) measurements and homology modelling/docking studies were performed confirming the hypothesis formulated on the IET of FDH.

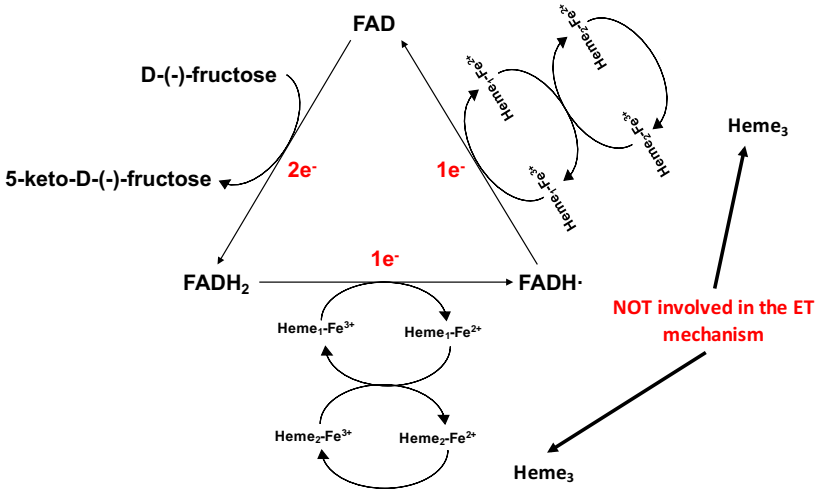

Scheme 1. Suggested ET mechanism of the oxidation reaction of FDH. D-(-)-fructose is oxidized to 5-keto-D-(-)-fructose releasing 2 electrons, which are transferred one by one initially through the FAD, followed by two heme *c* working as monoelectronic acceptors.

2. Material and methods

2.1 Chemicals

D-(-)-fructose, calcium chloride ($CaCl_2$), magnesium chloride hexahydrate ($MgCl_2 \cdot 6\ H_2O$), sodium chloride (NaCl), potassium chloride (KCl), cytochrome *c* from bovine heart (≥95% based on MW 12,327 Da, prepared using TCA), 2,6-dichloroindophenol (DCIP), sodium acetate (CH_3COONa, NaAc), 3-(N-morpholino)propanesulfonic acid (MOPS), 2-amino-2-(hydroxymethyl)-1,3-propanediol (TRIS), sodium dihydrogen phosphate (NaH_2PO_4), hydrochloric acid (HCl), sodium hydroxide (NaOH) were purchased from Sigma Aldrich (St. Louis, MO, USA). D-Fructose dehydrogenase from *Gluconobacter japonicus* (FDH; EC 1.1.99.11) was purified from the culture supernatant of *Gluconobacter japonicus* NBRC 3260 obtained from the National Institute of Technology and Evaluation (Nishinomiya, Hyogo Pref., Japan) and solubilized in PBS buffer at pH 6 (50~500 mM) containing 0.1 mM 2-mercaptoethanol and 0.1% v/v Triton X-100 (volumetric activity measured with potassium ferricyanide at pH 4.5 = 420±30 U mL^{-1}, specific activity = 250±30 U mg^{-1}, protein concentration = 1.7±0.2 mg mL^{-1}) [50]. All solutions were prepared using Milli-Q water (R = 18.2 MΩ cm at 25 °C; TOC < 10 µg L^{-1}, Millipore, Molsheim, France).

2.2 Electrochemical measurements

Graphite rods (Alfa Aesar GmbH & Co KG, AGKSP grade, ultra "F" purity, and 3.05 mm diameter, Karlsruhe, Germany) were polished on wet emery paper (Turfbak Durite, P1200) and then carefully rinsed with Milli-Q water [57]. The enzyme-modified electrodes were prepared by allowing 5 µL of an FDH solution (volumetric activity measured with potassium ferricyanide at pH 4.5 and found to be 420±30 U mL^{-1}, specific activity = 250±30 U mg^{-1}, protein concentration = 1.7±0.2 mg mL^{-1}) to physically adsorb on the top of the graphite rod electrodes, overnight at 4 ºC. The FDH modified graphite electrode, an Ag|AgCl (0.1 M KCl) reference electrode and a platinum wire counter electrode were fitted into a flow through wall-jet electrochemical cell [64] connected to a flow injection analysis (FIA) system consisting of a peristaltic pump (Gilson, Villier-le-Bel, France) and a six-port valve electrical injector equipped with a 50 µL-loop (injection volume 50 µL) (Rheodyne, Cotati, CA, USA) [64]. A potentiostat (Zäta Elektronik, Höör, Sweden) controlled the flow through cell and the response of the injected samples was shown on a strip chart recorder

(Kipp & Zonen, Utrecht, The Netherlands) [65].

2.3 Spectrophotometric measurements

Two spectrophotometric assays have been performed to measure the activity of FDH in solution as a function of both pH and the concentration of cations/ionic strength. In the first assay, the activity of the DH_{FDH} domain was monitored measuring the time dependent variation of the absorbance at λ=520 nm (ε=6.9 mM^{-1} cm^{-1}) of a mixture containing 100 µL of 300 mM D-(-)-fructose, 780 µL of 50 mM NaAc buffer, 20 µL of enzyme solution and 100 µL of 3 mM DCIP as two-electrons/two protons acceptor [57]. In the second assay, the activity of FDH and the internal electron transfer (IET) between the DH_{FDH} and CYT_{FDH} domains was monitored by using the one-electron acceptor cyt *c*, which communicates only with the CYT_{FDH} domain due to steric hindrance because of its dimensions. The absorption is followed at 550 nm (ε=19.6 mM^{-1} cm^{-1}) of a mixture of 20 µL of a 1 mM cyt *c* solution, 100 µl of 300 mM D-(-)-fructose, 860 µl of 50 mM NaAc buffer pH 4.5, and 20 µl of the enzyme solution [66]. One unit of DCIP and cyt *c* activity was defined as the amount of FDH that reduces 1 µmol of DCIP or cyt *c*, respectively, per min under the applied conditions. All measured enzyme activities are the average of three measurements at 25 °C, whereas the average activity values in 50 mM NaAc buffer without additions of "extra" KCl, NaCl, $MgCl_2$ or $CaCl_2$ were set to 100% and the average activity values in the presence of divalent and monovalent cations in 50 mM NaAc buffer were related to those values. All measurements were carried out using a UV-Vis spectrophotometer 1800 (Shimadzu Europe GmbH, Duisburg, Germany).

2.4 Circular dichroism (CD) measurements

Changes in the secondary structure of FDH as a function of pH and addition of divalent cations to the solution were investigated through CD measurements using a CD spectrometer (J-815 Circular Dichroic Spectrometer, Jasco, Easton, MD, USA) [67]. These measurements were carried out in a 0.1 cm cuvette at 25 °C using a final protein concentration of 0.15 mg mL^{-1}, diluted in 50 mM NaH_2PO_4 at pH 4.5 (unfortunately we could not use NaAc because the –COOH groups adsorb the light so we needed to use a non-adsorbing medium to obtain reliable data [68]). Then, the concentration of $CaCl_2$ or $MgCl_2$ was increased in the range of 0-100 mM to receive information about any changes in the secondary structure. The obtained spectra were further fitted with a method called β-structure selection (BeStSel) that takes into account the twist of β-structures for estimation of the secondary structure. This method can reliably distinguish parallel and antiparallel β-sheets and accurately estimate the secondary structure for a broad range of proteins [69,70]. Moreover, the secondary structure components applied by the method are characteristic to the

protein fold, which in turn can be predicted to the level of topology in the CATH classification from a single CD spectrum.

2.5 Homology modeling and docking

The homology models of the individual DH_{FDH} and CYT_{FDH} domains of FDH (GenBank accession number A0A164AQ58_9SYNE were generated using the Protein Homology/analogY Recognition Engine V 2.0 server (http://www.sbg.bio.ic.ac.uk/) [71] with the individually crystallized DH domains of FAD-glucose dehydrogenase (GDH) from *Aspergillus flavus* (PDB ID 4YNT [72]) and thiosulfate dehydrogenase (tsdba) from *Marichromatium purpuratum* "as2 isolated" (PDB ID 5LO9 [73]) as templates. The FIREDOCK webserver (http://bioinfo3d.cs.tau.ac.il/FireDock/firedock.html) [74,75] was used for protein–protein docking of the individual FDH domains. In total, 10 models from three clusters per enzyme were evaluated. The best model has been selected based on the lowest free energy [76]. Structures were visualized using the PyMOL MOLECULAR GRAPHICS SYSTEM, version 1.4 (Schroeodinger, New York, NY, USA).

3. Results and discussion

3.1 Influence of pH and divalent/monovalent cations on the direct electron transfer (DET) reaction of FDH: electrochemical study.

In order to study the influence of pH on the DET reaction of FDH with graphite electrodes, we have performed amperometric measurements with graphite electrodes simply modified with adsorbed FDH. The measurements were performed with 5 mM D-(-)-fructose as substrate and by varying the pH in the running buffer between 3 and 7 using NaAc buffer between pH 3 and 5.5, MOPS buffer between pH 5 and 7. Figure 1a shows the current dependence on pH. The optimum pH was found at 4.5. The response current rapidly decreased when increasing the pH above 4.5, thus assessing no DET activity starting at pH 7. These results are in good agreement with previous values reported in the literature [77].

Next, the influence of divalent ($CaCl_2$ and $MgCl_2$) and monovalent (NaCl and KCl) cations was studied through registering calibration curves for D-(-)-fructose at pH 4.5 and varying the salt concentrations in the range of 0-100 mM. Figure 1b shows the dependence of maximum current, I_{max}, on the concentration of $CaCl_2$, $MgCl_2$, NaCl and KCl for FDH at pH 4.5. The I_{max} values were obtained from the calibration curves and were set to 100% in the absence of extra added cations. All values obtained in the presence of the different cations are related to those values. Surprisingly, when increasing the concentration of $CaCl_2$ a marked increase in I_{max} was observed, with a

maximum increase of 237%, corresponding to an average maximal current of 33.0±2.7 μA for 10 mM $CaCl_2$. However, at higher concentrations of $CaCl_2$ than 10 mM an unexpected I_{max} decrease was registered, yielding I_{max} values of 140% and of 80%, at 50 mM 100 mM $CaCl_2$, respectively. This particular trend for $CaCl_2$ is probably due to the presence of side-chain carboxyl functions of surface-exposed aspartic acid (pK_a= 3.86) and glutamic acid (pK_a= 4.07) residues at the interface of the DH_{FDH} and CYT_{FDH} domains. These -COOH groups are ~90% deprotonated at pH 4.5, creating a strong electrostatic repulsion between the two domains [78]. It can be supposed that a possible complexation of Ca^{2+} with the carboxylic groups of the aspartic and glutamic acid residues takes place resulting in a closer interaction and shortening the distance between the DH_{FDH} and CYT_{FDH} domains thus increasing the rate of the IET [59]. On the other hand, the decrease in response signal when the concentration of Ca^{2+} is higher than 10 mM can probably be ascribed to a possible saturation of the aspartate/glutamate residues available at the interface between the DH_{FDH} and CYT_{FDH} domains [79]. Therefore, at concentrations higher than 10 mM, Ca^{2+} is now available for complexation of other aspartate/glutamate residues present on the surface of both subunits. Both the DH_{FDH} and CYT_{FDH} subunits show a partial positive charge at pH 4.5, which might now create a slight repulsion between the two subunits, which is, however, counter-balanced by the attractive interactions. A possible explanation for the inhibition effect observed at 100 mM $CaCl_2$ could be the interaction with other enzyme molecules through a Ca^{2+}-bridge [80].

Contrary to the effect by addition of $CaCl_2$, addition of $MgCl_2$ showed a 90% decrease in I_{max} already at 10 mM $MgCl_2$. This result could be ascribed to a lower affinity of Mg^{2+} compared to Ca^{2+} towards the carboxylic functions available at the interface of the DH_{FDH} and CYT_{FDH} domains. Mg^{2+} is expected mainly to be involved in the complexation reaction occurring between different enzyme molecules (Mg^{2+}-bridge), which will partially hinder the substrate access to the active site of FDH and will therefore show a slight inhibition behavior evident already at low $MgCl_2$ concentrations. Figure 1c shows that the enhanced effect on the catalytic current by addition of $CaCl_2$ occurs only in the pH range between 3.5 and 5.5 without any shift in the optimum pH of the enzyme activity, due to its presumed effect on the IET as described and discussed above.

In a series of previous investigations the effect of ionic strength and addition of Ca^{2+} and Mg^{2+} on the catalytic performance of various CDHs was investigated both in solution and when adsorbed on graphite [81,57,59,82]. The results obtained here for FDH are both similar and dissimilar with respect to those obtained for the various CDHs. E.g., for two ascomycete CDHs the addition of both Ca^{2+} and Mg^{2+} had a similar increasing effect on the catalytic efficiency and could even lead to a drastic shift in the pH optimum of the enzyme activity [81]. Thus it seems as though further investigations on the background reasons for the effect by both ionic strength and by individual

cations on the interactions between the various domains participating in the ET pathways in such multidomain redox enzymes are necessary.

For the monovalent cations, further additions of both KCl and NaCl showed a slight linear increase in I_{max} up to 100 mM, which is more evident in Fig. 1d, where the I_{max} is plotted versus the ionic strength of the buffer. The concentration of the monovalent cations is directly related to the ionic strength, leading to a general increase in the catalytic current, as already reported in literature for many enzymes, whereas monovalent cations are usually not involved in any complexation reactions occurring at the protein surface [57].

3.2 Influence of pH and divalent/monovalent cations on the catalytic reaction of FDH: spectrophometric study

Two different spectrophotometric assays have been performed to follow the catalytic reaction of FDH in solution; one with cyt *c* and one with DCIP, acting as mono and bielectronic acceptors, respectively. DCIP may have a direct connection with subunit I (DH_{FDH}), where the catalytic oxidation of D-fructose to 5-keto-D-fructose occurs [60], whereas cyt *c* can only interact with the subunit II (CYT_{FDH}) due to its dimensions. Figure 2a shows the dependence of the activity of FDH with pH using DCIP as electron acceptor and one can see that the highest activity is found between 3 and 6 corresponding to an activity of 3086 U mL^{-1} at pH 5.5. For pH values higher than 6, the activity rapidly decreases and reaches zero at approximately pH 7, indicating a progressive inactivation of DH_{FDH} (subunit I). The dependence of the activity of FDH with pH when using cyt *c* is shown in Fig. 2b. In this case the activity exhibits two pH optima: one at 4.5 and one at 7, in agreement with previous results already reported in the literature [83]. These results could be ascribed to the different mechanisms of the interaction between FDH and cyt *c*: (i) ET may either proceed from the active site (FAD containing subunit I, DH_{FDH}) via the heme groups (subunit II containing the three heme centers, CYT_{FDH}) toward cyt *c* or (ii) directly from the DH_{FDH} to cyt *c*. A similar conclusion was found by Ferapontova et al. when investigating the ET between FDH and cyt *c* by cyclic voltammetry at different scan rates [84].

As far as for the influence of mono and divalent cations, the results of the spectrophotometric activity assays are shown in Figs. 3a and b. The results obtained with cyt *c* (Fig. 3a) are comparable with those obtained with the amperometric measurements (Fig. 1b) for immobilized FDH on graphite electrodes, as Ca^{2+} ions may affect the rate of the IET and therefore the rate of overall DET reaction. Figure 3b shows that there is no influence of either divalent or monovalent cations on the activity of FDH using DCIP as electron acceptor, because DCIP is reduced directly by the FAD deeply buried within the DH_{FDH} (subunit I) and is thus not affected by any change in the IET.

The obtained results unequivocally confirm the influence of $CaCl_2$ on the rate of the IET reaction, whereas there is no influence observed on the catalytic oxidation reaction of D-(-)-fructose at the DH_{FDH} domain by $CaCl_2$ or by the other cations tested.

3.3 Influence of $CaCl_2$ on the secondary enzyme structure

In order to confirm the results obtained with the amperometric and spectrophotometric assays, CD measurements of FDH have been performed increasing the concentration $CaCl_2$ or $MgCl_2$ in the range of 0-100 mM. Figure 4 shows the CD spectra recorded for FDH in the presence of $CaCl_2$. It is possible to observe that the secondary structure only to some extent shows minor changes up to a concentration of 10 mM, whereas at higher concentrations of $CaCl_2$ the spectra reveal large changes that can be explained by agglomeration with other FDH molecules due to Ca^{2+}-bridge interactions between enzyme molecules. Therefore, at low $CaCl_2$ concentrations it is possible to observe an intra-complexation caused by Ca^{2+} ions, which might increase the rate of the IET reaction, whereas at high $CaCl_2$ concentrations inter-complexation reactions occur due to aggregation of enzyme molecules caused by the high $CaCl_2$ concentration. These qualitative results were further confirmed from the quantitative fitting of the CD spectra recorded in the presence of $CaCl_2$ shown in Table 1. The α-helix content of FDH decreased to 5%, whereas the antiparallel β-sheets content did not change (36%) and the random coiled protein was found to be approximately 59% of the secondary structure by increasing the $CaCl_2$ concentration. This unequivocally proves the formation of an aggregated state of FDH when increasing the $CaCl_2$ concentration.

3.4 Structural analysis and docking of FDH domains

The already characterized FAD-glucose dehydrogenase from *Aspergillus flavus* (4YNT) and thiosulfate dehydrogenase (tsdba) from *Marichromatium purpuratum* "as2 isolated" (5LO9) were used for modeling and docking studies, of the DH_{FDH} and CYT_{FDH} domains, respectively. Figure 5a shows the homology models of the DH_{FDH} and CYT_{FDH} domains highlighting in the insets the position of the FAD cofactor (subunit I) and the three heme *c* (subunit II), respectively, while subunit III was not possible to model, because of the absence of a similar structure. From previous studies [50] it was already stated that subunit III has no influence on the DET reaction but it is important for the overall stability of the enzymatic complex.

Moreover, the docking between the DH_{FDH} and CYT_{FDH} domains was needed to highlight those amino acids expected to be involved in the interaction between the two domains, viz., Asp, Glu, Lys, Arg and Tyr. DH_{FDH} exhibits five amino acid residues negatively charged at the interface, while CYT_{FDH} contains three such amino acid residues. The occurrence of these residues could

partially explain the reason for the highest rate of the IET reaction at pH 4.5, where the repulsion between the two domains is lowest, whereas at pHs between 7 and 10 the repulsion between the two domains is high and will cause the low rate of the IET reaction. However, this model does not give any information about Ca^{2+}-bridging interactions. Nevertheless, a concentration of 10 mM $CaCl_2$ results in the upper limit in terms of an enhanced IET probably due to that only a few possible matches between the negatively charged amino acids residues and Ca^{2+} ions are found at the interface between the DH_{FDH} and the CYT_{FDH}, while the number of negatively charged amino acids residues exposed on the other parts of the enzyme surface is much higher confirming the possibility of other Ca^{2+}-bridging interactions between different individual enzyme molecules allowing the aggregation process [85,86].

4. Conclusions

This paper demonstrates the possibility to enhance the measurable activity of FDH either in solution or when immobilized onto an electrode surface about 2.5-fold by adding 10 mM $CaCl_2$ to the buffer solution, whereas $MgCl_2$ had no such effect. Additions of KCl or NaCl led to a slight linear increase in I_{max} of about 10%. However, $CaCl_2$ had an effect only at pH 4.5, because there was no shift in the optimum pH, in contrast to what was shown for ascomycete CDHs in previous papers [82,59,81,57]. Moreover, the amperometric and spectrophotometric results were confirmed also through conformational changes observed in the secondary structure of FDH, revealing unfolding of the protein occurring at high $CaCl_2$ concentrations (50 mM and 100 mM) followed by aggregation.
By the homology models, it was assumed that Ca^{2+} at lower concentrations was chelated by the few amino acids residues negatively charged shortening the distance between the DH_{FDH} and CYT_{FDH} domains, leading to an enhanced IET, while at higher concentrations of Ca^{2+}, they give Ca^{2+}-bridging interactions with other enzyme molecules.
These results show that studies of the mechanism of the IET between the DH_{FDH} and CYT_{FDH} domains are of great interest to shed further light into the physiological functions of FDH, as well as for the development of third generation biosensors and enzymatic fuel cells based on FDH.

Acknowledgments

The authors would like to thank the following agencies for financial support: The Swedish Research Council (Vetenskapsrådet project 2014-5908) and the European Commission (project “Bioenergy” FP7-PEOPLE-2013-ITN-607793). PB also acknowledges a scholarship of the Erasmus+ Project

Unipharma-Graduates, promoted by a Consortium of Italian Universities and coordinated by Sapienza University of Rome.

References

1. Leger C, Bertrand P (2008) Direct electrochemistry of redox enzymes as a tool for mechanistic studies. Chem Rev 108 (7):2379-2438. https://doi:10.1021/cr0680742.
2. Frew JE, Hill HAO (1988) Direct and indirect electron-transfer between electrodes and redox proteins. Eur J Biochem 172 (2):261-269. https://doi:10.1111/j.1432-1033.1988.tb13882.x.
3. Frew JE, Hill HAO (1988) Direct and indirect electron transfer between electrodes and redox proteins. FEBS J 172 (2):261-269. https://DOI:10.1111/j.1432-1033.1988.tb13882.x.
4. Falk M, Blum Z, Shleev S (2012) Direct electron transfer based enzymatic fuel cells. Electrochim Acta 82:191-202. https://DOI: 10.1016/j.electacta.2011.12.133.
5. Ghindilis AL, Atanasov P, Wilkins E (1997) Enzyme-catalyzed direct electron transfer: Fundamentals and analytical applications. Electroanalysis 9 (9):661-674. https://DOI: 10.1002/elan.1140090902.
6. Gorton L, Lindgren A, Larsson T, Munteanu F, Ruzgas T, Gazaryan I (1999) Direct electron transfer between heme-containing enzymes and electrodes as basis for third generation biosensors. Anal Chim Acta 400 (1):91-108. https://doi:10.1016/S0003-2670(99)00610-8.
7. Cracknell JA, Vincent KA, Armstrong FA (2008) Enzymes as working or inspirational electrocatalysts for fuel cells and electrolysis. Chem Rev 108 (7):2439-2461. https://doi:10.1021/cr0680639.
8. Armstrong FA, Hill HAO, Walton NJ (1988) Direct electrochemistry of redox proteins. Acc Chem Res 21 (11):407-413. https://doi:10.1021/ar00155a004.
9. Wang L, Wang E (2004) Direct electron transfer between cytochrome c and a gold nanoparticles modified electrode. Electrochem Commun 6 (1):49-54. https://doi:10.1016/j.elecom.2003.10.004.
10. Ju H, Liu S, Ge B, Lisdat F, Scheller FW (2002) Electrochemistry of cytochrome c immobilized on colloidal gold modified carbon paste electrodes and its electrocatalytic activity. Electroanalysis 14 (2):141. https://doi:10.1002/1521-4109(200201)14:2<141::AID-ELAN141>3.3.CO;2-P.
11. Eddowes MJ, Hill HAO (1979) Electrochemistry of horse heart cytochrome-*c*. J Am Chem Soc 101 (16):4461-4464. https://doi:10.1021/ja00510a003.
12. Yeh P, Kuwana T (1977) Reversible electrode-reaction of cytochrome-*c*. Chem Lett (10):1145-1148. https://doi:10.1246/cl.1977.1145.
13. Yagati AK, Lee T, Min J, Choi J-W (2011) Amperometric sensor for hydrogen peroxide based on direct electron transfer of spinach ferredoxin on Au electrode. Bioelectrochemistry 80 (2):169-174. https://doi:10.1016/j.bioelechem.2010.08.002.
14. Armstrong FA, Heering HA, Hirst J (1997) Reactions of complex metalloproteins studied by protein-film voltammetry. Chem Soc Rev 26 (3):169-179. https://doi:10.1039/cs9972600169.
15. Lancaster KM, Farver O, Wherland S, Crane III EJ, Richards JH, Pecht I, Gray HB (2011) Electron transfer reactivity of type zero *Pseudomonas aeruginosa* azurin. J Am Chem Soc 133 (13):4865-4873. https://doi:10.1021/ja1093919.
16. Chi QJ, Zhang JD, Andersen JET, Ulstrup J (2001) Ordered assembly and controlled electron transfer of the blue copper protein azurin at gold (111) single-crystal substrates. J Phys Chem B 105 (20):4669-4679. https://doi:10.1021/jp0105589.
17. Ferapontova EE, Shleev S, Ruzgas T, Stoica L, Christenson A, Tkac J, Yaropolov AI, Gorton L (2005) Direct Electrochemistry of Proteins and Enzymes. In: Palecek E, Scheller F, Wang J (eds) Electrochemistry of Nucleic Acids and Proteins: Towards Electrochemical Sensors for Genomics and Proteomics, vol 1. Perspectives in Bioanalysis. pp 517-598. https://doi:10.1016/s1871-0069(05)01016-5.
18. Olloqui-Sariego JL, Zakharova GS, Poloznikov AA, Calvente JJ, Hushpulian DM, Gorton L, Andreu R (2015) Interprotein Coupling Enhances the Electrocatalytic Efficiency of Tobacco Peroxidase Immobilized at a Graphite Electrode. Anal Chem 87 (21):10807-10814. https://doi:10.1021/acs.analchem.5b01710.

19. Li W-T, Wang M-H, Li Y-J, Sun Y, Li J-C (2011) Linker-free layer-by-layer self-assembly of gold nanoparticle multilayer films for direct electron transfer of horseradish peroxidase and H 2 O 2 detection. Electrochim Acta 56 (20):6919-6924. https://doi:10.1016/j.electacta.2011.06.023.
20. Ruzgas T, Csöregi E, Emnéus J, Gorton L, MarkoVarga G (1996) Peroxidase-modified electrodes: Fundamentals and application. Anal Chim Acta 330 (2-3):123-138. https://doi:10.1016/0003-2670(96)00169-9.
21. Christenson A, Dimcheva N, Ferapontova EE, Gorton L, Ruzgas T, Stoica L, Shleev S, Yaropolov AL, Haltrich D, Thorneley RNF, Aust SD (2004) Direct electron transfer between ligninolytic redox enzymes and electrodes. Electroanalysis 16 (13-14):1074-1092. https://doi:10.1002/elan.200403004.
22. Ferapontova EE (2004) Direct peroxidase bioelectrocatalysis on a variety of electrode materials. Electroanalysis 16 (13-14):1101-1112. https://doi:10.1002/elan.200403003.
23. Luis Olloqui-Sariego J, Zakharova GS, Poloznikov AA, Jose Calvente J, Hushpulian DM, Gorton L, Andreu R (2016) Fenton-like Inactivation of tobacco peroxidase electrocatalysis at negative potentials. ACS Catal 6 (11):7452-7457. https://doi:10.1021/acscatal.6b01839.
24. Gazaryan IG, Gorton L, Ruzgas T, Csöregi E, Schuhmann W, Lagrimini LM, Khushpul'yan DM, Tishkov VI (2005) Tobacco peroxidase as a new reagent for amperometric biosensors. J Anal Chem 60 (6):558-566. https://doi:10.1007/s10809-005-0139-1.
25. Vincent KA, Parkin A, Armstrong FA (2007) Investigating and exploiting the electrocatalytic properties of hydrogenases. Chem Rev 107 (10):4366-4413. https://doi:10.1021/cr050191u.
26. Salaj-Kosla U, Pöller S, Schuhmann W, Shleev S, Magner E (2013) Direct electron transfer of *Trametes hirsuta* laccase adsorbed at unmodified nanoporous gold electrodes. Bioelectrochemistry 91:15-20. https://doi:10.1016/j.bioelechem.2012.11.001.
27. Shleev S, Tkac J, Christenson A, Ruzgas T, Yaropolov AI, Whittaker JW, Gorton L (2005) Direct electron transfer between copper-containing proteins and electrodes. Biosens Bioelectron 20 (12):2517-2554. https://doi:10.1016/j.bios.2004.10.003.
28. Shleev S, Jarosz-Wilkolazka A, Khalunina A, Morozova O, Yaropolov A, Ruzgas T, Gorton L (2005) Direct electron transfer reactions of laccases from different origins on carbon electrodes. Bioelectrochemistry 67 (1):115-124. https://doi:10.1016/j.bioelechem.2005.02.004.
29. Pita M, Gutierrez-Sanchez C, Olea D, Velez M, Garcia-Diego C, Shleev S, Fernandez VM, De Lacey AL (2011) High redox potential cathode based on laccase covalently attached to gold electrode. J Phys Chem C 115 (27):13420-13428. https://doi:10.1021/jp203643h.
30. Ferapontova EE, Ruzgas T, Gorton L (2003) Direct electron transfer of heme- and molybdopterin cofactor-containing chicken liver sulfite oxidase on alkanethiol-modified gold electrodes. Anal Chem 75 (18):4841-4850. https://doi:10.1021/ac0341923.
31. Frasca S, Rojas O, Salewski J, Neumann B, Stiba K, Weidinger IM, Tiersch B, Leimkuehler S, Koetz J, Wollenberger U (2012) Human sulfite oxidase electrochemistry on gold nanoparticles modified electrode. Bioelectrochemistry 87:33-41. https://doi:10.1016/j.bioelechem.2011.11.012.
32. Ikeda T, Kobayashi D, Matsushita F, Sagara T, Niki K (1993) Bioelectrocatalysis at electrodes coated with alcohol-dehydrogenase, a quinohemoprotein with heme-*c* serving as a built-in mediator. J Electroanal Chem 361 (1-2):221-228. https://doi:10.1016/0022-0728(93)87058-4.
33. Ramanavicius A, Habermüller K, Csöregi E, Laurinavicius V, Schuhmann W (1999) Polypyrrole entrapped quinohemoprotein alcohol dehydrogenase. Evidence for direct electron transfer via conducting-polymer chains. Anal Chem 71 (16):3581-3586. https://doi:10.1021/ac981201c.
34. Tasca F, Gorton L, Harreither W, Haltrich D, Ludwig R, Nöll G (2008) Highly efficient and versatile anodes for biofuel cells based on cellobiose dehydrogenase from *Myriococcum thermophilum*. J Phys Chem C 112 (35):13668-13673. https://doi:10.1021/jp805092m.
35. Bollella P, Mazzei F, Favero G, Fusco G, Ludwig R, Gorton L, Antiochia R (2017) Improved DET communication between cellobiose dehydrogenase and a gold electrode modified with a rigid self-assembled monolayer and green metal nanoparticles: The role of an ordered nanostructuration.

Biosens Bioelectron 88 (Supplement C):196-203.
https://doi:https://doi.org/10.1016/j.bios.2016.08.027.
36. Bollella P, Ludwig R, Gorton L (2017) Cellobiose dehydrogenase: Insights on the nanostructuration of electrodes for improved development of biosensors and biofuel cells. Appl Mater Today 9:319-332. https://doi.org/10.1016/j.apmt.2017.08.009.
37. Ludwig R, Harreither W, Tasca F, Gorton L (2010) Cellobiose dehydrogenase: A versatile catalyst for electrochemical applications. ChemPhysChem 11 (13):2674-2697. https://doi:10.1002/cphc.201000216.
38. Ludwig R, Ortiz R, Schulz C, Harreither W, Sygmund C, Gorton L (2013) Cellobiose dehydrogenase modified electrodes: advances by materials science and biochemical engineering. Anal Bioanal Chem 405 (11):3637-3658. https://doi:10.1007/s00216-012-6627-x.
39. Kawai S, Yakushi T, Matsushita K, Kitazumi Y, Shirai O, Kano K (2014) The electron transfer pathway in direct electrochemical communication of fructose dehydrogenase with electrodes. Electrochem Commun 38:28-31. https://doi:10.1016/j.elecom.2013.10.024.
40. Kamitaka Y, Tsujimura S, Kano K (2006) High current density bioelectrolysis of D-fructose at fructose dehydrogenase-adsorbed and Ketjen black-modified electrodes without a mediator. Chem Lett 36 (2):218-219. https://doi:10.1246/cl.2007.218.
41. Khan GF, Kobatake E, Shinohara H, Ikariyama Y, Aizawa M (1992) Molecular interface for an activity controlled enzyme electrode and its application for the determination of fructose. Anal Chem 64 (11):1254-1258. https://doi:10.1021/ac00035a011.
42. Khan GF, Shinohara H, Ikariyama Y, Aizawa M (1991) Electrochemical-behavior of monolayer quinoprotein adsorbed on the electrode surface. J Electroanal Chem 315 (1-2):263-273. https://doi:10.1016/0022-0728(91)80075-2.
43. Page CC, Moser CC, Dutton PL (2003) Mechanism for electron transfer within and between proteins. Current opinion in chemical biology 7 (5):551-556. https://doi:10.1016/j.cbpa.2003.08.005.
44. Murgida DH, Hildebrandt P (2005) Redox and redox-coupled processes of heme proteins and enzymes at electrochemical interfaces. Phys Chem Chem Phys 7 (22):3773-3784. https://doi:10.1039/b507989f.
45. Bollella P, Schulz C, Favero G, Mazzei F, Ludwig R, Gorton L, Antiochia R (2017) Green synthesis and characterization of gold and silver nanoparticles and their application for development of a third generation lactose biosensor. Electroanalysis 29 (1):77-86. https://doi:10.1002/elan.201600476.
46. Hibino Y, Kawai S, Kitazumi Y, Shirai O, Kano K (2017) Construction of a protein-engineered variant of D-fructose dehydrogenase for direct electron transfer-type bioelectrocatalysis. Electrochem Commun 77:112-115. https://doi:10.1016/j.elecom.2017.03.005.
47. Sugimoto Y, Kawai S, Kitazumi Y, Shirai O, Kano K (2015) Function of C-terminal hydrophobic region in fructose dehydrogenase. Electrochim Acta 176:976-981. https://doi:10.1016/j.electacta.2015.07.142.
48. Funabashi H, Murata K, Tsujimura S (2015) Effect of pore size of MgO-templated carbon on the direct electrochemistry of D-fructose dehydrogenase. Electrochemistry (Tokyo, Jpn) 83 (5):372-375. https://doi:10.5796/electrochemistry.83.372.
49. Kizling M, Bilewicz R (2017) Fructose dehydrogenase electron transfer pathway in bioelectrocatalytic reactions. ChemElectroChem, in press. https://doi:10.1002/celc.201700861.
50. Kawai S, Goda-Tsutsumi M, Yakushi T, Kano K, Matsushita K (2013) Heterologous overexpression and characterization of a flavoprotein-cytochrome *c* complex fructose dehydrogenase of *Gluconobacter japonicus* NBRC3260. Appl Environ Microbiol 79 (5):1654-1660. https://doi:10.1128/AEM.03152-12.
51. Tsujimura S, Nishina A, Hamano Y, Kano K, Shiraishi S (2010) Electrochemical reaction of fructose dehydrogenase on carbon cryogel electrodes with controlled pore sizes. Electrochem Commun 12 (3):446-449. https://doi:10.1016/j.elecom.2010.01.016.

52. Tominaga M, Nomura S, Taniguchi I (2009) D-Fructose detection based on the direct heterogeneous electron transfer reaction of fructose dehydrogenase adsorbed onto multi-walled carbon nanotubes synthesized on platinum electrode. Biosens Bioelectron 24 (5):1184-1188. https://doi:10.1016/j.bios.2008.07.002.
53. Antiochia R, Lavagnini I, Magno F (2004) Amperometric mediated carbon nanotube paste biosensor for fructose determination. Anal Lett 37 (8):1657-1669. https://doi:10.1081/AL-120037594.
54. Antiochia R, Gorton L (2014) A new osmium-polymer modified screen-printed graphene electrode for fructose detection. Sens Actuat B 195:287-293. https://doi:10.1016/j.snb.2014.01.050.
55. Antiochia R, Vinci G, Gorton L (2013) Rapid and direct determination of fructose in food: a new osmium-polymer mediated biosensor. Food Chem 140 (4):742-747. https://doi:10.1016/j.foodchem.2012.11.023.
56. Privé GG (2007) Detergents for the stabilization and crystallization of membrane proteins. Methods 41 (4):388-397. https://doi:10.1016/j.ymeth.2007.01.007.
57. Schulz C, Ludwig R, Micheelsen PO, Silow M, Toscano MD, Gorton L (2012) Enhancement of enzymatic activity and catalytic current of cellobiose dehydrogenase by calcium ions. Electrochem Commun 17 (Supplement C):71-74. https://doi:https://doi.org/10.1016/j.elecom.2012.01.031.
58. Saboe PO, Conte E, Farell M, Bazan GC, Kumar M (2017) Biomimetic and bioinspired approaches for wiring enzymes to electrode interfaces. Energy Environ Sci 10 (1):14-42. https://doi:10.1039/c6ee02801b.
59. Kracher D, Zahma K, Schulz C, Sygmund C, Gorton L, Ludwig R (2015) Inter-domain electron transfer in cellobiose dehydrogenase: modulation by pH and divalent cations. FEBS J 282 (16):3136-3148. https://doi:10.1111/febs.13310.
60. Zamocky M, Ludwig R, Peterbauer C, Hallberg B, Divne C, Nicholls P, Haltrich D (2006) Cellobiose dehydrogenase-a flavocytochrome from wood-degrading, phytopathogenic and saprotropic fungi. Curr Prot Pept Sci 7 (3):255-280. https://doi:10.2174/138920306777452367
61. Tan T-C, Kracher D, Gandini R, Sygmund C, Kittl R, Haltrich D, Hallberg BM, Ludwig R, Divne C (2015) Structural basis for cellobiose dehydrogenase action during oxidative cellulose degradation. Nat Commun 6. https://doi:10.1038/ncomms8542.
62. Sezer M, Spricigo R, Utesch T, Millo D, Leimkuehler S, Mroginski MA, Wollenberger U, Hildebrandt P, Weidinger IM (2010) Redox properties and catalytic activity of surface-bound human sulfite oxidase studied by a combined surface enhanced resonance Raman spectroscopic and electrochemical approach. Phys Chem Chem Phys 12 (28):7894-7903. https://doi:10.1039/b927226g.
63. Feng C, Kedia RV, Hazzard JT, Hurley JK, Tollin G, Enemark JH (2002) Effect of solution viscosity on intramolecular electron transfer in sulfite oxidase. Biochemistry 41 (18):5816-5821. https://doi:10.1021/bi016059f.
64. Appelqvist R, Marko-Varga G, Gorton L, Torstensson A, Johansson G (1985) Enzymatic determination of glucose in a flow system by catalytic oxidation of the nicotinamide coenzyme at a modified electrode. Anal Chim Acta 169:237-247. https://doi:10.1016/S0003-2670(00)86226-1.
65. Harreither W, Coman V, Ludwig R, Haltrich D, Gorton L (2007) Investigation of graphite electrodes modified with cellobiose dehydrogenase from the ascomycete *Myriococcum thermophilum*. Electroanalysis 19 (2-3):172-180. https://doi:10.1002/elan.200603688.
66. Baminger U, Subramaniam SS, Renganathan V, Haltrich D (2001) Purification and characterization of cellobiose dehydrogenase from the plant pathogen *Sclerotium* (*Athelia*) *rolfsii*. Appl Environ Microbiol 67 (4):1766-1774. https://doi:10.1128/AEM.67.4.1766-1774.2001.
67. Greenfield NJ, Fasman GD (1969) Computed circular dichroism spectra for the evaluation of protein conformation. Biochemistry 8 (10):4108-4116. https://doi:10.1021/bi00838a031.
68. Johnson WC (1990) Protein secondary structure and circular dichroism: A practical guide. Proteins: Structure, Function, and Bioinformatics 7 (3):205-214. https://doi:10.1002/prot.340070302.

69. Micsonai A, Wien F, Kernya L, Lee Y-H, Goto Y, Réfrégiers M, Kardos J (2015) Accurate secondary structure prediction and fold recognition for circular dichroism spectroscopy. Proc Nat Acad Sci 112 (24):E3095-E3103. https://doi:10.1073/pnas.1500851112.
70. Lees JG, Miles AJ, Wien F, Wallace B (2006) A reference database for circular dichroism spectroscopy covering fold and secondary structure space. Bioinformatics 22 (16):1955-1962. https://doi:10.1093/bioinformatics/btl327.
71. Kelley LA, Mezulis S, Yates CM, Wass MN, Sternberg MJ (2015) The Phyre2 web portal for protein modeling, prediction and analysis. Nat Protoc 10 (6):845-858. https://doi:10.1038/nprot.2015.053.
72. Yoshida H, Sakai G, Mori K, Kojima K, Kamitori S, Sode K (2015) Structural analysis of fungus-derived FAD glucose dehydrogenase. Sci Rep 5:13498. https://doi:10.1038/srep13498.
73. Kurth JM, Brito JA, Reuter J, Flegler A, Koch T, Franke T, Klein E-M, Rowe SF, Butt JN, Denkmann K (2016) Electron accepting units of the diheme cytochrome c TsdA, a bifunctional thiosulfate dehydrogenase/tetrathionate reductase. J Biol Chem 291 (48):24804-24818. https://doi:10.1074/jbc.M116.753863.
74. Andrusier N, Nussinov R, Wolfson HJ (2007) FireDock: fast interaction refinement in molecular docking. Proteins: Struc Func Bioinform 69 (1):139-159. https://doi:10.1002/prot.21495
75. Duhovny D, Nussinov R, Wolfson HJ (2002) Efficient unbound docking of rigid molecules. Lect Notes Comput Sc 2452:185-200.
76. Schneidman-Duhovny D, Inbar Y, Nussinov R, Wolfson HJ (2005) PatchDock and SymmDock: servers for rigid and symmetric docking. Nucleic Acids Res 33 (suppl_2):W363-W367. https://doi:10.1093/nar/gki481.
77. Garcia C, de Oliveira Neto G, Kubota L (1998) New fructose biosensors utilizing a polypyrrole film and D-fructose 5-dehydrogenase immobilized by different processes. Anal Chim Acta 374 (2):201-208. https://doi:10.1016/S0003-2670(98)00259-1.
78. Arthur EJ (2015) Exploring the Solvent Environment of Biomolecular Systems.
79. Warshel A, Sharma PK, Kato M, Parson WW (2006) Modeling electrostatic effects in proteins. BBA-Proteins Proteom 1764 (11):1647-1676. https://doi:10.1016/j.bbapap.2006.08.007.
80. Armstrong FA, Cox PA, Hill HAO, Lowe VJ, Oliver BN (1987) Metal ions and complexes as modulators of protein-interfacial electron transport at graphite electrodes. J Electroanal Chem 217 (2):331-366. https://doi:10.1016/0022-0728(87)80228-0.
81. Schulz C, Ludwig R, Gorton L (2014) Polyethyleneimine as a promoter layer for the immobilization of cellobiose dehydrogenase from *Myriococcum thermophilum* on graphite electrodes. Anal Chem 86 (9):4256-4263. https://doi:10.1021/ac403957t.
82. Kielb P, Sezer M, Katz S, Lopez F, Schulz C, Gorton L, Ludwig R, Wollenberger U, Zebger I, Weidinger IM (2015) Spectroscopic observation of calcium-induced reorientation of cellobiose dehydrogenase immobilized on electrodes and its effect on electrocatalytic activity. ChemPhysChem 16 (9):1960-1968. https://doi:10.1002/cphc.201500112.
83. Wettstein C, Kano K, Schäfer D, Wollenberger U, Lisdat F (2016) Interaction of flavin-dependent fructose dehydrogenase with cytochrome *c* as basis for the construction of biomacromolecular architectures on electrodes. Anal Chem 88 (12):6382-6389. https://doi:10.1021/acs.analchem.6b00815.
84. Ferapontova EE, Gorton L (2005) Direct electrochemistry of heme multicofactor-containing enzymes on alkanethiol-modified gold electrodes. Bioelectrochemistry 66 (1):55-63. https://doi:10.1016/j.bioelechem.2004.04.004.
85. Blondin G, Girerd JJ (1990) Interplay of electron exchange and electron transfer in metal polynuclear complexes in proteins or chemical models. Chem Rev 90 (8):1359-1376. https://doi:10.1021/cr00106a001.
86. Bendall DS (1996) Protein electron transfer, in Interprotein Electron Transfer (Ed. Bendall DS). Garland Science, pp. 43-68.

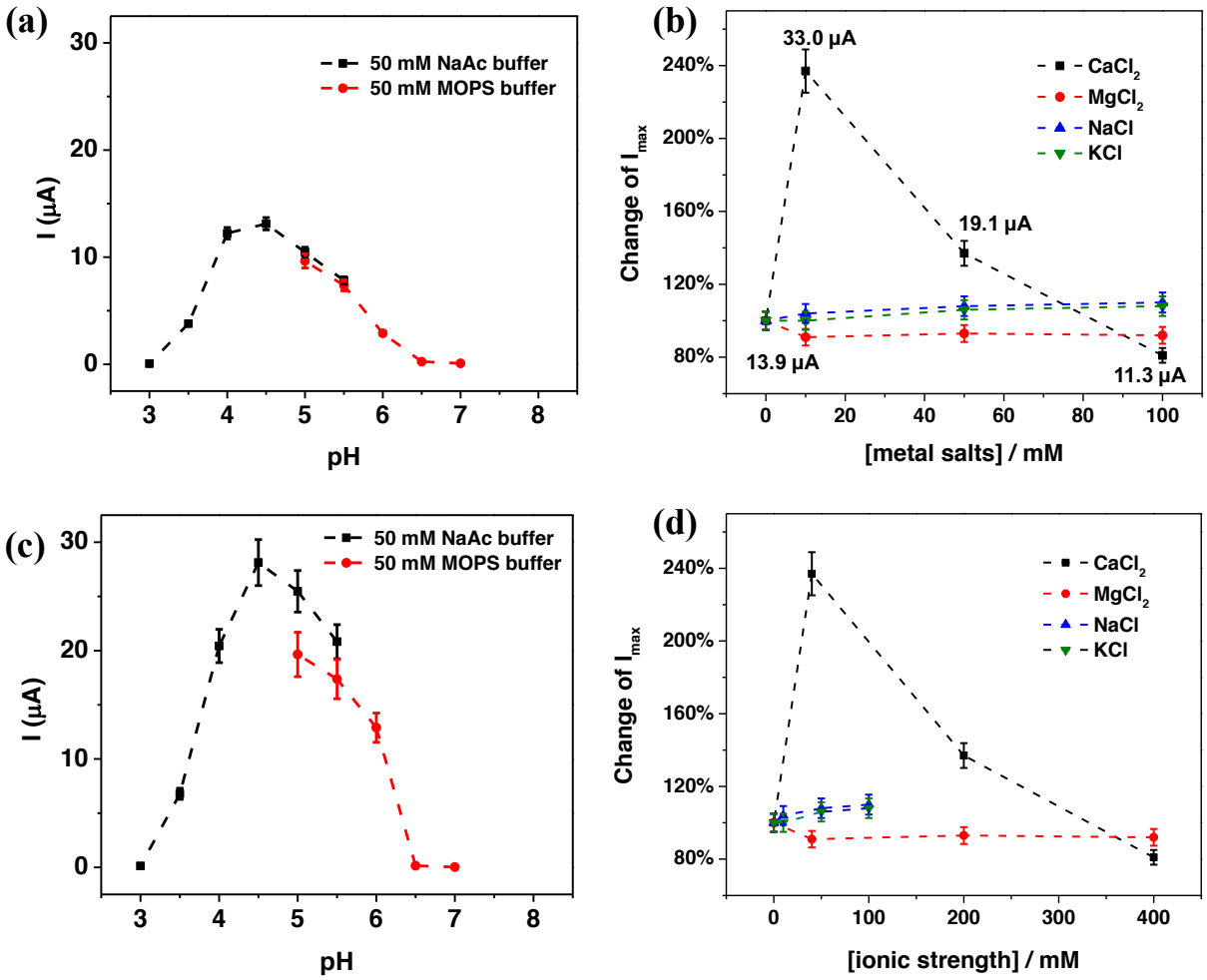

Figure 1. Dependence of the current on pH **(a)** in the absence and **(c)** in the presence of 10 mM $CaCl_2$ carried out in 50 mM NaAc buffer (pH 3-5.5, black), 50 mM MOPS buffer (pH 5-7, red) and 50 mM TRIS buffer (pH 7-10, blue) in the presence of 5 mM D-(-)-fructose; the relative maximal catalytic currents (I_{max}) on the concentration **(b)** and ionic strength **(d)** of $CaCl_2$ (black), $MgCl_2$ (red), NaCl (blue) and KCl (green) solutions (50 mM NaAc buffer pH 4.5) calculated from calibration curves performed in presence of different concentrations of D-(-)-fructose. Experimental conditions: applied potential (E_{app}): +0.2 V vs. $Ag|AgCl_{sat}$, flow rate: 0.5 mL min^{-1}; injection volume 50 μL.

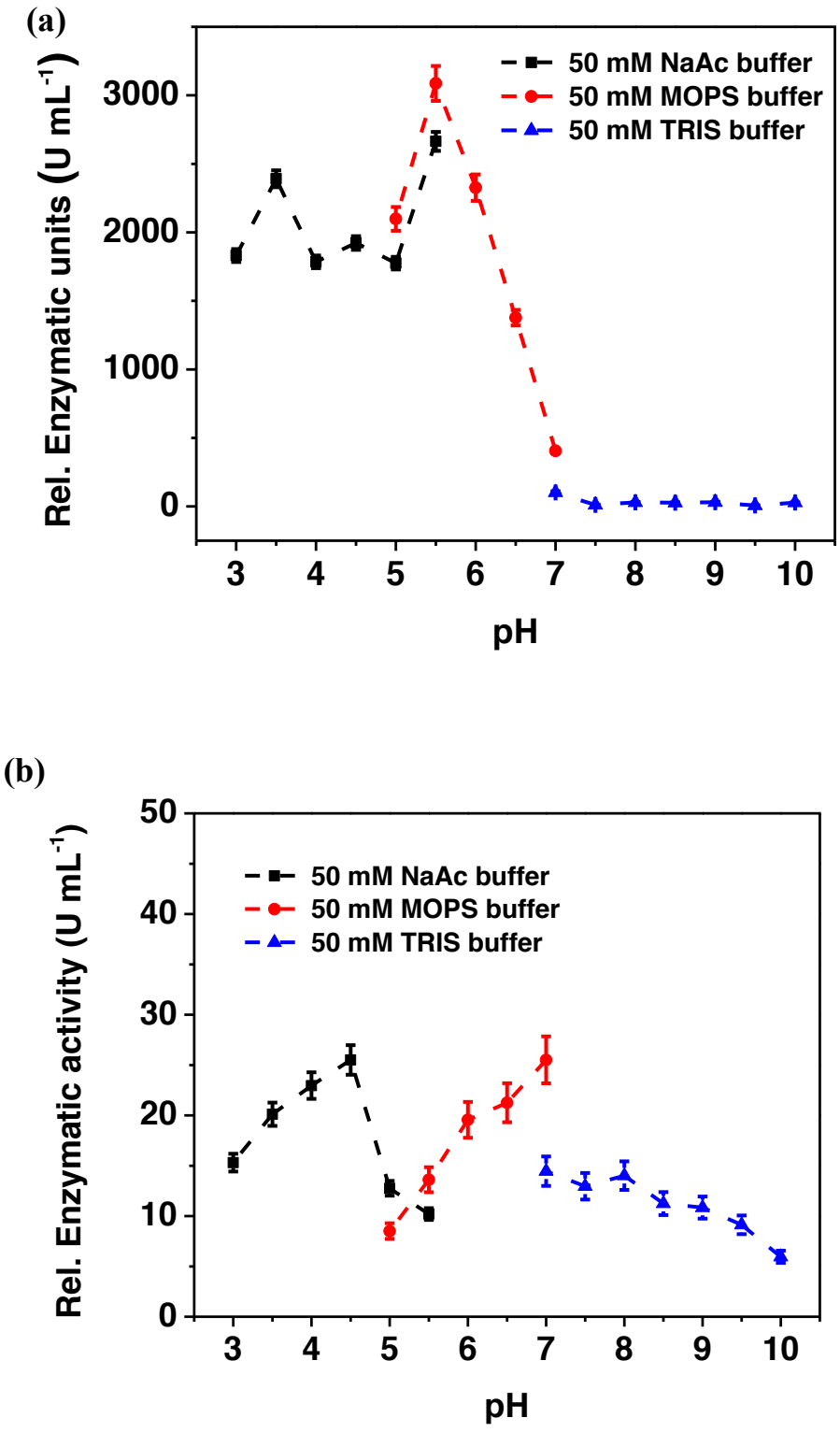

Figure 2. Dependance of the relative activities of **(a)** DCIP and **(b)** cyt *c* on pH carried out in 50 mM NaAc buffer (pH 3-5.5, black), 50 mM MOPS buffer (pH 5-7, red) and 50 mM TRIS buffer (pH 7-10, blue). Experimental conditions: [Fructose]: 30 mM, [cyt *c*]: 100 µM and [2,6-dichloroindophenol, DCIP]: 300 µM.

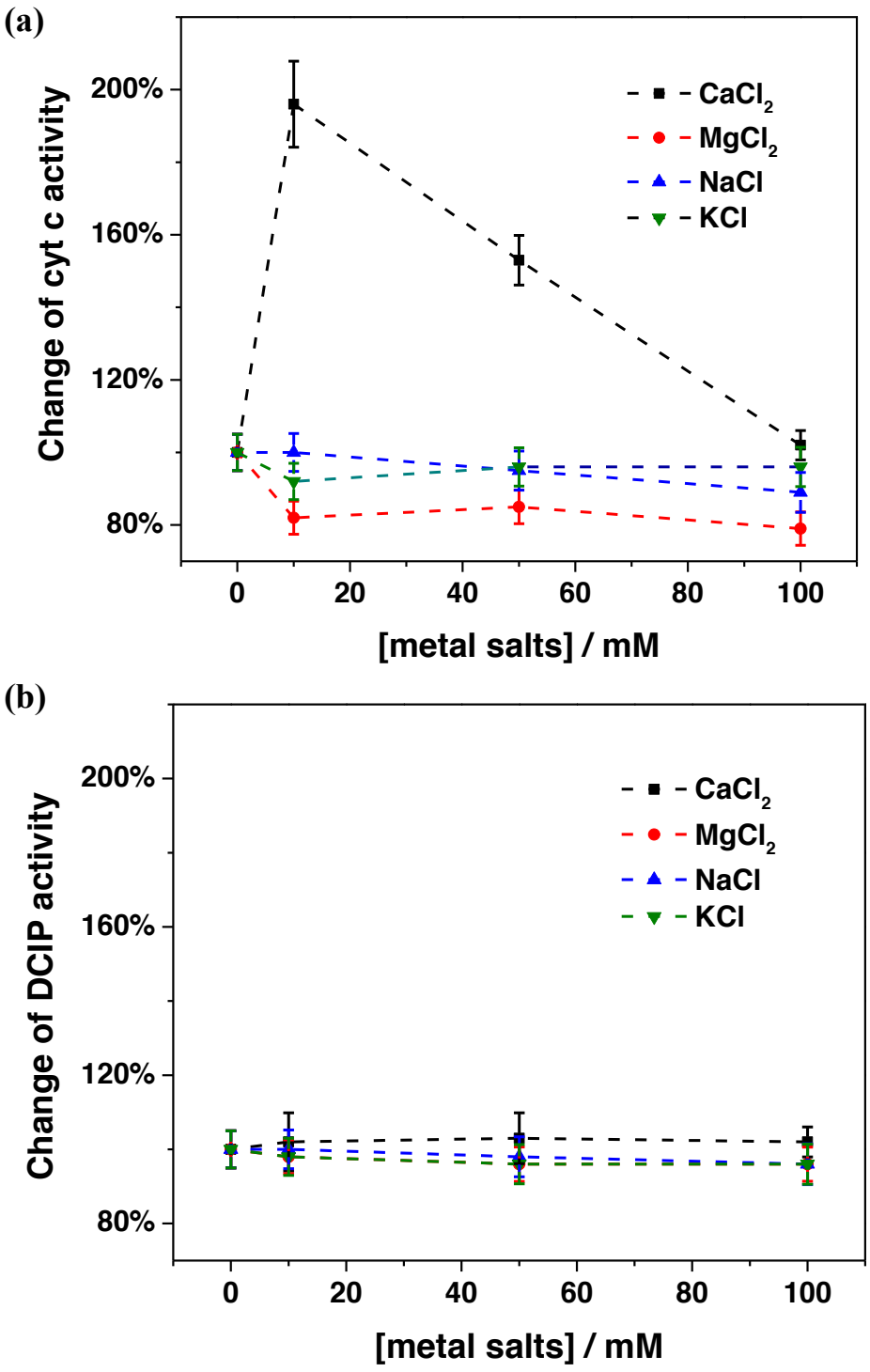

Figure 3 Dependence of the relative **(a)** cyt *c* and **(b)** DCIP activities on different concentrations of $CaCl_2$ (black), $MgCl_2$ (red), NaCl (blue) and KCl (green) in 50 mM NaAc buffer pH 4.5. Experimental conditions: [Fructose]: 30 mM, [cyt *c*]: 100 µM and [2,6-dichloroindophenol, DCIP]: 300 µM.

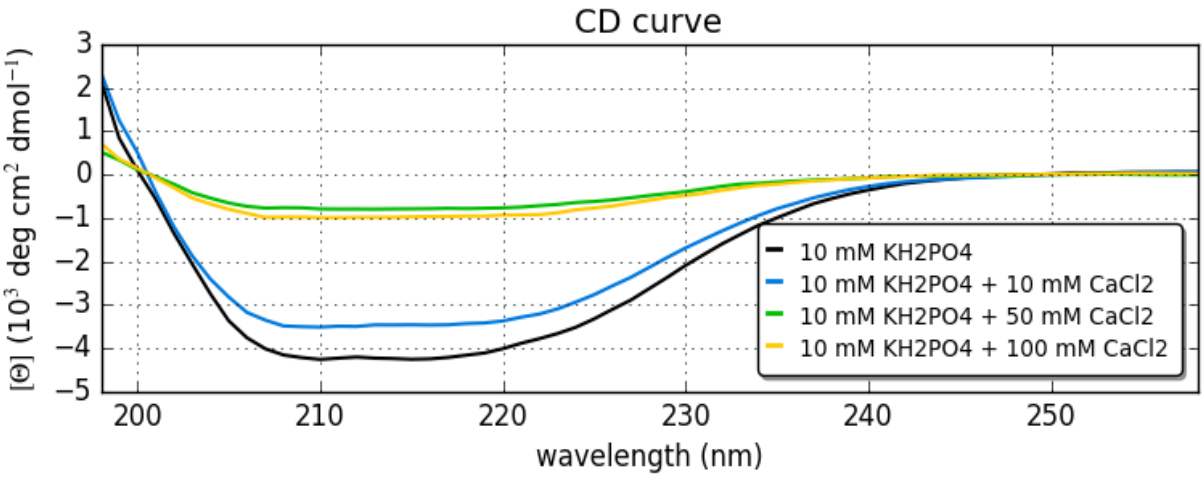

Figure 4 Circular dichroism (CD) spectra of FDH obtained in 10 mM KH_2PO_4 pH 4.5 at different Ca^{2+} concentrations: 0 mM (**black**), 10 mM (**blue**), 50 mM (**green**) and 100 mM $CaCl_2$ (**yellow**).

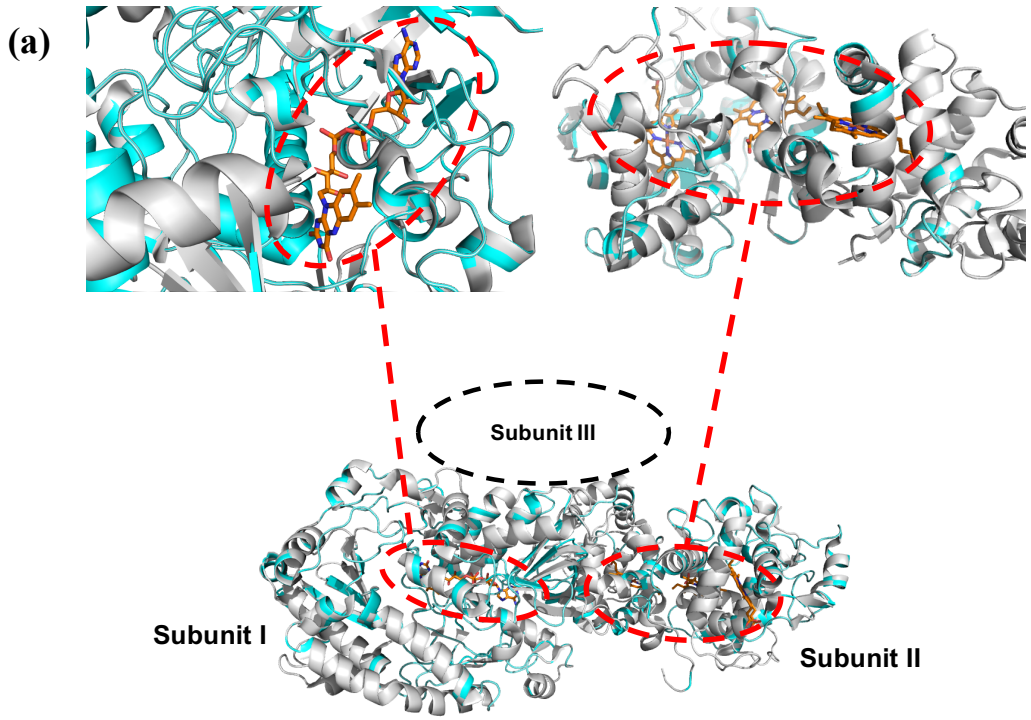

(b)

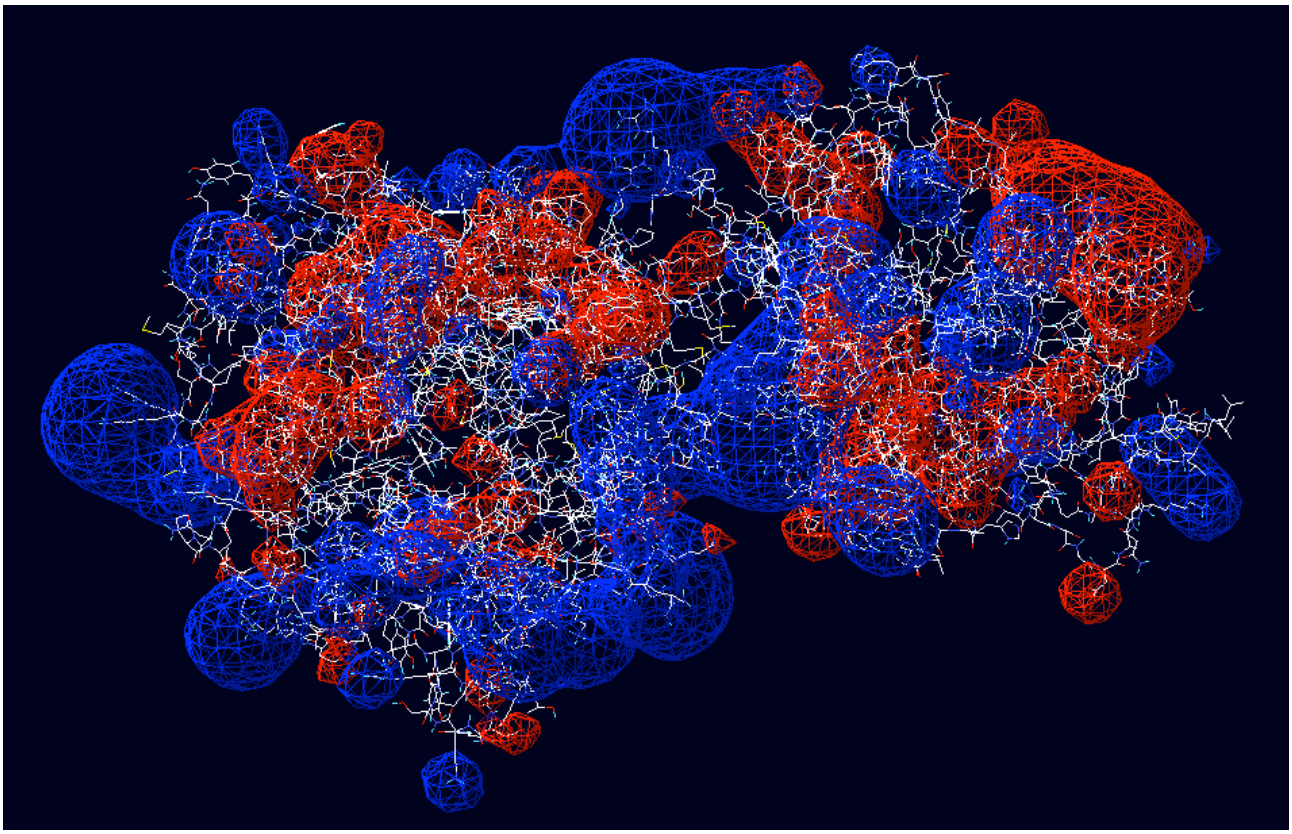

Figure 5 (a) Detailed representation of structural alignment between Subunit I of FDH (homology model, grey structure) and *Aspergillus niger* FAD-Glucose Dehydrogenase (PDB ID: 4ynt, light blue structure); and between Subunit II of FDH (homology model) and thiosulfate dehydrogenase (tsdba) from *Marichromatium purpuratum* "as2 isolated" form (PDB ID: 5lo9); **(b)** Electrostatic map of the Subunit I and II after docking obtained from the homology models.

Table 1. CD data obtained fitting CD spectra (Figure 4) performed in 10 mM KH_2PO_4 at pH 4.5 (**black**) increasing Ca^{2+} concentrations up to 10 mM (**blue**), 50 mM (**green**) and 100 mM $CaCl_2$ (**yellow**).

	10 mM KH_2PO_4 pH 4.5	**10 mM KH_2PO_4 pH 4.5 + 10 mM $CaCl_2$**	**10 mM KH_2PO_4 pH 4.5 + 50 mM $CaCl_2$**	**10 mM KH_2PO_4 pH 4.5 + 100 mM $CaCl_2$**
Alpha Helix	10.9	9.9	5.1	5.3
Antiparallel	34.2	34.6	36.3	36.2
Parallel	0.0	0.0	0.0	0.0
Turns	13.0	13.3	14.3	14.0
Others	41.9	42.2	44.2	44.4
RMSD	0.0149	0.0192	0.0283	0.0229
NRSMD	0.00969	0.01356	0.03911	0.02654

Paper VII

Enhanced Direct Electron Transfer of Fructose Dehydrogenase Rationally Immobilized on 2-Amino Anthracene Diazonium Cation Grafted Single-Walled Carbon Nanotube Based Electrode

Paolo Bollella[a,b], Yuya Hibino[c], Kenji Kano[c], Lo Gorton[b,*], Riccarda Antiochia[a,*]

[a]Department of Chemistry and Drug Technologies, Sapienza University of Rome P.le Aldo Moro 5, 00185 – Rome, Italy

[b]Department of Analytical Chemistry/Biochemistry, Lund University, P.O. Box 124, 221 00 – Lund, Sweden

[c]Division of Applied Life Sciences, Graduate School of Agriculture, Kyoto University, Sakyo, Kyoto 606-8502, Japan

ABSTRACT

In this paper, an efficient direct electron transfer (DET) reaction was achieved between fructose dehydrogenase (FDH) and a glassy carbon electrode onto which anthracene modified single walled carbon nanotubes were deposited. The SWCNTs were in situ activated with a diazonium salt synthesized through the reaction of 2-amino anthracene with $NaNO_2$ in acidic media (0.5 M HCl) for 5 min at 0 °C. After the in situ reaction, the 2-amino anthracene diazonium salt was electrodeposited by running cyclic voltammograms from +1000 mV to -1000 mV vs. $Ag|AgCl_{sat}$. The anthracene-SWCNT modified glassy carbon electrode was further incubated in a FDH solution to allow the enzyme to adsorb. Cyclic voltammograms of the FDH modified electrode revealed two couple of redox waves possibly ascribed to the heme c_1 and heme c_3 of the cytochrome domain. In the presence of 10 mM fructose two catalytic waves could clearly be seen and were correlated with the two heme *c*:s, with a maximum current density of 485 μA cm^{-2} at 0.4 V vs. $Ag|AgCl_{sat}$ at a sweep rate of 10 mVs^{-1}. In contrast, for the plain SWCNT modified glassy carbon electrode only one catalytic wave and one couple of redox waves were observed. Adsorbing FDH directly onto a glassy carnon electrode showed no non-turn over electrochemistry of FDH and in the presence of fructose only a slight catalytic effect could be seen. These differences can be explained by considering the hydrophobic pocket close to heme c_1 and heme c_3 of the cytochrome domain at which the anthracenyl aromatic structure could interact through π-π interactions with the aromatic side chains of the amino acids present in the hydrophobic pocket of FDH.

KEYWORDS: fructose dehydrogenase (FDH), 2-aminoanthracene (2-ANT), diazonium coupling, hydrophobic pocket, single-walled carbon nanotubes (SWCNTs)

INTRODUCTION

In the last decades, the mechanism of the direct electron transfer (DET) reactions of several redox proteins have been widely investigated in order to gain fundamental bioelectrochemical knowledge but also to develop 3rd generation biosensors and enzymatic fuel cells (EFCs) based on DET.[1-6] DET reactions have been observed both for smaller electron transfer redox proteins[7] such as cytochrome *c*[8], azurin[9], ferredoxin, as well as for a whole range of the larger more complex redox enzymes of great relevance in recent studies of biosensors and biofuel cells, e.g., hydrogenases[10-12] cellobiose dehydrogenase,[13-15] multi-copper oxidases,[16-18] peroxidases,[19-21] fructose dehydrogenase (FDH)[22-26], alcohol PQQ dehydrogenase[27-31], sulphite oxidase[32-33] etc. Nevertheless, several strategies to improve DET like the deglycosylation[34-39] or bioengineering of redox enzyme[40-41] and the electrode nanostructuration[42-43] by using both carbon or metal nanomaterials (e.g. carbon nabotubes, graphene, metal nanoparticles, highly porous gold etc.).[44-48]

Among the carbon nanomaterials, single-walled carbon nanotubes (SWCNTs) have a very well defined cylindrical geometry and are readily synthesized with a diameter in the nanometer range.[49] Their high conductance, tensile strength, and chemical stability have attracted much attention for the development of electronic devices.[50] They can be prepared by variety of methods, and recently, significant progress has been made in both their chemical functionalization and their manipulation.[51] Although graphitic side-wall functionalization will unavoidably lead to a disruption of the nanotube delocalized system, this offers a convenient and controllable means of tethering molecular species or proteins.[52-53] E.g., SWCNTs can be functionalized by using EDC-NHS covalent coupling, glutaraldehyde or other cross-linkers, or chemical modification with aryl diazonium salts etc.[54-56]

Covalent modification of carbon surfaces via electrochemically reductive adsorption of aryl diazonium salts has attracted wide attention for the development of new electrode platforms used both as biosensors and as EFCs.[57-60] The modification of electrodes with aryl diazonium salts is achieved by a one electron reductive adsorption of the aryl diazonium salt either in acetonitrile or aqueous acid solutions with a pH below 2.[61] The reductive adsorption of aryl diazonium salts can be performed through the use of cyclic voltammetry.[62]

This approach to nanostructure the electrode surface has been exploited by Armstrong and co-workers, where 2-anthracenecarboxylic acid was electrodeposited onto a multi-walled carbon nanotube (MWCNT) modified electrode surface to orient laccase from *Trametes versicolor* through the π-π interaction between the anthracenyl groups available onto the electrode surface and the aromatic groups present in the hydrophobic pocket of the enzyme, greatly facilitating an enhanced

DET reaction without enzyme activity loss.[63] This approach has been widely used in the last 10 years to obtain high potential cathode for EFCs.[64-68] In this work we consider a linker able to penetrate and remain in the hydrophobic region of FDH in a similar way as was used for multi-copper oxidases and thus provide the equivalent of an 'electric plug' to achieve a faster DET, useful for biosensors and EFCs development.[69]

Fructose dehydrogenase (FDH, EC 1.1.99.11) from *Gluconobacter japonicus* has been widely exploited to develop biosensors based on mediated and direct electron transfer as well as bioanode for enzymatic fuel cells (EFCs).[23, 70-71] FDH is a membrane-bound flavocytochrome oxidoreductase also belongs to the hemoflavoproteins family.[72] FDH from *Gluconobacter japonicus* NCBR 3260 is a heterotrimeric membrane-bound enzyme complex with a molecular mass of 146.4 kDa, consisting of three subunits: viz., subunit I, which is equivalent to the catalytic dehydrogenase domain, DH_{FDH}, with a covalently bound flavin adenine dinucleotide (FAD) cofactor, where D-(-)-fructose is involved in a $2H^+/2e^-$ oxidation to 5-dehydro-D-(-)-fructose; subunit II, which is equivalent to the cytochrome domain, CYT_{FDH}, which acts as a "built-in" electron transfer domain[27] with three heme *c* moieties covalently bound to the enzyme scaffold and two of them are involved in a sequential one by one electron transfer pathway[23, 73]; and subunit III, which is not involved in the electron transfer but plays a key role for the enzyme complex stability.[74-75]

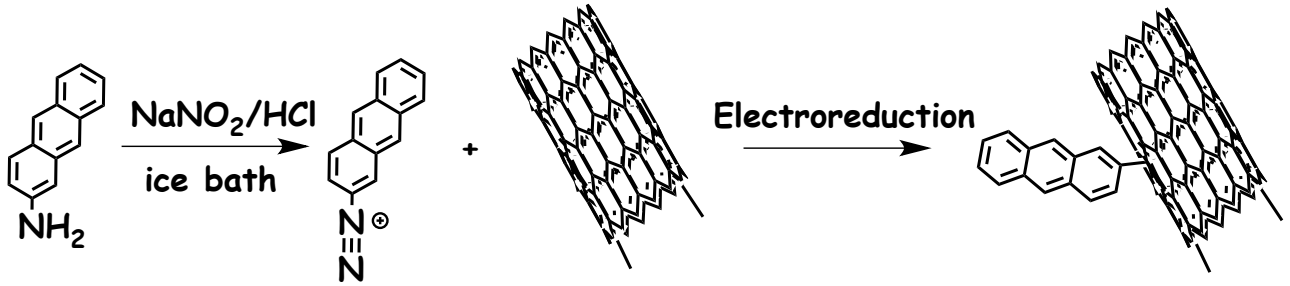

Figure 1. Schematic representation of the reaction pathway and synthesis of 2-aminoanthracene diazonium (2-ANT) salt and electroreduction on single-walled carbon naotubes (SWCNTs) performed by using cyclic voltammetry from +1000 mV to -1000 mV vs. $Ag|AgCl_{sat}$ at 100 mV s^{-1}.

In this paper, we aim at obtaining an efficient DET reaction pathway between FDH and a SWCNTs/GC electrode further modified through diazonium coupling of an aromatic compound. In particular, we have electrodeposited anthracene onto SWCNTs through electroreduction of 2-aminoanthracene diazonium (2-ANT) by using cyclic voltammetry from +1000 mV to -1000 mV vs. $Ag|AgCl_{sat}$ at 100 mV s^{-1}, according to the electrochemical reduction mechanism reported in Figure 1. Next the electrode was further modified through drop-casting of FDH allowing the interaction between the aromatic anthracenyl groups available onto the electrode surface and the

hydrophobic pocket within the enzyme. This region is located on subunit II of FDH leading to the improvement of DET reactions of the enzyme probably shortening the distance between the prosthetic groups (e.g. heme), deeply buried, and the electrode surface.[75] The redox potential of each heme has been carefully determined both by cyclic and square wave voltammetry in order to establish which heme was highly exposed toward the electrode surface with this modification. Finally, the kinetics and analytical properties of 2-ANT/SWCNTs/GC have been thoroughly investigated to prove the advantages of using this electrode platform both as 3rd generation biosensor and EFCs bioanode.

EXPERIMENTAL SECTION

Chemicals

2-aminoanthracene (2-ANT), sodium nitrite ($NaNO_2$), hydrochloric acid (HCl), D-(-)-fructose, sodium acetate (NaAc), sodium hydroxide (NaOH), single-walled carbon nanotubes (SWCNTs) were purchased from Sigma Aldrich (St. Louis, MO, USA). D-Fructose dehydrogenase from *Gluconobacter japonicus* (FDH; EC 1.1.99.11) was purified from the culture supernatant of *Gluconobacter japonicus* NBRC 3260 obtained from the National Institute of Technology and Evaluation (Nishinomiya, Hyogo Pref., Japan), and solubilized in PBS buffer pH 6 (50~500 mM) containing 0.1 mM 2-mercaptoethanol and 0.1% v/v Triton X-100 (volumetric activity measured with potassium ferricyanide at pH 4.5 = 420±30 U mL^{-1}, specific activity = 250±30 U mg^{-1}, protein concentration = 1.7±0.2 mg mL^{-1}).[72] All solutions were prepared using Milli-Q water (R = 18.2 MΩ cm at 25 °C; TOC < 10 μg L^{-1}, Millipore, Molsheim, France).

Electrode Modification

Glassy carbon (GC) electrodes (Bioanalytical Systems Inc., West Lafayette, IN, USA, Ø=3 mm; $A_{geometric}$=0.073 cm^2) were polished with aqueous alumina (Al_2O_3) slurry (Struers, Copenhagen, Denmark) solution in decreasing size, 1 and 0.1 mm, for 5 min and ultra-sonicated in Milli-Q water for 5 min and dried under a stream of N_2.

FDH/GC electrode – 3 μL of an FDH solution were drop-cast onto the electrode surface.

FDH/2-ANT/GC electrode – GC electrode was immersed into an ice cold 1 mM solution of 2-aminoanthracene (2-ANT) diazonium cation *in situ* generated, purged with argon for 20 min to achieve anaerobicity. After, the aryl diazonium cation was electrochemically reduced by scanning the potential between +1000 mV and – 1000 mV vs. $Ag|AgCl_{sat}$ at 100 mV s^{-1} for two cycles.

Finally, the electrode was abundantly rinsed with Milli-Q water, dried under a stream of N_2 and 3 µL FDH solution were drop-cast onto the so modified electrode surface.[76]

FDH/SWCNTs/GC electrode - 3 µL of an SWCNTs aqueous suspension (30 mg mL^{-1}), previously ultra-sonicated for 1 week, was drop-cast onto the electrodes and let it dry at room temperature. Thus, 3 µL of an FDH solution were drop-cast onto the electrode surface.

FDH/2-ANT/SWCNTs/GC electrode - 3 µL of an SWCNTs aqueous suspension (30 mg mL^{-1}), previously ultra-sonicated for 1 week, was drop-cast onto the electrodes and let it dry at room temperature. The modified electrode was further immersed into the 2-aminoanthracene (2-ANT) diazonium cation solution and electrochemically reduced as above. After rinsing, 3 µL of an FDH solution were drop-cast onto the electrode surface.[76]

The *in situ*-generated 2-aminoanthracene diazonium cation solution was prepared by mixing a 0.5 mM HCl:ethanol (50 % v/v) solution containing 1 mM 2-aminoanthracene and 5 mM $NaNO_2$ for 5 min, under stirring.

SEM Characterization

Scanned electron microscopy (SEM) measurements were performed with a JSM-7600F Schottky Field Emission Scanning Electron Microscope (JEOL Nordic AB, Sollentuna, Sweden). All samples were prepared according to the electrode modification protocol, reported above, using glassy carbon plates (25 x 25 x 1 mm, ALS Co. Ltd., Tokyo, Japan) instead of GC electrodes. In particular, two samples namely SWCNT/GC and 2-ANT/SWCNT/GC were analysed. The samples were paced on a clip SEM sample holder (JEOL Nordic AB).

Electrochemical measurements and apparatus

Cyclic voltammetry (CV) experiments were carried out using a Autolab potentiostat (model PGSTAT30, Metrohm Autolab B.V. Ecochemie, Utrecht, The Netherlands) equipped with GPES, version 4.9. A conventional three-electrode electrochemical cell was used for all experiments performed with an Ag|AgCl (sat. KCl) as reference electrode, a platinum wire as counter electrode and a modified glassy carbon electrode as working electrode. Square wave voltammetry (SWV) experiments were performed using a PalmSens potentiostat (model Emstat2, Palm Instruments BV, Utrecht, The Netherlands) equipped with PSTrace, version 4.5. All measurements were performed under temperature control by using a cryostatic bath (T ± 0.01 ºC, LAUDA RM6, Delran, NJ, USA).

Flow injection experiments were performed with a three electrode potentiostat (Zäta Elektronik, Höör, Sweden). The enzyme-modified GC electrode, inserted into a wall-jet flow-through

amperometric cell[77] and positioned at a constant distance (1–2 mm) from the inlet nozzle, was used as working electrode, an Ag|AgCl (0.1 KCl) electrode as reference electrode and a platinum wire as counter electrode. The electrochemical cell was connected to a flow injection system consisting of a peristaltic pump (Gilson, Villier-le-Bel, France) and a six-port valve electrical injector (Rheodyne, Cotati, CA, USA). A 50 µl aliquot of the substrate was applied by a loop mounted onto the injector. The resulting electrical current was recorded on a strip chart recorder (Kipp & Zonen, Utrecht, The Netherlands).

RESULTS AND DISCUSSION

Electrochemical reduction of in-situ generated 2-aminoanthracene diazonium cation

GC and SWCNTs/GC electrodes were grafted with in-situ generated 2-aminoanthracene diazonium cations as previously described in order to access directly the hydrophobic region of FDH located in the subunit II close to the heme *c* moieties and enhance the DET reaction of FDH occurring at the electrode surface. After the preliminary in-situ generation of the 2-aminoanthracene diazonium cations, the electrochemical reduction was performed by scanning the potential between +1000 mV and – 1000 mV vs. Ag|AgClsat at 100 mV s^{-1} for two cycles as outlined in Figure 1a and b, on GC and GC/SWCNTs, respectively.

Figure 2A and B present CVs showing the electrochemical reduction of the 2-aminoanthracene diazonium salt on GC and SWCNTs/GC, respectively. In the first case, the CV showed one wave in the first scan (black curve) with a potential close to -0.090 V vs. $Ag|AgCl_{sat}$, which partially disappeared in the second scan (red curve), indicating that the GC surface was partially covered by 2-aminoanthracene diazonium salt. In the latter case, the CV showed two waves in the first scan (black curve) with a potential close to +0.070 V and -0.145 V vs. $Ag|AgCl_{sat}$, which totally disappeared in the second scan (red curve), indicating that the SWCNTs/GC surface has been totally covered by 2-aminoanthracene diazonium salt. This aryl amine provides a rigid, hydrophobic, π-electron conductor with the right length, width and projection angle to insert snugly into the hydrophobic region of FDH.

The SWCNTs/GC electrodes were characterized with SEM microscopy before and after the electrodeposition of 2-aminoanthracene diazonium salt in order to investigate possible morphological changes occurring at the electrode surface, as shown in Figure 2C and D. Unfortunately, it was not possible to appreciate any difference because the instrument could not reach the atomic resolution to distinguish between the anthracenyl groups and the SWCNTs.

Cyclic Voltammetric Characterization of GC Modified Electrodes

To investigate the role of the anthracenyl groups on the catalytic current density, several CV experiments have been performed in absence and in presence of D-(-)-fructose. In several papers, it has been proven that the orientation of the enzyme is a key issue to obtain an efficient DET reaction due to the enzyme structure, especially considering the access to a particular part of the enzyme (e.g. a hydrophobic region) giving a correct immobilization strategy beneficial both for the development of biosensors and EFCs.[63-65]

Figure 3A shows the CV for FDH/GC modified electrode in non-turnover conditions in a 50 mM NaAc buffer at pH 4.5, where it is not possible to observe any redox wave related to a DET reaction of heme *c* probably due to the random orientation of FDH onto the electrode surface and the low roughness of glassy carbon electrode not allowing a high enzyme loading. After the addition of 10 mM D-(-)-fructose, the FDH/GC modified electrode showed a slight electrocatalytic wave starting at E_{ONSET} = -0.058 V vs. $Ag|AgCl_{sat}$ rising up to 18 μA cm^{-2} at 0.4 V vs. $Ag|AgCl_{sat}$, as shown in Figure 3B.

Afterwards, the GC electrode was modified electrodeposition of the 2-aminoanthracene diazonium cation in order to highlight the effect of the anthracenyl group on the orientation of FDH. The CV of the FDH/2-ANT/GC modified electrode in 50 mM NaAc at pH 4.5 is depicted in Figure 3C, showing a couple of redox waves with a formal potential of $E^{0'}$= -0.002 V vs. $Ag|AgCl_{sat}$ and another wave in the forward scan at a potential of E= +0.140 vs. $Ag|AgCl_{sat}$, which are actually close to the values reported in literature[73] for heme c_3 (E=-0.010 Vvs. $Ag|AgCl_{sat}$) and heme c_1 ($E^{0'}$= +0.150 V vs. $Ag|AgCl_{sat}$), respectively. These results could be ascribed to the interaction between the anthracenyl groups exposed onto the electrode surface and the hydrophobic region of FDH located on the subunit II of the enzyme. However, the modified electrode was tested in the presence of the substrate showing an electrocatalytic wave starting at E_{ONSET}= + 0.028 V vs. $Ag|AgCl_{sat}$ rising up to 13.3 μA cm^{-2} at 0.4 V vs. $Ag|AgCl_{sat}$, as shown in Figure 3D. Despite the great results obtained in non-turnover conditions for FDH/2-ANT/GC modified electrode, the electrocatalytic wave showed a lower current density values compared to that of the FDH/GC electrode probably due to the low amount of anthracenyl groups grafted onto the electrode surface not enough to orient all FDH molecules and the low roughness of the electrode surface.

In order to enhance the roughness of the electrode surface, the following experiments have been performed modifying the GC electrodes with SWCNTs. Figure 4A shows the CV for an FDH/SWCNTs/GC modified electrode in non-turnover conditions (50 mM NaAc buffer at pH 4.5), where it is possible to observe a couple of redox waves with a formal potential of $E^{0'}$= +0.142 V vs. $Ag|AgCl_{sat}$ close to the formal potential of heme c_1 ($E^{0'}$= +0.150 V vs. $Ag|AgCl_{sat}$), as reported in

the literature[73]. This result is ascribable to the random orientation of FDH onto the electrode surface and to the position of heme c_1, which is probably close to the edge of the enzyme. After the addition of 10 mM D-(-)-fructose, the FDH/SWCNTs/GC electrode showed a great electrocatalytical wave starting at E_{ONSET}= -0.052 V vs. Ag|$AgCl_{sat}$ rising up to 223 μA cm^{-2} at 0.4 V vs. Ag|$AgCl_{sat}$, as shown in Figure 4A. The great electrocatalytical wave is probably due to the high enzyme loading directly related with the enhanced roughness of the electrode surface achieved with the deposition of the SWCNTs.

Finally, the CV of an FDH/2-ANT/SWCNTs/GC modified electrode in 50 mM NaAc at pH 4.5 is depicted in Figure 4B, showing two couples of redox waves with a formal potential of $E^{0'}$= -0.006 V vs. Ag|$AgCl_{sat}$ and of $E^{0'}$= +0.169 V vs. Ag|$AgCl_{sat}$, respectively. In both cases, the E°' values of the redox waves are in agreement with the E°' of heme c_3 (E=-0.010 V vs. Ag|$AgCl_{sat}$) and heme c_1 ($E^{0'}$= +0.150 V vs. Ag|$AgCl_{sat}$)[73]. Afterwards, the modified electrode was tested in the presence of substrate, showing a larger electrocatalytical wave compared to that of the SWCNTs/GC starting at E_{ONSET}= -0.095 V vs. Ag|$AgCl_{sat}$ rising up to 485 μA cm^{-2} at 0.4 V vs. Ag|$AgCl_{sat}$, as shown in Figure 4B. In the overall electrocatalytic wave, it is possible to clearly distinguish two electrocatalytic waves ascribable to heme c_1 and c_3 highlighting the contribution of each heme to the electron transfer mechanism and therefore also individually to the electrocatalytical wave. This result could be explained with the enhanced roughness of the electrode surface improving the enzyme loading and the correct orientation of FDH due to the interaction between the anthracenyl group and the hydrophobic part of subunit II. In particular, the interaction occurs between the aromatic rings of the anthracenyl group and the aromatic rings available on the side chain of the amino acids present into the hydrophobic portion of subunit II (π-π interaction).[78]

The effect of the scan rate of the CVs was investigated for the non-turn over DET reaction of the immobilized FDH at the SWCNTs/GC and 2-ANT/SWCNTs/GC electrodes. The CVs at different scan rates for FDH/SWCNTs/GC and FDH/2-ANT/SWCNTs/GC are presented in Figure 4A and B, respectively. It is possible to see that the anodic and cathodic peak current densities were linearly dependent on the scan rate in the range between 2 and 100 mV s^{-1}, shown in the insets of both Figure 4A and B, indicating a surface controlled electrochemical process.

Further analysis of the CVs allowed to calculate the apparent heterogeneous electron transfer rate constants (k_s) for the redox reaction between FDH and SWCNTs/GC, considering the peak current for heme c_1 (Figure 5A), and 2-ANT/SWCNTs/GC, considering both peak currents for heme c_1 and c_3 (Figure 5B), using Laviron's method.[79] From the slopes of the linear part of the trumpet plot (data not shown), the α values can be determined and found to be 0.43 for the SWCNTs/GC electrode, 0.60 (heme c_1) and 0.37 (heme c_3) for the 2-ANT/SWCNTs/GC modified electrode. Thereafter, the

k_s values were calculated according to Laviron's derivation of the Butler-Volmer theory (Eq. (1)) and resulted in 2.5 ± 0.1 s^{-1} for the SWCNTs/GC electrode, and 3.7 ± 0.3 s^{-1} (heme c_1) and 4.2 ± 0.6 s^{-1} (heme c_3) for the 2-ANT/SWCNTs/GC electrode (ν between 2 and 100 mV s^{-1}):

$$\log k_s = \alpha \log(1-\alpha) + (1-\alpha)\log(RT/nF\upsilon) - \alpha(1-\alpha)nF\Delta Ep/2.3RT \quad (1)$$

where α is the electron transfer coefficient, n is the number of electron, ΔEp is the separation of the redox peak potentials, ν the scan rate and F, T and R have their usual meanings (F=96.495 C mol^{-1}; T=298 K; R=8.31 J mol^{-1} K^{-1}).[79]

By integrating of the redox peaks relative to the DET of heme *c* depicted in Figure 5A (scan 2 mVs^{-1}) for the SWCNTs/GC electrode and in Figure 5B (scan 2 mVs^{-1}) for the 2-ANT/SWCNTs/GC electrode, it was possible to evaluate the enzyme surface coverage using the Faraday's law[80] (Equation (2)):

$$\Gamma_T = Q/(nFA) \quad (2)$$

where Γ_T is the total surface concentration of electroactive enzyme (mol cm^{-2}), A the electrode area (cm^2), F the Faraday's constant (96 495 C mol^{-1} of electrons), Q the charge under the redox wave and n the number of electrons. Γ_T resulted to be 19.4±0.7 nmol cm^{-2} and 9.1±0.3 nmol cm^{-2} for the FDH/SWCNTs/GC electrode and the FDH/2-ANT/SWCNTs/GC electrode, respectively. Despite the lower amount of FDH immobilized onto the 2-ANT/SWCNTs/GC electrode, this electrode showed better performance in terms of electron transfer rate, which resulted in a twice higher value compared to that of the SWCNTs/GC electrode. This result could be ascribed to a correct orientation of the FDH molecules on the 2-ANT/SWCNTs/GC electrode compared to the random orientation of FDH on the SWCNTs/GC electrode, achieved through the interaction between the anthracenyl groups immobilized onto the electrode surface and the aromatic groups present in the hydrophobic portion of subunit II of FDH.

SWV characterization of GC modified electrodes

After careful CV characterization performed both in the absence and the presence of substrate, several SWV experiments were performed in 50 mM NaAc at pH 4.5 with the different electrode platforms to unequivocally prove the role of the anthracenyl groups on the orientation of FDH through its hydrophobic region, as shown in Figure 6. The peaks herein reported were integrated

allowing the determination of the width at half-height (FWHM), which is proportional to the number of electrons involved in the faradic process according to equation (3):

$$FWHM = 3.53RT/nF \quad (3)$$

where F, T and R have their usual meanings (F=96.495 C mol^{-1}; T=298 K; R=8.31 J mol^{-1} K^{-1}) and n is the number of electrons involved in the faradic process.[81] By considering the FDH/2-ANT/SWCNTs/GC electrode, it was possible to clearly identify two redox peaks both ascribable to heme *c*:s, since the FWHM resulted in values close to 90 mV (Table 1). Both peak potentials were actually close to the values reported in the literature for heme c_1 and heme c_3. Moreover, the other electrode platforms showed only redox peaks related to heme c_1 due to the random orientation of FDH onto the SWCNTs/GC and the GC electrodes and the low roughness of the electrode surface as in the case of the 2-ANT/GC electrode.

All the electrochemical parameters determined using SWV have been summarised in Table 1, showing unequivocally the role of the anthracenyl groups for the orientation of FDH allowing a deeper investigation of the internal electron transfer (IET), since different co-factors seem to be involved in the DET mechanism according to the orientation.[78]

Kinetic characterization of GC modified electrodes

The amperometric response to fructose was studied by injecting fructose solutions at different concentrations by using the flow injection analysis (FIA) system, in order to investigate the electroanalytical and kinetic parameters of the FDH/2-ANT/SWCNTs/GC electrode platform. The FDH/2-ANT/SWCNTs/GC electrode showed the shortest response time (3 s), probably due to the correct orientation of FDH onto the electrode surface through the π-π interaction between the anthracenyl groups and the hydrophobic region of FDH. Moreover, the calibration curve showed a linear range between 0.05 and 5 mM (R^2 = 0.998, n = 5) with a sensitivity of 47 ± 1 μA mM^{-1} cm^{-2}, as shown in the inset of Figure 7A. The detection limit for the FDH/2-ANT/SWCNTs/GC electrode was found to be 0.9 μM, calculated using the relation 3σ/S, where σ is the absolute standard deviation of the intercept and S is the slope of the calibration curve. The analytical performance of the FDH/2-ANT/SWCNTs/GC electrode and the kinetic parameters are listed in Table 2. The apparent kinetic parameters (J_{max}, K_M^{app}) are in good agreement with the values reported in the literature for nanostructured electrodes.[22, 74, 82]

Finally, the stability and lifetime of the FDH/2-ANT/SWCNTs/GC electrode was evaluated using the FIA system by monitoring the signal decrease within 60 days when the biosensor is used for one

measurement per day, as shown in Figure 7B. The modified biosensor seems to retain about 90% of its initial activity after 60 days, probably due to the stability of the enzyme layer directly related to the correct orientation of FDH onto the electrode surface and the strength of the π-π interaction between the anthracenyl groups and the aromatic groups in the side chain of the amino acids present in the hydrophobic region[78] as was previously also shown for laccase[63].

CONCLUSIONS

We demonstrate unequivocally the possibility to access the hydrophobic region of FDH by exploiting the π-π interaction between an anthracenyl group immobilized onto the electrode surface and the aromatic groups in the side chain of the amino acids present in the hydrophobic region. This electrode modification is easy to perform and time-saving. Furthermore, the FDH/2-ANT/SWCNTs/GC electrode platform showed two clearly separated electrocatalytic waves ascribable to heme c_1 and heme c_3, which play key roles in the ET mechanism with the enzyme in the current orientation. The overall electrocatalytic wave for the proposed electrode platform resulted in a current density of 485 μA cm^{-2} at 0.4 V vs. $Ag|AgCl_{sat}$, underling the positive features of this electrode modification both as a potential fructose biosensor, showing fast-response time, a great stability (about 90% of retained signal after 60 days), selectivity and sensitivity (47 ± 1 μA mM^{-1} cm^{-2}) with the lowest detection limit (0.9 μM), or EFCs bioanode considering the great electrocatalytical wave and the low E_{ONSET} close to -100 mV vs. $Ag|AgCl_{sat}$.

ACKNOWLEDGMENTS

Dr. Crispin Hetherington (Lund University, Department of Chemistry, Centre for Analysis and Synthesis, National Center for High-Resolution Electron Microscopy nCHREM) is greatly ackonowledged for the SEM characterization of the highly porous gold electrodes. The authors thank the following agencies for financial funding: The Swedish Research Council (Vetenskapsrådet project 2014-5908), the European Commission (project "Bioenergy" FP7-PEOPLE-2013-ITN-607793) and a scholarship of the Erasmus+ Project Unipharma-Graduates, promoted by a Consortium of Italian Universities and coordinated by Sapienza University of Rome.

AUTHORS INFORMATION:

Corresponding authors:

Prof. Riccarda Antiochia

e-mail: riccarda.antiochia@uniroma1.it

Prof. Lo Gorton

e-mail: lo.Gorton@biochemistry.lu.se

REFERENCES

1. Frew, J. E.; Hill, H. A. O., *The FEBS Journal* 1988, 172 (2), 261-269.
2. Gorton, L.; Lindgren, A.; Larsson, T.; Munteanu, F.; Ruzgas, T.; Gazaryan, I., *Analytica Chimica Acta* 1999, 400 (1), 91-108.
3. Leger, C.; Bertrand, P., *Chemical Reviews* 2008, 108 (7), 2379-2438.
4. Ferapontova, E. E.; Shleev, S.; Ruzgas, T.; Stoica, L.; Christenson, A.; Tkac, J.; Yaropolov, A. I.; Gorton, L. In *Electrochemistry of Nucleic Acids and Proteins: Towards Electrochemical Sensors for Genomics and Proteomics*, Palecek, E., Scheller, F., Wang, J., Eds. 2005; Vol. 1, pp 517-598.
5. Cracknell, J. A.; Vincent, K. A.; Armstrong, F. A., *Chemical Reviews* 2008, 108 (7), 2439-2461.
6. Falk, M.; Blum, Z.; Shleev, S., *Electrochimica Acta* 2012, 82, 191-202.
7. Armstrong, F. A.; Hill, H. A. O.; Walton, N. J., *Accounts of Chemical Research* 1988, 21 (11), 407-413.
8. Aghamiri, Z. S.; Mohsennia, M.; Rafiee-Pour, H.-A., *Talanta* 2018, 176, 195-207.
9. Alessandrini, A.; Corni, S.; Facci, P., *Phys. Chem. Chem. Phys.* 2006, 8 (38), 4383-4397.
10. Vincent, K. A.; Parkin, A.; Armstrong, F. A., *Chemical Reviews* 2007, 107 (10), 4366-4413.
11. Liebgott, P.-P.; Leroux, F.; Burlat, B.; Dementin, S.; Baffert, C.; Lautier, T.; Fourmond, V.; Ceccaldi, P.; Cavazza, C.; Meynial-Salles, I.; Soucaille, P.; Fontecilla-Camps, J. C.; Guigliarelli, B.; Bertrand, P.; Rousset, M.; Leger, C., *Nature Chemical Biology* 2010, 6 (1), 63-70.
12. Lojou, E., *Electrochimica Acta* 2011, 56 (28), 10385-10397.
13. Ludwig, R.; Harreither, W.; Tasca, F.; Gorton, L., *Chemphyschem* 2010, 11 (13), 2674-2697.
14. Ludwig, R.; Ortiz, R.; Schulz, C.; Harreither, W.; Sygmund, C.; Gorton, L., *Analytical and Bioanalytical Chemistry* 2013, 405 (11), 3637-3658.
15. Bollella, P.; Ludwig, R.; Gorton, L., *Appl. Mater. Today* 2017, 9, 319-332.
16. Shleev, S.; Tkac, J.; Christenson, A.; Ruzgas, T.; Yaropolov, A. I.; Whittaker, J. W.; Gorton, L., *Biosensors and Bioelectronics* 2005, 20 (12), 2517-2554.
17. Shleev, S.; El Kasmi, A.; Ruzgas, T.; Gorton, L., *Electrochemistry Communications* 2004, 6 (9), 934-939.
18. Christenson, A.; Dimcheva, N.; Ferapontova, E. E.; Gorton, L.; Ruzgas, T.; Stoica, L.; Shleev, S.; Yaropolov, A. L.; Haltrich, D.; Thorneley, R. N. F.; Aust, S. D., *Electroanalysis* 2004, 16 (13-14), 1074-1092.
19. Ruzgas, T.; Csöregi, E.; Emnéus, J.; Gorton, L.; Marko-Varga, G., *Analytica Chimica Acta* 1996, 330 (2-3), 123-138.
20. Lindgren, A.; Ruzgas, T.; Gorton, L.; Csöregi, E.; Ardila, G. B.; Sakharov, I. Y.; Gazaryan, I. G., *Biosensors and Bioelectronics* 2000, 15 (9), 491-497.
21. Ferapontova, E. E., *Electroanalysis* 2004, 16 (13-14), 1101-1112.
22. Kamitaka, Y.; Tsujimura, S.; Kano, K., *Chemistry letters* 2007, 36 (2), 218-219.
23. Kawai, S.; Yakushi, T.; Matsushita, K.; Kitazumi, Y.; Shirai, O.; Kano, K., *Electrochemistry Communications* 2014, 38, 28-31.
24. Khan, G. F.; Kobatake, E.; Shinohara, H.; Ikariyama, Y.; Aizawa, M., *Analytical Chemistry* 1992, 64 (11), 1254-1258.
25. Khan, G. F.; Shinohara, H.; Ikariyama, Y.; Aizawa, M., *Journal of Electroanalytical Chemistry* 1991, 315 (1-2), 263-273.
26. Kamitaka, Y.; Tsujimura, S.; Setoyama, N.; Kajino, T.; Kano, K., *Physical Chemistry Chemical Physics* 2007, 9 (15), 1793-1801.
27. Ikeda, T.; Kobayashi, D.; Matsushita, F.; Sagara, T.; Niki, K., *Journal of Electroanalytical Chemistry* 1993, 361 (1-2), 221-228.

28. Ramanavicius, A.; Habermuller, K.; Csoregi, E.; Laurinavicius, V.; Schuhmann, W., *Analytical Chemistry* 1999, 71 (16), 3581-3586.
29. Aquino Neto, S.; Suda, E. L.; Xu, S.; Meredith, M. T.; De Andrade, A. R.; Minteer, S. D., *Electrochim. Acta* 2013, 87, 323-329.
30. Takeda, K.; Matsumura, H.; Ishida, T.; Samejima, M.; Igarashi, K.; Nakamura, N.; Ohno, H., *Bioelectrochemistry* 2013, 94, 75-78.
31. Yakushi, T.; Matsushita, K., *Appl. Microbiol. Biotechnol.* 2010, 86 (5), 1257-1265.
32. Ferapontova, E. E.; Ruzgas, T.; Gorton, L., *Analytical Chemistry* 2003, 75 (18), 4841-4850.
33. Zeng, T.; Pankratov, D.; Falk, M.; Leimkuehler, S.; Shleev, S.; Wollenberger, U., *Biosensors & Bioelectronics* 2015, 66, 39-42.
34. Courjean, O.; Gao, F.; Mano, N., *Angewandte Chemie-International Edition* 2009, 48 (32), 5897-5899.
35. Ferapontova, E. E.; Grigorenko, V. G.; Egorov, A. M.; Borchers, T.; Ruzgas, T.; Gorton, L., *Biosensors & Bioelectronics* 2001, 16 (3), 147-157.
36. Lindgren, A.; Tanaka, M.; Ruzgas, T.; Gorton, L.; Gazaryan, I.; Ishimori, K.; Morishima, I., *Electrochemistry Communications* 1999, 1 (5), 171-175.
37. Presnova, G.; Grigorenko, V.; Egorov, A.; Ruzgas, T.; Lindgren, A.; Gorton, L.; Borchers, T., *Faraday Discussions* 2000, 116, 281-289.
38. Ortiz, R.; Matsumura, H.; Tasca, F.; Zahma, K.; Samejima, M.; Igarashi, K.; Ludwig, R.; Gorton, L., *Analytical Chemistry* 2012, 84 (23), 10315-10323.
39. Yakovleva, M. E.; Killyeni, A.; Ortiz, R.; Schulz, C.; MacAodha, D.; Conghaile, P. O.; Leech, D.; Popescu, I. C.; Gonaus, C.; Peterbauer, C. K.; Gorton, L., *Electrochemistry Communications* 2012, 24, 120-122.
40. Ortiz, R.; Rahman, M.; Zangrilli, B.; Sygmund, C.; Micheelsen, P. O.; Silow, M.; Toscano, M. D.; Ludwig, R.; Gorton, L., *ChemElectroChem* 2017, 4 (4), 750-750.
41. Durand, F.; Stines-Chaumeil, C.; Flexer, V.; Andre, I.; Mano, N., *Biochemical and Biophysical Research Communications* 2010, 402 (4), 750-754.
42. De Poulpiquet, A.; Ciaccafava, A.; Lojou, E., *Electrochimica Acta* 2014, 126, 104-114.
43. Walcarius, A.; Minteer, S. D.; Wang, J.; Lin, Y.; Merkoci, A., *Journal of Materials Chemistry B* 2013, 1 (38), 4878-4908.
44. Wang, J., *Electroanalysis* 2005, 17 (1), 7-14.
45. Bollella, P.; Fusco, G.; Tortolini, C.; Sanzò, G.; Favero, G.; Gorton, L.; Antiochia, R., *Biosensors and Bioelectronics* 2017, 89 (Part 1), 152-166.
46. Yanez-Sedeno, P.; Pingarron, J., *Analytical and bioanalytical chemistry* 2005, 382 (4), 884-886.
47. Sanzó, G.; Taurino, I.; Antiochia, R.; Gorton, L.; Favero, G.; Mazzei, F.; De Micheli, G.; Carrara, S., *Bioelectrochemistry* 2016, 112, 125-131.
48. Merkoci, A.; Pumera, M.; Llopis, X.; Perez, B.; del Valle, M.; Alegret, S., *Trac-Trends in Analytical Chemistry* 2005, 24 (9), 826-838.
49. Azamian, B. R.; Davis, J. J.; Coleman, K. S.; Bagshaw, C. B.; Green, M. L., *Journal of the American Chemical Society* 2002, 124 (43), 12664-12665.
50. Heller, I.; Kong, J.; Heering, H. A.; Williams, K. A.; Lemay, S. G.; Dekker, C., *Nano Letters* 2005, 5 (1), 137-142.
51. Dettlaff-Weglikowska, U.; Benoit, J.-M.; Chiu, P.-W.; Graupner, R.; Lebedkin, S.; Roth, S., *Current Applied Physics* 2002, 2 (6), 497-501.
52. Hirsch, A., *Angewandte Chemie International Edition* 2002, 41 (11), 1853-1859.
53. Karajanagi, S. S.; Vertegel, A. A.; Kane, R. S.; Dordick, J. S., *Langmuir* 2004, 20 (26), 11594-11599.
54. Gao, Y.; Kyratzis, I., Covalent immobilization of proteins on carbon nanotubes using the cross-linker 1-ethyl-3-(3-dimethylaminopropyl) carbodiimide—a critical assessment. ACS Publications: 2008.

55. Trojanowicz, M., *TrAC trends in analytical chemistry* 2006, 25 (5), 480-489.
56. Schmidt, G.; Gallon, S.; Esnouf, S.; Bourgoin, J. P.; Chenevier, P., *Chemistry-A European Journal* 2009, 15 (9), 2101-2110.
57. Gooding, J. J., *Electroanalysis* 2008, 20 (6), 573-582.
58. Gooding, J. J., *Electrochimica Acta* 2005, 50 (15), 3049-3060.
59. Gooding, J. J.; Wibowo, R.; Liu, J. Q.; Yang, W. R.; Losic, D.; Orbons, S.; Mearns, F. J.; Shapter, J. G.; Hibbert, D. B., *Journal of the American Chemical Society* 2003, 125 (30), 9006-9007.
60. Yang, W.; Ratinac, K. R.; Ringer, S. P.; Thordarson, P.; Gooding, J. J.; Braet, F., *Angewandte Chemie-International Edition* 2010, 49 (12), 2114-2138.
61. Liu, G.; Böcking, T.; Gooding, J. J., *Journal of Electroanalytical Chemistry* 2007, 600 (2), 335-344.
62. Tasca, F.; Harreither, W.; Ludwig, R.; Gooding, J. J.; Gorton, L., *Analytical chemistry* 2011, 83 (8), 3042.
63. Blanford, C. F.; Heath, R. S.; Armstrong, F. A., *Chemical Communications* 2007, (17), 1710-1712.
64. Meredith, M. T.; Minson, M.; Hickey, D.; Artyushkova, K.; Glatzhofer, D. T.; Minteer, S. D., *ACS Catalysis* 2011, 1 (12), 1683-1690.
65. Giroud, F.; Minteer, S. D., *Electrochemistry Communications* 2013, 34, 157-160.
66. Sosna, M.; Chretien, J.-M.; Kilburn, J. D.; Bartlett, P. N., *Physical Chemistry Chemical Physics* 2010, 12 (34), 10018-10026.
67. Stolarczyk, K.; Sepelowska, M.; Lyp, D.; Zelechowska, K.; Biernat, J. F.; Rogalski, J.; Farmer, K. D.; Roberts, K. N.; Bilewicz, R., *Bioelectrochemistry* 2012, 87, 154-163.
68. Thorum, M. S.; Anderson, C. A.; Hatch, J. J.; Campbell, A. S.; Marshall, N. M.; Zimmerman, S. C.; Lu, Y.; Gewirth, A. A., *Journal of Physical Chemistry Letters* 2010, 1 (15), 2251-2254.
69. Minson, M.; Meredith, M. T.; Shrier, A.; Giroud, F.; Hickey, D.; Glatzhofer, D. T.; Minteer, S. D., *Journal of The Electrochemical Society* 2012, 159 (12), G166-G170.
70. Antiochia, R.; Vinci, G.; Gorton, L., *Food chemistry* 2013, 140 (4), 742-747.
71. Antiochia, R.; Gorton, L., *Sensors and Actuators B: Chemical* 2014, 195, 287-293.
72. Kawai, S.; Goda-Tsutsumi, M.; Yakushi, T.; Kano, K.; Matsushita, K., *Applied and environmental microbiology* 2013, 79 (5), 1654-1660.
73. Hibino, Y.; Kawai, S.; Kitazumi, Y.; Shirai, O.; Kano, K., *Electrochemistry Communications* 2016, 67, 43-46.
74. Hamano, Y.; Tsujimura, S.; Shirai, O.; Kano, K., *Bioelectrochemistry* 2012, 88, 114-117.
75. Xia, H.-q.; Hibino, Y.; Kitazumi, Y.; Shirai, O.; Kano, K., *Electrochimica Acta* 2016, 218, 41-46.
76. Ortiz, R.; Ludwig, R.; Gorton, L., *ChemElectroChem* 2014, 1 (11), 1948-1956.
77. Appelqvist, R.; Marko-Varga, G.; Gorton, L.; Torstensson, A.; Johansson, G., *Analytica Chimica Acta* 1985, 169, 237-247.
78. Sugimoto, Y.; Kawai, S.; Kitazumi, Y.; Shirai, O.; Kano, K., *Electrochimica Acta* 2015, 176, 976-981.
79. Laviron, E., *Journal of Electroanalytical Chemistry and Interfacial Electrochemistry* 1979, 101 (1), 19-28.
80. Zhang, Z.; Rusling, J. F., *Biophysical chemistry* 1997, 63 (2-3), 133-146.
81. Mirceski, V.; Komorsky-Lovric, S.; Lovric, M., *Square-wave voltammetry: theory and application*. Springer Science & Business Media: 2007.
82. Tominaga, M.; Shirakihara, C.; Taniguchi, I., *Journal of Electroanalytical Chemistry* 2007, 610 (1), 1-8.

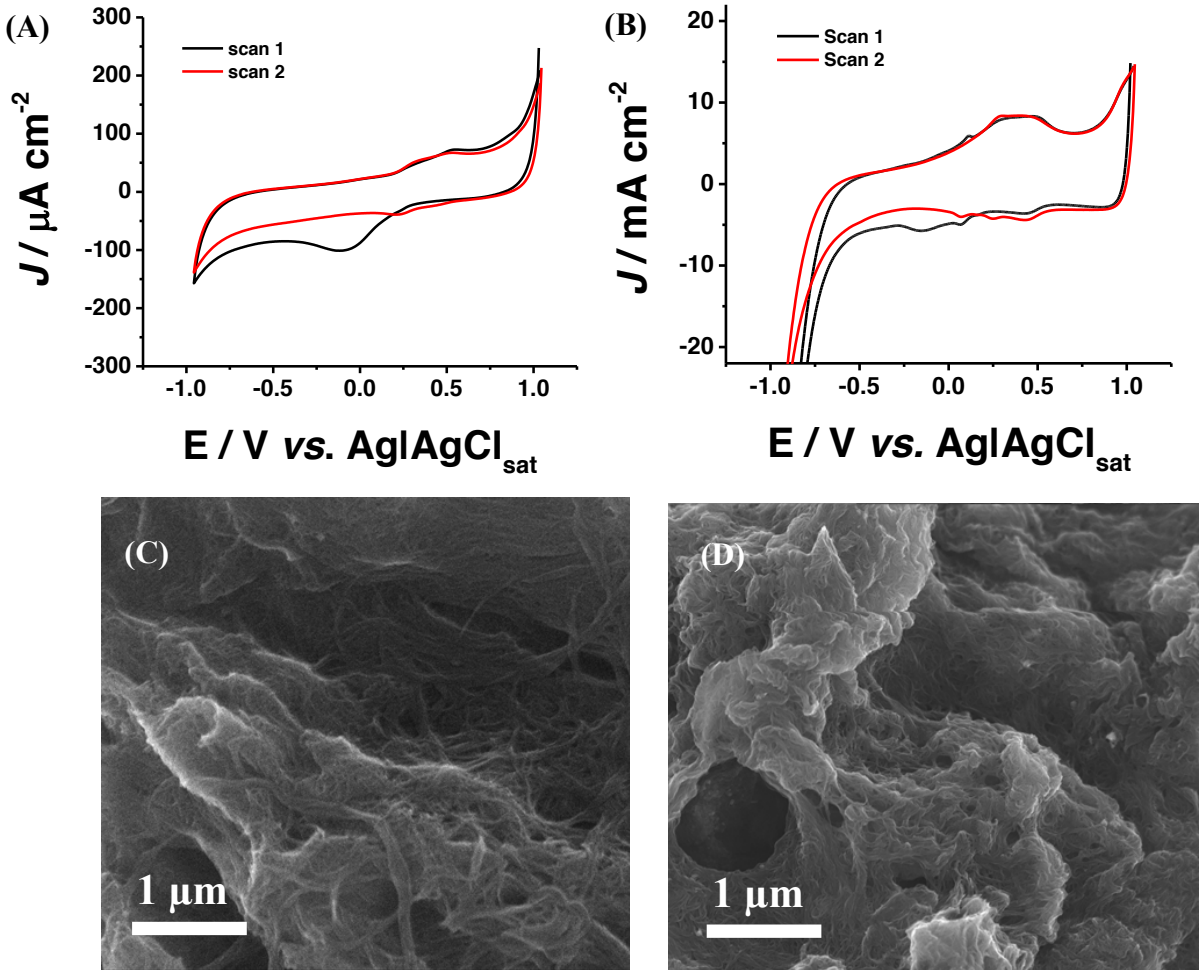

Figure 2. (A) CVs of GCE in 1 mM 2-Amino-anthracene solution with 5 mM $NaNO_2$ in a 0.5 M HCl solution scanning the electrode from +1000 to -1000 mV vs. $Ag|AgCl_{sat}$ at 100 mV s^{-1} for 2 cycles (scan 1: black curve; scan 2: red curve), purged previously for 20 min with Ar to achieve anaerobicity; **(B)** CVs of SWCNT/GCE in 1 mM 2-Amino-anthracene solution with 5 mM $NaNO_2$ in a 0.5 M HCl solution scanning the electrode from +1000 to -1000 mV vs. $Ag|AgCl_{sat}$ at 100 mV s^{-1} for 2 cycles (scan 1: black curve; scan 2: red curve), purged previously for 20 min with Ar to achieve anaerobicity; SEM pictures **(C)** before and **(D)** after electroreduction of 2-Amino Anthracene diazonium salt onto SWCNTs/GC modified electrodes.

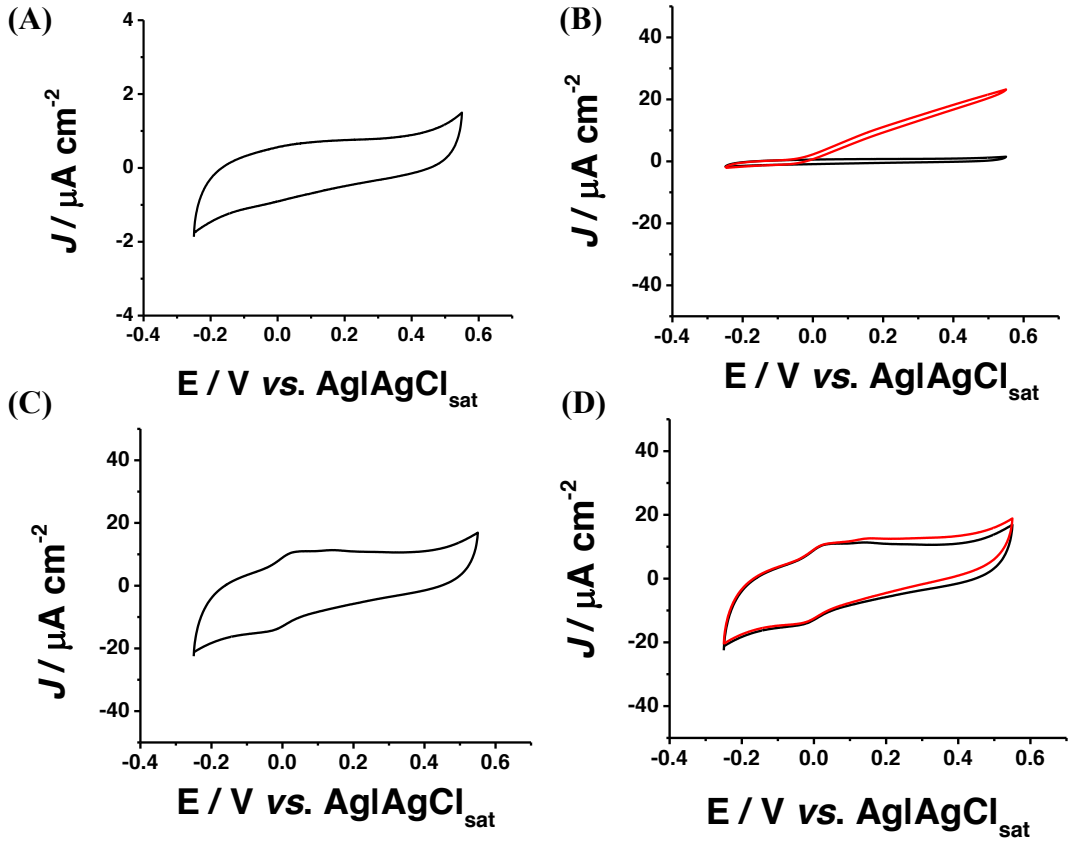

Figure 3. (A) CV of FDH/GC in 50 mM NaAc buffer pH 4.5 without substrate at 10 mV s^{-1}; **(B)** CVs of FDH/GC in 50 mM NaAc buffer pH 4.5 in absence (black) and in presence of 10 mM D-(-)-fructose at 10 mV s^{-1}; **(C)** CV of FDH/2-ANT/GC in 50 mM NaAc buffer pH 4.5 without substrate at 10 mV s^{-1}; **(D)** CVs of FDH/2-ANT/GC in 50 mM NaAc buffer pH 4.5 in absence (black) and in presence of 10 mM D-(-)-fructose at 10 mV s^{-1}. All measurements have been carried out at T= 25 °C.

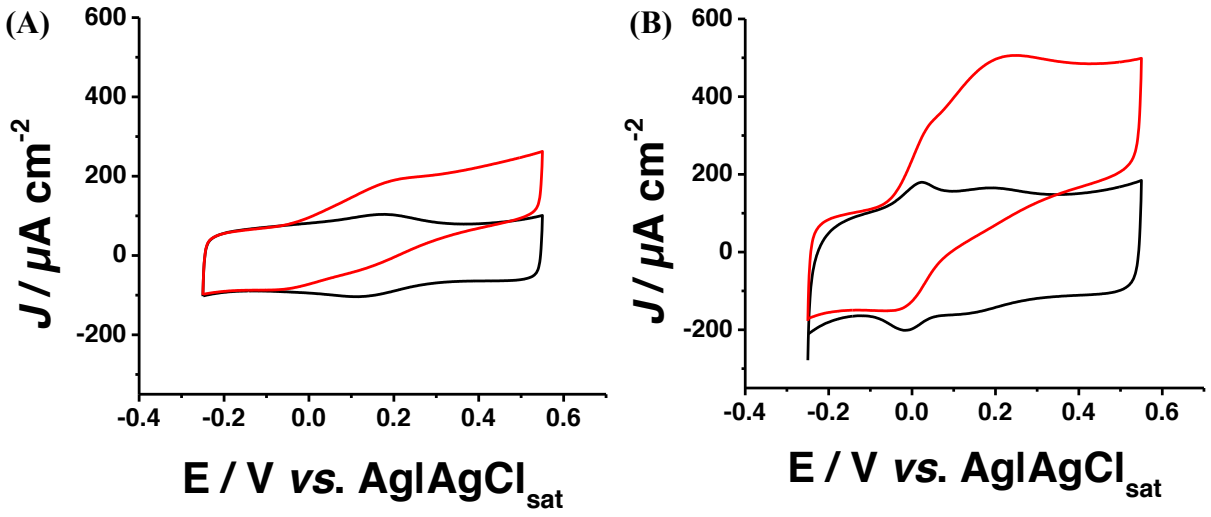

Figure 4. (A) CVs of FDH/SWCNTs/GC in 50 mM NaAc buffer pH 4.5 in absence (black) and in presence of 10 mM D-(-)-fructose at 10 mV s^{-1}; **(B)** CVs of FDH/2-ANT/SWCNTs/GC in 50 mM NaAc buffer pH 4.5 in absence (black) and in presence of 10 mM D-(-)-fructose at 10 mV s^{-1}. All measurements have been carried out at T= 25 °C.

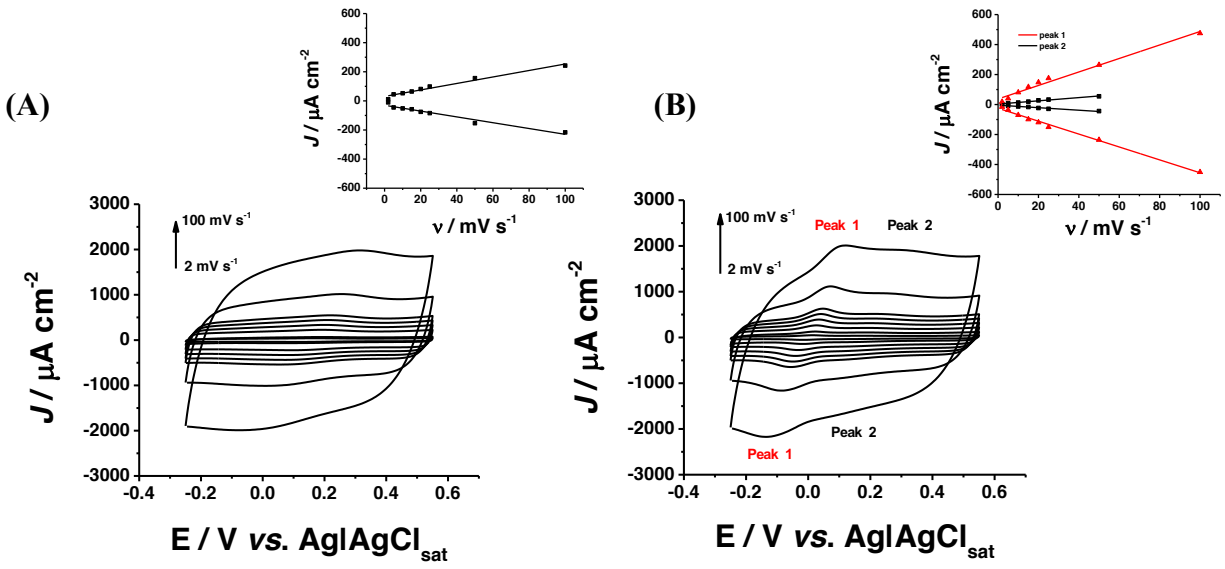

Figure 5. (A) CVs of FDH/SWCNTs/GC in 50 mM NaAc pH 4.5 at different scan rates from 2 mV s^{-1} to 100 mV s^{-1}, inset: current densities of the anodic peak (J_{pa}) and cathodic peak (J_{pc}) vs. scan rate (ν); **(B)** CVs of FDH/2-ANT/SWCNTs/GC in 50 mM NaAc pH 4.5 at different scan rates from 2 mV s^{-1} to 100 mV s^{-1}, inset: current densities of the anodic peak (J_{pa}) and cathodic peak (J_{pc}) vs. scan rate (ν) for peak 1 (red) and peak 2 (black). All measurements have been carried out at T= 25 °C.

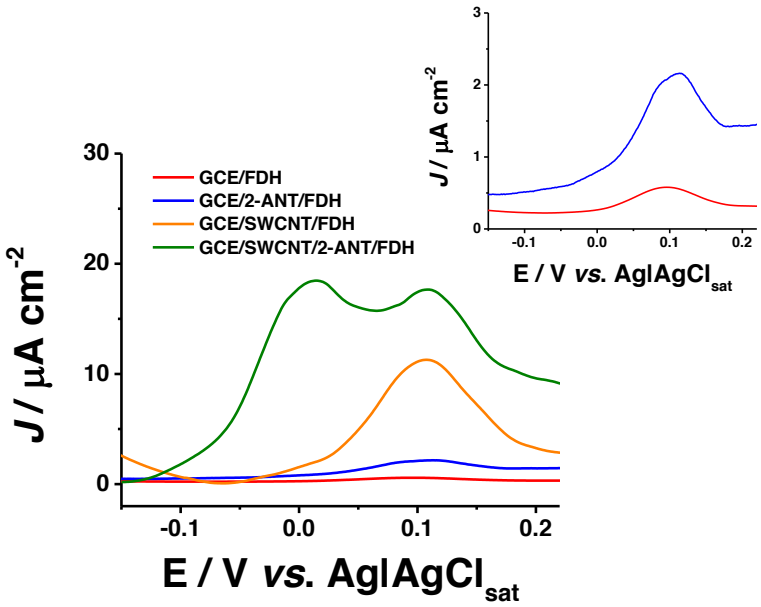

Figure 6. SWVs of FDH/GCE (red), FDH/2-ANT/GCE (blue), FDH/SWCNT/GCE (orange) and FDH/2-ANT/SWCNT/GCE (green) in 50 mM NaAc buffer pH 4.5 at f= 1 Hz Amp.= 10 mV between -150 mV and +220 mV vs. $Ag|AgCl_{sat}$. All measurements have been carried out at T= 25 °C.

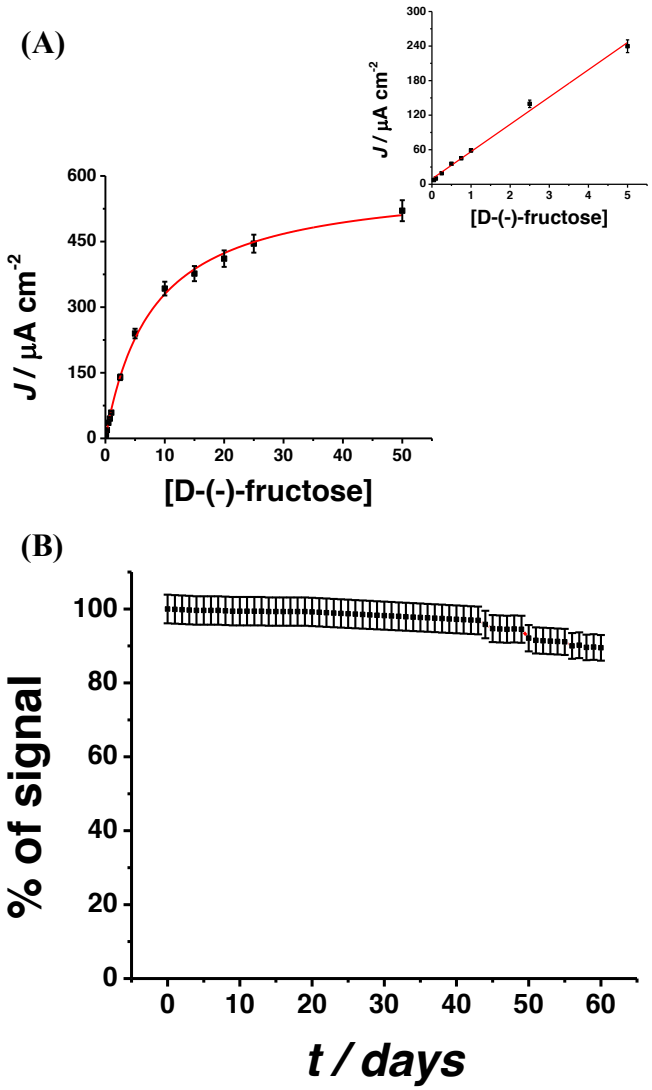

Figure 7. (A) D-(-)-fructose biosensor calibration graph of FDH/2-ANT/SWCNTs/GC in 50 mM NaAc buffer pH 4.5, inset: linear range; (B) . Experimental contitions: **(B)** lifetime FDH/2-ANT/SWCNTs/GC in presence of 10 mM D-fructose solution E_{app} = 0.250 vs. Ag|AgCl$_{sat}$; flow rate 0.5 mL min^{-1}; injection volume 50 µL; T = 25 °C.

Table 1. Electrochemical parameters obtained by using SWV. Experimental conditions: 50 mM NaAc buffer pH 4.5 at f= 1 Hz Amp.= 10 mV between -150 mV and +220 mV vs. $Ag|AgCl_{sat}$ T = 25 °C.

	E_{P1}/ mV	E_{P2} / mV	$W_{1/2P1}$ / mV	$W_{1/2P2}$ / mV	$E^{0'}{}_{P1}$/ mV	$E^{0'}{}_{P2}$/ mV
GCE bare	-	+125 ± 3	-	83 ± 2	-	-
2-ANT	-	+106 ± 5	-	78 ± 1	-	-
SWCNT	-	+119 ± 1	-	86 ± 3	-	+142 ± 4
SWCNT+2-ANT	+15 ± 2	+109 ± 7	81 ± 2	92 ± 4	-6 ± 2	+169 ± 5

Table 2. Electrochemical and kinetics parameters of the FDH/2-ANT/SWCNTs/GC electrode.

	FDH/2-ANT/SWCNTs/GC
E_{app}/ (V vs. $Ag|AgCl_{sat}$)	+ 0.250
K_M^{app}/mM	7.9 ± 0.4
J_{max}/µA cm^{-2}	592 ± 11
LOD/µM	0.9
Linear range/mM	0.05-5
Sensitivity/µA mM^{-1} cm^{-2}	47 ± 1
R^2	0.99

GRAPHICAL ABSTRACT

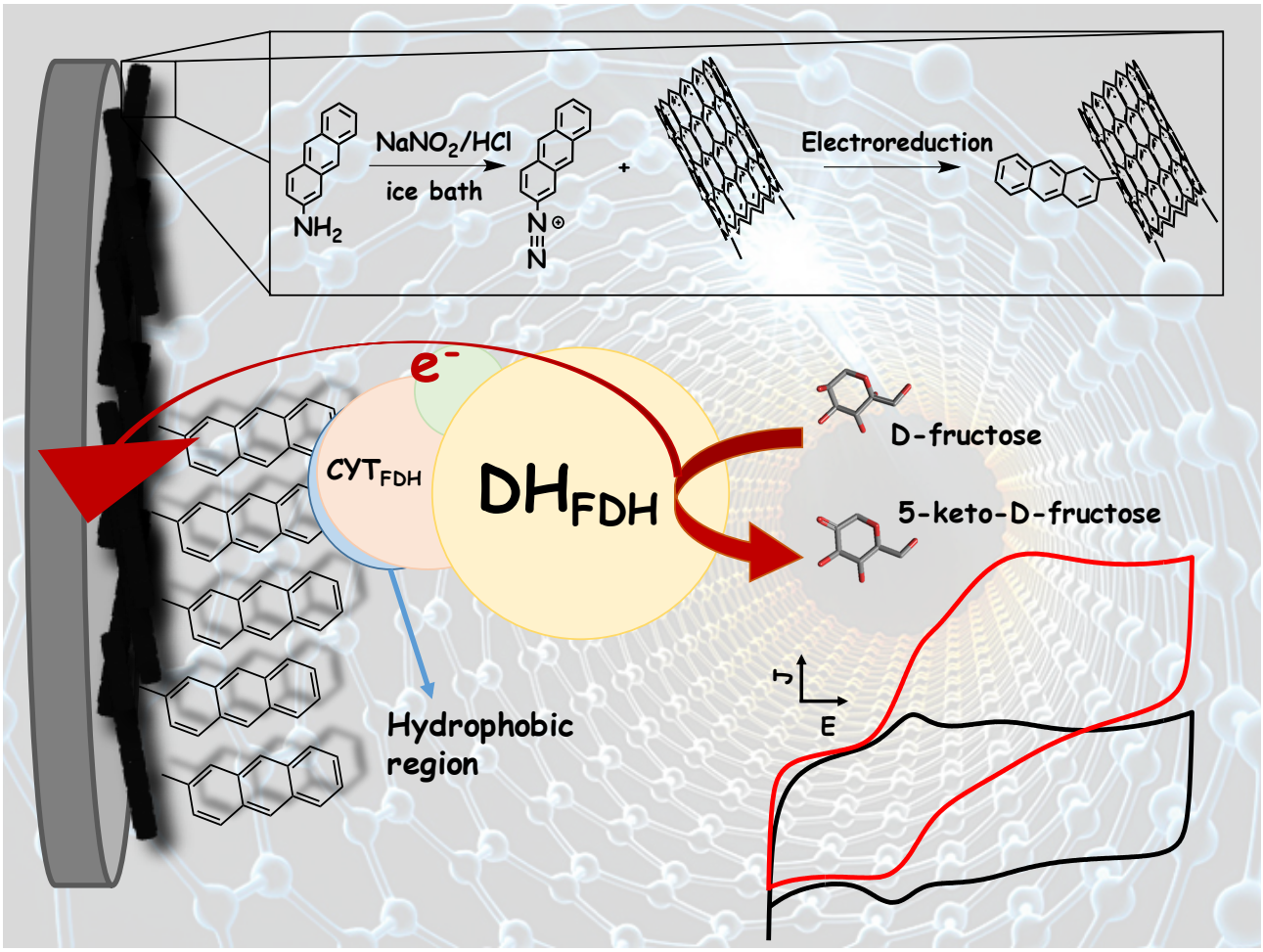

Paper VIII

Highly Sensitive Membrane-less Fructose Biosensor Based on Fructose Dehydrogenase Immobilized onto Aryl Thiols Modified Highly Porous Gold Electrode: Characterization and Application in Food Samples

Paolo Bollella[a,b], Yuya Hibino[c], Kenji Kano[c], Lo Gorton[b,*], Riccarda Antiochia[a,*]

[a]Department of Chemistry and Drug Technologies, Sapienza University of Rome P.le Aldo Moro 5, 00185 – Rome, Italy

[b]Department of Analytical Chemistry/Biochemistry, Lund University, P.O. Box 124, 221 00 – Lund, Sweden

[c]Division of Applied Life Sciences, Graduate School of Agriculture, Kyoto University, Sakyo, Kyoto 606-8502, Japan

Abstract

In this paper we present a new method to electrodeposit highly porous gold (h-PG) onto a polycrystalline solid gold electrode without any templates. The electrodeposition is carried out by first cycling the electrode potential between +0.8 and 0 V in 10 mM $HAuCl_4$ with 2.5 M NH_4Cl and then applying a negative potential for the production of hydrogen bubbles at the electrode surface. After that the modified electrode was characterized in sulphuric acid to estimate the real surface area (A_{real}) to be close to 24 cm^2. The electrode was further incubated overnight with different thiols in order to produce self assembled monolayers (SAMs), i.e., 4-mercaptobenzoic acid (4-MBA), 4-mercaptophenol (4-MPh), and 4-aminothiophenol (4-APh), in order to obtain differently charged electrode surfaces. Finally a fructose dehydrogenase (FDH) solution was drop-cast onto the electrodes. All the modified electrodes were investigated by cyclic voltammetry both under non-turnover and turnover conditions revealing the best performance for the FDH/4-MPh/h-PG observing a clear electrochemistry of both heme c_2 and heme c_3 of the cytochrome domain of FDH and as well a great catalytic efficiency (about 1000 μA cm^{-2} in the presence of 10 mM fructose) an effect of correct orientation of FDH through the electrostatic interactions between enzyme and SAM and the stabilization of FDH due to the presence of –OH groups on the electrode surface. The FDH/4-MPh/h-PG based electrode showed the best analytical performances with an excellent stability (90% retained activity over 90 days), a detection limit of 0.3 μM, a linear range between 0.05 and 5 mM, and a sensitivity of 175±15 μA cm^{-2} mM^{-1}. These

properties were favourably compared with other fructose biosensors reported in the literature. The biosensor was successively tested to quantify the fructose content in food and beverage samples. No significant interference present in the sample matrices was observed.

Keywords: highly porous gold (h-PG), 4-mercaptophenol (4-MPh), fructose dehydrogenase (FDH), fructose biosensor, direct electron transfer (DET)

*Corresponding Author:
Prof. Riccarda Antiochia
e-mail: riccarda.antiochia@uniroma1.it
Prof. Lo Gorton
e-mail: lo.gorton@biochemistry.lu.se

1. Introduction

In the last decades direct electron transfer (DET) reactions between redox enzymes and electrodes has been widely investigated to develop both 3rd generation biosensors and biofuel cells (Falk et al. 2012; Freire et al. 2003; Ghindilis et al. 1997; Gorton et al. 1999; Gray and Winkler 1996; Leger and Bertrand 2008; Wu and Hu 2007; Zhang and Li 2004). Although there are a lot of papers dealing with DET, most redox enzymes do not show DET properties mainly because the prosthetic (e.g. FAD, PQQ) and redox (e.g. heme *b*, heme *c*) co-factors are deeply buried within the protein structure (Frew and Hill 1988; Gorton et al. 1999; Schuhmann 2002). Nevertheless, a lot of efforts have been addressed towards nano-structuration of electrode surfaces in order to improve DET reactions as an effect of enlarging the surface area, which would contribute to increasing the enzyme loading (Holzinger et al. 2014; Wang 2005b) as well as the possibility for chemical modification (e.g., self-assembled monolayer SAM, diazonium coupling etc.) enabling a correct orientation of the enzyme onto the electrode surface to minimize the distance between the bound cofactor and the electrode surface (Chekin et al. 2015; Gooding 2008; Gooding and Ciampi 2011; Samanta and Sarkar 2011).

A lot of nanomaterials have been exploited to improve DET (Bollella et al. 2017b; Favero et al. 2015; Mazzei et al. 2015) such as single- and multi-walled carbon nanotubes (Chekin et al. 2015; Gooding 2005; Wang 2005a), graphene (Bollella et al. 2017a; Carbone et al. 2015), highly-/nano-porous gold (Du Toit and Di Lorenzo 2014; Sanzó et al. 2016) and metal

nanoparticles (Bollella et al. 2017c; Bollella et al. 2017d; Pingarrón et al. 2008; Yanez-Sedeno and Pingarron 2005). Among the aforementioned nanomaterials, nano-porous gold (nPG, porous gold with pores in the nanometer range) electrodes represent a very promising alternative for the development of new implantable bioelectronics (Adiga et al. 2008; Deng et al. 2008). These electrodes exhibit remarkable properties such as high conductivity, large surface area, three-dimensional open porosity, and biocompatibility (Dixon et al. 2007). Besides the nPG electrodes, highly porous gold (hPG) electrodes seem to be even more promising for the development of highly sensitive biosensors. hPG electrodes present larger pores (micrometer range) compared to nPG electrodes. In particular, each micropore presents an internal complex nano-structuration based on nano-pores. As a consequence, hPG electrodes show a very broad pore size distribution, drastically increasing the surface area and thus the current densities compared to the conventional nPG based electrodes (Li et al. 2007). Generally, h-PG can be obtained by using mainly two approaches (Zhang and Olin 2014): the chemical dealloying or the templating and self-templating methods. Chemical de-alloying/etching is a corrosive process performed by dissolving metal elements such as Ag, Sn, and Cu in the alloy except for gold (Siepenkoetter et al. 2016; Xiao et al. 2016). According to the chemical activity of the elements in the alloys, different reagents such as nitric acid, hydrochloric acid, or NaOH can be used (Ding et al. 2004). Contrary to the chemical dealloying, the templating method is a simple approach combining different techniques like flow-stream technique, sputter deposition and electrochemical methods to create nano-porous gold films. In this method, there are three main steps: preparation of template, followed by deposition of gold, and then the removal of the template. Different templates could be used such as a layer of assembled particles, biologically made templates or ion etched substrates. Polystyrene latex and silica particles have been widely used to make assembled particles as templates (Ben-Ali et al. 2003; Gloria et al. 2011; Szamocki et al. 2006; Xia et al. 2011).

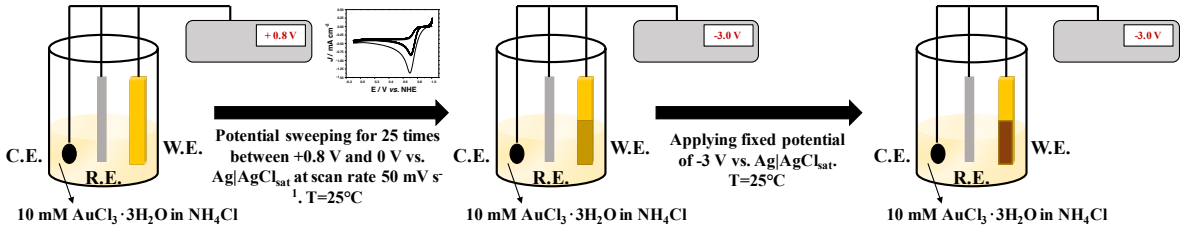

Scheme 1. Schematic representation of the electrodeposition method for h-PG performed in two steps: potential sweeping for 25 scans between +0.8 V and 0 V vs. $Ag|AgCl_{sat}$ at a scan rate of 50 mV s^{-1}, applying a fixed potential of -3 V vs. $Ag|AgCl_{sat}$ for 120 s in 10 mM $AuCl_3$ solution containing 2.5 M NH_4Cl.

In contrast to previous methods, self-templating methods present two steps: gold electrodeposition and gas bubbling used as self-template. Accordingly we have developed a novel two step method, where first a layer of gold is electrodeposited onto the electrode surface followed by hydrogen bubbling at the electrode realized through applying a really negative potential in a solution containing NH_4Cl as supporting electrolyte and hydrogen source. This technique is a really time saving and cost-effective way to produce highly porous gold avoiding all removal steps or chemical dissolution like in the dealloying procedures (Hsu et al. 2008; Plowman et al. 2015; Siepenkoetter et al. 2016; Siepenkoetter et al. 2017; Tsai et al. 2002; Xiao et al. 2016).

Besides the nano-structuration, also the immobilization of the enzymes is a key issue for the development of highly sensitive and stable biosensors. There are several immobilization methods such as drop-casting, physical entrapment, and chemical modification of the electrode surface by the use of self-assembled monolayers (SAMs) (Chaki and Vijayamohanan 2002). SAMs are ordered ultrathin organic films obtained through strong chemisorption between the substrate and the head group of the selected organic molecule. This procedure has been widely used for studying several fundamental phenomena such as distance dependent electron transfer (Collinson et al. 1992; Song et al. 1993; Tarlov and Bowden 1991), mechanism of single electron transistor, and observations of molecular events such as coulomb staircase etc. (Andres et al. 1996). In addition, the strong inter-chain interactions ensure a tight packing and stability of the monolayers leading to several applications including chemical sensing, control of surface properties such as wettability and friction, corrosion protection, patterning, semiconductor passivation, and optical second order harmonic generation (Love et al. 2005; Prime and Whitesides 1993; Ulman 1996). Herein, we have used three different aromatic SAMs based on 4-mercaptobenzoic acid (4-MBA), 4-mercaptophenol (4-MPh), and 4-aminothiophenol (4-APh) in order to obtain three different

tail groups, *viz.* –COOH, -OH and $–NH_2$ exposed toward the enzyme layer driving the orientation of the enzyme molecules by means of electrostatic and van der Waals interactions (Malem and Mandler 1993; Ostuni et al. 1999).

Fructose dehydrogenase (FDH, EC 1.1.99.11) from *Gluconobacter japonicus* has been widely exploited to develop fructose biosensors based on mediated and direct electron transfer (Antiochia and Gorton 2014; Antiochia et al. 2004; Antiochia et al. 2013; Begum et al. 1993; Khan et al. 1993a; Khan et al. 1992; Khan et al. 1991, 1993b; Kizling et al. 2015; Parellada et al. 1996; Siepenkoetter et al. 2017; Swann et al. 1997; Tominaga et al. 2009; Tominaga et al. 2007; Tsujimura et al. 2009) as well as bioanode for enzymatic fuel cells (EFCs) (Ikeda and Kano 2001, 2003; Kamitaka et al. 2007; Meredith et al. 2011; Miyake et al. 2011; Murata et al. 2009; Sakai et al. 2009; So et al. 2014). FDH is a membrane-bound flavocytochrome oxidoreductase also belongs to the hemoflavoproteins family. FDH from *Gluconobacter japonicus* NCBR 3260 is a heterotrimeric membrane-bound enzyme complex with a molecular mass of 146.4 kDa, consisting of three subunits: namely subunit I (DH_{FDH}), which is the catalytic domain with a covalently bound flavin adenine dinucleotide (FAD) cofactor, where D-(-)-fructose is involved in a $2H^+/2e^-$ oxidation to 5-dehydro-D-(-)-fructose; subunit II (CYT_{FDH}), which acts as a built-in electron acceptor with three heme *c* moieties covalently bound to the enzyme scaffold and two of them are involved one by one in the electron transfer pathway; and subunit III, which is not involved in the electron transfer but plays a key role for the enzyme complex stability (Hibino et al. 2017; Kawai et al. 2013; Kawai et al. 2016; Kawai et al. 2014; Tsujimura et al. 2010).

The aim of this paper was to improve the DET rate between FDH and a novel developed highly porous gold electrode, driving the enzyme orientation through the electrostatic interaction between the enzyme and the different SAMs used. The h-PG electrodes were produced through a two-step process involving the electrodeposition of a gold layer followed by hydrogen bubbling at the electrode surface as self-template. Three different platforms have been compared in order to investigate the effect of the surface charge on the catalytic efficiency, which in turn is expected to mirror the enzyme orientation: *viz.* FDH/4-MBA/h-PG, FDH/4-MPh/h-PG, and FDH/4-APh/h-PG. FDH/4-MPh/h-PG showed the best performance due to the correct orientation of the enzyme directly related to the electrostatic attraction between FDH (p*I* 6.59 according to the enzymatic sequence) and 4-MPh modified h-PG (pK_a 6.81 according to (Rankin 2009)) and to the role of exposed –OH groups on the stabilization of immobilized layer FDH on the electrode surface. The electrochemical characterization and optimization of the fructose biosensor obtained with FDH/4-MPh/h-PG

electrode are herein presented. Finally, the feasibility of the developed biosensor for *in-situ* analysis was tested in real food samples.

2. Experimental

2.1 Chemicals and Reagents

4-mercaptobenzoic acid (4-MBA), 4-mercaptophenol (4-MPh), 4-aminothiophenol (4-APh), ammonium chloride (NH_4Cl), sodium acetate (NaAc), hydrochloric acid (HCl), sodium hydroxide (NaOH), D-fructose, D-glucose, D-galactose, D-mannitol, ascorbic acid, gold chloride ($AuCl_3$ H_2O), 3-(N-morpholino)propanesulphonic acid (MOPS), sulphuric acid (H_2SO_4), 2-amino-2-(hydroxymethyl)-1,3-propanediol (TRIS) were purchased from Sigma Aldrich (St. Louis, MO, USA). D-Fructose dehydrogenase from *Gluconobacter japonicus* (FDH; EC 1.1.99.11) was purified from the culture supernatant of *Gluconobacter japonicus* NBRC 3260 obtained from the National Institute of Technology and Evaluation (Nishinomiya, Hyogo Pref., Japan) ANY REFERENCE?, and solubilized in PBS buffer pH 6 (50~500 mM) containing 0.1 mM 2-mercaptoethanol and 0.1% v/v TritonX-100 (volumetric activity measured with potassium ferricyanide at pH 4.5 = 420 ± 30 U mL^{-1}, specific activity = 250 ± 30 U mg^{-1}, protein concentration = 1.7 ± 0.2 mg mL^{-1}). All solutions were prepared using Milli-Q water (ρ= 18.2 MΩ cm at 25 °C; Total Organic Compounds (TOC) < 10 µg L^{-1}, Millipore, Molsheim, France).

2.2 Electrode Preparation and Modification

Polycrystalline gold electrodes (Ø=1.6 mm, BASi, West Lafayette, IN, USA) were cleaned by incubation in Piranha solution for 2 min (1:3 mixture of conc. H_2O_2 with H_2SO_4, (*CAUTION: Piranha solution is especially dangerous, corrosive and may explode if contained in a closed vessel, it should be handled with special care*), then with polishing cloths with deagglomerated alumina slurry of 1 µm diameter (Struers, Ballerup, Denmark), successively sonicated in ultrapure water for 5 min and finally electrochemically cleaned in 0.5 M H_2SO_4 by running 20 cyclic voltammograms (CVs) between −0.3 and 1.7 V vs. $Ag|AgCl_{sat}$ at a scan rate of 0.3 V s^{-1} and thoroughly rinsed with Milli-Q water between each polishing step. Au electrodes were successively modified by electrodeposition of highly porous gold (h-PG) by initially sweeping the potential for 25 scans between +0.8 V and 0 V vs. $Ag|AgCl_{sat}$ at a scan rate of 50 mV s^{-1} and then applying a fixed potential of -3 V vs.

$Ag|AgCl_{sat}$ in a 10 mM $AuCl_3$ solution containing 2.5 M NH_4Cl. Then, the modified electrodes were activated in 0.5 M H_2SO_4 by running CVs between 0 and +1.7 vs. $Ag|AgCl_{sat}$ at a scan rate of 0.1 V s^{-1} until a well-defined CV was obtained. The real surface area (A_{real}) was evaluated by running CVs between 0 and +1.7 vs. $Ag|AgCl_{sat}$ at a scan rate of 0.1 V s^{-1} and integrating the peak related to the formation of gold oxide (amount of charge relative to the adsorption of oxygen), which was normalized by the reference charge 390±10 μC cm^{-2} reported in the literature (Trasatti and Petrii 1991).

The so modified electrode was next incubated overnight in a 10 mM ethanol solution containing one of three different thiols: 4-MBA, 4-MPh, or 4-APh, to form a SAM on the electrode surface. Then, the electrode was thoroughly rinsed with ethanol and dried under a N_2 stream. For the biomodification, 3 μL of an FDH solution (1.7 mg mL^{-1}) were drop-cast on the top of the thiol-modified h-PG electrode and allowed to react in a moisturised atmosphere for 2 h to avoid evaporation of the reactants. Finally, the electrode was gently rinsed with a 50 mM NaAc buffer (pH 4.5) in order to remove any possible unbound enzyme molecules.

2.3 SEM Experiments

Scanning electron microscopy (SEM) measurements were carried out with a JSM-7600F Schottky Field Emission Scanning Electron Microscope (JEOL Nordic AB, Sollentuna, Sweden). All samples were prepared according to the electrodeposition protocol as reported above in Section 2.2 by using gold plates (25 × 25 × 1 mm, ALS Co. Ltd., Tokyo, Japan) instead of gold electrodes. The samples have been placed on a clip SEM sample holder (JEOL Nordic AB).

2.4 Electrochemical Measurements and Apparatus

Cyclic voltammetry (CV) experiments were carried out using an Autolab potentiostat (model PGSTAT30, Metrohm Autolab B.V. Ecochemie, Utrecht, The Netherlands) equipped with GPES, version 4.9. A conventional three-electrode electrochemical cell was used for all experiments performed with an Ag|AgCl (sat. KCl) as the reference electrode, a platinum wire as the counter electrode, and the modified gold electrode as the working electrode.

Flow injection experiments were performed with a three-electrode potentiostat (Zäta Elektronik, Höör, Sweden). The enzyme-modified gold electrode, inserted into a wall-jet flow-through amperometric cell and positioned at a constant distance (1–2 mm) from the inlet

nozzle (Appelqvist et al. 1985), was used as the working electrode, an Ag|AgCl (0.1 KCl) electrode as the reference electrode and a platinum wire as the counter electrode. The electrochemical cell was connected to a flow injection system consisting of a peristaltic pump (Gilson, Villier-le-Bel, France) and a six-port valve electrical injector (Rheodyne, Cotati, CA, USA). A 50-μL aliquot of the substrate was applied by a loop mounted onto the injector. The resulting electrical current was recorded on a strip chart recorder (Kipp & Zonen, Utrecht, The Netherlands). All measurements were performed under temperature control by using a cryostatic bath (T ± 0.01 ºC, LAUDA RM6, Delran, NJ, USA).

2.5 Real Food Samples Collections and Pre-Treatment

Real samples (cola, honey, tomato juice, apple juice, pineapple juice, energy drink) were bought in a local supermarket and carefully diluted in 50 mM NaAc buffer at pH 4.5 in a ratio of 1:250, before the analysis, except for the honey samples, which required a particular pre-treatment. Honey samples were transferred into a beaker and heated for 5 min at 60 °C, stirring occasionally with a spatula, and finally allowed to cool. Next the samples were carefully diluted in 50 mM NaAc buffer at pH 4.5 in a ratio of 1:250 (Parellada et al. 1996; Piermarini et al. 2011). The results obtained for FDH/4-MPh/h-PG biosensor were compared with a commercially available enzymatic kit (K-FRUGL 02/17) purchased from Megazyme (Bray Business Park, Bray, Co. Wicklow, A98 YV29, Ireland).

3. Results and discussion

3.1 SEM and Electrochemical Characterization of Highly Porous Gold Electrodes (h-PG)

SEM experiments have been carried out in order to investigate the morphology of the highly porous gold (h-PG) substrates. In Figs. 1A-C it is possible to observe that the surfaces with deposited h-PG exhibit a multimodal distribution of well-defined porous, which have a diameter ranging from 5 to 25 μm. In this electrodeposition protocol, both steps have a crucial importance: i) the first step was needed to control the overall thickness and homogenous distribution of the gold layer electrodeposited by sweeping the potential, whereas ii) the second step ensures a high hydrogen evolution rate due to the high concentration of NH_4^+ contained in the electrodeposition solution as supporting electrolyte and the highly negative applied potential of -3.0 V vs. $Ag|AgCl_{sat}$. Since the importance of both the metal precursor and the NH_4Cl concentrations, they have been previously optimized

for both steps (data not shown). Du Toit and Di Lorenzo have developed a similar two-step method electrodepositing a gold porous structure applying two different potentials: namely -0.7 V vs. SCE for 5 s and -4.0 V for 15 s, which did not allow to obtain a high real surface area and a homogeneous pores distribution (Du Toit and Di Lorenzo 2014). Recently, Sanzò and coworkers developed a one-step electrodeposition method, which consists of applying a fixed negative potential for a certain time. Although the latter was a one-step electrodeposition method, so far time saving, it did not ensure a homogeneous distribution of the pores on the whole modified electrode, because the gold is deposited only in the interstitial spaces of the hydrogen bubbles in too short an electrodeposition time (Sanzó et al. 2016).

However, in order to prove unequivocally the improvements of our electrodeposition method, A_{real} was calculated by integrating the peak current related to the reduction of the gold oxide (~ +0.9 V vs. $Ag|AgCl_{sat}$) obtained by running CVs in 0.5 M H_2SO_4 at a scan rate of 100 mV s^{-1}, as shown in Fig. 2. The theoretical charge density considered for reduction of gold oxide is 390±10 μC cm^{-2}. Therefore, the A_{real} for the h-PG modified gold electrodes was 23.6±0.8 cm^2, which is roughly 300 times higher compared to the bare gold electrodes (0.08 ± 0.01 cm^2).

3.2 Electrochemical Characterization of FDH Immobilized on Self-Assembled Monolayer (SAM) Modified h-PG Electrodes

After preliminary characterization, the h-PG electrodes were further modified with one of three different thiols, *viz*. 4-MBA, 4-MPh, and 4-APh, to form self-assembled monolayers (SAMs) on the surface in order to investigate the effect of electrostatic attraction/repulsion between the differently charged electrode surfaces and FDH, which is expected to control the enzyme orientation (Ferretti et al. 2000; Gooding and Hibbert 1999). In a series of previously published papers, it has been proved that the orientation of a redox enzyme is a key issue to obtain efficient direct electron transfer (DET) communication between the enzyme active site and the electrode due to the enzyme structure, the position of both the prosthetic and other redox groups and the enzyme surface charge (isoelectric point) (Blanford et al. 2007; Gorton et al. 1999; Ludwig et al. 2013; Matsumura et al. 2012; Schuhmann 2002; Tasca et al. 2011; Tavahodi et al. 2017; Wang et al. 2012).

Figure 3A shows the CV for the FDH/4-MBA/h-PG modified electrode under non-turnover conditions (50 mM NaAc buffer pH 4.5), where it is possible to observe a tendency for a

couple of waves with a mid-point potential ($E°'$) of +0.045 vs. Ag|$AgCl_{sat}$, which is actually close to the value reported in the literature for heme c_2 (+0.060 V vs. Ag|$AgCl_{sat}$) (Kawai et al. 2014). In the presence of 10 mM D-(-)-fructose as substrate the FDH/4-MBA/h-PG electrode showed a slight electrocatalytical wave starting at E_{ONSET}= -0.070 V vs. Ag|$AgCl_{sat}$ rising up to 100 µA cm^{-2} at 0.2 V vs. Ag|$AgCl_{sat}$, as seen in Fig. 3B.

In contrast, the FDH/4-MPh/h-PG modified electrode showed two clear couples of redox waves while cycling in 50 mM NaAc buffer pH 4.5, as depicted in Fig. 3C. The more negative redox couple showed an $E°'$value of -0.032 vs. Ag|$AgCl_{sat}$, while the other one of +0.068 vs. Ag|$AgCl_{sat}$, which are in good agreement with the values reported in the literature for heme c_3 (-0.010 V vs. Ag|$AgCl_{sat}$) and heme c_2 (+0.060 V vs. Ag|$AgCl_{sat}$), respectively (Kawai et al. 2014). Furthermore, with the addition of substrate (10 mM D-(-)-fructose) the electrode exhibits a great electrocatalytical wave starting at E_{ONSET}= -0.115 V vs. Ag|$AgCl_{sat}$ rising up to 920 µA cm^{-2} at 0.2 V vs. Ag|$AgCl_{sat}$, as reported in Fig. 3D.

In the last case, the FDH/4-APh/h-PG electrode was scanned under non-turnover conditions (50 mM NaAc buffer pH 4.5), showing a non-reversible electrochemistry of FDH with only two oxidation peaks at +0.032 V vs. Ag|$AgCl_{sat}$ and +0.122 V vs. Ag|$AgCl_{sat}$, which might correspond to heme c_2 and heme c_1, as reported in Fig. 3E. Most probably the enzyme showed an irreversible electrochemistry probably due to the unfavorable orientation obtained on the positive charged surface. Nevertheless, the CV in presence of substrate showed an electrocatalytical wave starting at E_{ONSET}= -0.098 V vs. Ag|$AgCl_{sat}$ rising up to 314 µA cm^{-2} at 0.2 V vs. Ag|$AgCl_{sat}$, as shown in Fig. 3F.

The integration of the redox peaks relative to DET of heme *c*, allowed to compare the enzyme surface coverage for all the modified electrodes by using Faraday's law (equation (1)):

$$\Gamma_T = \frac{Q}{nFA} \qquad (1)$$

where Γ_T is the total surface concentration of electroactive protein in mol cm^{-2}, A is electrode area in cm^2, F is Faraday's constant (96 485.34 C mol^{-1} of electrons), Q is the charge underlying the redox wave and n is the number of electrons transferred in the reaction

(Rusling and Zhang). Γ_T resulted to be 192±13 pmol cm^{-2}, 356±10 pmol cm^{-2}, and 160±9 pmol cm^{-2} for FDH/4-MBA/h-PG, FDH/4-MPh/h-PG and FDH/4-APh/h-PG, respectively.
According to these results, it was possible to establish the FDH/4-MPh/h-PG as the best modified electrodes due to the quasi-reversible however, clearly visible non-turnover electrochemistry, the great electrocatalytical behavior and the amount of FDH immobilized. These results are related to the best correct orientation of the enzyme onto the electrode surface as a result of the interactions between the enzyme, that is slightly positively charged during the immobilization occurring at pH 6 (the p*I* of FDH was calculated to be 6.59 from the structure of the enzyme), and the mild negatively charged electrode surface due to the presence of –OH groups.

3.3 Fructose Biosensor Development

To investigate the electroanalytical and kinetic parameters of FDH/4-MBA/h-PG, FDH/4-MPh/h-PG and FDH/4-APh/h-PG, the amperometric responses toward D-(-)-fructose have been recorded by using the flow injection system (FIA) approach injecting D-(-)-fructose solutions at different concentrations, as reported in Fig. 4a. As expected from the results exhibited in Fig. 3, the FDH/4-MPh/h-PG modified electrode showed a faster and a much higher peak response (3 s) compared to FDH/4-MBA/h-PG and FDH/4-APh/h-PG, which exhibit a response time of 8 s and a much lower current response. The calibration curves exhibited a linear response range between 0.05 and 5 mM (R^2 = 0.99, n = 5) and with the following sensitivies: 175±15 μA mM^{-1} cm^{-2} for FDH/4-MPh/h-PG, 60 ± 3 μA mM^{-1} cm^{-2} for FDH/4-APh/h-PG, and 14±1 μA mM^{-1} cm^{-2} for FDH/4-MBA/h-PG, respectively, as shown in the inset of Fig. 4a. At higher concentrations than 5 mM the amperometric response is no longer linear due to the saturation of the enzyme active site. The detection limit resulted to be 0.3 μM for FDH/4-MPh/h-PG, 1.2 μM for FDH/4-APh/h-PG, and 1.5 μM for FDH/4-MBA/h-PG, respectively, calculated using the relation $3\sigma/S$, where σ is the absolute standard deviation of the intercept and S is the slope of the calibration curve (Shrivastava and Gupta 2011). The electroanalytical and kinetic parameters for FDH/4-MBA/h-PG, FDH/4-MPh/h-PG and FDH/4-APh/h-PG electrodes are reported in Table 1. The apparent kinetic parameters (I_{max}, K_M^{app}) are in good agreement with the values reported in the literature for nanostructured biosensors for fructose detection based on DET (Kawai et al. 2014; Tsujimura et al. 2010). The analytical results of the FDH/4-MPh/h-PG electrode were further compared with other platforms reported in the literature showing great improvements by considering

sensitivity, linear range, detection limit, selectivity, and stability (Table 2) (Antiochia and Gorton 2014; Campuzano et al. 2003; Damar and Demirkol 2011; Kinnear and Monbouquette 1997; Parellada et al. 1996; Siepenkoetter et al. 2017).

3.4 Effect of pH, Temperature, Interferences, and Stability Studies

Since the FDH/4-MPh/h-PG electrode platform exhibits the best analytical performance compared to the others, the following experiments where the effects of pH and temperature have been performed were only studied for the FDH/4-MPh/h-PG platform. The effects of pH and temperature are shown in Figs. 4b and c. The optimum pH was found to be pH 4.5 in 50 mM NaAc buffer at a temperature of 35 °C. The catalytic current density was rapidly decreasing when increasing the pH revealing only one optimum pH at 4.5 in the investigated pH range of 3 and 10, in perfect agreement with the results reported in literature (Damar and Demirkol 2011). Concerning the temperature dependence, the FDH/4-MPh/h-PG electrode showed its best performance at 35 °C. Nevertheless, the biosensor still exhibits good performance both at room temperature and at 45 °C, while at 50 °C the current density was drastically decreased probably due to denaturation of the enzyme.

The stability and lifetime of the FDH/4-MPh/h-PG electrode was evaluated using the FIA system by monitoring the signal decrease within 90 days when the biosensor was used for one measurement per day and stored in 50 mM NaAc buffer pH 4.5 at 4 °C, as reported in Fig. 4d. The modified biosensor seems to retain more than 90% of its initial activity after 90 days, probably due to the high stability of the enzyme layer directly related to the nano-structuration of the electrode surface and the modification with a slight negatively charged SAM namely 4-mercaptophenol, which is responsible for both electrostatic and Van der Waals interactions occurring at the interface between the enzyme and 4-MPh modified electrode. Nevertheless, we should consider that the –OH groups exposed on the electrode surface create a favorable environment for the immobilization of a membrane bound protein namely FDH.

Finally, the selectivity of the proposed biosensor was studied in order to see the influence of possible interfering compounds generally present in food samples such as D-glucose, D-galactose, D-mannitol and ascorbic acid. The signal obtained for a fixed concentration of D-(-)-fructose (10 mM) was compared to that obtained with a sample containing the same D-(-)-fructose concentration plus equal concentrations of the potential interfering compounds. The amperometric signal is lower than 10% for all the compounds tested except for ascorbic acid (about 20%), which may interfere in real measurements because of its direct oxidation on the

electrode surface occurring approximately at 0.2 V vs. $Ag|AgCl_{sat}$ close to formal potential of L-ascorbic acid oxidation ($E^{0'}$ = +0.170 V vs. $Ag|AgCl_{sat}$), as reported in literature (Rueda et al. 1978).

3.5 Fructose Detection in Food Samples

To demonstrate the feasibility of the modified electrode for the *in-situ* detection of D-(-)-fructose in food industry as a screening method for analytical process control, the proposed biosensor was used to detect the D-(-)-fructose concentration in food samples. The samples were collected and used according to the procedure reported in section 2.5., referred to the protocols reported in the literature and provided with guidelines of the spectrophotometric reference method. The reliability of the FDH/4-MPh/h-PG electrode platform was evaluated by comparing the results with those obtained with the spectrophotometric reference method. The proposed biosensor exhibits satisfactory results in all food samples with a recovery percentage above 94% (RSD values lower than 2.5%), as reported in Table 3.

4. Conclusions

This paper demonstrated the possibility to achieve efficient DET for FDH immobilized within the FDH/4-MPh/h-PG platform as a result of the highly porous gold electrode in combination with the exposed –OH groups of the SAM. The latter is responsible for the correct orientation of FDH onto the electrode surface due to both the electrostatic interaction between the enzyme (p*I* 6.59) and the electrode surface (4-MPh, pK_a 6.81), and to the stabilization effect of the exposed –OH groups of the SAM on FDH. The proposed biosensor based on the FDH/4-MPh/h-PG platform showed a really high catalytic current density of 920 μA cm^{-2} at 0.2 V vs. $Ag|AgCl_{sat}$, with a great improvement compared with the other platforms reported in the literature. The FDH/4-MPh/h-PG biosensor can be easily prepared through a two-step electrodeposition protocol (20 min), further modified with 4-mercaptophenol to form a SAM, and finally with the enzyme deposition. The fructose biosensor was fast-responding, showed a great stability (more than 90% of retained signal after 90 days), selectivity and sensitivity (175±15 μA mM^{-1} cm^{-2}) with the lowest detection limit (0.3 μM). According to these results, the proposed electrode platform namely FDH/4-MPh/h-PG exhibits great promises both as a 3rd generation biosensor for fructose detection and as a biofuel cell anode suitable to be integrated in industrial processes.

Acknowledgments

Dr. Crispin Hetherington (Lund University, Department of Chemistry, Centre for Analysis and Synthesis, The National Center for High-Resolution Electron Microscopy nCHREM) is particular acknowledged for help with SEM investigation of the highly porous gold electrodes. The authors would like to thank for the following agencies for financial funding: The Swedish Research Council (Vetenskapsrådet project 2014-5908), the European Commission (project "Bioenergy" FP7-PEOPLE-2013-ITN-607793) and a scholarship of the Erasmus+ Project Unipharma-Graduates, promoted by a Consortium of Italian Universities and coordinated by Sapienza University of Rome.

References

Adiga, S.P., Curtiss, L.A., Elam, J.W., Pellin, M.J., Shih, C.-C., Shih, C.-M., Lin, S.-J., Su, Y.-Y., Gittard, S.D., Zhang, J., 2008. Nanoporous materials for biomedical devices. JOM Journal of the Minerals, Metals and Materials Society 60(3), 26-32.

Andres, R., Datta, S., Dorogi, M., Gomez, J., Henderson, J., Janes, D., Kolagunta, V., Kubiak, C., Mahoney, W., Osifchin, R., 1996. Room temperature Coulomb blockade and Coulomb staircase from self‐assembled nanostructures. Journal of Vacuum Science & Technology A: Vacuum, Surfaces, and Films 14(3), 1178-1183.

Antiochia, R., Gorton, L., 2014. A new osmium-polymer modified screen-printed graphene electrode for fructose detection. Sensors and Actuators B: Chemical 195, 287-293.

Antiochia, R., Lavagnini, I., Magno, F., 2004. Amperometric mediated carbon nanotube paste biosensor for fructose determination. Analytical letters 37(8), 1657-1669.

Antiochia, R., Vinci, G., Gorton, L., 2013. Rapid and direct determination of fructose in food: a new osmium-polymer mediated biosensor. Food chemistry 140(4), 742-747.

Appelqvist, R., Marko-Varga, G., Gorton, L., Torstensson, A., Johansson, G., 1985. Enzymatic determination of glucose in a flow system by catalytic oxidation of the nicotinamide coenzyme at a modified electrode. Analytica Chimica Acta 169, 237-247.

Begum, A., Kobatake, E., Suzawa, T., Ikariyama, Y., Aizawa, M., 1993. NEW ELECTROCATALYTIC BIOMOLECULAR INTERFACE FOR FABRICATING A FRUCTOSE DEHYDROGENASE-BASED SENSING SYSTEM. Analytica Chimica Acta 280(1), 31-36.

Ben-Ali, S., Cook, D.A., Evans, S.A.G., Thienpont, A., Bartlett, P.N., Kuhn, A., 2003. Electrocatalysis with monolayer modified highly organized macroporous electrodes. Electrochemistry Communications 5(9), 747-751.

Blanford, C.F., Heath, R.S., Armstrong, F.A., 2007. A stable electrode for high-potential, electrocatalytic O-2 reduction based on rational attachment of a blue copper oxidase to a graphite surface. Chemical Communications(17), 1710-1712.

Bollella, P., Fusco, G., Tortolini, C., Sanzò, G., Favero, G., Gorton, L., Antiochia, R., 2017a. Beyond graphene: Electrochemical sensors and biosensors for biomarkers detection. Biosensors and Bioelectronics 89, 152-166.

Bollella, P., Ludwig, R., Gorton, L., 2017b. Cellobiose dehydrogenase: Insights on the nanostructuration of electrodes for improved development of biosensors and biofuel cells. Applied Materials Today 9, 319-332.

Bollella, P., Mazzei, F., Favero, G., Fusco, G., Ludwig, R., Gorton, L., Antiochia, R., 2017c. Improved DET communication between cellobiose dehydrogenase and a gold electrode modified with a rigid self-assembled monolayer and green metal nanoparticles: The role of an ordered nanostructuration. Biosensors and Bioelectronics 88, 196-203.

Bollella, P., Schulz, C., Favero, G., Mazzei, F., Ludwig, R., Gorton, L., Antiochia, R., 2017d. Green synthesis and characterization of gold and silver nanoparticles and their application for development of a third generation lactose biosensor. Electroanalysis 29(1), 77-86.

Campuzano, S., Galvez, R., Pedrero, M., de Villena, F.J.M., Pingarrón, J.M., 2003. An integrated electrochemical fructose biosensor based on tetrathiafulvalene-modified self-assembled monolayers on gold electrodes. Analytical and bioanalytical chemistry 377(4), 600-607.

Carbone, M., Gorton, L., Antiochia, R., 2015. An Overview of the Latest Graphene‐Based Sensors for Glucose Detection: the Effects of Graphene Defects. Electroanalysis 27(1), 16-31.

Chaki, N.K., Vijayamohanan, K., 2002. Self-assembled monolayers as a tunable platform for biosensor applications. Biosensors and Bioelectronics 17(1), 1-12.
Chekin, F., Gorton, L., Tapsobea, I., 2015. Direct and mediated electrochemistry of peroxidase and its electrocatalysis on a variety of screen-printed carbon electrodes: amperometric hydrogen peroxide and phenols biosensor. Analytical and Bioanalytical Chemistry 407(2), 439-446.
Collinson, M., Bowden, E.F., Tarlov, M.J., 1992. VOLTAMMETRY OF COVALENTLY IMMOBILIZED CYTOCHROME-C ON SELF-ASSEMBLED MONOLAYER ELECTRODES. Langmuir 8(5), 1247-1250.
Damar, K., Demirkol, D.O., 2011. Modified gold surfaces by poly (amidoamine) dendrimers and fructose dehydrogenase for mediated fructose sensing. Talanta 87, 67-73.
Deng, Y., Huang, W., Chen, X., Li, Z., 2008. Facile fabrication of nanoporous gold film electrodes. Electrochemistry Communications 10(5), 810-813.
Ding, Y., Kim, Y.J., Erlebacher, J., 2004. Nanoporous gold leaf:"Ancient technology"/advanced material. Advanced Materials 16(21), 1897-1900.
Dixon, M.C., Daniel, T.A., Hieda, M., Smilgies, D.M., Chan, M.H., Allara, D.L., 2007. Preparation, structure, and optical properties of nanoporous gold thin films. Langmuir 23(5), 2414-2422.
Du Toit, H., Di Lorenzo, M., 2014. Electrodeposited highly porous gold microelectrodes for the direct electrocatalytic oxidation of aqueous glucose. Sensors and Actuators B: Chemical 192, 725-729.
Falk, M., Blum, Z., Shleev, S., 2012. Direct electron transfer based enzymatic fuel cells. Electrochimica Acta 82, 191-202.
Favero, G., Fusco, G., Mazzei, F., Tasca, F., Antiochia, R., 2015. Electrochemical characterization of graphene and mwcnt screen-printed electrodes modified with aunps for laccase biosensor development. Nanomaterials 5(4), 1995-2006.
Ferretti, S., Paynter, S., Russell, D.A., Sapsford, K.E., Richardson, D.J., 2000. Self-assembled monolayers: a versatile tool for the formulation of bio-surfaces. TrAC Trends in Analytical Chemistry 19(9), 530-540.
Freire, R.S., Pessoa, C.A., Mello, L.D., Kubota, L.T., 2003. Direct electron transfer: An approach for electrochemical biosensors with higher selectivity and sensitivity. Journal of the Brazilian Chemical Society 14(2), 230-243.
Frew, J.E., Hill, H.A.O., 1988. DIRECT AND INDIRECT ELECTRON-TRANSFER BETWEEN ELECTRODES AND REDOX PROTEINS. European Journal of Biochemistry 172(2), 261-269.
Ghindilis, A.L., Atanasov, P., Wilkins, E., 1997. Enzyme‐catalyzed direct electron transfer: Fundamentals and analytical applications. Electroanalysis 9(9), 661-674.
Gloria, D., Gooding, J.J., Moran, G., Hibbert, D.B., 2011. Electrochemically fabricated three dimensional nano-porous gold films optimised for surface enhanced Raman scattering. Journal of electroanalytical chemistry 656(1), 114-119.
Gooding, J.J., 2005. Nanostructuring electrodes with carbon nanotubes: A review on electrochemistry and applications for sensing. Electrochimica Acta 50(15), 3049-3060.
Gooding, J.J., 2008. Advances in interfacial design for electrochemical biosensors and sensors: aryl diazonium salts for modifying carbon and metal electrodes. Electroanalysis 20(6), 573-582.
Gooding, J.J., Ciampi, S., 2011. The molecular level modification of surfaces: from self-assembled monolayers to complex molecular assemblies. Chemical Society Reviews 40(5), 2704-2718.
Gooding, J.J., Hibbert, D.B., 1999. The application of alkanethiol self-assembled monolayers to enzyme electrodes. TrAC Trends in Analytical Chemistry 18(8), 525-533.

Gorton, L., Lindgren, A., Larsson, T., Munteanu, F., Ruzgas, T., Gazaryan, I., 1999. Direct electron transfer between heme-containing enzymes and electrodes as basis for third generation biosensors. Analytica Chimica Acta 400(1), 91-108.
Gray, H.B., Winkler, J.R., 1996. Electron transfer in proteins. Annual review of biochemistry 65(1), 537-561.
Hibino, Y., Kawai, S., Kitazumi, Y., Shirai, O., Kano, K., 2017. Construction of a protein-engineered variant of D-fructose dehydrogenase for direct electron transfer-type bioelectrocatalysis. Electrochemistry Communications 77, 112-115.
Holzinger, M., Le Goff, A., Cosnier, S., 2014. Nanomaterials for biosensing applications: a review. Frontiers in chemistry 2, 63-63.
Hsu, P.-C., Seol, S.-K., Lo, T.-N., Liu, C.-J., Wang, C.-L., Lin, C.-S., Hwu, Y., Chen, C., Chang, L.-W., Je, J., 2008. Hydrogen bubbles and the growth morphology of ramified zinc by electrodeposition. Journal of The Electrochemical Society 155(5), D400-D407.
Ikeda, T., Kano, K., 2001. An electrochemical approach to the studies of biological redox reactions and their applications to biosensors, bioreactors, and biofuel cells. Journal of Bioscience and Bioengineering 92(1), 9-18.
Ikeda, T., Kano, K., 2003. Bioelectrocatalysis-based application of quinoproteins and quinoprotein-containing bacterial cells in biosensors and biofuel cells. Biochimica Et Biophysica Acta-Proteins and Proteomics 1647(1-2), 121-126.
Kamitaka, Y., Tsujimura, S., Setoyama, N., Kajino, T., Kano, K., 2007. Fructose/dioxygen biofuel cell based on direct electron transfer-type bioelectrocatalysis. Physical Chemistry Chemical Physics 9(15), 1793-1801.
Kawai, S., Goda-Tsutsumi, M., Yakushi, T., Kano, K., Matsushita, K., 2013. Heterologous overexpression and characterization of a flavoprotein-cytochrome c complex fructose dehydrogenase of Gluconobacter japonicus NBRC3260. Applied and environmental microbiology 79(5), 1654-1660.
Kawai, S., Kitazumi, Y., Shirai, O., Kano, K., 2016. Bioelectrochemical characterization of the reconstruction of heterotrimeric fructose dehydrogenase from its subunits. Electrochimica Acta 210, 689-694.
Kawai, S., Yakushi, T., Matsushita, K., Kitazumi, Y., Shirai, O., Kano, K., 2014. The electron transfer pathway in direct electrochemical communication of fructose dehydrogenase with electrodes. Electrochemistry Communications 38, 28-31.
Khan, G.F., Kobatake, E., Ikariyama, Y., Aizawa, M., 1993a. AMPEROMETRIC BIOSENSOR WITH PQQ ENZYME IMMOBILIZED IN A MEDIATOR-CONTAINING POLYPYRROLE MATRIX. Analytica Chimica Acta 281(3), 527-533.
Khan, G.F., Kobatake, E., Shinohara, H., Ikariyama, Y., Aizawa, M., 1992. MOLECULAR INTERFACE FOR AN ACTIVITY CONTROLLED ENZYME ELECTRODE AND ITS APPLICATION FOR THE DETERMINATION OF FRUCTOSE. Analytical Chemistry 64(11), 1254-1258.
Khan, G.F., Shinohara, H., Ikariyama, Y., Aizawa, M., 1991. ELECTROCHEMICAL-BEHAVIOR OF MONOLAYER QUINOPROTEIN ADSORBED ON THE ELECTRODE SURFACE. Journal of Electroanalytical Chemistry 315(1-2), 263-273.
Khan, G.F., Shinohara, H., Ikariyama, Y., Aizawa, M., 1993b. AN AMPEROMETRIC BIOSENSOR FOR FRUCTOSE USING A PQQ ENZYME. Sensors and Actuators B-Chemical 14(1-3), 673-674.
Kinnear, K.T., Monbouquette, H.G., 1997. An amperometric fructose biosensor based on fructose dehydrogenase immobilized in a membrane mimetic layer on gold. Analytical chemistry 69(9), 1771-1775.

Kizling, M., Draminska, S., Stolarczyk, K., Tammela, P., Wang, Z., Nyholm, L., Bilewicz, R., 2015. Biosupercapacitors for powering oxygen sensing devices. Bioelectrochemistry 106, 34-40.
Leger, C., Bertrand, P., 2008. Direct electrochemistry of redox enzymes as a tool for mechanistic studies. Chemical Reviews 108(7), 2379-2438.
Li, Y., Song, Y.-Y., Yang, C., Xia, X.-H., 2007. Hydrogen bubble dynamic template synthesis of porous gold for nonenzymatic electrochemical detection of glucose. Electrochemistry Communications 9(5), 981-988.
Love, J.C., Estroff, L.A., Kriebel, J.K., Nuzzo, R.G., Whitesides, G.M., 2005. Self-assembled monolayers of thiolates on metals as a form of nanotechnology. Chemical reviews 105(4), 1103-1170.
Ludwig, R., Ortiz, R., Schulz, C., Harreither, W., Sygmund, C., Gorton, L., 2013. Cellobiose dehydrogenase modified electrodes: advances by materials science and biochemical engineering. Analytical and Bioanalytical Chemistry 405(11), 3637-3658.
Malem, F., Mandler, D., 1993. Self-assembled monolayers in electroanalytical chemistry: application of. omega.-mercapto carboxylic acid monolayers for the electrochemical detection of dopamine in the presence of a high concentration of ascorbic acid. Analytical Chemistry 65(1), 37-41.
Matsumura, H., Ortiz, R., Ludwig, R., Igarashi, K., Samejima, M., Gorton, L., 2012. Direct Electrochemistry of Phanerochaete chrysosporium Cellobiose Dehydrogenase Covalently Attached onto Gold Nanoparticle Modified Solid Gold Electrodes. Langmuir 28(29), 10925-10933.
Mazzei, F., Favero, G., Bollella, P., Tortolini, C., Mannina, L., Conti, M.E., Antiochia, R., 2015. Recent trends in electrochemical nanobiosensors for environmental analysis. International Journal of Environment and Health 7(3), 267-291.
Meredith, M.T., Minson, M., Hickey, D., Artyushkova, K., Glatzhofer, D.T., Minteer, S.D., 2011. Anthracene-Modified Multi-Walled Carbon Nanotubes as Direct Electron Transfer Scaffolds for Enzymatic Oxygen Reduction. Acs Catalysis 1(12), 1683-1690.
Miyake, T., Yoshino, S., Yamada, T., Hata, K., Nishizawa, M., 2011. Self-Regulating Enzyme-Nanotube Ensemble Films and Their Application as Flexible Electrodes for Biofuel Cells. Journal of the American Chemical Society 133(13), 5129-5134.
Murata, K., Kajiya, K., Nakamura, N., Ohno, H., 2009. Direct electrochemistry of bilirubin oxidase on three-dimensional gold nanoparticle electrodes and its application in a biofuel cell. Energy & Environmental Science 2(12), 1280-1285.
Ostuni, E., Yan, L., Whitesides, G.M., 1999. The interaction of proteins and cells with self-assembled monolayers of alkanethiolates on gold and silver. Colloids and Surfaces B: Biointerfaces 15(1), 3-30.
Parellada, J., Domínguez, E., Fernández, V.M., 1996. Amperometric flow injection determination of fructose in honey with a carbon paste sensor based on fructose dehydrogenase. Analytica chimica acta 330(1), 71-77.
Piermarini, S., Volpe, G., Esti, M., Simonetti, M., Palleschi, G., 2011. Real time monitoring of alcoholic fermentation with low-cost amperometric biosensors. Food chemistry 127(2), 749-754.
Pingarrón, J.M., Yáñez-Sedeño, P., González-Cortés, A., 2008. Gold nanoparticle-based electrochemical biosensors. Electrochimica Acta 53(19), 5848-5866.
Plowman, B.J., Jones, L.A., Bhargava, S.K., 2015. Building with bubbles: the formation of high surface area honeycomb-like films via hydrogen bubble templated electrodeposition. Chemical Communications 51(21), 4331-4346.

Prime, K.L., Whitesides, G.M., 1993. Adsorption of proteins onto surfaces containing end-attached oligo (ethylene oxide): a model system using self-assembled monolayers. Journal of the American Chemical Society 115(23), 10714-10721.
Rankin, D.W., 2009. CRC handbook of chemistry and physics, edited by David R. Lide. Taylor & Francis.
Rueda, M., Aldaz, A., Sanchez-Burgos, F., 1978. Oxidation of L-ascorbic acid on a gold electrode. Electrochimica Acta 23(5), 419-424.
Rusling, J.F., Zhang, Z., Thin Films on Electrodes for Direct Protein Electron Transfer-Chapter 2.
Sakai, H., Nakagawa, T., Tokita, Y., Hatazawa, T., Ikeda, T., Tsujimura, S., Kano, K., 2009. A high-power glucose/oxygen biofuel cell operating under quiescent conditions. Energy & Environmental Science 2(1), 133-138.
Samanta, D., Sarkar, A., 2011. Immobilization of bio-macromolecules on self-assembled monolayers: methods and sensor applications. Chemical Society Reviews 40(5), 2567-2592.
Sanzó, G., Taurino, I., Antiochia, R., Gorton, L., Favero, G., Mazzei, F., De Micheli, G., Carrara, S., 2016. Bubble electrodeposition of gold porous nanocorals for the enzymatic and non-enzymatic detection of glucose. Bioelectrochemistry 112, 125-131.
Schuhmann, W., 2002. Amperometric enzyme biosensors based on optimised electron-transfer pathways and non-manual immobilisation procedures. Reviews in Molecular Biotechnology 82(4), 425-441.
Shrivastava, A., Gupta, V., 2011. Methods for the determination of limit of detection and limit of quantitation of the analytical methods. Chronicles of Young Scientists 2(1), 21-21.
Siepenkoetter, T., Salaj-Kosla, U., Xiao, X., Belochapkine, S., Magner, E., 2016. Nanoporous Gold Electrodes with Tuneable Pore Sizes for Bioelectrochemical Applications. Electroanalysis 28(10), 2415-2423.
Siepenkoetter, T., Salaj‐Kosla, U., Magner, E., 2017. The Immobilization of Fructose Dehydrogenase on Nanoporous Gold Electrodes for the Detection of Fructose. ChemElectroChem 4(4), 905-912.
So, K., Kawai, S., Hamano, Y., Kitazumi, Y., Shirai, O., Hibi, M., Ogawa, J., Kano, K., 2014. Improvement of a direct electron transfer-type fructose/dioxygen biofuel cell with a substrate-modified biocathode. Physical Chemistry Chemical Physics 16(10), 4823-4829.
Song, S., Clark, R.A., Bowden, E.F., Tarlov, M.J., 1993. CHARACTERIZATION OF CYTOCHROME-C ALKANETHIOLATE STRUCTURES PREPARED BY SELF-ASSEMBLY ON GOLD. Journal of Physical Chemistry 97(24), 6564-6572.
Swann, M.J., Bloor, D., Haruyama, T., Aizawa, M., 1997. The role of polypyrrole as charge transfer mediator and immobilization matrix for D-fructose dehydrogenase in a fructose sensor. Biosensors & Bioelectronics 12(12), 1169-1182.
Szamocki, R., Reculusa, S., Ravaine, S., Bartlett, P.N., Kuhn, A., Hempelmann, R., 2006. Tailored mesostructuring and biofunctionalization of gold for increased electroactivity. Angewandte Chemie-International Edition 45(8), 1317-1321.
Tarlov, M.J., Bowden, E.F., 1991. ELECTRON-TRANSFER REACTION OF CYTOCHROME-C ADSORBED ON CARBOXYLIC-ACID TERMINATED ALKANETHIOL MONOLAYER ELECTRODES. Journal of the American Chemical Society 113(5), 1847-1849.
Tasca, F., Harreither, W., Ludwig, R., Gooding, J.J., Gorton, L., 2011. Cellobiose Dehydrogenase Aryl Diazoniunn Modified Single Walled Carbon Nanotubes: Enhanced Direct Electron Transfer through a Positively Charged Surface. Analytical Chemistry 83(8), 3042-3049.

Tavahodi, M., Ortiz, R., Schulz, C., Ekhtiari, A., Ludwig, R., Haghighi, B., Gorton, L., 2017. Direct Electron Transfer of Cellobiose Dehydrogenase on Positively Charged Polyethyleneimine Gold Nanoparticles. Chempluschem 82(4), 546-552.
Tominaga, M., Nomura, S., Taniguchi, I., 2009. D-Fructose detection based on the direct heterogeneous electron transfer reaction of fructose dehydrogenase adsorbed onto multi-walled carbon nanotubes synthesized on platinum electrode. Biosensors & Bioelectronics 24(5), 1184-1188.
Tominaga, M., Shirakihara, C., Taniguchi, I., 2007. Direct heterogeneous electron transfer reactions and molecular orientation of fructose dehydrogenase adsorbed onto pyrolytic graphite electrodes. Journal of Electroanalytical Chemistry 610(1), 1-8.
Trasatti, S., Petrii, O., 1991. Real surface area measurements in electrochemistry. Pure and applied chemistry 63(5), 711-734.
Tsai, W., Hsu, P., Hwu, Y., Chen, C., 2002. Building on bubbles in metal electrodeposition. Nature 417(6885), 139.
Tsujimura, S., Nishina, A., Hamano, Y., Kano, K., Shiraishi, S., 2010. Electrochemical reaction of fructose dehydrogenase on carbon cryogel electrodes with controlled pore sizes. Electrochemistry Communications 12(3), 446-449.
Tsujimura, S., Nishina, A., Kamitaka, Y., Kano, K., 2009. Coulometric D-Fructose Biosensor Based on Direct Electron Transfer Using D-Fructose Dehydrogenase. Analytical Chemistry 81(22), 9383-9387.
Ulman, A., 1996. Formation and structure of self-assembled monolayers. Chemical reviews 96(4), 1533-1554.
Wang, J., 2005a. Carbon‐nanotube based electrochemical biosensors: A review. Electroanalysis 17(1), 7-14.
Wang, J., 2005b. Nanomaterial-based electrochemical biosensors. Analyst 130(4), 421-426.
Wang, X., Falk, M., Ortiz, R., Matsumura, H., Bobacka, J., Ludwig, R., Bergelin, M., Gorton, L., Shleev, S., 2012. Mediatorless sugar/oxygen enzymatic fuel cells based on gold nanoparticle-modified electrodes. Biosensors & Bioelectronics 31(1), 219-225.
Wu, Y., Hu, S., 2007. Biosensors based on direct electron transfer in redox proteins. Microchimica Acta 159(1-2), 1-17.
Xia, Y., Huang, W., Zheng, J., Niu, Z., Li, Z., 2011. Nonenzymatic amperometric response of glucose on a nanoporous gold film electrode fabricated by a rapid and simple electrochemical method. Biosensors and Bioelectronics 26(8), 3555-3561.
Xiao, X., Si, P., Magner, E., 2016. An overview of dealloyed nanoporous gold in bioelectrochemistry. Bioelectrochemistry 109, 117-126.
Yanez-Sedeno, P., Pingarron, J., 2005. Gold nanoparticle-based electrochemical biosensors. Analytical and bioanalytical chemistry 382(4), 884-886.
Zhang, R., Olin, H., 2014. Porous gold films—a short review on recent progress. Materials 7(5), 3834-3854.
Zhang, W.J., Li, G.X., 2004. Third-generation biosensors based on the direct electron transfer of proteins. Analytical Sciences 20(4), 603-609.

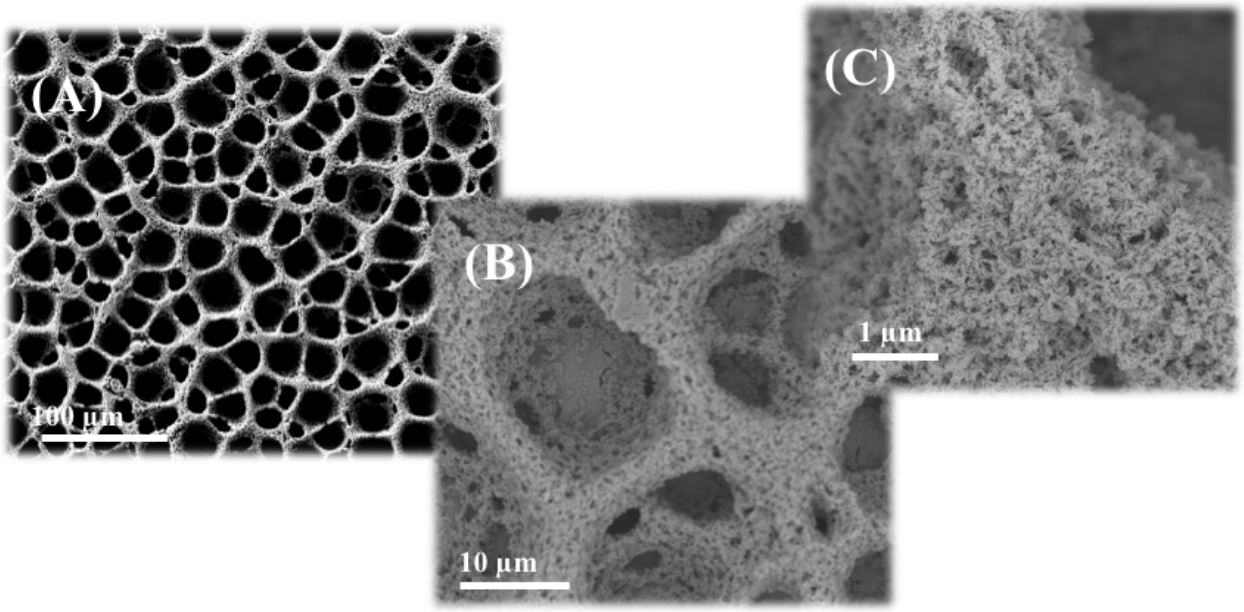

Figure 1. SEM images at different magnifications (A) 100 µm (B) 10 µm (C) 1 µm of the h-PGE obtained through a two step electrodeposition protocol: i) sweeping the potential for 25 scans between +0.8 V and 0 V vs. Ag|AgClsat, ii) applying a fixed potential of -3 V vs. Ag|$AgCl_{sat}$ for 120 s; both steps have been carried out in 10 mM $AuCl_3 \cdot H_2O$ containing 2.5 M NH_4Cl.

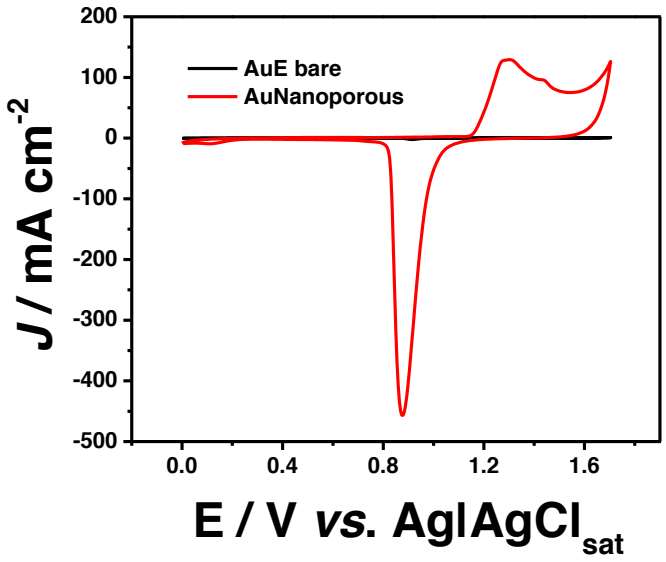

Figure 2. Cyclic voltammograms of AuE bare **(black)** and h-PG modified AuE **(red)** in 0.5 M H_2SO_4. Scan rate 100 mV s^{-1}. T = 25 °C.

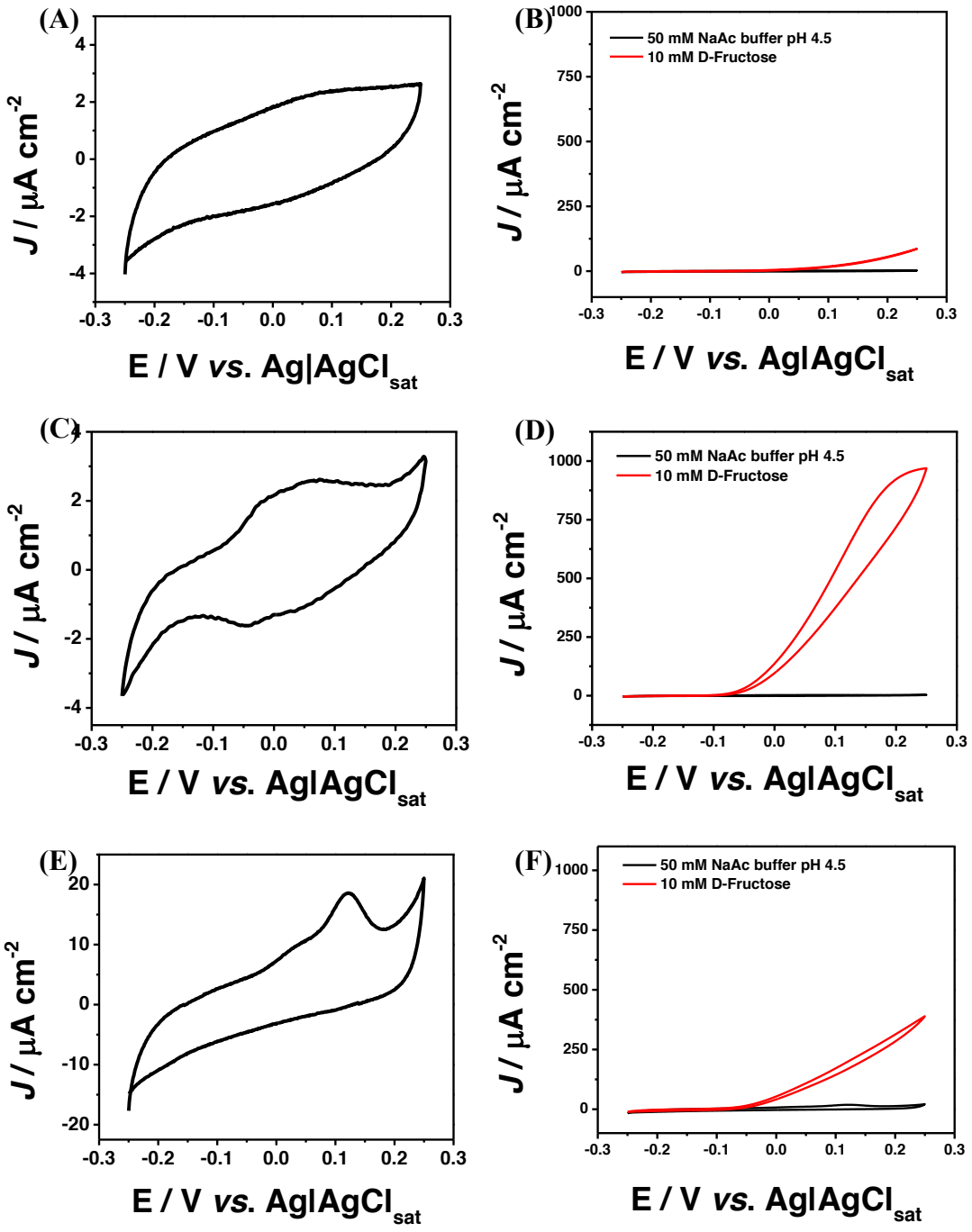

Figure 3. (A) CVs of FDH/4-MBA/h-PG in absence and **(B)** in presence of 10 mM D-(-)-fructose; **(C)** CVs of FDH/4-MPh/h-PG in absence and **(D)** in presence of 10 mM D-(-)-fructose; **(E)** CVs of FDH/4-APh/h-PG in absence and **(F)** in presence of 10 mM D-(-)-fructose; Experimental conditions: 50 mM NaAc buffer at pH 4.5, scan rate 5 mV s^{-1}, T = 25 °C.

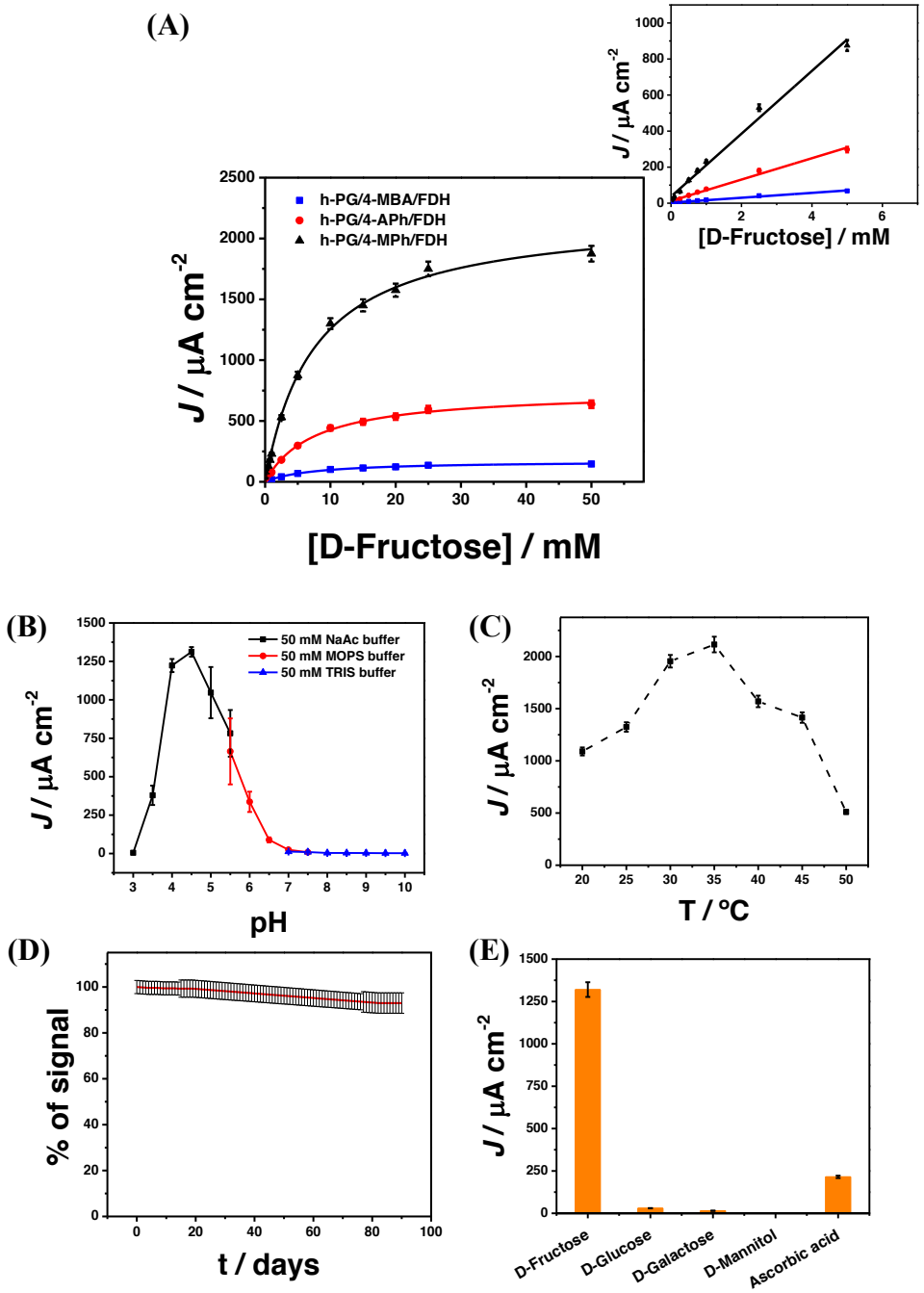

Figure 4. (A) D-(-)-fructose biosensor calibration graph of FDH/4-APh/hPG (**red**), FDH/4-MPh/h-PG (**black**), FDH/4-MBA/h-PG (**blue**) in 50 NaAc buffer pH 4.5. Insert: linear range; **(B)** FDH/4-MPh/h-PG biosensor response over the pH range (4.5–10): 50 mM acetate buffer (**black**), 50 mM MOPS buffer (**red**) and in 50 mM TRIS buffer (**blue**), with E_{app} = 0.250 vs. Ag|$AgCl_{sat}$; flow rate 0.5 mL min^{-1}; **(C)** FDH/4-MPh/h-PG biosensor response over the *T* range (20–45 °C) in TRIS buffer; **(D)** lifetime FDH/4-MPh/h-PG biosensor in presence of 10 mM D-Fructose solution; **(E)** influence of interfering compounds on fructose response in presence of 10 mM D-glucose, D-galactose, D-mannitol and ascorbic acid. Experimental conditions: 50 mM NaAc buffer E_{app} = 0.250 vs. Ag|$AgCl_{sat}$; flow rate 0.5 mL min^{-1}; injection volume 50 µL; *T* = 25 °C.

Table 1. Electroanalytical and kinetic parameters for FDH/4-APh/h-PG, FDH/4-MPh/h-PG and FDH/4-MBA/h-PG

	FDH/4-APh/h-PG	FDH/4-MPh/h-PG	FDH/4-MBA/h-PG
E_{app}/ (V vs. Ag|AgCl$_{sat}$)	+ 0.200	+ 0.200	+ 0.200
K_M^{app}/mM	8.7 ± 0.2	7.5 ± 0.4	9.2 ± 0.9
J_{max}/µA cm^{-2}	750 ± 10	2200 ± 40	170 ± 3
LOD/µM	1.5	0.3	1.2
Linear range/mM	0.05-5	0.05-5	0.05-5
Sensitivity/µA mM^{-1} cm^{-2}	60 ± 3	180 ± 20	14 ± 1
R^2	0.99	0.99	0.99

Table 2. Comparison with fructose biosensors reported in literature. List of abbreviations: 3-mercaptopropionic (3-MPA), 3,3'-dithiodipropionic acid (3,3'-DTDP), 4-mercaptophenol (4-MPh), carbodiimide metho-p-toluenesulfonate (CMC), carbon paste (CP), coenzyme ubiquinone-6 (CoQ), cystamine dihydrochloride (CYS), FAD-fructose dehydrogenase (FDH), glutaraldehyde (GA), gold electrode (AuE), graphene scree-printed electrode (GPH-SPE), hexacyanoferrate (HCF), highly porous gold (h-PG), nanoporous gold electrodes (n-PG), osmium polymer (Os-polymer), poly(amidoamine) dendrimer (PAMAM), poly(ethylene glycol) (400) diglycidyl ether (PEDGE), polyethyleneimine (PEI), PQQ-fructose dehydrogenase (PQQ-FDH), tetrathiafulvalene (TTF).

Electrode Platforms	**Linear Range (mM)**	**LOD (µM)**	**Sensitivity (µA mM^{-1} cm^{-2})**	**Applied Potential (V) vs. $Ag\|AgCl_{sat}$**	**Stability**	**Ref.**
FDH/TTF/GA/3-MPA/AuE	0.01-1.0	2.4	29.1	0.2	~ 30 days	(Campuzano et al. 2003)
FDH/CoQ/3,3'-DTDP/CYS/AuE	0.01-0.5	10	15	0.5	10% decrease in 4 days	(Kinnear and Monbouquette 1997)
FDH/CYS/PAMAM/AuE (with HCF in solution)	0.25-5.0	-	-	0.3	30% decrease after 5 h	(Damar and Demirkol 2011)
FDH/PEDGE/Os-polymer/GPH-SPE	0.1-5.0	2	1.6	0.15	10% decrease after 1 month	(Antiochia and Gorton 2014)
PQQ-FDH/PEI/CP	0.5-10	75	0.4	0.4	Operation stability 10 h	(Parellada et al. 1996)
FDH/CMC/3-MPA/nPG	0.05-0.3	1.2	3.7	0.15	40% remaining after ~6 days	(Siepenkoetter et al. 2017)
FDH/4-MPh/h-PG	0.05-5	0.3	175	0.2	10% decrease after 90 days	This work

Table 3. Results relative to the analysis of real food and beverage samples obtained with FDH/4-MPh/h-PG biosensor and a commercially available enzymatic kit.

Samples	Biosensor mmoL L^{-1}	Ref. Method mmol L^{-1}	Recovery (%)
Cola	180 ± 4	188 ± 6	95.7
Honey	2390 ± 30	2420 ± 30	98.5
Sport drink	44 ± 1	45 ± 1	97.8
Apple juice	1780 ± 30	1800 ± 10	98.8
Tomato juice	1430 ± 20	1460 ± 20	97.3
Orange juice	1640 ± 20	1720 ± 20	95.5
Beer	1490 ± 20	1520 ± 40	97.6
Red wine	1930 ± 30	2010 ± 20	96.3
White wine	1270 ± 30	1340 ± 30	94.3